Mondragon Unibertsitatea

DOCTORAL THESIS

EVALUATION AND ENHANCEMENT OF IEEE 802.11 AMENDMENTS FOR THE CONNECTED TRAIN

ERISLANDY MOZO BIGÑOTTE | Arrasate-Mondragón, 2022

ERISLANDY MOZO BIGÑOTTE | Evaluation and enhancement of IEEE 802.11 amendments for the connected train

Mondragon Unibertsitatea
Goi Eskola Politeknikoa

Evaluation and enhancement of IEEE802.11 amendments for the connected train

Erislandy Mozo Bigñotte

Mondragon Unibertsitatea

Electronics and Computer Science Department

February 2022

Evaluation and enhancement of IEEE802.11 amendments for the connected train

Thesis - Doctor of Philosophy presented at

Mondragon Goi Eskola Politeknikoa

to obtain the title of

Doctor in Applied Engineering

presented by:

Erislandy Mozo Bigñotte

Supervisors:

Dr. Mikel Mendicute Errasti

Dra. Arrate Alonso Gómez

Committee:

Chair: Dr. Ramiro Sámano Robles

Member: Dr. Jorge Portilla Berrueco

Member: Dr. Iker Sobrón Polancos

Member: Dr. Igor López Orbe

Secretary: Dr. Aitor Lizeaga Goikoetxea

Arrasate, February 2022

"Nunca consideres el estudio como una obligación, sino como una oportunidad para penetrar en el bello y maravilloso mundo del saber …"

— Albert Einstein

"La educación es el pasaporte hacia el futuro, el mañana pertenece a aquellos que se preparen para él en el día de hoy …"

— Malcolm X

Toda la gloria del mundo cabe en un grano de maíz …

— José Martí

Acknowledgments

I would like to express my deepest gratitude to all the people who in one way or another have contributed to the development of this Doctorate Thesis. First of all, to my thesis supervisors Mikel Mendicute Errasti and Arrate Alonso Gómez for their support and wise guidance. Nire irakasleei, nire prestakuntzan hondar ale bat jarri didatenei; Imitatzea merezi duen inspirazio bikaina izan dira guztiak. A todos mis compañeros por su respaldo a lo largo del camino, en especial a George Enrique Figueras por sus consejos oportunos y por siempre confiar en mi. A mis padres Angela y Humberto por su guía durante toda la vida, su sacrificio y entrega por completo a esta obra. A toda mi familia, mis hermanos Aymee, Yusel y Pocholo por su constante apoyo y amor durante toda mi vida. Sin ustedes habría sido imposible llegar hasta aquí, muchas gracias por estar a mi lado.

Declaración de originalidad

Hereby I, Erislandy Mozo Bigñotte declare, that this Doctorate Thesis is my original authorial work, which I have worked out by my own. All sources, references and literature used or excerpted during elaboration of this work are properly cited and listed in complete reference to the due source.

Yo Erislandy Mozo Bigñotte declaro que este trabajo de Tesis de Doctorado es original, fruto de mi trabajo personal, y que no ha sido previamente presentado para obtener otro título o calificación profesional. Las ideas, formulaciones, imágenes, ilustraciones tomadas de fuentes ajenas han sido debidaente citadas y referenciadas.

Erislandy Mozo Bigñotte -k adierazten dut Doktorego Tesi lan hau jatorrizkoa dela, nire lan pertsonalaren emaitza dela, eta ez dela aurretik aurkeztu beste titulu edo titulu profesional bat lortzeko. Kanpoko iturrietatik hartutako ideiak, formulazioak, irudiak, ilustrazioak behar bezala aipatu eta erreferentzia egin dira .

Arrasate, February 2022

Erislandy Mozo Bigñotte

Abstract

The Vehicle-to-Everything (V2X) communication is a wireless technology aimed at enabling data exchanges between a vehicle and its surroundings, which is standardized and has great popularity in industry and academia. In the railway domain, even though the use of wireless communications for signalling purposes is not new, the use of a subset of V2X technologies for traffic safety-related services is currently under research since the current communication systems deployed do not provide the requirements demanded by these services. Thus, they allow increasing the safety, reliability and performance of this transportation medium.

In this thesis we focus on the 802.11p/bd amendments where we evaluate their performance to support Train-to-Infrastructure (T2I) and Train-to-Train (T2T) communication links, that will enable traffic-safety related services and eventually the implementation of different degrees of automation in the railway. In addition, an adaptation of the Comb-type Pilot-based Channel Estimation (CPCE) method is proposed for channel tracking for 802.11bd and improving its performance in scenarios with high Doppler spread. It is also benchmarked against the Midamble-based Channel Estimation (MCE) method which is the candidate method used in 802.11bd.

In order to evaluate the performance of 802.11bd in railway, it is essential to consider the propagation characteristics of railway environments with dedicated channel models for simulation and testing. For the T2I propagation link, we have used a parametrized Winner II channel model for simulation purposes, whereas for T2T a gap has been identified in the current state of the art. Therefore, an effort has been made in collaboration with the German's Research Center for Aeronautics and Space (DLR). Based on measurement campaign data, six Tapped Delay Line (TDL) channel models have been derived for T2T communications as well as their stochastic parameters. The proposed TDL channel models and the measured propagation characteristics have been used in a 802.11p/bd simulation framework in order to validate its performance as well as to evaluate the performance of the used communication protocols.

The provided simulation results show a very good match between the proposed TDL channel models and the measurement data, indicating a good accuracy of the theoretical derivations and the simulation method. These channel models have been used to prove that CPCE achieves a higher performance that MCE. Moreover, the results show also that 802.11bd supports reliable V2X communications in railway environments.

Resumen

La comunicación *Vehicle-to-Everything* (V2X) es una tecnología inalámbrica que permite el intercambio de datos entre un vehículo y su entorno, la cual está estandarizada y tiene gran popularidad en la industria y la academia. En el ámbito ferroviario, si bien el uso de enlaces de comunicación inalámbrica con fines de señalización no es nuevo, actualmente se está investigando el uso de tecnologías V2X para soportar servicios relacionados con seguridad vial. Lo antes mencionado es debido a que los sistemas de comunicación desplegados actualmente no proporcionan los requerimientos exigidos por estos servicios. They permiten aumentar la seguridad, confiabilidad y desempeño del ferrocarril.

En esta tesis nos enfocamos en los protocolos 802.11p/bd, donde evaluamos su desempeño para soportar enlaces de comunicación *Train-to-Infrastructure* (T2I) y *Train-to-Train* (T2T), permitiendo de esta forma el soporte de servicios relacionados con seguridad vial y eventualmente la implementación de diferentes grados de automatización en el ferrocarril. Además, se propone un método *Comb-type Pilot-based Channel Estimation* (CPCE) para seguir el canal en 802.11bd. Mejorando de esta forma su desempeño en escenarios con alto *Doppler*. También el método propuesto se compara con el método *Midamble-based Channel Estimation* (MCE), el cual es el método candidato utilizado para 802.11bd.

Para evaluar el desempeño de 802.11bd en el ferrocarril, es esencial considerar las características de propagación de un escenario ferroviario con modelos de canal dedicados para simulación. Para el enlace de propagación T2I, nosotros hemos utilizado el modelo de canal Winner II, mientras que para T2T se ha identificado una brecha en la literatura y ningún modelo ha sido identificado. Por ello, se ha hecho un esfuerzo de colaboración con el Centro de Investigación Alemán (DLR). Usando datos medidos de una campaña de medida, se derivaron seis modelos de canal *Tapped Delay Line* (TDL) para comunicaciones T2T, así como sus parámetros estocásticos. Los modelos TDL propuestos y las características de propagación medidas se han utilizado en un simulador 802.11p/bd para validar su desempeño, así como para evaluar el desempeño de los protocolos utilizados.

Los resultados de simulación muestran una buena correlación entre los modelos de canal TDL propuestos y los datos medidos, indicando una buena precisión de la derivación teórica y el método de simulación. Estos modelos se han utilizado para demostrar que CPCE obtiene un mayor desempeño que MCE. Además, los resultados muestran también que 802.11bd soporta comunicaciones V2X fiables en entornos ferroviarios.

Laburpena

Vehicle-to-Everything (V2X) komunikazioa haririk gabeko teknologia bat da, ibilgailu baten eta bere inguruaren artean datuak trukatzeko aukera ematen duena, estandarizatua eta industrian eta akademian ospe handia duena. Trenbide-jabarian, haririk gabeko komunikazioak seinaleztapenerako erabiltzea berria ez bada ere, gaur egun ikerketapean dago V2X teknologia erabiltzea trafiko-segurtasunerako, egungo komunikazio sistemek ez baitituzte zerbitzu horien eskakizunak betetzen. Horrela, garraiobide honen segurtasuna, fidagarritasuna eta errendimendua handitzeko aukera ematen dute.

Tesi hau 802.11p/bd zuzenketetan oinarritzen da, non hauen errendimendua ebaluatzen den *Train-to-Infrastructure* (T2I) eta *Train-to-Train* (T2T) komunikazioak bermatzeko. Horrek, trafiko segurtasunarekin lotutako zerbitzuak eta trenbidean automozio maila desberdinak ezartzea ahalbidetuko du. Horrez gain, *Comb-type Pilot-based Channel Estimation* (CPCE) metodoaren egokitzapen bat proposatzen da 802.11bd-arekin kanalaren jarraipena egiteko eta *Doppler* altuko egoeretan bere errendimendua hobetzeko. Halaber, *Midamble-based Channel Estimation* (MCE) metodoarekin alderatzen da.

802.11bd errendimendua trenbidean ebaluatzeko, ezinbestekoa da trenbide inguruneetako hedapen ezaugarriak dituzten kanal dedikatuen modeloak kontuan hartzea, bai simulaziorako eta baita testeatzeko. T2I-aren hedapena simulatzeko, Winner II kanal eredu parametrizatu bat erabili da. T2Trako, berriz, ez da kanalaren modelorik aurkitu. Horregatik, Aeronautika eta Espazioko Alemaniako Ikerketa Zentroarekin (DLR) batera, sei *Tapped Delay Line* (TDL) modelo proposatu dira T2T komunikazioen neurketa kanpainanetan oinarrituta. Modelo hauek eta neurtutako hedapen parametroak erabili dira 802.11p/bd simulazio esparru batean protokoloaren errendimendua frogatzeko.

Lortutako emaitzek, proposatutako TDL modeloen eta neurketen arteko antzekotasuna balioztatu dute. Modelo hauek, CPCE-k MCE-k baino errendimendu hobeagoa duela baieztatu dute. Gainera, lortutako emaitzek 802.11bd-ak trenbide inguruneetako V2X komunikazio fidagarriak mantentzeko gai direla adierazi dute.

Index

1 Introduction

In this chapter, the context in which the current doctoral thesis has been carried out is introduced. First, the main opportunities that motivated this research are presented. Then, in order to solve them, the objectives and hypotheses are detailed, as well as the methodology followed to fulfill the proposed objectives. In addition, the scope and the framework in which it is carried out are briefly explained. Finally, the structure of this doctoral report is presented and described.

1.1 Motivation

Telecommunication systems play an important role in the railway transportation system and have a direct impact on its safety and efficiency. Thanks to the development of electronics, semiconductor devices and signal processing techniques, there has been an increase in the use of critical and non-critical communication applications in the railway infrastructure. Initially, these applications were aimed at train safety (critical) oriented services and later also dedicated to the railway operator and end-users (non-critical) oriented services. Today, there is no single communication system to support all services requirements, mainly motivated by the nature of the service to be provided (critical and non-critical). These applications require a Train-to-Infrastructure (T2I) or Train-to-Train (T2T) communication link that meets the demands of the type of service offered, based on packet switching, and require high reliability.

Currently, the most widely used communication technology in the mainline and high-speed segment is Global Systems for Mobile Communication-Railway (GSM-R), which supports only T2I communication links. This is a circuit-switched network, where each connection, whether a call or data one, requires a dedicated end-to-end virtual circuit. This means that network resources are exclusively reserved for a particular connection on both the radio access link and the backbone network, which is suboptimal under burst data transmission. Because of the aforementioned, GSM-R is an obsolete and inefficient technology to support packet-switched applications [1]. Besides, it is a narrowband technology without the capabilities to support Device-to-Device (D2D) communications. Thus, it cannot support applications that require this type of communication.

Given the known limitations of GSM-R, railway operators generally rent the service of public mobile networks or use commercially available technologies to support critical and non-critical applications in other railway segments. Although in theory this solves

the need for connection, it can lead to interference problems, as well as an increase in installation and maintenance costs. In addition, these technologies, generally based on Orthogonal Frequency Division Multiplexing (OFDM), are not optimized to be exploited in railway scenarios. Highly time varying channels (high mobility speeds up to 300 km/h) and a variety of propagation settings (free space, tunnels, bridges, and so on) characterize these scenarios. For example, 802.11a is a technology widely used to support critical applications such as Communication Based Train Control (CBTC) systems, but it was initially conceived for indoor and low mobility environments. Furthermore, it is known that OFDM-based systems are sensitive to the loss of orthogonality between subcarriers, which is frequent in double-dispersive railway channels.

On the other hand, the T2T communication link enables a secure radio connection capable of transferring data directly between trains. In addition, a wireless communication channel is created parallel to the existing T2I radio link. This type of communication can handle time-critical events much better than a centralized system, since the communication is direct and no intermediate equipment is required in the communication. This lack of intermediate elements decreases communication latency. In this sense, there is no standardized technology currently in the railway environment to support T2T communications, which enables the implementation of time-critical applications such as collision avoidance systems, virtual coupling or decentralized CBTC systems. The potential advantages of these emerging applications for train safety and operation have been presented in [2].

Some private solutions of these applications have already been implemented. For instance, in [3], the German Aerospace Center (DLR) presents a Railway Collision Avoidance System (RCAS) based on the Terrestrial Trunked Radio (TETRA) system, which allows the driver to have an accurate knowledge of the state of movement of trains in their vicinity without the help of equipment on ground (i.e. T2I) and they can make decisions in the face of dangerous situations. In [4] a decentralized CBTC system is modelled, in which the functions of the equipment on ground are transferred to the train, increasing its autonomy. This control philosophy was implemented by Alstom in [5] and it is able to double the capacity of the track, reduce the separation between trains to 66 seconds and reduce the number of equipment on ground by 20 %.

Commercial technologies such as Cellular Vehicular-to-Everything (C-V2X), TETRA, 802.11, and WiMAX can support T2T links. An emerging research topic is T2T communication, where a lot of research is required to evaluate the channel characteristics and subsequently the design and evaluation of the communication system used. Thus, technologies such as 802.11p and TETRA have been experimentally evaluated in T2T. However, further research is required because of the variety of propagation environments and the dispersive nature of the railway channel. For instance, the analysis of ITS-G5 based on 802.11p was presented in a T2T link under high speed railway (HSR) conditions [6]. In addition, new communication protocols are being standardized which enable use cases in railway scenarios since a part of the 5.9 GHz band has been assigned for railway purpose. The successor of 802.11p, 802.11bd will add new advanced processing techniques to its physical layer [7]. Another one is New Radio Vehicular-to-Everything (NR-V2X), which is expected to be standardized in the next release (17) by the 3rd Generation Partnership Project (3GPP).

It is known that the insufficient number of pilot carriers and the channel estimation method used in 802.11p limit its use in double-dispersive channels [8]. These channels are characteristic of vehicular and railway scenarios, where the vehicle speed can be

up to 300 km/h. Currently, standardization efforts are underway within European Telecommunications Standards Institute (ETSI) for the design and evaluation of the 802.11bd protocol, which maintains compatibility with its predecessor. The specifications and processing techniques candidates for 802.11bd are presented in [7].

The new protocol increases the numbers of active subcarriers to 56 with a mandatory bandwidth of 10 MHz. 802.11bd uses Low Density Parity Check (LDPC) coding to increase robustness against channel impairments as well as Dual Constellation Modulation (DCM) to increase the transmission range. Also, midambles are used to update estimation of Channel Impulse Response (CIR) by periodically inserting training symbols into the sequence of data OFDM symbols, tracking the wireless channel in this way. Alternative channel estimation schemes for 802.11p have been shown in [9], which could be used with 802.11bd. For example, the authors propose in [10] to use a Comb-type Pilot-based Channel Estimation (CPCE) method, which increases the number of pilot subcarriers to track the channel. Thus, a performance evaluation of these advanced processing techniques is required and necessary during the 802.11bd standardization process.

The performance evaluation of the previous mentioned wireless technologies requires accurate channel models and measurement campaigns carried out in railway scenarios. In [11], the authors provide a rich literature analysis of existing railway channel models based on measurement only for T2I communications. Some Tapped Delay Line (TDL) channel models were identified and used to evaluate the performance of the Emulradio4Rail platform. Also, the WINNER II model is a TDL model used by 3GPP for railway applications with frequencies up to 6 GHz [12].

Several channel models, measurement campaigns and propagation studies have been carried out for T2I communications [13],[14]. In comparison, only a few studies have been reported for T2T communications and a research gap is observed. The first studies in relation to T2T communications based on measurements were carried out in [15], [3], [16]. These articles cover different radio phenomena in the 400 MHz band which include path loss, Doppler shift, fading, and delay spread. In [17], a geometric channel model is presented for a viaduct T2T environment in the 900 MHz band. The wireless channel is characterized with the path loss, the k-factor and the covariance of the envelope. Please note that the channel models shown in [15] and [17] were not tested with a communication system to validate its performance, and they are valid for frequency bands below 1 GHz.

In addition, some measurement campaigns have been carried out to characterize the propagation phenomenon in T2T scenario and the results have been reported in [6],[2],[18]. In [19], a wideband channel sounding was performed in the 5.9 GHz band, and time-variant statistical parameters of the T2T channel were derived for different use cases and driving maneuvers. Also in [20], the authors present an exhaustive study of time-varying stochastic channel parameters for different scenarios and variation of the propagation characteristics with the T2T distance. From the literature, it is observed that no T2T railway scenario is represented by a model that can be used for simulation and evaluation of the radio link performance in the 5.9 GHz band.

1.2 Thesis objectives

In the above exposed context, the focus is on the research of 802.11bd protocol performance to support T2T and T2I communication links, as well as on the improvement of its physical layer. The scope of this thesis includes also the T2T channel modeling, which

is a key element to evaluate the performance of a communication protocol. Considering the previously mentioned, the following main objectives for the current thesis are defined:

- To implement an 802.11p/bd framework to evaluate the physical layer performance of these wireless communication protocols supporting T2T and T2I communication links, considering different channel estimation methods. The performance evaluation is based on numerical simulations and considers different performance metrics.
- To model the small-scale propagation characteristics of the T2T communication channel based on field measurements, in order to provide more realistic simulations, results and conclusions.
- To propose recommendations for the on-going 802.11bd protocol standardization process, contributing to its physical layer definition in order to enable safe automatic train operation.

1.3 Hypotheses

In the current doctoral thesis, 802.11bd physical layer, different channel estimation methods, and multipath propagation in T2T scenarios, as well as channel models for T2I communications available in the state of the art are analyzed. Based on initial results obtained in previous performance analysis and related works in the literature, the following hypotheses were stated:

- The 802.11bd protocol supports critical applications on T2T and T2I links.
- The performance of current OFDM systems on double-dispersive channels is improved by an enhanced distribution of pilot subcarriers.
- The propagation characteristics of a T2T wireless channel can be modeled using the time-varying channel impulse response, which can be measured with channel sounding.

1.4 Methodology

To achieve the main results and contributions of the thesis, the aim is to prove the hypotheses above stated. The research strategy followed for this task consists on processing data obtained in previous measurement campaigns and numerical simulations carried out in Matlab, which is a computational tool that facilitates the design and simulation of wireless systems. This tool is used to perform a link-level simulation of the 802.11p/bd protocol, to model the railway wireless channel, as well as to evaluate the set of candidate signal processing techniques proposed for 802.11bd.

Using these simulations, the performance of 802.11bd is evaluated in terms of Bit Error Rate (BER) and Packet Error Rate (PER) against E_b/N_0 for different railway communication scenarios and configurations, being E_b the energy per bit and N_0 the power density of the noise . In addition, two channel estimation methods available for 802.11bd are compared using these performance metrics. Monte Carlo simulations are

applied, which are configured in such a way that a confidence interval between 10^{-1} and 10^{-3} is provided. The E_b/N_0 ratio is defined taking into account the Modulation and Coding Scheme (MCS) used, the packet length and the simulated Signal to Noise Ratio (SNR).

To model the propagation characteristics of the railway channel, a TDL model is used in this doctorate thesis. The Winner II model is used to simulate the wireless channel for communications with infrastructures (T2I link), which is standardized by 3GPP, and widely used in the literature for railway propagation investigations. Since no model for communications without infrastructure (T2T link) has yet been standardized, the T2T channel is modeled using a TDL model based on a measurement campaign carried out by DLR. In the T2T model, the measured CIR is used to obtain all the parameters of the TDL model.

In order to simulate these models, the channel statistics for them are used to parameterize the channel object *comm.RicianChannel* in Matlab. These parameters include Power Delay Profile (PDP), k-factor, and the distribution of the simulated Doppler spectrum, among others. During the simulations, the same channel model, is used to run a whole cycle of Monte Carlo iterations, but different channel realization at each iteration are used.

Specific considerations on the simulation criteria will be explained in their corresponding sections along with the results obtained.

1.5 Scope of the doctoral thesis

This doctoral thesis is part of a line of research carried out during the Secure Connected Trustable Things (SCOTT) project (www.scott-project.eu) within the working groups 19 and 20. The objectives of these working groups were to propose and evaluate communication solutions for T2T and T2I links, which should support time critical applications. Among the time critical applications worked on in this project are Smart Trains Composition Coupling (STCC) and Trustable Warning Systems (TWS). Both applications are intended to increase the capacity and efficiency of the railway system, as well as safety along the railway track and at level crossing [2].

SCOTT was a Electronic Component and Systems for European Leadership (ECSEL)-funded H2020 project under grant agreement No 737422, which includes 57 commercial partners from 12 countries, including USA and Brazil. Among the participating partners were companies such as Nokia, Ericsson, Siemens, Embraer, NXP or Indra. SCOTT focused on the use of wireless sensor and actuator networks applied to different areas such as mobility, transport, buildings, infrastructures and health, which allowed solving several European social objectives such as integration, life quality upgrading, reduction of energy consumption and improvement in infrastructure management.

During the project, the 802.11p protocol was used as the base access technology to support T2T and T2I wireless communications. In addition, characterization and modeling activities were carried out paying special attention to characteristics such as, catenaries, reflecting objects, other trains, locomotives, Line of Sight (LoS) condition, and bridges, among others. These adversities in the channel hinder the propagation of the radio signal. Moreover, this doctoral thesis has been also supported by the Intelligent Secure Trustable Things (InSecTT) project (https://www.insectt.eu/). InSecTT has

received funding from the ECSEL Joint Undertaking (JU) under grant agreement No 876038.

Throughout the doctoral thesis process there was also a research stay carried out at the Institute of Communications and Navigation in DLR, Munich, Germany [21]. The research stay was a joint collaboration between the Vehicular Communications team in DLR and the Signal Processing & Communications team of Mondragon Unibertsitatea. The joint collaboration was carried out at the end of the year 2020 for a period of three months. The main objective of the stay was to evaluate the performance of the 802.11p/bd protocol in railway scenarios, to support applications related to safety, maintenance and train operation.

1.6 Outline

The doctoral thesis is divided into six chapters, which are briefly described below:

- Chapter 2, Vehicular communications: In this chapter some theoretical aspects on vehicular communications related to our research are taken into account, and a state-of-the-art analysis is performed. Furthermore, the 802.11bd protocol is introduced as a novel technology to support road safety related applications. Besides, the structure of an 802.11bd transceiver is detailed, highlighting its main signal processing techniques including those related to 802.11bd signal timing and detection.
- Chapter 3, Railway communication technologies: In this chapter, some concepts and definitions used in railway communications are introduced. First, the types of services, scenarios and use cases applied to the railway domain are shown. Then, the main characteristics of wireless technologies are summarized where those that support use cases in railway for T2T and T2I links are highlighted.
- Chapter 4, Train-to-Train channel models: This chapter deals with the problem of channel modeling in railway scenarios in the 5.9 GHz band. First, the theoretical aspects of modeling the small-scale propagation characteristics of a wireless channel are examined. Based on field measurements carried out by DLR, the T2T propagation characteristics of two railway scenarios for different distances are analyzed: Railway station and Hilly Terrain. In addition, the channel impulse response was measured and stored using a channel sounder As a result of the examination of stored data, six TDL channel models are proposed. Both the proposed TDL models and the measured impulse response are incorporated into an 802.11bd framework to validate the accuracy of the theoretical derivations and the simulation method.
- Chapter 5, Channel estimation methods for 802.11-based technologies: This chapter addresses the problem of channel estimation in 802.11p/bd. Channel estimation is an essential requirement in the design of any radio receiver. First, the different channel estimation methods exposed in the literature for 802.11p/bd are presented and analyzed. Then, the performance of two channel estimation methods adapted to the 802.11bd frame structure is assessed. The first method, Midamble-based Channel Estimation (MCE), is based on midambles and proposed by ETSI, while the second one, CPCE which is based on pilots, is examined in this thesis, as well. Then, performance results of 802.11p/bd in railway scenarios are shown considering different MCS, payload and communication scenarios.

- Chapter 6, Conclusions and future work. In this chapter, the main conclusions derived from the current doctoral research are presented. In addition, the main contributions are described. Finally, the lines and future works that could be derived from this research are briefly explained.

2 Vehicular communication

In this chapter, Vehicular Ad-hoc Networks (VANET) are introduced which are an essential element in the development of Cooperative-Intelligent Transportation Systems (C-ITS). The main features of the access technologies used in VANET are described. In addition, the 802.11p/bd protocols are described with a focus on the physical layer, where the functional structure of a 802.11bd transceiver is analyzed. Also, a summary of the work in the C-V2X approach and its main features are shown, where C-V2X has had two development paths. Finally, a comparison of vehicular communication technologies is presented and two approaches are analyzed in order to choose a candidate or leading technology.

2.1 Introduction

Mobile Ad-hoc Network (MANET) systems seek to connect mobile devices to each other to create a network, allowing any device in the network to exchange information with all of the devices that are currently around them at any time [22]. The ad-hoc term refers to lack of managing infrastructure devices like routers or phone towers in the network. The MANET systems led to the development of another field of mobile networking systems that sought to connect together devices that are being moved around by vehicles. This field was originally treated as a subcategory of MANETs, but given its unique characteristics such a high mobility, it has been investigated using the term VANET. Hence, the general definition of the term VANET refers to the possibility of having a communication node on-board a vehicle able to establish a wireless communication spontaneously with other surrounding communication nodes visible in its radio range.

The nodes in a VANET system are very dynamic, which can cause quick, frequent or abrupt changes in network topology. These changes can be seen as connections and disconnections of network nodes which introduce a communication overhead for the exchange of signaling. Another characteristic of VANET is the autonomy of the network nodes, which have the capacity to process the information that is exchanged in the network. Also, the control of the network does not depend on an central infrastructure, but it is distributed between all the nodes of the network, thus being more tolerant to failures.

VANET is a fundamental component of the so-called Intelligent Transportation Systems (ITS) [23]. This concept has emerged strongly as a result of traffic problems and

significant growth of information technologies. ITS is defined as a system that collects, stores, processes and distributes information with aim to improve road safety, traffic efficiency, and infotainment needs of passengers (critical and non-critical applications). These applications can range from broadcasting of emergency messages to real-time traffic monitoring, as well as applications related to road safety and collision prevention. In all these applications, there are message exchanges between nodes, in order to improve the response capacity of the driver before possible dangerous situations.

The effectiveness of ITS systems can be increased if there is a cooperation between the nodes of the vehicular network (C-ITS), in which joint actions can be taken to increase safety and travel efficiency. The approach behind VANET is not restricted to vehicular transportation only (car, truck, cart, etc), but it will also include other transportation modes that will equally benefit from a gradual adoption of C-ITS in order to make the mobility of people and freight safer, more efficient, environmentally-friendly and economically sustainable [24]. These new transportation modes include train, aircraft and boat. This vision is represented by Fig. 2.1 showing the vehicle as one of the elements of an integrated communication ecosystem.

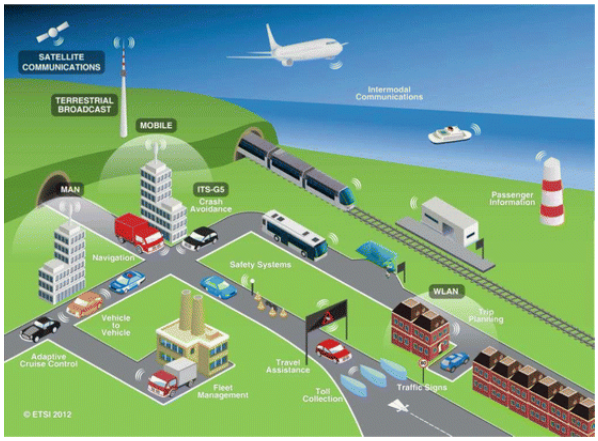

Figure 2.1: C-ITS scenario in an integrated communication ecosystem [24].

2.1.1 Types of V2X communication links

Vehicular networks allow different kind of communication links which can be included within of the term of Vehicular-to-Everything (V2X) communications. This approach describes the exchange of information from a vehicle to other entities within the transport ecosystem that may have an effect on the vehicle. The information that has been exchanged can then be used for a number of applications covering safety, traffic management and user comfort among other.

A node in a vehicular network can be a vehicle equipped with an On-Board Unit (OBU). It includes a wireless short-range communications system with which the vehicle can form an ad-hoc network. In addition, a node can also corresponds to road-side equipment, called Road-Side Unit (RSU), which it is used to connect a vehicle to a wired network infrastructure. Based on which node forms the vehicular network, different kind of communication links can be identified in Fig. 2.2, which were defined by 3GPP in [25] as:

- Vehicle-to-Vehicle (V2V): The vehicles in a close proximity can form a Ad-Hoc network and communicate directly between them. The exchange information is generally transmitted through broadcast messages, both periodic or aperiodic. The V2V applications are used to increase the efficiency and road safety, which allow reducing the number of fatal accidents and saving human lives.
- Vehicle-to-Infrastructure (V2I): The communication link is carried out between vehicle and the RSU to exchange mainly critical information related to road safety. RSU are processing devices that are placed in fixed positions along the road or at specific points on the road to assist vehicles traveling in their area of coverage at all times.
- Vehicle-to-Network (V2N): The vehicles supporting ITS applications can also communicate with an application server located in the cloud. For instance, the vehicles can receive alerts about accidents or warnings of congestion on the route, and take preventive action.
- Vehicle-to-Pedestrian (V2P): It involves direct communications between a vehicle and a pedestrian or multiple pedestrians within close proximity. In addition, the transmission can be targeting other vulnerable road users, such as cyclists. V2P is conducted directly or through the use of a network infrastructure.

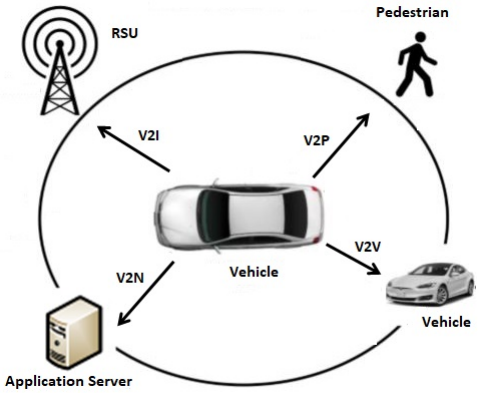

Figure 2.2: Types of vehicular-to-everything application [26].

The vehicles also incorporate a series of sensors such as front and rear radar, speed sensor, position sensor or steering sensor among others. They can capture useful information from the environment that the driver is usually unable to perceive by himself. The vehicles can include too a Global Positioning System (GPS), necessary to locate the vehicle and provide driving assistance. For instance, the driver can use the GPS application to obtain the best route towards a point of arrival which saves time and avoids traffic jam. Finally, some manufacturers propose the use of an electronic license plate to identify a vehicle, and not to use the conventional one for security reasons. The electronic license plate can be remotely updated by the authorities when the driver's license is invalid or if the car is reported as stolen.

The communication links shown in Fig. 2.2 enable V2X applications that can use cooperative awareness to provide more intelligent services for end-users [25]. This means that entities, such as vehicles, roadside infrastructure, application server and pedestrians, can collect and process local environment knowledge and share that information in order

to provide more intelligent services, such as cooperative collision warning or autonomous driving. The shared knowledge can be related to information received from other vehicles, sensor equipment in proximity, localization or speeds, among others.

2.1.2 Applications

VANET provides an opportunity for the development of applications that improve traffic and transportation conditions through the use of collaborative systems based on V2X communications [27]. For instance, the RSU can detect the risk of an imminent collision between two vehicles and warns drivers via the OBU. This action could avoid accidents and save human lives. Furthermore, vehicles stopped in a traffic congestion could send information about their situation using the infrastructure. This information could be made available to other drivers, who can even access external elements of the VANET network itself and calculate an alternative route. This action allows improving the traffic efficiency on the road. Depending on the function, vehicular applications fall into four main categories: road safety, road efficiency, and public and information services.

1. Road safety: It is considered as the most service demanded from VANET and its objective is to reduce the probability of traffic accidents and to reduce damages and injuries caused by traffic accidents. Drivers are notified with alarm messages associated with road events, information about nearby vehicles and incident management. These applications are divided into three subcategories
    - Collision avoidance: Intersection collision warning, pre-collision warning, lane change warning, dangerous area warning.
    - Road sign notifications: Curve speed warning, traffic signal violation warning.
    - Incident management: Emergency vehicle alarm, post-collision/crash warning.
2. Road efficiency: The purpose of these applications is to improve traffic conditions by managing and monitoring vehicle traffic and road conditions. These applications are divided into two subcategories:
    - Traffic monitoring: Road condition monitor, vehicle tracking and tracing agent
    - Traffic management: Intelligent traffic control, speed control, tolls, navigation etc.
3. Public service: The purpose of these applications is to facilitate the work of public security and emergency services. For instance, an active emergency vehicle, like an ambulance or an police car, could indicate to other vehicles on the road to clear the lanes. This information can be relayed in the same environment by other vehicles and RSUs available in the area. These applications are divided into two subcategories:
    - Emergency vehicle warning: Emergency vehicle alert approaches, emergency call.
    - Support for authorities: Electronic license plate, electronic driver's license, security vehicle inspection, stolen vehicle tracking.

4. Infotainment: These are focused on providing drivers and passengers with entertainment and information services. For instance, they offer drivers information on places of interest, local attractions and location-based services. In addition, they offer the possibility to vehicle occupants to make use of VANET resources for recreational purposes. Hence, using Wireless Fidelity (WiFi) hotspots set up on the road or cellular network, the users can surf internet, play online games or view multimedia content, among other activities. These applications are divided into two subcategories:

   - Entertainment: Access to internet resources, tele-diagnosis and on-line help.
   - Context information: Updating and downloading maps, location and parking reservation, information on places of interest.

2.1.3 Standards for vehicular networks

Vehicular networks are an important field of research in the area of Intelligent Transportation Systems. As a result, different vehicle communication protocols have been standardized. Dedicated Short-Range Communications (DSRC) is a wireless technology that has been designed to support a variety of applications based on V2X communications. Vehicular communications supported by DSRC systems operate in the 5.9 GHz licensed band and have an approximate maximum range of 1000 m [23]. There are two main protocol architectures for vehicular communication systems, one developed by Institute of Electrical and Electronics Engineers (IEEE) and the other one by ETSI, as shown in Fig. 2.3.

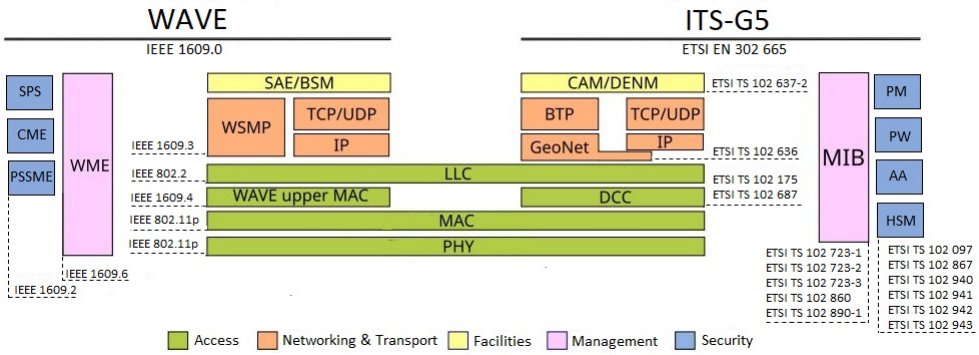

Figure 2.3: WAVE/ITS-G5 protocol stacks in vehicular communication systems [28].

The protocol stack in United State (US) is known as Wireless Access in Vehicular Environment (WAVE), while in Europe it has been named ITS-G5. Both standards rely on 802.11p for the implementation of physical layer and Medium Access Control (MAC) layer, which allow the reliable and timely data transfer necessary in highly variable vehicular channels. In order to manage the channel congestion by decreasing the packect transmission time, 802.11p defines an operation mode called Outside the Context of a Basic Service Set (OC-BSS). Using this mode, the devices enable with 802.11p avoid the registration and authentication procedures, commonly present in typical wireless local area networks.

Using the TCP/IP reference model, Fig. 2.3 shows that vehicular protocol stacks are divided in five layers: Access, Networking & Transport, Facilities, Management and

Security. Several protocols are defined over these layers, as well as procedures and rules to meet V2X application requirements with the most stringent performance specifications and robustness. For instance, the facilities layer gives support to different V2X applications by facilitating the access to information at the ITS stations. In addition, basic V2V safety messages have been defined by IEEE, named Basic Safety Message (BSM), and by ETSI, named Cooperative Awareness Message (CAM). These messages contain information about the vehicle status and are used to assess potential threats by surrounding vehicles. A more detailed description of functionalities of these layers can be found in official documents from IEEE and ETSI (see Fig. 2.3).

The Federal Communications Commission (FCC) in the United States allocated a dedicated spectrum band at 5.9 GHz for vehicular communications. In America, a bandwidth of 75 MHz was reserved, while in Europe only 50 MHz were assigned. This spectrum was divided into smaller 10 MHz wide channels and in the American case, a 5 MHz guard band at the low end was also included. As a result, there are 7 different channels for WAVE operation and 5 for the case of ITS-G5. These channels are divided in Control Channels (CCH) and Service Channels (SCH), as seen in Fig. 2.4. The control channels are used to transmit cooperative road safety and control information [23]. In addition in Europe, the frequency band can be divided into ITS bands, where the ITS-G5A band is reserved for road safety, the ITS-G5B band is assigned for general purpose ITS services, and the ITS-G5D band, initially reserved for future applications, was recently assigned to Urban Rail ITS by ETSI [29].

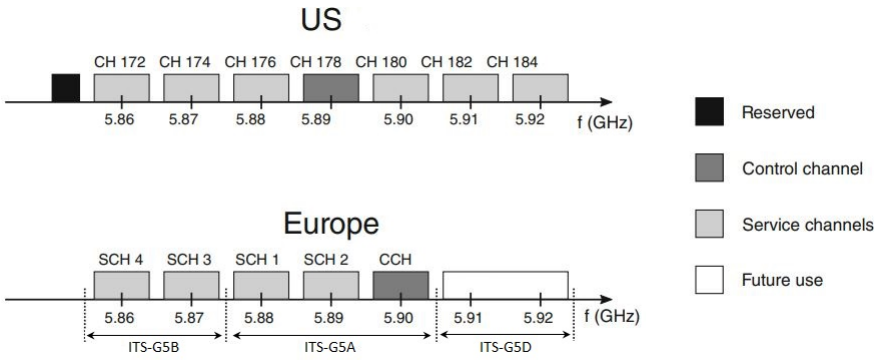

Figure 2.4: Spectrum allocation for vehicular communications used in WAVE and ITS-G5 [23].

Although, the WAVE/ITS-G5 standards allow the multi-channel operation necessary in the vehicle safety context, they carry out this operation in different ways. While ITS-G5 considers units as dual-radio devices with a dedicated radio for safety, WAVE periodically and synchronously switches between the CCH and SCH using only one radio. In addition, Internet Protocol (IP) based communications are supported in both cases, which allows for instance that a vehicular entity can communicate with an application server.

The Access layer based on 802.11p has more than a decade of exploitation and supports basic non-critical and critical applications. In the last year, Europe and US have taken different positions on which vehicular communication protocol to implement in their region as the successor of 802.11p in next years. The FCC will abandon 802.11p in the US and allow the use of cellular technology in the access network. This communication approach is named C-V2X. In addition, the bandwidth for ITS application will decrease from 75 to 30 MHz, and unlicensed wireless users will be allowed to operate in the freed

spectrum.

In contrast, the CAR 2 CAR Communication Consortium supports a hybrid communication approach for Europe. In this approach, both technologies (802.11p/bd and C-V2X) are complemented to provide distinct functions facilitating connected and automated mobility in the access network. Furthermore, ETSI is working in the next evolution of 802.11p named 802.11bd since the former does not comply with the requirements demanded by advanced vehicular services such as latency, reliability, and quality of services among others [30]. These protocols will be explained in detail in the following sections.

It is worth mentioning that DSRC and C-V2X technologies are addressing the similar use cases. They have identical network, security, and application layers, only difference in the access layer. Therefore, some companies are delivering dual-mode functionality device to support both DSRC and C-V2X technologies. It is yet to be seen which one will be the market prefer. For instance, Autotalks is a company that develops vehicle technology which offers dual-mode chipset supporting both DSRC and C-V2X. CRATON2 is a second-generation chipset specifically designed by Autotalks for connected autonomous vehicles [31]. It is actually the most advanced, secure, global V2X communication solution.

2.2 IEEE 802.11p

Currently, the 802.11p standard constitutes one of the protocols under which vehicular networks are supported, as it was mentioned in Section 2.1.3. This protocol defines the communication requirements, procedures, and algorithms at the physical and MAC layer. This section describes the main features of 802.11p in terms of its physical layer.

2.2.1 Main features

802.11p is a modified version of 802.11a that uses OFDM as a modulation technique with 48 data sub-carriers and 4 pilot sub-carriers. Also, it defines 8 coding and modulation schemes where 64QAM-5/6 is the scheme of higher order [32]. The main parameters of 802.11p are shown in Table 2.1. To adapt 802.11p from 802.11a to vehicular environment, some modifications were made. For instance, 10 MHz channels are used instead of 20 MHz channels which reduces the unwanted effect of Inter-Carrier Interference (ICI) caused by high Doppler spread seen in high-mobility vehicular channels. As a consequence of this modification, the timing parameters of OFDM are doubled.

In addition, to increase the communication range and reduce co-channel interference, the Effective Isotropic Radiated Power (EIRP) is increased up to 33 W and 4 new spectral masks are defined which are more restrictive than those used in 802.11 devices. To increase the accuracy of synchronization and channel estimating techniques, the training sequence duration time of the physical layer header is increased as well, and pilot signals are still used to correct the frequency offset and phase noise [33]. The 5.9 GHz band has been licensed for vehicular communications use, where 802.11p divides the spectrum from 5.850-5.925 GHz into multiple channels, including a CCH and six SCH. The former is dedicated to the transmission of critical messages related to vehicle safety and the latter for the transmission of non-critical vehicular applications.

The 802.11p physical layer is composed of two sub-layers, Physical Layer Convergence Protocol (PLCP) and Physical Medium Dependent (PMD). The PLCP is responsible

Table 2.1: 802.11p physical layer main features based on the OFDM modulation.

Parameter	Value	Unit
Number of sub-carriers	52	...
Number of pilot sub-carriers	4	...
Number of data sub-carriers	48	...
Guard time	1.6	μ
OFDM symbol time	8	μ
STS duration	1.6	μ
LTS duration	6.4	μ
Modulation type	BPSK,QPSK,16QAM, 64QAM	...
Coding rate	1/2,2/3,3/4	...
Coding type	Convolutional	...
Separation between carriers	0.15625	MHz
Bandwidth	10	MHz
Data rate	3,4.5,6,9,12,18,24,27	Mbps

STS= Short Training Symbol;LTS=Large Training Symbol

for the communication with the MAC layer, and carries out a convergence process, in which the Packet Data Unit (PDU) coming from the MAC layer is transformed into an OFDM frame, thus forming a Protocol Packet Data Unit (PPDU). On the other hand, the PMD is an interface with the physical transmission medium, whose role is to manage data coding and modulation.

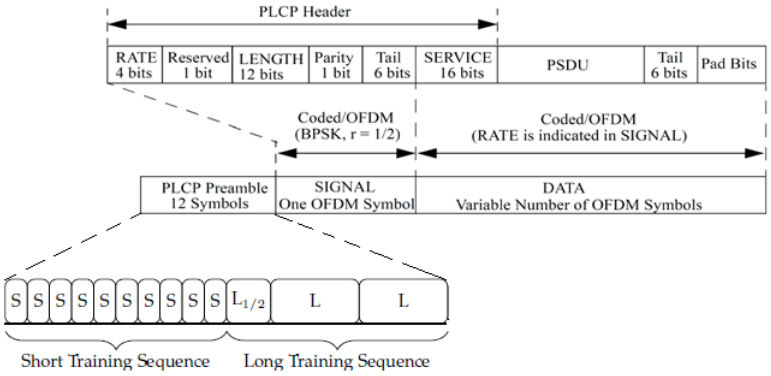

Figure 2.5: 802.11p PPDU frame format.

The PPDU frame consists of a preamble, a signal field, and a data field as shown in Fig. 2.5. The preamble field is used to mark the beginning of the physical frame, antenna diversity, and correct the frequency and time offset (synchronization). This field is composed by 12 training symbols distributed in a short and a large training sequence. The short training sequence is composed by 10 repetitions of short symbols that form two Short Training Symbol (STS), whose role is to detect the signal and control the automatic gain [34]. While the large training sequence is composed by 2.5 repetitions of a Large Training Symbol (LTS). A STS consists of 12 subcarriers $\{\pm4, \pm8, \pm12, \pm16, \pm20, \pm24\}$ generated by the sequence S as follows:

$$S_{-26..26} = \sqrt{\frac{13}{6}}\{0,0,1+j,0,0,0,-1-j,0,0,0,1+j,0,0,0-1-j,$$
$$0,0,0,-1-j,0,0,0,1+j,0,0,0,0,0,0,-1-j,0,0,0,-1-j,0,0,0,1+j,$$
$$0,0,0,1+j,0,0,0,1+j,0,0\}. \quad (1)$$

The LTS consists of 53 sub-carriers, whose role is essential for channel estimation. LTS is

defined by the training sequence L as:

$$S_{-26..26} = \{1, 1, -1, -1, 1, 1, -1, 1, -1, 1, 1, 1, 1, 1, 1, -1, -1, 1, 1, \\ -1, 1, -1, 1, 1, 1, 1, 0, 1, -1, -1, 1, 1, -1, 1, -1, 1, -1, -1, -1, -1, \\ -1, 1, 1, -1, -1, 1, -1, 1, -1, 1, 1, 1, 1\}. \quad (2)$$

A guard time is inserted between the STS and LTS to avoid inter-symbol interference, the total preamble time is 32 us.

The signal field consists of 24 bits and contains important information about the transmitted signal. This field is transmitted using the most robust MCS, BPSK modulation and 1/2 coding. The signal field is composed by a rate field (4 bits) which specifies the MCS used in the transmission; a reserved field (1 bit), a length field (12 bits) with the length of transmitted packet; a parity field (1 bit) used to enable error detection in the receiver; and a tail field (6 bits zero) used to reset the convolutional coder registers.

Finally, the data field consists of a service field, a PLC Service Data Unit (PSDU) field, tail bits, and a padding field. The Service field has 16 zeros to initialize the data coder, avoiding long sequences of the same bit. Thus improving the distribution of ones and zeros in the payload. The PSDU is a variable length frame from the MAC upper layer, while the tail bits are used to initialize the shift registers of the convolutional coder once the coding process is finished. Six bits are required for each coder, that is, six tail bits for each coded frame. Finally, padding bits are used to ensure that the PLCP data field occupies an integer number of OFDM symbols.

As MAC layer protocol, 802.11p uses Enhanced Distributed Channel Access (EDCA), which is an extension of the Carrier Sense Multiple Access with Collision Avoidance (CSMA/CA) protocol, to provide Quality of Service (QoS) over transmitted packets [35]. EDCA is a contention-based, decentralized, and low-complexity protocol that provides the use of four Access Category (AC) stacks. Each AC stack works as an independent Distributed Coordination Function (DCF) station with its own EDCA parameters to contain channel access opportunities [36]. These functions are called Enhanced Distributed Channel Access Functions (EDCAF).

2.3 IEEE 802.11bd

In May 2018, the IEEE and the IEEE Standards Association announced the formation of a new study group focused on the evolution of the 802.11 technology for Next Generation Vehicle-to-Everything (NGV). They are now preparing the amendment to 802.11bd. In January 2019, Task Group 802.11bd (TGbd) was created with the goal of investigating and evaluating the requirements and technologies in the upcoming amendments [37]. This group defined the main design objectives in [38], where interoperability, co-existence, backward compatibility and fairness were defined as essential requirements. In this section, the frame structure, the transceiver structure, use cases and processing techniques that are expected to be included in 802.11bd are briefly described based on studies presented in [39] by TGbd.

2.3.1 Main features

New advanced vehicle applications demand low latency (below 10 ms), ultra-high reliability (99.999 % in term of PER for remote driving) and very high efficiency of

bandwidth used [40]. Hence, the new protocol must be designed considering these requirements, introducing novel processing techniques, and in keeping with the constrains of backward compatibility. An 802.11bd specification framework was presented in [37] and [7], where the following setting candidates were proposed:

- 10/20 MHz bandwidth: Mandatory use of 56 active carriers over a bandwidth of 10 MHz. In addition, a 20 MHz bandwidth can be used to increase the throughput.
- Channel tracking: Use of midamble to combat Doppler, every 4, 8 or 16 symbols. The midamble are training symbols that are periodically inserted into the sequence of data OFDM symbols.
- LDPC coding: To increase robustness against channel impairments. Different parity check matrices are defined and chosen depending on the packet length.
- Retransmissions: To increase reliability, TGbd proposes an adaptive retransmission scheme, where the decision of retransmission is based on the congestion level [41].
- MIMO techniques: They can increase the reliability or throughput and can support two spatial streams for unicast transmissions as an optional feature.
- DCM technique: Increases the reliability, and was firstly introduced in 802.11ax in orden to improve BER and decrease the receiver sensitivity [42].
- Aggregation of messages: Increases efficiency and enables both aggregate MAC service data unit and aggregate MAC protocol data unit operations to work with unicast messages as defined in 802.11ac.

Most of the techniques will be implemented in the physical layer, keeping OFDM as the radio access interface, while the working frequency band is kept at 5.9 GHz, which was licensed for vehicular applications. In addition, the basis of the 802.11bd design can be deployed in $mmWave$ frequency band for short-range applications. This approach was already used in 802.11ad and its enhancement 802.11ay. On the other hand, the MAC layer will be extended to provide upper layers with the ability to control NGV transmissions.

Use cases

The following use cases and scenarios have been defined in [7] and [43] for 802.11bd :

- Basic safety messages
- Sensor sharing
- Multi-channel operation
- Infrastructure applications
- Vehicular positioning and location
- Automated driving assistance
- Aerial vehicle ITS application

- Train to Train (T2T)
- Vehicle to Train (V2T)

Basic safety messages initially defined in 802.11p are maintained to provide backward compatibility. In this use case, all vehicles periodically broadcast a message containing their basic information, which alerts the driver of an upcoming safety risk. For this use case, the transmission range of 802.11p needed to be increased by 25 % for urban intersections [43]. The requirements, limitations and deployment time of these advanced vehicle use cases are under test by TGbd, and the requirements of some have been studied by 3GPP in [40].

On the other hand, sharing sensors allows the exchange of processed data collected through local sensors or video cameras with other V2X entities. In this manner, vehicles can improve the perception of their own environment beyond what they can detect and have a more holistic view of their local situation. Autonomous driving allows a driver or a V2X application to operate a vehicle remotely. Both use cases require that the packet carries a higher number (50 % greater) of transmitted bytes than a 802.11p packet under the same conditions (packet duration, PER, range, wireless channel) [43].

These advanced V2X use cases are applications that can also assist in better traffic management and greater operating efficiency. For example, within the T2T use case, different applications were defined in [41]: collision avoidance, remote control, automatic coupling, train integrity, and virtual coupling (platooning). In this use case, a reliable radio link is capable of transferring data directly between both trains, and a additional wireless communication channel is created along with the T2I link already available. The T2T link can handle critical time events more effectively than a centralized system. Thus, trains can exchange information about their composition, position, power controls, relative speed and train lengths among others. In this scenario, NGV must provide at least a data rate of 1 Mbps, a ranging accuracy of 1 % of distance, and latency of 10 ms (within a transmission range of 2000 m and a speed of 500 km/h).

2.3.2 **Frame structure**

The 802.11bd frame structure for 10 MHz is shown in the upper part of Fig. 2.6, where the preamble is extended to enable backward compatibility. The first three fields of the preamble are formed by the legacy preamble: Short Training Field (STF), Large Training Field (LTF) and Signal Field (SIG). This format allows the coexistence of both protocols (new and legacy). A new signal field is defined, the NGV Signal Field (NGV-SIG), to describe other parameters of the transmitted signal, such as used bandwidth, midamble rate, and number of spatial streams. In addition, both signal fields are duplicated to improve the detection probability of the received signal, and they form the Repeated SIG (R-SIG) and Repeated NGV-SIG (RNGV-SIG). Finally, the two last fields in the preamble are the new version of short and large training fields, NGV Short Training Field (NGV-STF) and NGV Large Training Field (NGV-LTF), respectively. The NGV modulated data is inserted on the NGV Data Field (NGV-Data) using the information on both signal fields.

Fig. 2.6 also shows the number of OFDM symbols of each field of the 802.11bd frame. Please note that the number of symbols in NGV Data Field (NGV-Data), N_{Data}, is variable and depends on the size of the packet, data rate and bandwidth used. Also, the

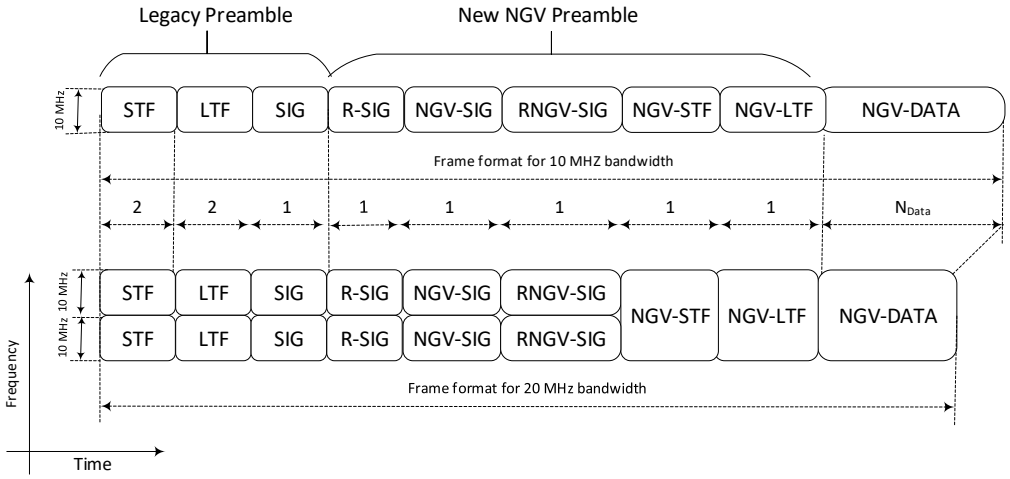

Figure 2.6: 802.11bd frame structure for channels of 10 and 20 MHz bandwidth[7].

802.11bd frame format for 20 MHz bandwidth is too presented in this figure, where the preamble of the transmitted signal is repeated and transmitted over two adjacent channels of 10 MHz bandwidth. This approach assures the compatibility between 802.11bd devices that are transmitting with different bandwidth. A detailed description of the structure of each field in the frame can be seen in [7].

Signal bits and NGV-LTF format

The SIG and NGV-SIG fields contain signal bits which carry control and signalling information that indicates to receiver how the signal has been generated. Then, the receiver uses this information in orden to recover properly the transmitted data bits. This process will be explained in detail in next sections. SIG and NGV-SIG fields are composed of an OFDM symbol that contains 24 signalling bits. Table 2.2 shows the description and distribution that the signalling bits shall have in NGV-SIG. Remember that the SIG field is similar a to signal field standardized for 802.11p, which was described in Section 2.2.1.

Table 2.2: Description of signaling bits in the NGV signal field [7].

Signal bits	Field	Description
0-1	Version	Set to 0 for 11bd, other three options are reserved
2	Bandwidth	Set to 0 for 10 MHz, and set to 1 to 20 MHz
3-6	MCS index	Binary code of the MCS index, see table 2.4
7	Stream	set to 0 for one stream, and set to 1 for two stream
8-9	Midamble	set to 0 for M=4, set to 0 for M=8, set to 0 for M=16, value 3 is reserved
10	NGV-LTF	set to 0 for NGV-LTF-2x, and set to 1 for NGV-LTF-1x
11	Extra symbol	Set to 0 if there are a extra OFDM symbol in LDPC encoding process, otherwise set to 1
12-13	Reserved	Set to 1
14-17	CRC	CRC computation
18-23	Tail	Used to reset the convolutional decoder

MCS= modulation and coding scheme; M= Midamble periodicity; CRC= Check Redundancy Cyclic;LDPC= Low Density Parity Check;

Table 2.2 shows the three options of midamble that are available in the protocol, which

are signalled using two bits (bits seven and eight). The use of midamble is a relevant feature of 802.11bd for channel tracking compared to 802.11p. However, its use has a penalty in throughput or effective data rate since overhead is increased. The midambles have same format that NGV-LTF. Using the bit 10 of NGV-SIG, 802.11bd defines two NGV-LTF formats: NGV-LTF-2x normal format ($\mathrm{LTF}_{2\mathrm{x}}$) and NGV-LTF-1x reduced format ($\mathrm{LTF}_{1\mathrm{x}}$). The use of NGV-LTF-1x decreases considerably the overhead since it reduces the symbol length by half regarding to NGV-LTF-2x.

In a 10 MHz transmission where total number of subcarriers $N = 64$, the NGV-LTF-2x is defined in frequency domain by

$$\mathrm{LTF}_{2\mathrm{x}}[k] = \{0, 0, 0, 0, 1, 1, \mathrm{LTF}_{\mathrm{L}}, 0, \mathrm{LTF}_{\mathrm{R}}, -1, -1, 0, 0, 0\}\,, \tag{3}$$

being $k = -32, ..., 31$ the carrier index, and the 14-length sequences

$$\mathrm{LTF}_{\mathrm{L}} = [1, 1, -1, -1, 1, 1, -1, 1, -1, 1, 1, 1, 1, 1, 1, -1, -1, 1, 1, \\ -1, 1, -1, 1, 1, 1, 1]$$

and

$$\mathrm{LTF}_{\mathrm{R}} = [1, -1, -1, 1, 1, -1, 1, -1, 1, -1, -1, -1, -1, -1, -1, 1, 1, -1, -1, 1, \\ -1, 1, -1, 1, 1, 1, 1].$$

The $\mathrm{LTF}_{1\mathrm{x}}[k]$ is obtained from $\mathrm{LTF}_{2\mathrm{x}}[k]$ by putting to zero all subcarriers with even index, and defined by

$$\mathrm{LTF}_{1\mathrm{x}}[k] = \begin{cases} \mathrm{LTF}_{2\mathrm{x}}[k] & \text{for } k \text{ odd} \\ 0 & \text{else.} \end{cases} \tag{4}$$

As a result of assigning zeroes in frequency domain, the NGV-LTF-1x in time domain $\mathrm{LTF}_{1\mathrm{x}}[n']$ is a periodic sequence with period 32, where $n' = 1, .., 64$ represents the sample index. The last result means that $\mathrm{LTF}_{1\mathrm{x}}[n'] = \mathrm{LTF}_{1\mathrm{x}}[n' + 32]$. Then, it is not necessary to transmit all $\mathrm{LTF}_{1\mathrm{x}}[n']$ symbols. Instead, only the half of the symbol is transmitted. Using this approach, the overhead is reduced by transmitting only half midamble. In the receiver side, the reverse process must be done together with an interpolation process in order to estimate amplitude in the even sub-carriers. The reader can check [7] to see the definition of $\mathrm{LTF}_{1\mathrm{x}}[k]$ for 20 MHz transmission.

2.3.3 **802.1bd transceiver**

This section describes the structure of a 802.1bd transceiver based on studies presented in [39] by TGbd. The section is divided in two parts where the structure of transmitter and receiver are described. Firstly, the 802.11bd signal model is presented and implemented using a block diagram where relevant parameters of the signal are shown. In the second part of the section, a block diagram of the receiver is depicted and analyzed. The synchronization process of the 802.11bd received signal is explained in detail, as well as its implementation using a real signal as a reference.

2.3.3.1 Structure of 802.1bd transmitter

The 802.11bd transceiver is based on an OFDM system which uses N subcarriers and a Cyclic Prefix (CP) with a length of N_{g} samples. The spacing between the subcarriers is chosen such that the orthogonality between the carriers is maintained, which is possible by setting the number of samples of an OFDM symbol equal to $N_{\mathrm{s}} = N + N_{\mathrm{g}}$. As result, each OFDM symbol is preceded by a CP of length N_{g}. This choice allows to avoid Inter-Symbols Interference (ISI) which could cause a distortion in the recovered signal. In addition, each OFDM symbol is composed by N complex symbols $a_{p,k}$, where p denotes the OFDM symbol index and k denotes the subcarrier index. The complex symbols contain data symbols and signaling symbols as well as null symbols. The data symbols carry the information bits, the signalling symbols are used to control and signalling purpose, and the null symbols located in the edges of the band provide guard bands to manage adjacent channel interference. Using these guard bands, the signal spectrum can be limited by using an appropriate discrete transmission filter with an impulse response $g[\tau]$.

The transmitter is frame-oriented with frame length equal to N_{ofdm} OFDM symbols. The 802.11bd frame structure was presented in Section 2.3.2, where the frame contains preamble symbols, data symbols and midamble symbols. The discrete complex baseband signal for a transmitted frame $s[n]$ can then be defined by

$$s[n] = \frac{1}{N} \sum_{p=1}^{N_{\mathrm{ofdm}}} \sum_{k=-N/2}^{N/2-1} a_{p,k} \psi_{p,k}[n] * g[\tau] \tag{5}$$

being the complex subcarrier

$$\psi_{p,k}[n] = e^{j2\pi \frac{k}{N}(n - N_{\mathrm{g}} - pN_{\mathrm{s}})} g_{\mathrm{s}}[n - pN_{\mathrm{s}}], \tag{6}$$

where * denotes convolution. Please note, although the training symbols (symbols with indexes $p = 1, 2, 3, 4, 9, 10$) and midambles have been included in (5), they are predefined in 802.11bd protocol. Moreover, each OFDM symbol is shaped using a pulse shape $g_{\mathrm{s}}[n]$ which minimizes the energy leakage out the band. Using a raised cosine shaping filter, $g_{\mathrm{s}}[n]$ is defined by

$$g_{\mathrm{s}}[n] = \begin{cases} \frac{\sin(n\pi)}{n\pi} \frac{\cos(\beta_{\mathrm{c}} n\pi)}{1-(2\beta_{\mathrm{c}} n\pi)^2} & 0 \leq n \leq N_{\mathrm{s}} \\ 0 & \text{else,} \end{cases} \tag{7}$$

being β_{c} the roll-off factor. Furthermore, when $g_{\mathrm{s}}[n]$ is a rectangular pulse, the upper branch of (7) equals 1. Table 2.3 shows the main parameters of the 802.11bd signal, which can be set using two options of bandwidth: 10 and 20 MHz.

The block diagram of an 802.11bd transmitter based on (5) is shown in Fig. 2.7. The diagram has been divided into four processing blocks for convenience, which have been numbered from one to four. The data bit stream b_i is modulated in block number 1 following a processing chain composed by padding-scrambler-encoder-constellation sub-blocks. Firstly, service bits and padding bits are added to b_i to reset the scrambler and to ensure that the frame contains a whole number of OFDM symbols, respectively. Next, the obtained bits are scrambled in orden to randomize the data pattern, which may contain long strings of 1s or 0s. After that, the scrambled data is passed to a LDPC encoder, which introduces, in a controlled manner, some redundancy into the bit stream.

Table 2.3: Parameters of 802.11bd signal.

Parameter	BW10	BW20	Description
N_{sd}	52	108	Number of data subcarriers
N_{p}	4	6	Number of pilot subcarriers
N_{n}	8	14	Number of null subcarriers
N	64	128	Total number of subcarriers, $N = N_{\mathrm{sd}} + N_{\mathrm{p}} + N_{\mathrm{n}}$
$\mathrm{T_s}$	100 ns	50 ns	Sampling period
Δf	156.25 KHz		Spacing between subcarriers
$\mathrm{T_g}$	1.6 μs		Guard interval duration
$\mathrm{T_{sym}}$	8 μs		OFDM symbol duration, $\mathrm{T_{sym}} = 1/\Delta\mathrm{f} + \mathrm{T_g}$
$\mathrm{T_{NGV-LTF-1x}}$	4.8 μs		Duration of NGV-LTF-1x symbol
$\mathrm{T_{NGV-LTF-2x}}$	8 μs		Duration of NGV-LTF-2x symbol

BW10=10 MHz bandwidth setting;BW20=20 MHz bandwidth setting

This redundancy is used for error correcting coding which allows the receiver to combat the detrimental effects of the channel and, hence, achieve reliable communications in spite of these effects. The specifications of the LDPC encoder have been defined by ETSI in [44]. Finally, the output of block 1, modulated data stream a_{d}, is achieved by modulating encoded bits using a digital constalation.

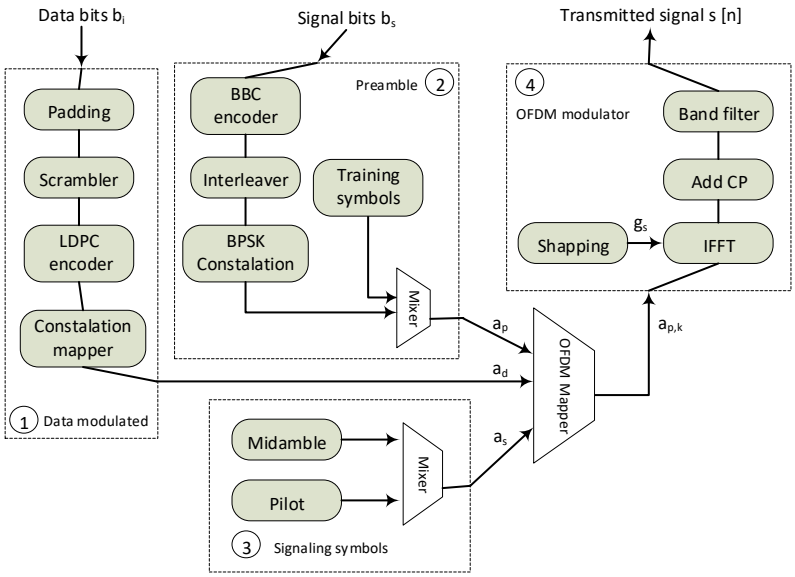

Figure 2.7: Block diagram of an 802.11bd transmitter.

The preamble a_{p} defined in Section 2.3.2 is generated in block number 2 (Fig. 2.7). It is divided in training symbols and control symbols. While the training symbols are predefined and do not need to be generated, the other ones are obtained following a processing chain composed by BBC_Encoder-Interleaver-BPSK_Constellation sub-blocks. In this way, the control symbols are obtained from signal bits b_{s} which were introduced in the previous section, please see Table 2.2. More extra signalling symbols a_{s} are introduced in block number 3: pilot symbols and midambles. These symbols are predefined too and are used for phase tracking and channel estimation purposes in the receiver.

Now, the a_{p}, a_{d}, and a_{s} symbol streams are mapped on the OFDM time-frequency grid of complex symbols $a_{p,k}$, which represent a complex matrix of $N_{\mathrm{OFDM}} \times N$ elements. The mapping is performed in the block named OFDM Mapper. Finally, the transmitted signal $s[n]$ is the output of block number 4. This block implements a OFDM modulator

using directly (5). Please note, the first sum in (5) is implemented in Add_CP sub-block where each OFDM symbol is extended in length with a CP and aligned in time. In the next subsections, we give more detail about some relevance sub-blocks in Fig. 2.7.

Modulation and coding: data rates

The MCS is a parameter that describes the modulation type and channel code rate R_c used for transmission of a wireless signal. The 802.11bd draft defines 11 modes of MCS from MCS0 up to MCS10. For instance, the MCSO mode combines the BPSK modulation and the coding rate 1/2. The MCS is transmitted in the signal field of frame and used by the receiver to decode properly the received data symbols. Also, it determines how many data bits are contained into an OFDM symbol, denoted by N_{DBPS}. This parameter is used in the padding sub-block in orden to calculate the number of padding bits that are necessary. Table 2.4 shows the MCS modes that the 802.11bd draft defines as well as other parameters that are dependent on MCS. Given that 802.11bd supports two options of bandwidth, the (a_0, a_1) pair shown in the table corresponds to the obtained values when the used bandwidth is 10 and 20 MHz, respectively.

Table 2.4: Transmission parameters and data rates R_b supported by 802.11bd [7] using a SISO systems.

MCS mode	**Modulation**	R_c	N_{CBPC}	N_{SD}	N_{DBPS}	R_b**(Mb/s)**
0	BPSK	1/2	1	(52,108)	(26,54)	(3.3,6.8)
1	QPSK	1/2	2	(52,108)	(52,108)	(6.5,13.5)
2	QPSK	3/4	2	(52,108)	(78,162)	(9.8,20.3)
3	16QAM	1/2	4	(52,108)	(104,216)	(13.0,27.0)
4	16QAM	3/4	4	(52,108)	(156,324)	(19.5,40.5)
5	64QAM	2/3	6	(52,108)	(208,432)	(26.0,54.0)
6	64QAM	3/4	6	(52,108)	(234,486)	(29.3,60.8)
7	64QAM	5/6	6	(52,108)	(260,540)	(32.5,67.5)
8	256QAM	3/4	8	(52,108)	(312,648)	(39.0,81.0)
9*	256QAM	5/6	8	(-,108)	(-,720)	(-,90.0)
10	BPSK-DCM	1/2	1	(52,108)	(13,27)	(1.6,3.4)

* mode used only for 20 MHz bandwidth;N_{DBPS} = data bit per OFDM symbol;N_{SD}= number of data sub-carriers; N_{CBPC}= coded bit per sub-carrier

The table shows that 802.11bd includes a new modulation scheme compared to 802.11p, 256QAM modulation. This modulation combined with a $R_c = 5/6$ in MCS9 mode allows to obtain the higher data rate equal to 90 Mbps. The parameters shown in table 2.4 are defined for a Single-Input Single-Output (SISO) system, hence a single transmitting antenna is used. The reader can check [39] in orden to see how these parameters can vary if two transmitting antennas are used in a 2×2 Multiple-Input Multiple-Output (MIMO) system.

Furthermore, the MCS10 mode introduces another relevant feature of 802.11bd, the DCM. DCM was initially introduced in 802.11ax to extend the transmission range. It modulates the same information (one complex symbol) in a pair of data carriers within the same OFDM symbol. Both data carriers are typically separated far apart in frequency, allowing to get a diversity gain. DCM is an appropriate solution to deal with narrowband interference, which is very common in wireless channels. In addition, DCM can significantly improve the packet error rate and increase the transmission range. In [45], the performance of DCM was reported for 802.11ax, showing that a gain of 2 dB is obtained when DCM is applied to LDPC-coded transmissions.

Different mapping schemes have been reported in the literature for DCM modulation, showing its potential to combat phase noise and narrowband interference[45],[46]. In [7], TGbd proposes mapping the complex symbols $a_{p,k}$ using the next expression:

$$a_{p,k'+N_{\mathrm{D}}} = a_{p,k'} \cdot e^{j\cdot(k'+N_D)\cdot\pi} \qquad k' \in [1, N_{\mathrm{D}}], f \quad (8)$$

being $N_{\mathrm{D}} = N_{\mathrm{SD}}/2$ the half of total data carriers. Equation (8) means that symbols modulated in the second frequency segment $a_{p,k'+N_{\mathrm{D}}}$ carry a rotated version of the symbols modulated in the first frequency segment $a_{p,k'}$. Using this approach, each data OFDM symbol is transmitted in two OFDM symbols, which include both redundant and data symbols. Also, it is implemented on the OFDM block in Fig. 2.7. On the receiver, the soft demodulated symbols in both frequency segments are coherently combined and weighted by the channel power in the corresponding carriers. This combination obtains a certain diversity gain, but decreases the throughput to a half.

2.3.3.2 Structure of 802.11bd receiver

The design and implementation of a radio receiver is an important part in performance of any communication system where basically are carried out the reverse operations performed on the radio transmitter such as demodulation, decoding, de-scrambler among others. Additional to these tasks, more processing must be done in other to decode properly the complex symbols received. For instance, the received signal must be first detected, synchronized, and equalized.

In this section, we describe the implementation of a 802.11bd receiver which is mainly described by its frame structure shown in Fig. 2.6. Each frame, similar to 802.11p frame, starts with two STS composed by a short pattern that repeats 10 times, and followed by two LTS composed by a longer pattern that repeats 2.5 times. In addition, 802.11bd incorporates new training symbols in its frame: NGV-STS and NGV-LTS. The training symbols are used in essential tasks such as detection, synchronization, antenna selection, channel estimation, automatic gain control, among other.

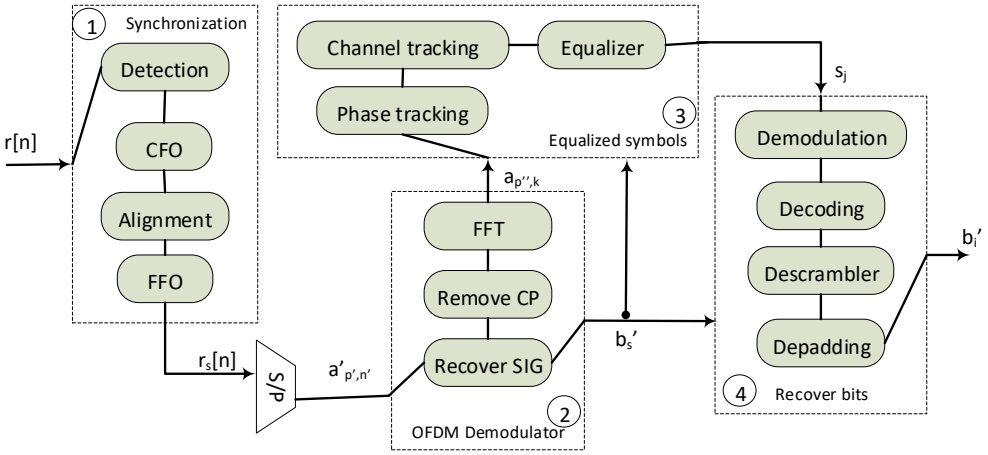

Figure 2.8: Block diagram of an 802.11bd receiver.

The complex received signal $r[n]$, output of multipath channel, can be expressed in terms of the transmitted signal $s[n]$ by

$$r[n] = s[n] * h[n] + w[n], \tag{9}$$

where h represents the CIR and w represents samples of Additive White Gaussian Noise (AWGN). The block diagram of 802.11bd receiver is shown in Fig. 2.8 which has been divided into four processing blocks for convenience. The blocks are numbered from one to four. Firstly, in block one, $r[n]$ is processed in Detection sub-block where the receiver must determine if one frame has been transmitted or not. Next, the detected frame is aligned or synchronized in time domain and frequency offset is estimated and corrected. The frequency offset correction is divided into two parts: Coarse Frequency Offset (CFO) and Fine Frequency Offset (FFO). The tasks carried out in block 1 will be explain in detail in next section.

Next, using a serial-parallel converter (S/P block), the synchronized signal $r_{\mathrm{s}}[n]$ is divided into groups of N_{s} samples where each group represents an OFDM symbol. Then, the groups are clustered into a complex matrix $a'_{p',n'}$, where $p' = 1, ..., N_{\mathrm{OFDM}} - 2$ represents of OFDM symbol index and $n' = 1, ..., N_{\mathrm{s}}$ represents the sample index. At this point, the first two symbols corresponding to STF have been removed. On block two, each OFDM symbol is demodulated by removing the CP and applying the Fast Fourier Transform (FFT) of length N. The first four OFDM symbols correspond to the signal symbols. They must be firstly processed in the Recover_SIG sub-block, to recover the signal bits b'_{s}. The relevant information contain in these bits will be used in the blocks three and four for processing the rest of OFDM symbols.

The demodulated OFDM symbols $a_{p'',k}$ are processed on block 3, where three tasks are performed: phase tracking, channel tracking and equalization. At this point, the first nine symbols of the frame are not included in $a_{p'',k}$, being symbol index $p'' = 1, ..., N_{\mathrm{OFDM}} - 9$. The phase tracking is implemented using the pilot sub-carries in each OFDM symbol. A part of phase offset is common for all sub-carries and it is calculated based on the correlation between pilots sub-carriers of two consecutive OFDM symbols. In other to reverse the channel unwanted effect, the midamble symbols are used to periodically estimate the channel. Then, this estimation is used to equalize the data sub-carriers of an OFDM symbol. Remember that the sub-carriers of an OFDM symbol are clustered into data, pilot and null sub-carriers. More detail about these tasks will be given in next section. Finally on block 4, equalized data symbols s_{j} are processed by the following sequence of sub-blocks: demodulation, decoding, de-scrambler, and depadding. As a result, the transmitted bits are recovered, b'_{i}, which are delivered to the upper layer.

Fig. 2.9 shows a snapshot of the module of $r[n]$ during a T2T approaching maneuver in measurement campaign shown in [6]. In this snapshot, $r[n]$ includes four received frames, using the MCS1 mode (QPSK-1/2) and measured with a software defined radio USRP N201. The used transmission rate was of 0.7 ms. Then, we will use this data to describe how some processing algorithms shown in Fig. 2.8 are implemented.

Frame detection

The detection algorithm was designed based on the correlator structure, as shown in Fig. 2.10. The receiver exploits the periodicity of the short training sequence, by calculating the normalized autocorrelation coefficient $c[n]$ of the received signal. Once

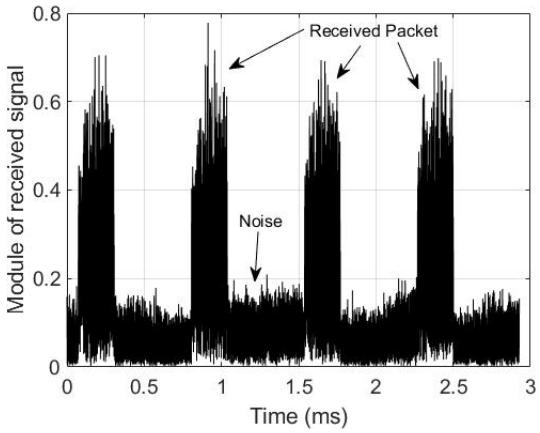

Figure 2.9: Snapshot of the module of the received signal during a T2T approaching maneuver.

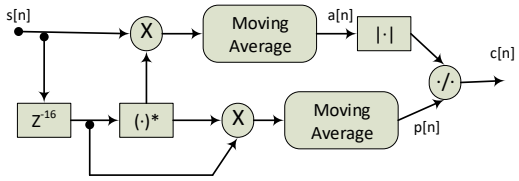

Figure 2.10: The block diagram of signal detection algorithm used.

$c[n]$ exceeds a configurable threshold η, the receiver considers that a frame has been received and the subsequent processing blocks are triggered. For the estimation of $c[n]$, the input signal $s[n]$ is firstly correlated with its delayed version $s[n-16]$. The delay of 16 samples corresponds to the periodicity of the short training sequence. After that, the correlated samples are averaged in the moving average block over a period of time L to suppress AWGN. The result is denoted by $a[n]$ and defined as

$$a[n] = \sum_{k=0}^{L+15} s[n+k]\bar{s}[n+k-16], \tag{10}$$

being $\bar{s}[n]$ the conjugate complex of $s[n]$. The lower branch in Fig. 2.10 was used to calculate the input average power $p[n]$ and to normalize the correlation output as

$$c[n] = \frac{|a[n]|}{p[n]}, \tag{11}$$

being $|\cdot|$ the module function and

$$p[n] = \sum_{k=0}^{L-1} s[n+k-16]\bar{s}[n+k-16]. \tag{12}$$

As a consequence of the normalization process, $c[n]$ is independent from the received power level, and it is not affected by sudden peaks in the input signal. Fig. 2.11 shows the normalized correlation coefficient for the first received frame. In the figure, the duration of the short training sequence can be identified as a plateau since the correlation takes

a maximum value in this time. Please note, a peak around of 847 sample index is too observed and can be used for the detection. This peak is due to NGV_LTS symbols which is correlated with the LTS symbols. Detection algorithm using (11) has been used in [47] to detect the 802.11p signal in a hardware platform USRP N201. Alternative detection algorithms can be found in [48], classified according to their computational complexity.

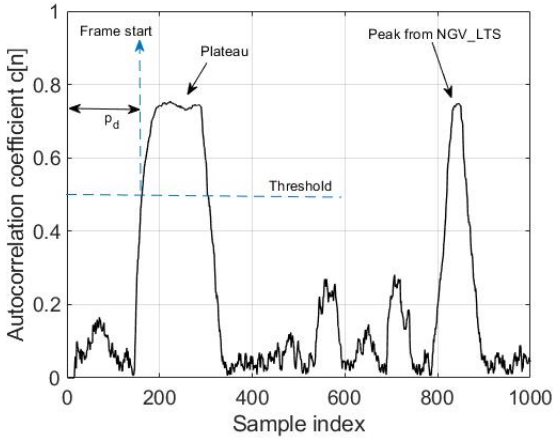

Figure 2.11: Normalized autocorrelation coefficient in the detection task. Only the first 1000 samples of $c[n]$ are shown which contain the relevant information for frame detection.

Frame synchronization

The frame synchronization process is related to the symbol alignment, where the receiver determines with accuracy the first complex sample of the LTS. It is marked as the starting point of a frame, and denoted by p_{s}. This process can be carried out in two steps in orden to decrease the computational complexity of its implementation in real time. Firstly, the frame start is marked in the detection point p_{d} shown in Fig. 2.11. Then, the samples with indexes below p_{d} are considered as noise and are discarded. However, the autocorrelation cannot accurately determine the start of the frame using p_{d}. Then, in a second step, we employ a matched filter to cross-correlate the detection signal $s_{\mathrm{d}}[n]$ with the known pattern of the long training sequence L_{L}.

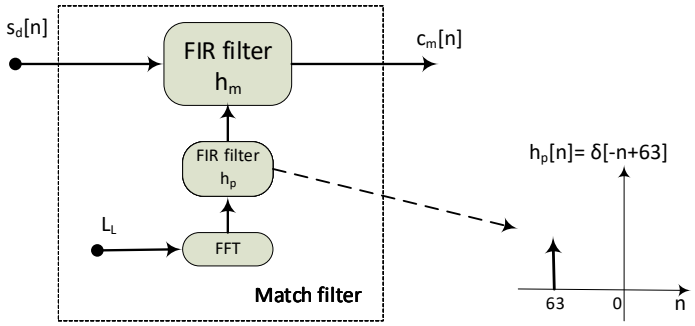

Figure 2.12: Structure of match filter for the cross-correlation.

The coefficients of matched filter h_{m} are calculated using the vertical branch in Fig.

2.12, where the Fourier transform of L_{L} is filtered using an delayed inverter filter with an impulse response $h_{\mathrm{p}}[n'] = \delta[-n' + 63]$. The delay introduced by the filter corresponds to the length of L_{L} minus one. The output of the match filter $c_{\mathrm{m}}[n]$ is determined using the convolution of $s_{\mathrm{d}}[n]$ and $h_{\mathrm{m}}[n]$ as:

$$s_{\mathrm{m}}[n] = \sum_{k=-\infty}^{\infty} s_{\mathrm{d}}[n-k] h_{\mathrm{m}}[k]. \tag{13}$$

Now we need to analyze the module of $c_{\mathrm{m}}[n]$ to find a common pattern that can allow us to determine the frame start with accuracy. For instance, Fig. 2.13 shows the result of matched signal. The spikes in the figure indicate the position where L_{L} pattern matches with the filter input signal $s_{\mathrm{d}}[n]$. Since the peaks are very narrow, this method introduced in [47], allows us to determine the OFDM symbol boundaries accurately. Then, the frame start p_{s} corresponds with the point of the first peak which has less amplitude. Please note, as LTS symbols in the 802.11bd frame are composed by 2.5 times L_{L}, we can see three equidistant peaks where two of them have similar power and the other one has half the power. Exploring the separation between these peaks, it is possible to find efficiently p_{s}. Also, another peak is observed with a sample index close to 800. This peak determine the start point of the NGV_LTS symbol and would be used to align the OFDM symbols too.

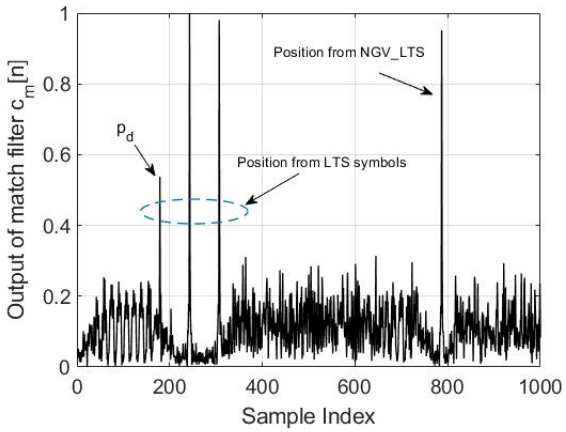

Figure 2.13: Normalized output of the match filter.

Frequency offset correction

In any digital radio receptor, the received signal is down-converted, filtered and sampled which are carried out in Analog Digital Coverter (ADC). This process allows to process the desired signal with a smaller number of samples in the discrete domain. Then, complex baseband signal is processed following the block diagram shown in Fig. 2.8 to recover the information bits. Both carrier frequency f_{c} and sampling frequency f_{s} used in ADC, are generated using a Local Oscillator (LO) which has a frequency offset ε. Due to imperfections in LO, two frequency offset are perceived in the receiver: carrier frequency offset $\varepsilon f_{\mathrm{c}}$ and sampling frequency offset $\varepsilon f_{\mathrm{s}}$. In addition, the frequency offset can be too caused by the mobility of the transmitter and/or receiver, which is known by Doppler effect. In the following, we refer to frequency offset by ε.

The frequency offset causes an undesirable phase rotation to OFDM carriers and creates ICI. This effect is observed in the received constellation, as shown in Fig. 2.14a. In the figure, the black points represent the received symbols in the constellation with a frequency offset. Then, it is not possible to identify the transmitted constellation and the received symbols would be decoded with errors.

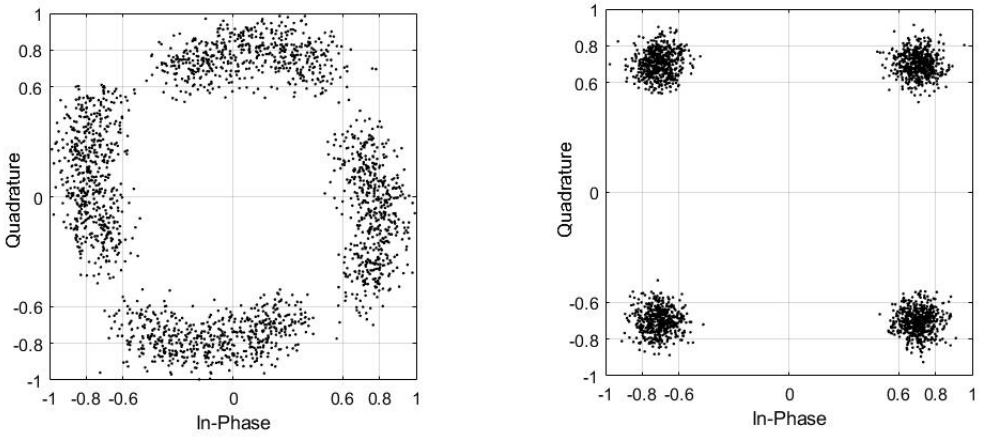

(a) With frequency offset (b) With frequency offset correction

Figure 2.14: Output of quadrature-phase modulator which represents the constellation used in received signal s[n].

Fig. 2.14b shows the constellation of received symbols after the frequency offset is estimated and corrected. Now, the symbols are distributed around the ideal QPSK constellation points ($\pm\frac{\sqrt{2}}{2} \pm \frac{\sqrt{2}}{2}$) due to AWGN noise. The frequency offset ε causes a phase offset α in the received signal $s[n]$ given by

$$\alpha = 2\pi\varepsilon f_{\mathrm{c}} T_{\mathrm{s}}, \tag{14}$$

being $T_{\mathrm{s}} = 1/f_{\mathrm{s}}$ the sampling period. Once α is estimated, it must be corrected by multiplying the received signal by a complex exponential as

$$s[n] = s[n]e^{-jn\alpha}. \tag{15}$$

The phase offset estimation is performed in two steps. The receiver firstly makes an initial estimate of phase offset α_{o} using the training symbols. In a second step, it uses the pilots sub-carriers to continuously estimate residual phase offset which represents phase error that cannot be compensated during the first step. The correction of residual phase offset or phase tracking is very necessary in orden to improve the efficiency of the system [49]. The initial phase estimation is performance in block one in Fig. 2.8 and it is summarised by

(a) The received signal $s[n]$ is detected and the detection point p_{d} is determined.

(b) The coarse phase offset ε_{d} is estimated using STS symbols as

$$\varepsilon_{\mathrm{d}} = \frac{1}{16}\arctan(a[n = p_{\mathrm{d}}]), \tag{16}$$

where the complex auto-correlation coefficient $a[n]$ and p_{d} were defined in Section 2.3.3.2.

(c) ε_{d} is corrected using (15) over the detected signal $s_{\mathrm{d}}[n] = s_{\mathrm{d}}[n]e^{-jn\alpha_{\mathrm{d}}}$.

(d) After compensating ε_{d}, the OFDM symbols are aligned and frame start p_{s} is determined.

(e) The fine phase offset ε_{m} is estimated using LTS as

$$\varepsilon_{\mathrm{m}} = \frac{1}{64}\arctan(c_{\mathrm{m}}[n = p_{\mathrm{s}} - 64] * \bar{c}_{\mathrm{m}}[n = p_{\mathrm{s}} - 128]), \tag{17}$$

where the complex cross-correlation function $c_{\mathrm{m}}[n]$ and p_{s} were defined in Section 2.3.3.2.

(f) ε_{m} is corrected using (15) over the synchronized signal $s_{\mathrm{m}}[n] = s_{\mathrm{m}}[n]e^{-jn\alpha_{\mathrm{m}}}$.

(g) The initial phase offset estimation $\alpha_{\mathrm{o}} = \alpha_{\mathrm{d}} + \alpha_{\mathrm{m}}$ is stored which will be used in the next step (phase tracking).

Please note that α_{d} and α_{m} are estimated and corrected in the CFO and FFO sub-blocks in Fig. 2.8. Now, the phase tracking is performed in orden to remove as much as possible the residual frequency offset. The authors in [50] showed that the signal in frequency domain $S_{\mathrm{p}}[k]$ still contains an ICI component in addition to desired signal and AWGN noise, although α_{d} and α_{m} have been previously compensated. Using the notation $S_{\mathrm{p}}[k]$, m and k represents the OFDM symbol and carrier indexes. The OFDM symbols contain N carriers, N_{p} pilot carriers, and N_{g} samples of cyclic prefix. As was explained before, this ICI component induces an extra phase rotation $\phi_{\mathrm{p}}[k]$ in the received symbol [49] given by

$$\phi_{\mathrm{p}}[k] = 2\pi p\left(\varepsilon_{\mathrm{r}} f_{\mathrm{c}} T_{\mathrm{s}} - \frac{N + N_{\mathrm{g}}}{N}\varepsilon_p k\right). \tag{18}$$

where $\varepsilon_{\mathrm{r}} = \varepsilon_p - \varepsilon_{\mathrm{o}}$ is the residual carrier frequency offset.

The first part in the right hand side of (18) is due to the residual carrier frequency offset not corrected after first step. This term is equal for all sub-carriers of the same OFDM Symbol. The second part is due to the continuous drift in the sampled signal of the OFDM Symbol due to sampling offset [49] which depends linearly on N. These terms are independently corrected in the phase tracking sub-block in Fig. 2.8. The algorithm used to correct these terms, which is applied to each OFDM symbol, can be summarised by

(a) The second term in (18) is compensated by introducing a lineal phase rotation to each carrier in a OFDM symbol as

$$S_p[k] = S_p[k]e^{2\pi jp\frac{N+N_{\mathrm{g}}}{N}\varepsilon_{p-1}k}, \tag{19}$$

being $k = -N/2, ..., N/2$. Please note, ε_{o} is obtained from the initial correction step and, the first OFDM symbol $S_0[k]$ corresponds to the signal field symbol as shown Fig. 2.6.

(b) Now, the pilot carrier are used to compensate the first term in (18) which is the same for all carriers. This phase is denoted by β_p and estimated as

$$\beta_p = \arctan\left(\sum_{i=1}^{N_{\mathrm{p}}} S_p[k = i_{\mathrm{p}}(i)]m_p P[i]\right), \tag{20}$$

where $P[i]$ is the pilot pattern used and, i_{p} is a vector with the indexes of pilot carriers. For instance, 802.11bd uses four pilot carriers in a 10 MHz bandwidth where $P[i] = \{1, -1, 1, 1\}$ and $i_{\mathrm{p}} = \{-24, -8, 8, 22\}$. Also, $m_p \in \{1, -1\}$ removes the polarity of pilot carriers which it is necessary to remove the dc component from spectrum of transmitted signal. The first two terms of the sum in (20), $P_p[i] = S_p[k = i_{\mathrm{p}}(i)]m_p$, represents an estimation of complex channel gain. It will be used in the next step to achieve a finer estimation of the frequency offset estimation ε_p. Also, $P_p[i]$ can be used to estimate the channel frequency response using interpolation techniques, but this approach will be analyzed in chapter III.

(c) Using $P_p[i]$, we can obtain an estimate of the residual phase increase, first term in (18), using the following expression:

$$\varepsilon_{\mathrm{r}} = \frac{1}{2\pi f_{\mathrm{c}} T_{\mathrm{s}}} \arctan\left(\sum_{i=1}^{N_{\mathrm{p}}} P_p[i] P_{p-1}[i]\right). \tag{21}$$

Now, $\varepsilon_p = \varepsilon_{\mathrm{r}} + \varepsilon_o$ and $P_p[i]$ are stored and use with next OFDM symbol in (19) and (21) respectively.

(d) Finally, to remove the phase rotation completely from all received symbols, we correct the residual frequency error as follows:

$$S_p[k] = S_p[k] e^{-j\beta_p} \tag{22}$$

This algorithm is applied to a received frame which has N_{s} OFDM symbols, where the preamble symbols are not included. Also, it removes the phase offset and it is divided in 3 steps as mentioned before: correct sampling offset, correct residual carrier frequency, and finer frequency offset estimation The algorithm also allows a phase tracking continually across all OFDM symbols in the frame. At this point, the $S_p[k]$ symbols are ready for channel equalization and the receiver processing.

2.3.3.3 **Performance indicators**

In order to evaluate the performance of a communication system, it is necessary to use magnitudes or parameters that characterize the quality of the communication link. These parameters are known as metrics or performance indicators, which can be measured or quantified based on field measurements or numerical simulations. The most relevant metrics related to the reliability of a link-level system are presented in this part.

BER is a performance indicator that is defined as the ratio between the number of received wrong bits regarding to the number of transmitted bits. Similar to BER, PER is a performance indicator that indicates the relation between the total number of received and transmitted packets. These metrics are suitable for measuring the performance of a wireless link as long as pseudo-random bit sequences are used. Then, they are frequently used in Monte Carlo simulations to evaluate the performance of communication algorithm. For instance, they were used in [10] where the author presented a link level simulator to evaluate the physical layer of 802.11p protocol.

Root mean square of error vector magnitude (EVM_{rms}) is another metric, which is a measure used to quantify the performance of a digital radio transceiver. This metric is

derived from the transmitted symbol S and received symbol $\hat{S}$ in a transmitted frame, as well as the number of received packets N_R during one Monte Carlo run, as shown the following equation:

$$EVM_{\mathrm{rms}} = \frac{1}{N_{\mathrm{R}}} \cdot \sum_{j=1}^{N_{\mathrm{R}}} \sqrt{\frac{\sum_{i=1}^{N_{\mathrm{S}}} |S_{i,j} - \hat{S}_{i,j}|^2}{\sum_{i=1}^{N_{\mathrm{S}}} |S_{i,j}|^2}} \cdot 100, \quad N_{\mathrm{R}} \in [1, N_{\mathrm{T}}], \tag{23}$$

where N_{S} is the total number of symbols within a frame according to the chosen MCS and payload size. Note that N_{R} is less than or equal to the number of transmitted packets N_{T}, due to the fact that some packets can be discarded in the receiver side. The packets can be discarded because they are not detected or their signal field is decoded with errors.

The average rate of successful packets delivered over a communication channel, named throughput TP and expressed in bit/s, was defined by [51] as

$$TP = (1 - PER) \cdot \frac{N_{\mathrm{b}}}{T_{\mathrm{p}}}, \tag{24}$$

where N_{b} is the number of data bits per packet, $T_{\mathrm{p}} = N_{\mathrm{samp}} T_{\mathrm{s}}$ is the frame duration, T_{s} is sampling period, and N_{samp} is the number of complex samples per packet.

The behaviour of these performance indicators will be shown versus E_{b}/N_0, where E_{b} denotes the energy per bit and N_0 denotes the noise power spectral density. The computed SNR in simulations was computed according to [51] as

$$SNR = \rho \cdot E_{\mathrm{b}}/N_0, \tag{25}$$

being ρ the spectral efficiency which includes the effect of varying the payload size, modulation and coding scheme, and configuration parameters of OFDM modulation. This metric is defined by

$$\rho = \frac{N_{\mathrm{b}} N_{\mathrm{ds}}}{N_{\mathrm{dp}} N_{\mathrm{samp}}}, \tag{26}$$

where N_{ds} indicates the number of data symbols per OFDM symbol, and N_{dp} indicates the number of data bits per OFDM symbol.

2.4 Overview of C-V2X

C-V2X is a recent term introduced for cellular technologies optimized for transportation and connected vehicles. In particular, the C refers to both 4G Long Term Evolution (LTE) and 5G New Radio (5G NR) releases of specification, whereas X refers to multiple things vehicles may connect with. C-V2X supports all types of V2X communications links described in Section 2.1.1 such as V2V, V2I, V2P and V2N. LTE-V2X is the 3GPP nomenclature for direct vehicular communications as specified in Releases 14 and 15, whereas NR-V2X is from Release 16 onward. NR-V2X has been designed to complement LTE-V2X. Then, while LTE-V2X supports basic safety and traffic management applications, NR-V2X supports advanced application with a higher automation level.

C-V2X also introduces additional possibilities for deployment, including public-private-partnerships, which can change the deployment strategy by leveraging roll-out of

mobile infrastructure, as well as leveraging cellular technology integration and economies of scale, instead of building independently operated infrastructure. For instance, railway use cases will be supported by C-V2X to take advantage of existing market opportunities in this scenario. In this section, we briefly introduce the C-V2X technology and we show its main features incorporated from Release 14. The reader can find a detailed description of C-V2X in [52], [53].

2.4.1 C-V2X communication modes

C-V2X uses two complementary transmission modes. The first is direct communications to vehicles, infrastructures, and road pedestrians, which is called Sidelink (SL). In this mode, C-V2X works independently of the cellular networks. It uses a PC5 interface for communication using the 5.9 GHz band. SL is relevant in this thesis because it allows V2V and Vehicle-to-Infrastructure (V2I) communications. The second mode is cellular network communications, in which C-V2X employs the conventional mobile network to enable vehicles to receive information about road and traffic conditions in the area. It uses Uu interface for communication using the licensed spectrum of the 3.5 GHz mobile band. Table 2.5 shows some of the differences between both communication interfaces.

Table 2.5: Main features of transmission modes in C-V2X [54].

Transmission mode	**Sidelink**	**Cellular network**
Radio interface	PC5	Uu
Communication Link	V2V, V2P, V2I	V2N
Link type	Sidelink	Uplink/downlink
Frequency Band (GHz)	5.9	3.5
Traffic	groupcast/broadcast/unicast	unicast/multicast
Type of traffic	IPv6, non-IP	IPv6

Furthermore, the communication in cellular network, outside of SL context, can support two different ways of traffic: unicast and groupcast. Unicast communication allows bidirectional data exchange between a User Equipment (UE) and the Evolved Node B (eNodeB) throught the downlink and uplink. For example, UEs request radio resources to eNodeB and they are in connected mode to avoid initial access delay due to random access. While groupcast communication allows that V2X messages can be efficiently broadcast to a group of multiple UE over downlink via Evolved Multicast Multimedia Broadcast Service (eMBMS) developed by 3GPP. Please note, while eNodeB is a node that manages and integrates all functions of LTE radio access network, UE is related to vehicles, infrastructure equipment, or mobile devices that are carried out by pedestrians.

On the other hand, using SL mode, UEs can use broadcast messages in addition to groupcast/unicast to send a message to all users in its network coverage area. For instance, road safety messages like CAM can be broadcated to all users in the network to prevent accidents. Compared to LTE-V2X which supports only broadcast transmissions in the SL, NR-V2X provides physical layer support for unicast, groupcast, and broadcast transmissions in the SL, which are shown in Fig. 2.15.

Both LTE-V2X and NR-V2X operate on SL and use two resource allocation modes. The resource allocation includes selecting and configuring the communication resources such as sub-channels. In mode 1, the resource allocation is managed by eNodeB in NR-V2X. However, the communication takes places directly between UEs, thus cellular

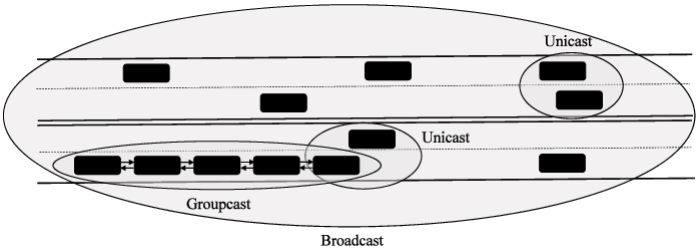

Figure 2.15: Communication types in NR-V2X [52].

coverage of UE is required [55]. In addition in mode 2, the vehicles autonomously select, manage, and configure the sub-channels. In this case, the vehicles can operate with out of network coverage. One of the tasks of Release 17 will be to improve the Sidelink resource allocation strategies.

NR-V2X modes 1 and 2 have the same characteristic as modes 3 and 4 defined for LTE-V2X in [56]. Mode 3 resource scheduling algorithms are not detailed in the 3GPP specifications and each operator can develop its own solution. For this mode, according to [57] a possible option is dynamic scheduling in which vehicles request sub-channels to the eNodeB for each packet transmission. On the other hand, in mode 4, the vehicles do not need to be in the coverage zone of the base station, because vehicles implement a mechanism for autonomous radio resource selection based on sensing before transmission with Semi-Persistent Scheduling (SPS).

2.4.2 **Main features**

LTE mobile technology has evolved rapidly to meet the needs of V2X communications. This evolution has been carried out by 3GPP and began with the introduction of direct D2D communications for proximity services (ProSe), using cellular technologies in Release 12. This approach allows that mobile devices can communicate directly without the help of the infrastructure, similar to how it is done in an AdHoc networks. Thus, the capacity and coverage range of cellular networks can be increased providing service to mobile users close to or outside the cell coverage limit.

Using the D2D approach, the first C-V2X standard based on 4G LTE air interface was developed by 3GPP below Release 14 (in short Rel. 14), called LTE-V2X. It allows the SL communication in the 5.9 GHz band given support to basic safety applications. After that, LTE-V2X was improved in Rel.15 to solve some design flaws and added new features like the 64QAM modulation and transmission diversity. Next, below Release 16 (Rel. 16) 3GPP has developed a new C-V2X standard based on 5G NR, called NR-V2X. This standard has been designed to cover a wide range of transmission requirements given support to advanced safety & non-safety applications. Fig. 2.16 shows the timeline in the C-V2X developed process followed by 3GPP, where some interesting features introduced in each release are listed too. Please note, Release 17 has not been published yet, it will improve NR-V2X (Rel. 16) and add new features like Beamforming, UE power saving, multi-slot scheduling, among others.

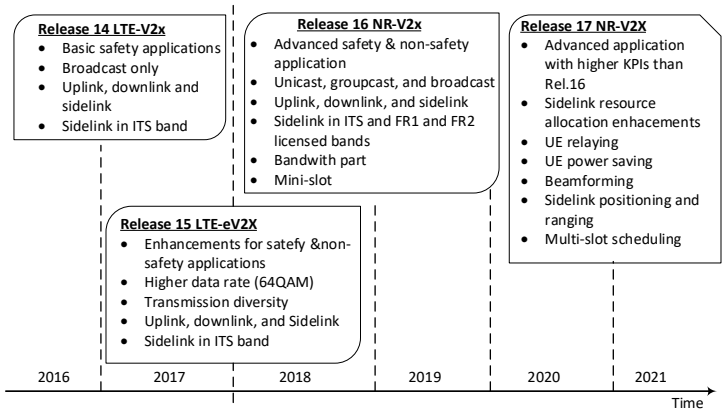

Figure 2.16: Progress of 3GPP work on V2X with a focus on radio access network [53].

2.4.2.1 LTE-V2X

LTE-V2X has been specified in Release 14 by 3GPP, and later improved on Release 15. It operates on the 5.9 GHz band reserved for ITS services where SL communication is carried out using the PC5 interface. LTE-V2X supports similar services as those supported by DSRC or its European counterpart ITS-G5. These services rely on the broadcast transmission of small awareness messages such as CAM in ITS-G5 or BSM in DSRC to regularly provide basic information such as the location, direction, speed, and acceleration of the transmitting vehicle [53].

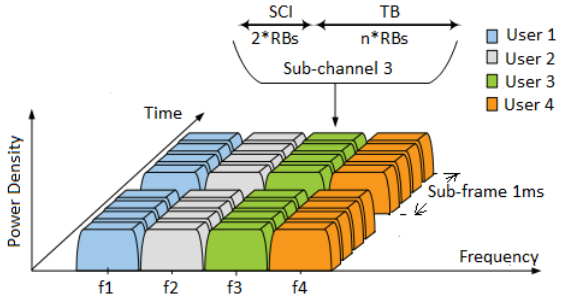

Figure 2.17: Distribution of resource blocks in LTE-V2X using SC-FDMA modulation [58].

LTE-V2X defines a new access layer with respect to 802.11p which is based on Single-Carrier Frequency Division Multiple Access (SC-FDMA) and uses 10 MHz and 20 MHz channels. Fig. 2.17 shows how using SC-FDMA the available bandwidth can be shared by several users in frequency-time domain. SC-FDMA has lower Peak to Average Power Ratio (PAPR) when compared to OFDM while at the same time combining the advantages of multipath interference resilience and flexible sub-carrier frequency allocation provided by OFDM.

The LTE-V2X channelization divides the channel into Resource Blocks (RBs) of 180 KHz that correspond to 12 carriers of 15 KHz each. RBs constitute the smallest spectral unit assigned to the UE by the eNodeB's scheduler or queue manager. This results in a frequency-time grid which consists of all RBs available in the system. Depending on data requirements demanded by the users and the availability of resources, the scheduler can

dynamically allocate one or more RBs to each active user to guarantee this demand.

Furthermore, the RBs associated to a same sub-frame are grouped into sub-channels. Then, the sub-channels are used to transmit data and control information. The data is organized in Transport Blocks (TB) that are carried in the Physical Sidelink Shared Channel (PSSCH) and contain a full packet like CAM or BSM. A TB can occupy one or several sub-channels depending on the size of the packet, the number of TB per sub-channel and MCS used [56]. TB can be transmitted using QPSK, 16QAM or 64QAM modulations and turbo coding. Each TB has an associated Sidelink Control Information (SCI) message that occupies 2 RBs (Fig 2.17) that is carried in the Physical Sidelink Control Channel (PSCCH). The SCI includes critical information for the correct reception of the TB such as the MCS used, priority of the message, number of RBs occupied among other. The SCI message has the same role that the signal field in the 802.11p frame structure.

Physical channel is another term used in 3GPP systems, which corresponds to a set of resource elements carrying information originating from higher layers. The last statement means that the frequency-time resource grid assigned to one user in Fig. 2.17 is divided together physical channels. SL in LTE-V2X defined four physical channel in release 14 [59] which are:

- Physical Sidelink Control Channel: carries control information in the sidelink with resource allocation of the physical sidelink shared channel.
- Physical Sidelink Shared Channel: carries data payload in the sidelink and additional control information. Sidelink transmission is defined as a one-to-many scheme, meaning that the data is to be received by multiple UEs that belong to a group.
- Physical Sidelink Broadcast Channel (PSBCH): carries information for supporting synchronization in the sidelink.
- Physical Sidelink Discovery Channel (PSDCH): it relates to direct discovery services.

The physical channels have been improved from Release 14 onward in order to increased the system performance. Release 16 in LTE-V2X introduced a new physical channel called Physical Sidelink Feedback Channel (PSFCH), which carries feedback related to the successful or failed reception of a sidelink transmission. This information can be used by the transmitter to optimize the transmitted signal through a previous precoding process.

In the time domain, downlink, uplink and sidelink transmissions are organized into radio frames with 10 ms duration. Using frame structure type 1 which applies only to both full duplex and half duplex Frequency Division Duplex (FDD), the frame is divided into 10 subframes with 1 ms duration. Each subframe has 14 OFDM symbols with normal cyclic prefix distributed in two slots of 0.5 ms. Nine of these symbols are used to transmit data and four of them (3rd, 6th, 9th, and 12th) are used to transmit Demodulation Reference Signals (DMRS) for channel estimation and mitigate the Doppler effect at high speeds [53]. The last symbol is used as a guard symbol for timing adjustments and for allowing vehicles to switch between transmission and reception across subframes.

2.4.2.2 **5G NR-V2X**

NR-V2X has been specified in Release 16 by 3GPP [60], and will be improved on Release 17. It reuses some of the concepts of NR-V2X, with the introduction of additional

procedures for providing physical layer suppoort for unicast and groupcast transmissions. NR-V2X is designed to cover a wide range of transmission requirements. It supports V2X applications with varying degrees of complexity, throughput, latency and reliability demands. Hence the NR-V2X physical layer is much more flexible than LTE-V2X and has a higher degree the complexity.

NR-V2X can operate in two frequency bands defined in Release 16, which allows to extend the use of C-V2X towards the millimeter band. The frequency ranges are define as:

- Frequency range (FR1): 410 MHz - 7.125 GHz, this band includes among others the LTE cell phone band and the 5.9 GHz band licensed.
- Frequency range (FR2): 24.25 GHz-52.6 GHz, this band offers a higher allocation of radio resources allowing high data rate and capacity.

Table 2.6: OFDM numerologies supported in NR-V2X [53].

n	SCS (KHz)	Frequency band	Cyclic prefix	Symbols per slot	Slot number per subframe 2^n	Slot duration 2^{-n} (ms)	Maximun carrier bandwidth (MHz)
0	15	FR1	Normal	14	1	1	50
1	30	FR1	Normal	14	2	0.5	100
2	60	FR1,FR2	Normal	14	4	0.25	200
			Extended	12			
3	120	FR2	Normal	14	8	0.125	400
4	240	FR2	Normal	14	16	0.0625	400

The NR-V2X transmission is based on the OFDM modulation with both normal and extended cyclic prefix. Different OFDM numerologies can be obtained with a scalable Subcarrier Spacing (SCS) given by $2^n \times 15$ KHz, being n the SCS configuration factor. While LTE-V2X was defined with $n = 0$, configuration factors for NR-V2X can be $n = 0, 1, 2, 3, 4$ such that the SCS can be equal to 15, 30, 60, 120 or 240 KHz, respectively. Table 2.6 shows the OFDM numerologies supported by NR-V2X. Please note, when SCS is increased by a factor of 2, the slot duration is reduced to half since the OFDM symbols are shorter. Thus, a NR-V2X frame is formed by 10 subframes of 1 ms duration, where the slot number per subframe depends on SCS (Fig. 2.18). In addition, supporting higher SCS improves robustness of the OFDM waveform against frequency impairments caused by Doppler effect and carrier frequency offset.

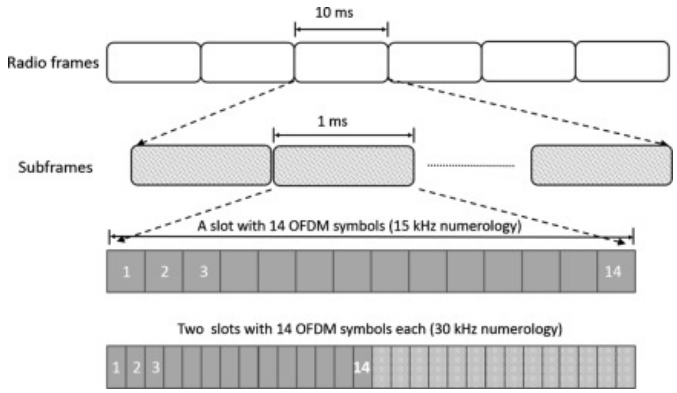

Figure 2.18: NR-V2X frame structure for different OFDM numerologies [61].

In contrast to 802.11bd, NR-V2X used a smaller SCS in the 5.9 GHz band included in FR1, hence it might be more sensitive to Doppler shift. Table 2.6 also shows that for a

60 kHz subcarrier spacing ($n = 2$), both CPs can be used, being 12 the number of OFDM symbols per slot for extended CP, and 14 for normal CP. The extended CP is used in channels with large delay spread and adds an extra protection against multipath effect.

NR-V2X supports QPSK, 16-QAM, 64-QAM, 256 QAM modulation schemes with LDPC codes for user data transfer and polar codes for control data transmission. For error detection, a Cyclic Redundancy Check (CRC) code of 24 parity bits is appended to a TB. Also, the use of DMRS is flexible, which can be transmitted in 2, 3, or 4 symbols at different locations within a slot. This choice improves the channel tracking in environments with high Doppler shift, which are very common in vehicular communications.

Another interesting feature of NR-V2X is the use of Bandwidth Part (BWP) concept which was inherited from LTE-V2X (Release 15). Using this approach, the UEs can use a contiguous portion of bandwidth within the carrier bandwidth where a single numerology is employed. Please note, the maximum carrier bandwidth is 200 MHz for FR1 and 400 MHz for FR2, as shown in Table 2.6. Hence, some UEs might not be able to handle large bandwidth since this requires higher power consumption, which is a limited resource in the UE. Then, defining a small BWP, the computational complexity and power consumption of a UE can be reduced. Thus, BWP enables a more flexible and efficient use of the radio resources.

2.4.3 **Use cases**

3GPP is a collaboration of groups of telecommunications associations, whose objective is to organize, manage and develop the standards of mobile communications. 3GPP has released the technical specifications for the support of V2X communications in 3GPP systems, by means of documents TS-22.185 [62] and TS-22.186 [40] , in its Releases 14 and 15, respectively . These documents establish the application types and services of V2X communications, as well as the technical requirements of the different communication scenarios to support V2X communications carried out under LTE. Then, the following use cases and scenarios have been defined in [62] as:

- Platooning
- Advanced driving
- Extended sensors
- Remote driving

Platooning enables the vehicles to dynamically form a group travelling together. All the vehicles in the platoon receive periodic data from the leading vehicle, in order to carry on platoon operations. In this way, it is possible to increase the safety and efficiency of the trip, to reduce the distance between the vehicles and the autonomous driving of the same. Advanced Driving enables semi-automated or fully-automated driving. Longer inter-vehicle distance is assumed. Each vehicle and/or RSU shares data obtained from its local sensors with vehicles in proximity, thus allowing vehicles to coordinate their trajectories or maneuvers. In addition, each vehicle shares its driving intention with vehicles in proximity. The benefits of this use case group are safer traveling, collision avoidance, and improved traffic efficiency.

Extended sensors allow the exchange of processed data or not with other V2X entities, collected through local sensors or video cameras. In this way, vehicles can improve the perception of their own environment beyond what they can detect and have a more holistic view of their local situation. And finally, autonomous driving allows a driver or a V2X application to operate a remote vehicle. In our project this type of service will be not of interest, it will be not analyzed in the document.

Table 2.7: Requirement ranges for the 3GPP uses case [40].

Use case	Payload (Bytes)	Tx rate (message/sec)	Reliability (%)	Data rate (Mbps)	Maximun Latency (ms)	Required range (m)
Vehicles platooning	50-6000	2-50	90-99.99	<= 65	10-25	80-350
Advanced driving	SL:300-1200 UL:450	SL:10-100 UL:50	90-99.999	SL:10-50 UL:0.25-10 DL:50	10-100	360-700
Extended sensors	1600	10	90-99.999	10-1000	3-100	50-1000
Remote driving	16000-41700	33-200	90-99.999	UL:25 DL:1	5	1000+

Table 2.7 summarizes the range of required values for the previous use cases as identified by 3GPP in [40]. Each range is defined by the minimum and maximum requirements based on [40]. Use cases typically do not need to meet all of the most stringent requirements simultaneously. For example, platooning might require relatively low latency and high reliability, but the required data rate is moderate (exchange of maneuver information among the platoon members). We note that higher degrees of automation generally lead to more stringent requirements

2.5 Comparison between 802.11p/bd and C-V2X

The use of V2X communication in ITS has been essential to achieve much safer and efficient transportation systems. Table 2.8 shows some of mean features of the present V2X technologies. Although 802.11p and LTE-V2X were already standardized and there are commercial devices in the market using these standards, 802.11bd and NR-V2X are in the process of standardization yet.

Table 2.8: Comparison between V2X communication technologies.

Feature	802.11p	802.11bd	LTE-V2X	5G NR-V2X
Frequency Band (GHz)	5.9	5.9/60	5.9	5.9/0.41-7.125/24.25-52.6
Bandwidth (MHz)	10	10/20	1.4/5/10/20	100/400 *
Waveform	OFDM	OFDM	SCFDMA	OFDM/DFT-OFDM
Carrier spacing (KHz)	156.25	156.25	15	15/30/60/60*/120*
Modulations	BPSK/QPSK/16QAM 64QAM	BPSK/QPSK/16QAM 64QAM/256QAM	QPSK/16QAM 64QAM	QPSK/16QAM/64QAM
Coding	BCC	LDPC	Turbo	LDPC
Number of MCS	8	10	>20	>20
Spatial streams	one	two	two	two
Re-transmission	none	Congestion dependent	Blind	HARQ
Channel estimation	Preamble	Preamble and midamble	DMRS4/sub-frame	DMRS: flexible
Traffic	Broadcast	Broadcast/groupcast/unicast	Broadcast	Broadcast/groupcast/unicast
Compatibility with	802.11bd	802.11p	—	—
Multiplexing	TDM	TDM	FDM	TDM
Available for railway	no	yes	no	yes

LTE-V2X is more advanced considering physical layer aspects. It uses Turbo codes with different bandwidth options, up to two spatial streams (2×2 MIMO), and DMRS symbols for channel tracking. Please note, 802.11p uses convolutional codes with single bandwidth, single spatial streams (SISO), and channel tracking is not enabled. The channel is estimated in 802.11p using the training symbols only in the frame beginning, and it is held during whole frame. However, the small sub-carrier spacing of 15 kHz in LTE-V2X, carried on from the cellular bands (typically in the 2 or 3 GHz region), is not suited to

the 5.9 GHz band [63]. This results in LTE-V2X might be more sensitive to frequency offsets than 802.11p whose sub-carrier spacing is 156.25 KHz.

The performance of 802.11p based on field measurements and numerical simulations has been widely reported in the literature [47],[8],[64], whereas LTE-V2X has neither been deployed nor sufficiently tested [65],[63]. It may take years until it can be deployed to the same extent as 802.11p, which is already up and working [66]. Both protocols were originally designed to support a basic set of vehicular applications which issue driver alerts to indicate potentially dangerous situations. These applications require an *end-to-end* latency of around 100 ms and the transmission of periodic messages. However, they do not achieve the quality of service demanded by advanced applications, and fail to provide consistent high data rate transmissions [52],[30]. Advanced applications require latencies of less than 10 ms and reliability (in term of PER) of 99.999 % in some use cases as was shown in Section 2.4.3. They are thus much more stringent than those of basic safety applications. Nevertheless, the next generation communication solutions, NR-V2X and 802.11bd will enable more advanced applications in fully automated vehicles, such as cooperative maneuver execution.

In addition, the comparison in [64] shows that LTE-V2X has superior performance in terms of data rates and reliability, whereas 802.11p is better in terms of transmission latency. Also the author in [67] shows a system level comparison of the performance of 802.11p and LTE-V2X. The results show that LTE-V2X can achieve better performance than 802.11p under low channel loads as it has a better physical layer performance. However, the results also show that 802.11p generally outperforms LTE-V2X when transmitting aperiodic messages of variable size, except when the channel load is very low. In contrast, the author in [63] concludes that LTE-V2X (Rel. 14) is a significant step back in performance compared to 802.11p, and maturity and testing level of LTE-V2X are still very low. This conclusion was obtained based on an analysis made for LTE-V2X regarding its range, readiness, and compatibility.

After reviewing the literature, we have seen that there is a great debate about which physical layer technology is used in the vehicular access network: 802.11p or LTE-V2X. In addition to this, there is a group of stakeholders that suggest a hybrid communication approach in which both technologies work together:

- 802.11p delivering safety messages in the 5.9 GHz spectrum allocated to V2X applications.
- LTE-V2X providing V2I information for more infrastructure related services like traffic management information in the 3.2-3.8 GHz spectrum allocated to cellular.

On the other hand, 802.11bd and LTE-V2X are advanced technologies with a greater degree of flexibility and performance in comparison to their predecessors, with multiple configuration options. For instance, the authors in [68] show the better performance and higher flexibility of NR-V2X over LTE-V2X based on simulations where both physical and MAC layers are tested. Remember that, while 802.11bd evolves from 802.11p which guarantees compatibility between them, LTE-V2X and NR-V2X are complementary technologies which are not compatible. Both are based on OFDM with multiples numerologies, LDPC codes, multiple spatial streams, and different message types (unicast, groupcast, and broadcast), being multiband technologies that operate in both the 5.9 GHz band and in the millimeter band.

In the literature, there is little evidence of the NR-V2X and 802.11bd performance since their standardization processes are not over yet. However, it can be expected that NR-V2X is superior than 802.11bd in terms of transmission latency and data rates. These results were obtained based on theoretical calculations by [30]. Also, comparisons based on the simulation results show that considering the same modulation and code rate, 802.11bd performs better than NR-V2X in terms of PER. Although these results are not conclusive, they indicate that an exhaustive evaluation of both technologies should be carried out based on simulations and field measurements. Thus, an optimal communication solution could be chosen to support all critical and no-critical applications. These solutions could be hybrid (802.11p/bd and LTE-V2X/NR-V2X) or standalone (802.11p/bd or LTE-V2X/NR-V2X).

2.6 Summary and conclusions

Vehicular networks provide an opportunity for the development of applications that improve traffic and transportation conditions through the use of collaborative systems based on V2X communications. In this chapter, we have introduced VANET, highlighting its main features and applications. Two communication approaches have been standardized depending on geographic deployment area: WAVE at US and ITS-G5 at Europe. Both standards use the 802.11p protocol in their access layers. 802.11p is based on OFDM, uses 10 MHz bandwidth, achieves date rate up to 27 Mbps, and was designed to support basic safety applications.

Nowadays, the ETSI standardization body is working in the next evolution of 802.11p since this protocol begins to be obsolete compared to the requirements demanded by new advanced applications. These applications demand high date rate, asymmetric and symmetric messages, variable length messages, among others. Thus, 802.11bd will be the most advanced wireless solution by IEEE for vehicular communications which comes from 802.11p. The structure of an 802.11bd transceiver has been explained using a block diagram for the transmitter and receiver. Furthermore, the synchronization process of 802.11bd received signal is shown in a realistic setting.

Similar to ETSI, 3GPP has been working in cellular solutions to support V2X applications from Release 14. Being LTE-V2X and NR-V2X, the protocols standardized by 3GPP which complement each other but they are not compatible. Their main features have been listed; they are based on OFDM, use DMRS symbols for channel tracking, and support high data rates. While LTE-V2X is adrressed to support basic safety application, NR-V2X supports advanced applications. 3GPP has defined the requirements of four advanced application: platooning, advanced driving, extended sensors and remote driving.

After introducing the vehicular communication technologies, a comparison between them is shown with a focus in physical layer. The results show that LTE-V2X has a more advanced physical layer than 802.11p, which uses polar codes and training symbols to channel tracking. In addition, 802.11bd and NR-V2X are advanced technologies with a greater degree of flexibility and performance in comparison to their predecessors, with multiple configuration options. Thus, both technologies are ready to support the requirements demanded by current vehicular applications and use cases. It is important to point out that both 802.11bd and NR-V2X have been designed to support railway use cases. Thus, railway transport could progressively incorporate the potential and proven advantages of V2X vehicular communications into railway.

3

Railway communication technologies

In recent years the railway community has proposed and pushed the increasing use of communication technologies to support critical and non critical applications, and thus allowing the safe operation of trains as well as increasing user comfort. In this chapter, we firstly introduce some basic terms and topics in railway communication such as communication scenarios, use cases, and railway services. Next, the main rail signalling systems are described and the train virtual coupling concept is introduced. Finally, the communication technologies used in railway are presented highlighting their main features. They do not follow any harmonized specification and are based on a set of requirements.

3.1 Introduction

The development of trade, industry and commerce of a country largely depends on the development of railways. Railway is one of the safest form of transport, with lower emission of carbon dioxide CO_2. The chances of accidents and breakdown of railways are minimum as compared to other modes of transport. Also, it allows both passengers and freight transport. The carrying capacity of the railways is extremely large, being elastic its capacity which can easily be increased by adding more wagons [69]. In addition, railway facilitates long distance travel and transport of bulky goods which are not easily transported through motor vehicles.

In contrast, railway transport cannot provide door to door service as it is tied to a particular track. This means that the freight can only be transported as far as the end of the track and cannot reach specific warehouses or production centers. Thus, it would be necessary to use another transport mode to transfer the cargo to the storage site or the place of operations. As result, the railway transport is considered as a multi-mode systems in general. Intermediate loading or unloading involves greater cost, more wear and tear and waste of time. The time cost of terminal operations are a great disadvantage of rail transport.

For more than 50 years, railway has been subjected to competition from road and air transport. While road transport has been taking over the short and medium distance traffic, the other one has taken a long distance traffic. However, the development of these successful modes has carried out congestion problems on highways and at airports, which

have led to the reemergence of the railway as an interesting alternative. Obviously, the railway cannot support all types of traffic, but it has to specialize in those for which its characteristics are suitable. For instance, long-distance inter-urban transport is a scenario where railway can compete with air transport.

If railway has to compete with other modes of transport, it will need the highest technology available in the fields of power electronics, industrial engineering, process engineering, information systems, and telecommunications. Following this approach, common policies have been outlined by European Union (EU) to all its member countries for the development of the railways and their integration with other modes of transport [70]. These policies have allowed the creation of a single European railway area (interoperability) as well as the increase of railway lines. Thus, the popularity gap with respect to other modes of transport has decreased progressively. In next sections, we address some topics in railway telecommunication field, showing how railway communication has been essential to improve the train safety, operation and efficiency.

3.1.1 Evolution of railway communication

The telecommunication system associated with railway infrastructure is a strategic element not only for train safety, but also for the efficiency and capacity of entire transport system. This statement is due to the characteristics of the railway environment, which implies several complex factors to establish a wireless communication. For instance, catenaries and metal objects on the track as well as metallic structure of the train cause important losses on the transmission signal. As a general rule, the tendency has been to use proprietary technologies specifically dedicated to railway applications, since the extremely high reliability required was not achievable by any of the products available on the market. It should be noted that telecommunications in a railway system are strictly linked to a signaling system, which is a set of technologies and systems that enable the safe movement of the train. Also, signaling system makes possible to maximize efficiency by increasing the capacity and regularity of the line.

The first communication system used to assist railway signaling was the telegraph and it began in the United Kingdom. The first telegraph installed in Spain was used on the railway line between Madrid and Aranjuez in 1851. Telegraphy was essential to establish communication between train stations to know the status and occupation of the track between them. The first electronic telegraph system was the Breguet telegraph, which was later replaced by the Morse telegraph. It used Morse code to transmit symbols, which were automatically written on paper at the receiver [71]. Optionally they could be decoded acoustically by an operator. The Morse telegraph significantly increased the speed of message transmission compared to its predecessor. For both types of telegraphs, the physical medium used for the transmission of the electrical signal was the railway line.

At the ending of the 19th century, the telephone was invented by Alexander Graham Bell making voice transmissions possible which marked a milestone in telecommunications. After that, voice calls were progressively incorporated into railway signaling and control equipment. Although it was only possible to establish calls between consecutive railway stations. From 1922, a two-wire circuit was deployed along the entire railway line connecting the main stations, so that direct connections could be established between them. The electric current flowing in the wires induces a magnetic field which allows the continuous transmission of information detected by a magnetic antenna on board the

train [72]. This type of communication was mainly used for messages related to railway management (dispatching operation), but not for safety.

In addition to safety and management related communication systems, other schemes were deployed for maintenance tasks, logistics management and others. In the mid-1950s the classic telegraph was replaced by the teleprinter, which used a wireless link between stations. Other communication systems were also introduced such as telephones and portable radio stations, which made it possible for the train operator or maintenance team to contact the maintenance section or a railway station.

Starting in 1967 with the electrification of the railroads, the obsolete communication lines began to be modernized. About 2000 km of cables were installed in order to avoid electromagnetic interference generated by catenaries, and to increase robustness. Several improvements in communication technology were introduced, such as the introduction of fiber optic cable, fax, automatic teleprinter, and the most important of all, the introduction of T2I that established a permanent communication channel between the train driver and the operator on the ground.

The first analog communication system between train and operators on ground was developed according to the UIC-751-3 specification and implemented in 1982. This system allowed voice calls and short teleprinter messages [73]. Also, it was the predecessor of GSM-R, which is still widely used today. In 1987, the Train-to-Ground communication system was available along 3500 km of the railway line and the required devices were installed on all locomotives, while the coverage was extended to 6000 km along the track in 1997 [71].

This T2I system provided a continuous connection between the driver and the ground controllers, which allowed emergency alarms, selective telephone calls and low bit rate data transmission. The network architecture was composed of fixed ground sites as well as a central control center. Communication was established between the train driver and the nearest ground site, while a second cable connection was available between the central controller and the ground site.

The first Spanish high-speed train line was inaugurated between Madrid and Seville on April 1992. It allowed speeds of up to 300 km/h and was designed to be centrally controlled from a single control center. At this time, each country had its own high-speed signaling system; for example, Spain used the ASFA system and France the Crocodile system. From this time onwards, strict requirements were established for the availability, robustness and redundancy of the communication systems.

The proprietary wireless communications systems used for the T2I link were progressively migrated to GSM-R, a version of Global Systems for Mobile Communication (GSM) specially adapted for railway. It was used for both management communications and signaling. This fact was really important since GSM-R was presented as the first wireless communication system used for the transmission of safety information. On the other hand, GSM-R constitutes the current communication platform of European Rail Traffic Management System (ERTMS), which allowed unifying the different existing signaling systems in different countries. As a result, the ERTMS signaling system increases the capacity and efficiency of the railway system. The standardization and migration process of both systems began in 1993 and finished in 2003. They were installed on main and high-speed lines.

To increase capacity and safety on railroad, the approach of T2T communication was presented in 1998 by researchers. This approach allows direct communication between

drivers on adjacent trains in addition to T2I link [74]. In this way, time-critical events could be efficiently addressed. This philosophy did not gain much acceptance in its early days mainly due to technological reasons. However, currently it is an active research topic in both the scientific community and the industry, due to its tangible benefits for railway. Also, there is no standardized technology to support T2T communications in the railway infrastructure, although some proprietary solutions have been implemented.

GSM-R was designed to support the rail critical services such as voice and signalling. As a result, it is incapable of supporting non-critical services which are based on packet transmission. Then, parallel to the use of GSM-R other T2I networks are used to support non-critical services such as CCTV, traveler information, telemaintenance, etc. The first implementations of these technologies are based on IEEE 802.11 standards in the early years of the 21st century. In reality, they are much more prevalent in metropolitan operations, where the huge volumes of travelers make security scanners at access points impossible to implement. The current trend in rail radio communications is towards convergence to only one technology. In this way, radiotelephony, signaling and non-critical services would be provided from a single universal radio, with consequent cost savings.

3.1.2 **Railway environment**

The railway environment is characterized by several complex factors that difficult the implementation of a wireless communication. For instance, the radio propagation channel characteristics depend on the type of geographic environment encountered. Railway environment is characterized by specific scenarios, such as tunnels, cuttings, hilly terrain or railway stations. These scenarios have different propagation condition where the LoS component of the signal exists in the majority of them. Also, the high speed of train could lead to problems that are not encountered in road context [72]. Thus, channel parameters could change fast and cause a degradation in the communication link. Some of these complex factors are summarized below:

- Several propagation scenarios with different channel parameters, for instance tunnels, cuttings, hilly terrain, viaduct, railway stations among others.
- Trains can drive to speed higher than 250 km/h, increasing the channel variability with Doppler frequency higher than 2 KHz in the high speed context.
- The metallic structure of the train behaves as a Faraday cage causing important losses on transmission signals.
- High vibration and high interferences which can lead to a need of isolation of communication devices.
- High density of obstacles and metal objects such as catenary, noise barrier signalling system, roof, buildings, cross bridge and others. Being the railway environment a scenario rich in multipath.
- Cohabitation between high power and low power systems, which induces strong magnetic fields that can cause inferences.

These factors must be taken in account in the design of any railway communication system. In the context of high speed and main lines, there are multiples special scenarios

or environments with a marked difference in terms of propagation conditions. These railway scenarios differ greatly from the road communication scenarios, since catenaries, metal structures, sources of interference, and other moving trains are frequent. Fig. 3.1 shown some of these special scenarios which can be classified as

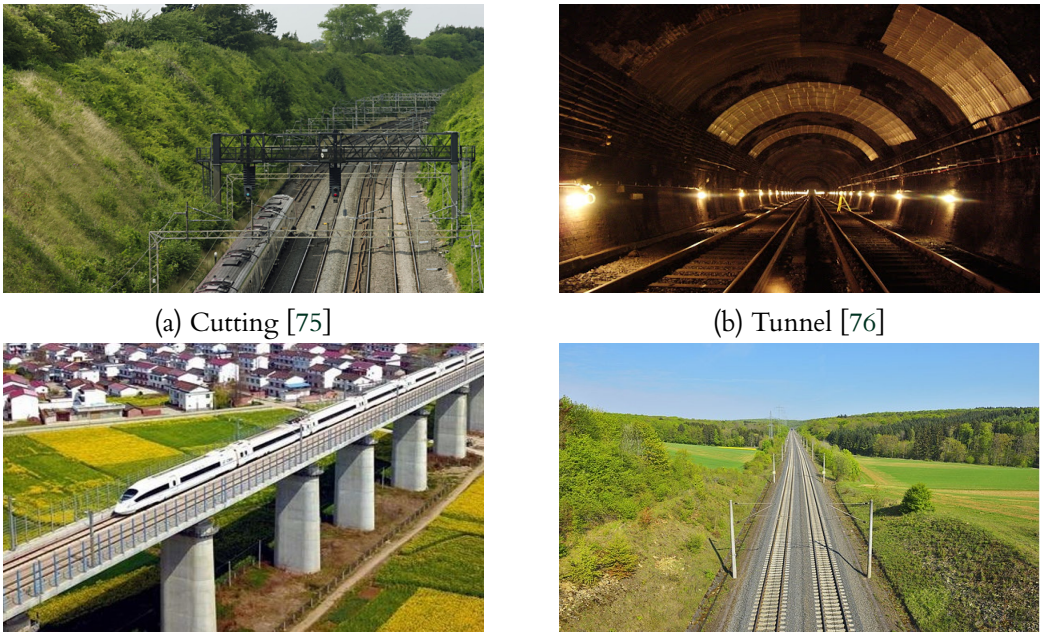

(a) Cutting [75] (b) Tunnel [76]

(c) Viaduct [77] (d) Open field [78]

Figure 3.1: Special scenario in Railway communication.

- Cutting: It is a typical environment in which a train moves between small hills, usually with similar heights and slopes. The hills are made by man with concrete and stone with some vegetation on its surface, as seen in Fig. 3.1a. Although the LoS component is still observed, it is not as dominant as in the open field scenarios [71]. The statistical propagation condition of a cutting scenario was analyzed in [79] where the small-scale fading characteristics such as delay spread and Doppler spread are shown. The cutting sometimes includes bridges spanned across cutting that allows for vehicles and pedestrian crossing. The crossing bridge leads to a Non Line of Sight (NLoS) propagation within short periods of time, which increases the path loss.

- Tunnels: It is an artificial closed environment and widely used in railways. The length of tunnel mostly ranges from several to dozens of kilometers. Due to the smooth walls and the close structure of tunnel (Fig. 3.1b), there are rich reflection and scattering components inside tunnel, where wave guide effect dominates radio propagation [80]. In addition, leaky coaxial cable is widely used for wireless coverage in tunnels where they are uniformly distributed. Furthermore, [81] shows that the radio channel characteristics in subway tunnels are highly dependent on the tunnel size, cross-section shape, distance of transmitter and receiver as well as their location. The waveguide effect was checked in [82] in high speed context where the performance of ITS-G5 was evaluated. In addition, the results reveal that additional losses in the receiver, located inside the tunnel, can be seen if the transmitter is located outside. This finding is caused by the diffraction effects.

- Viaducts: A viaduct is a long bridge across uneven ground in rural or urban areas with a series of piers, as seen in Fig. 3.1c. These are frequently used in typical railway line. For instance, they cover almost 70% of the Beijing–Shanghai high speed line in China. In a viaduct scenarios the LoS component is dominant and the scatters have a minor impact on the receiver. However, the author in [83] showed that the viaduct height, together with the number of surrounding scatterers, significantly affects the small and large scale channel parameters.

- Open Field: This scenario is shown in Fig. 3.1d and it is very common in high speed environment. In the Train-to-Ground (T2G) communication context, this environment focuses on large and continuous coverage where antenna in infrastructure is much higher than the surroundings. As a result, the LoS component is normally dominant. However, the impact of the scatterers will be noticed at the receiver after a certain distance. It is called breakpoint distance. Then, NLoS components can be seen in CIR. The author in [84] concludes that the breakpoint distance is mainly determined by the antenna height, while slightly affected by environments.

- Hilly Terrain: It is characterized by dense scatterers throughout the environment with objects distributed irregularly and non uniformly. The LoS path can be observable along the entire railway line because there are no larger obstacles. This scenario is analyzed in [85] where the relationship between the delay spreads and the transceiver distances is shown and a TDL model is proposed based on a measurement campaign at 2.4 GHz.

- Railway station: Railway station generally consists of a platform close to rail track and a depot providing related services. This scenario is composed by metallic carriages, signaling systems, overhead line masts, building, metallic structures among other. As a consequence of that, it usually result in complex multipath structure and rich reflection and scattering components. In [86], the author shows how the railway infrastructure influences in stochastic channel parameters in the T2T context. For instant, the average k-factor can decrease from 9 to 5.6 if the railway station has roof or not.

3.1.3 Types of Services

The value-added features that the communication technologies (telecommunications) have provided to the railway fall into three types of services or applications [87]:

- Critical services: These services are directly related to the train operation, safety and efficiency, being responsible for its safe movement. Examples of these are: signalling systems like ERTMS, collision avoidance systems, virtual coupling futuristic application (discussed in further detail in the next section), Train Control and Monitoring System (TCMS) and some types of emergency voice calls, among others. Without these applications, the train cannot operate or it operates in a degraded mode with a reduction of its efficiency and/or safety.

- Non-critical services: These services improve the internal operation of the railway company, but they are not in direct relation to the train operation nor have direct impact on its safety and efficiency. Examples of these applications can be video

surveillance systems for safety purposes, tele-maintenance, remote software updates, and passenger broadcast systems.

- Information and entertainment services: These are non-critical services specifically addressed to train passengers, such as Internet access, video transmission like TV and news, among others.

Currently, the GSM-R network is almost exclusively used to provide critical applications, and less frequently, the network supports non-critical low bit rate applications. This small range of applications cannot be exceeded due to the limited capacity offered by GSM-R, which will be discussed in more detail in the following sections. That is why railway companies often look for alternative solutions to provide non-critical applications. For example, Universal Mobile Telecommunications System (UMTS), Worldwide Interoperability for Microwave (WIMAX), 802.11 and satellite communications are very popular ways of providing non-critical applications. All these alternative communication solutions evidence the current demand for new services and applications, which cannot be fully supported by GSM-R, initially conceived for voice services.

Additionally, the critical and non critical applications can be addressed mainly into four use cases or application areas. A distinctive feature of these is that they use a different communication link. They were defined by TGbd in standardization reports [41] as

- Onboard Train: It includes all TCMS applications whose communication links are carried out inside the train (Inside train communication). For instance, Human to Machine Interface (HMI), Passenger Information System (PIS), Heating Ventilation & Air Conditioning (HVAC) system, system, Closed Circuit Television (CCTV), ligths and doors management systems, among others. Wired communication networks were standardized for supporting onboard railway applications in the end of the 1990s, called Wire Train Network (WTN). Nowadays, these networks have been progressively migrating towards wireless solutions in order to reduce maintenance costs and remove cabling and connectors that suffer from mechanical and environmental stress [88]. Fig. 3.2 shows how some TCMS applications are deployed inside the train.

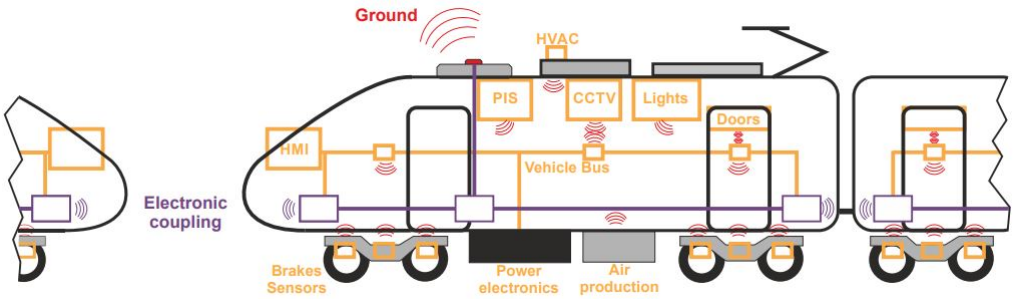

Figure 3.2: Diagram summarizing wireless train communication [16].

- Train-to-Train (T2T): It includes all services which use a direct communication links between trains without the help of any infrastructure equipment (Fig. 3.2), allowing the implementation of novel applications like collision avoidance and virtual or electronic coupling. This topic will be introduced in the next section, and a detailed analysis of T2T wireless channel will be provided in chapter III for two railway scenarios.

- Train-to-Infrastructure (T2I): It includes all services which use a communication link between a train and a infrastructure equipment or ground (Fig. 3.2). It allows the implementation of signaling systems and thus the safe operation of train. The next section introduces the main signaling systems used in railway.
- Vehicle-to-Train (V2T): It includes all services which use a communication link between a train and a vehicle. This use case allows the shared spectrum use of 5.9 GHz ITS band between V2X and urban rail communications. Also, it can be used to shared space in level crossings where both trains and vehicles use the same space.

Similar to IEEE, 3GPP has been working to define the railway communications scenarios and requirements for voice, data and video transmissions. Thus, the rail communication scenarios have been included in the use cases of 5G systems. For instance, Table 3.1 shows the scenarios and Key Performance Indicator (KPI) that 5G systems (Rel. 16) must comply in railway scenarios for main lines. In general, the communication systems must support speeds up to 500 km/h, *end-to-end* latency of 10 ms and data rates of 20 Mbps. The reader can found a more detailed description of these KPIs in [89].

Table 3.1: Performance requirements for rail scenarios in main line [89].

Scenario	Latency (ms)	Reliability (%)	Speed limit (Km/h)	Data rate (Mbps)	Payload
Voice Communication	≤ 100	99.9	≤ 500	0.1-0.3	Small
Critical video Communication	≤ 100	99.9	≤ 500	10	Medium
Critical video communication	≤ 100	99.9	≤ 500	10-20	Medium
with direct impact on train safety	≤ 10	99.9	≤ 40	10-30	Medium
Data Communication	≤ 500	99.9	≤ 500	1-10	Small to large
Critical data communication	≤ 500	99.999	≤ 500	0.1-0.5	Small to medium
Very critical data communication	≤ 10	99.9999	≤ 40	0.1-1	Small to medium
Messaging	—	99.9	≤ 500	0.1	Small

Small = payload $\leq$ 256 bytes;Medium= payload $\leq$ 512 bytes; Large = payload 513-1500 bytes

3.2 Signaling systems and Virtual coupling

In railway environments, telecommunication radio links allow providing critical and non-critical services aimed at improving the efficiency, safety and availability of this means of transport. Railway signalling systems are an example of critical services enabling safe and efficient operation. The most popular ones are ERTMS and CBTC; they are incompatible with each other and are used in different segments of the rail infrastructure. CBTC is used for passenger mass traffic of low capacity and short distances main lines, such as the subway system, and tramway, among others [90], while ERTMS is mostly used in long distances, high speed and complex networks main lines [91].

This section, first presents a classification of the different types of services provided in the railway, devoting a segment to the main signaling systems currently used, as well as a novel form of signaling, such as virtual coupling.

3.2.1 Communication Based Train Control (CBTC)

CBTC is a critical service where a high-capacity continuous radio link is used to exchange control information between train and wayside equipment [92], enabling the achievement of certain Grades of Automation (GoA), distributed as follows:

- GoA 0: No automation.

- GoA 1: Automatic Train Protection (ATP), the driver brakes and accelerates the train, but under restrictions given by the system, which protects the train.
- GoA 2: Automatic Train Operation (ATO), where the system controls the train speed and the driver remains in the cab doing auxiliary activities such as opening and closing the doors, among others.
- GoA 3: Driver-Less Train Operation (DTO), where the presence of a driver is not necessary, but some service staff are required on the train.
- GoA 4: Unattended Train Operation (UTO), where there are no service staff on the train.

In urban railway systems, all grades of automation have been achieved, unlike in mainline and high-speed trains, reaching only GoA 1. The reason behind this is that the implementation of a higher grade of GoA does not imply a significant benefit for high-speed train drivers as it does for urban ones, such as the intensive operation of trains running at a shorter distance from each other or less staff requirements, among others. In addition, automation at high speeds requires a more rigorous level of safety. For instance, the driverless line of Barcelona Madrid installed by Traincom is one of the most famous implementation in CBTC.

In CBTC, the train continuously sends its current speed, travel direction, and exact position to wayside equipment via radio, as well as its braking capacity. Based on the information received from all trains currently in track, the traffic control center calculates the maximum speed and distance that the train can travel, known as Limit of Movement Authority (LMA), and sends it to the train [93]. Thus, the train continually adjusts speed accordingly and maintains the safety distance to any preceding train.

The speed and location of a train is determined by using a combination of devices such as speedometers, tachometers, transponders (balise), Doppler radars, odometers, and geolocation systems such as GPS. Location accuracy is very critical. It is not standardized in CBTC, but having several redundant systems is very common, being balise the primary system in use. Balises are fixed reference points set between rails, which act as mile markers. When a train passes over a balise, its location information is transmitted to the train using an antenna set under the train, then the odometer initiates a computation process to determine the speed and position up to the new balise on the track. Any inaccuracies or accumulated errors in distance or position are corrected when the train passes over the following balise [92].

There are some problems associated to the GPS use as the primary location system. The location accuracy of geolocation systems may not be high enough to differentiate two trains traveling close to each other. Satellite signals reception might be unreliable inside tunnels. Thus, CBTC providers are generally reluctant to rely on a system controlled by an external authority on which the safety of the train depends. Therefore, the use of a geolocation system in CBTC is usually a fallback.

Given the above, we can say that CBTC is built on two pillars: a bidirectional T2G communication and the knowledge of the accurate position of the trains. Each CBTC provider has its own implementations with some differences, but with many aspects in common among them. Although CBTCs are not standardized, most radio subsystems are built on the 802.11 family of standards, with greater use of its 802.11a variant. Technical

requirements include an end-to-end delay below 800 ms, short message lengths of 64 bytes and transmission intervals between 300 and 500 ms.

The CBTC technology is well established and healthy, but it can be improved. A reasonable way to reduce the distance between two adjacent trains and thereby increase track capacity is to reduce the time in the entire processing chain (processing at transmission and reception, reaction time, etc.). The aforementioned can sometimes be very difficult to achieve [94]. However, the solution may be creating a new communication channel. If direct communication is introduced between two consecutive trains without the intervention of any wayside equipment, the *end-to-end* delay can be drastically reduced. This philosophy implies having a T2T radio system capable of transmitting real-time information between both trains, in addition to the current T2I communication system, as shown in Fig. 3.3. This allows decentralizing the CBTC system by providing the train more autonomy to determine its own LMA. The practical realization of this philosophy is not exempt of problems since a great engineering effort is required before becoming a reality.

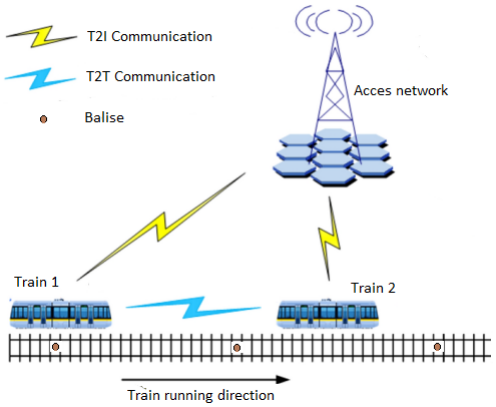

Figure 3.3: CBTC system with T2T capacity [95].

Alstom and other signaling system suppliers have been testing the feasibility of integrating this technology into their CBTC system. In this regard, they has developed a simplified CBTC system based on T2T communication tested in the Lille metro line [5], which allows doubling the trackside capacity and decreasing headways between trains to 66 s, at speeds up to 80 km/h. This proprietary solution also enhances the network architecture by using 20 % less wayside equipment reducing maintenance cost and time. This enables an extreme flexibility in train movement, higher operational availability (99.99 %) and improved performance. However, very little has been said about its technical requirements, thus fostering research in this field motivated by its proven results in train optimization and efficiency.

3.2.2 European Rail Traffic Management System (ERTMS)

At present, ERTMS is the most advanced signaling system, being the analogue of CBTC developed for high-speed trains and mainlines. At a train speeds over 200 km/h, the driver is unable to see the warning signals on both sides of the railway track, so it is necessary to transmit this information to the driver's cabine. Moreover, this information needs to be continuously transmitted to keep the safety and integrity of the train along

the track. This signaling system was designed to solve these drawbacks, as well as interoperability problems among different signaling systems. Before ERTMS standardization, each country had its own signaling system and to pass through a cross border, trains had to be equipped with both signaling systems, increasing maintenance and equipment cost [96]. Therefore, this system aims at enabling full interoperability among European Networks for high-speed lines, increasing traffic, improving all systems safety and reducing investment cost. The system facilitated the introduction of international high-speed corridors, reducing or eliminating travel delays caused by cross-border stops.

Today, ERTMS is a very popular system due to the many advantages it provides, evidenced by its current implementation by 38 countries across the world, including all member states of the European Union, and countries in Asia, such as China and South Korea. ERTMS is a critical service for train safety that is composed of two central elements. The first one is a command-based digital control system called European Train Control Systems (ETCS), on which the safety of train operation depends. It includes a set of OBU and RSU elements, creating a train movement supervising sub-system. Among the elements that make up the ETCS are a cab signaling system, an Radio Block Centre (RBC), Eurobalise, an ATP system, a block movement system, a driver machine interface, a positioning system and a braking curve, among others.

ETCS provides real-time information to both, the driver and traffic controllers, improving train management and operation flexibility. Furthermore, it can be applied at different levels, depending on the way the information is transmitted between the train and the infrastructure or how the network elements are allocated along the track. The second element in ERTMS is the GSM-R radio communication sub-system, which is the first mobile communication standard designed specifically for the railway environment, built on GSM, widely used in commercial mobil networks. GSM-R provides the following two essential railway services:

- T2I data communication for ETCS at levels 2 and 3, enabling a bidirectional data channel between the train driver and the traffic control center.
- A unified solution for all voice communications in the railway infrastructure (T2I communication, maintenance and shunting team members, and others). One of the advantages of this system is the possibility to make a Railway Emergency Call (REC) that is automatically accepted on all GSM-R terminal enabled devices within the current area, regardless of their function.

GSM-R is a dedicated railway network, which is independent from other networks (commercial GSM networks) and it is not shared with other entities or organizations (police, public service or others). Furthermore, GSM-R does not provide any services directly to passengers. Since GSM-R is built on GSM, in which roaming features are defined, there are few interoperability problems in GSM-R operation at cross borders.

Importance of the communication link

The ETCS is a distributed system whose functions are performed around the RBC network elements and the OBU, thanks to a logical communication link established between them, as shown in Fig. 3.4. However, its function does not depend on the communication technology on which it is built. Although GSM-R is the communication

technology standardized in EU for ERTMS, in other countries outside EU, such as Kazakhstan, ETCS has been deployed over a TETRA link due to the lower infrastructure costs of this technology. Euro-Radio made possible the aforementioned providing an interface between the ETCS and the communication technology, thus enabling reliable and secure connections over non-secure links [97].

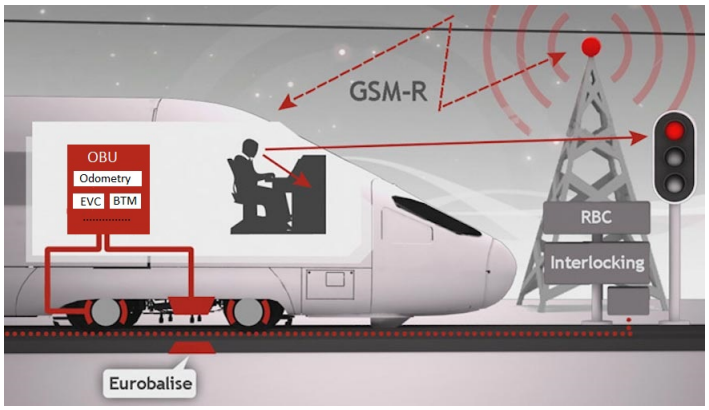

Figure 3.4: Architecture of an ETCS System Level 2 [98].

An ETCS section must be established between the OBU and the RBC to start ETCS operation (for example, train movement supervision). During the establishment process, the two network elements exchange configuration parameters necessary for the train operation. For example, the OBU sends data from the train to the RBC such as the length of the train, number of cars, and driver identifier among others. While the RBC sends pre-established data such as the speed limit on the rail, and level of protection, among others. The section establishment is the first scenario where the RBC and the OBU must communicate through a mobile network.

For RBC to maintain train management and supervision, each OBU periodically sends a position report message to its corresponding RBC, to which sometimes a Movement Authority (MA) request is attached. Taking into account the position report and other information (timetables, route schedules, and position reports of other trains within the RBC operating area, among others), the RBC issues a MA for the train. The MA defines the speed limit and the distance allowed to the train. Once in motion, the position report and the MA are constantly updated and exchanged between the OBU and the RBC, thus, a continuous communication between these elements is necessary. This implies that the radio subsystem uses short packet lengths (less than 100 bytes) and *end-to-end* delays lower than 500 ms [94].

Without continuous OBU-RBC connectivity, the main ETCS functionalities cannot be provided (ATP, cab signaling, MA distribution among others). For example, if a train approaches to End of Movement Authority (EoMA) and cannot update its MA, then it is forced to slow down and eventually stop. The OBU cannot allow the driver to exceed his EoMA unless an updated MA is received. As a result, a large delay in OBU-RBC communication can cause travel delays not only to the train affected, but also to others along the track, reducing the railway capacity. The aforementioned illustrates how the reliability and availability of the communication link affects the QoS (Quality of Service) of the ETCS system. Then we can say that in these systems a robust and efficient data communication is one of the pillars to have a punctual, efficient, and reliable rail service.

3.2.3 Virtual coupling

The current situation in Europe concerning freight traffic by rail is such that it is considered as an alternative to road freight transport. More and more customers prefer carrying their products by road, as the railway maximum capacity has been reached. This trend main reasons lie in technical and logistical aspects, resulting in the lack of economic attractiveness of rail transport. For example, railway-operating concepts such as signaling follow a long tradition and consequently, do not use modern technologies and still use block systems. Even modern approaches, such as Block Movement, follow these principles.

Increasing railway track capacity operated by a block system means, on the one hand, running more trains per time and extending the length of the train on the other. The latter contradicts many customers' demands, since the preparation time to build a long train also increases. This concept can only work properly on branchless railways carrying large amounts of cargo from a common origin to a common destination. So new operation concepts regarding both, customer´s demands and railway network topological structure must be considered.

To avoid the classic disadvantages of railway traffic, the authors in [99] propose the STCC approach, using independent train modules to form a train convoy, where the term train module refers to a conventional train. This means that trains use passive railways as flexibly as vehicles and trucks, which currently use the roads. So ideally, each train module would have its own propulsion system becoming intelligent and autonomous. By transmitting data using a highly reliable and low-latency radio communication system, the train modules would be driven one behind the other at a minimum distance, as short as possible and lesser than the braking distance, as shown in Fig. 3.5.

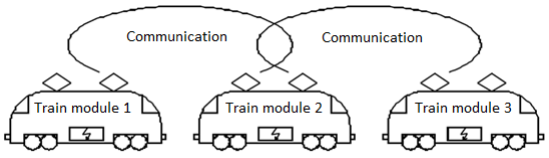

Figure 3.5: Smart Trains Composition Coupling Concept [99].

Train modules leave the alignment automatically when reaching or joining a line intersection. When approaching a danger point, the train modules that make up the convoy would have to maintain at least the absolute STCC breaking distance. Each module would determine on which track to continue to its final destination. This philosophy could increase the line capacity by 100 % and would imply that each train has a T2T radio system on-board, capable of transmitting real-time information between both train models. This direct communication execution could be performed now by different commercially available technologies such as LTE, TETRA, 802.11, and WIMAX among others. These technologies have been designed to support direct communication between devices, without intermediate or wayside equipment support.

A communication channel additional to the already available T2I link that can handle time critical events better than a centralized system is created with a reliable radio link capable of transferring data directly between trains. Unexpected events or potentially dangerous situations on the track can be communicated directly to the next train or approach it. This allows taking immediate action to mitigate potentially dangerous

situations, and increasing track capacity by effectively reducing the safety distance required between trains. Through the wireless link, they exchange information about their composition, position, power controls, relative speed, and length, among other aspects.

Figure 3.6: Trains manual coupling process.

Nowadays, trains coupling is done manually using electrical, pneumatic and mechanical connectors, as shown in Fig. 3.6. Trains coupling and uncoupling operations are highly risky and constitute a significant cost factor, requiring time and staff. Furthermore, only compatible trains can be coupled limiting interoperability, because their compositions must be, for example, of the same model. Hence, the STCC application is very attractive in the railway environment in the sense of improving track safety, increasing capacity and reducing operation and maintenance costs. Then, STCC complements the current T2I railway systems, but this philosophy requires a reliable and low-latency communication link.

Currently, the SCOTT and Shift2Rail projects conduct research on applications based on the same principles as TVC. The SCOTT project develops the STCC (Smart Train Composition Coupling) application intended to increase track capacity by 100 %. While Shift2Rail (S2R) is a public-private partnership in the railway sector, being the first European railway initiative to seek solutions focused on research and innovation (R&I) and oriented to the market. Presently, S2R is carrying out the Project S2R-CFM-IP2-01-2018-Advanced Signaling, Automation and Communication System **??**. It covers innovation and research activities based on communications, block movement, test methodologies and cybersecurity. It also works on researching new advanced signaling concepts, such as the set of virtually coupled trains.

In addition, the virtual coupling concept has been studied too within the MOVINGRAIL project in its deliverable *D3.1 Virtual Coupling Communication Solutions Analysis* [100]. The objective of this deliverable is to analyse the current technical communications solutions, that could be exploited to implement virtual coupling on a real railway. Please note, this analysis has been performed on a theoretical basis where TETRA, IEEE, 3GPP cellular based communication systems have been analyzed and compared. Then, performance results based on simulations or field measurements are missing in the literature. In Chapter IV, we address this topic where simulation based performance results are shown for T2T links using 802.11p/bd. In order to achieve this aims, we had to work in T2T channel modeling in Chapter III which is essential to obtain consistent simulation results.

3.3 Railway communication technologies

Railway communication technologies constitute an essential part of the railway system, since, as previously analyzed, they have a direct influence on the efficiency of the rail transport system. These communication technologies can be divided into three main application groups oriented to security-control, operation and user networks, that is, they are directed towards the type of traffic to be supported. Thus, at present there is no single communication technology capable to support all communication needs (critical and non-critical).

The first epigraph of this section shows the characteristics of the main wireless communication technologies currently deployed in railway infrastructure. In the following ones, a description of GSM-R and TETRA technologies are presented highlighting their shortcoming and drawback to support the current rail services. They have been deployed in T2I links but unlike to TETRA, GSM-R do not support T2T communication links. In addition, it is important to highlight that GSM-R is the most popular technology at present, but its life cycle is diminishing due to its inability to adapt to new services demands.

3.3.1 Wireless technologies

The deployment of wireless communication systems in the railway sector is in a booming stage, in which several technologies have been set up, evaluated or adapted to this means of transport. This has provided tangible benefits not only to rail operators but also to passengers. Table 3.2 shows some characteristics of these technologies. Also, these technologies have one of these features:

- Open standards such as TETRA, 802.11 family, among others.
- Open standards with slight modifications in some layers, a successful example is GSM-R built on GSM. Another future example would be 4G Long Term Evolution for Railway (LTE-R), based on C-V2X, which is expected to replace GSM-R.
- Proprietary communication solutions attractive to the market, such as TrainCom [101] and FLASH-OFDM [102].

Nowadays, GSM-R is the most used communication system between the train and the different control-operation elements in the railway infrastructure, that is, in the T2I link. It is very popular and has been deployed in more than 38 countries across the world, including all the member states of the EU and some in Asia and America. However, due to its low capacity and radio interface limitations, its useful life is depleting. It supports all critical communications related to train safety and control, and constitutes the communication platform in the ERTMS high-speed signaling system. Its main features are analyzed in the following section.

In T2I link, the 802.11 family of standards is also widely used in critical applications such as CBTC signaling system, being its 802.11a version the most used. This signaling system is railway operator's first choice for user mass traffic operations [93], such as the metro system, trams, etc. This family of standards is built on a set of technologies such as 802.11 a/b/g/n/p among others, working in unlicensed bands in general, and can have

Table 3.2: Main features of communication technology used in railway scenarios.

Technology	Frequency (GHz)	Bandwidth (MHz)	Peak bit rate (Mbps)	Modulation	Medium access	Support T2T
GsM-R	DL:0.921-0.925 UL:0.876-0.880	0.2	0.172	GMSK	TDMA	Not
TETRA	0.380-0.470 0.870-0.921	0.025	0.05/0.1	DPSK	TDMA	yes
802.11	2.4/5.8	20/40	>10	OFDM	CSMA/CA	yes
802.11p/bd *	5.9/60	10/20	>50	OFDM	EDCA	yes
WIMAX	2.4/2.5/3.5	1.3/20	>30	OFDM	DL:OFDMA UL:SC-FDMA	yes
UMTS	2.1	5	>2 (standby) >0.384 (mobile)	PSK	CDMA	Not
LTE-R	0.450/0.800 1.4/1.8	1.4,100	DL:50 UL:10	OFDM	DL:OFDMA UL:SC-FDMA	yes
C-V2X**	0.41-7.125 24.25-52.6	flexible	>50	OFDM, SC-FDMA	TDD, FDD	yes
RoF	variable	10,100	1000/10000	OFDM	...	Not
LCX	variable	30/1000	1000/10000	OFDMA	...	Not
Satellite	Limited	>20	>2	FSK,PSK	TDMA, FDMA, CDMA, ALOHA	Not
FLASH-OFDM	0.450	1.5,5	DL:5.3 UL:1.8	OFDM	FHSS	Not

UL= Uplink;DL=Downlink; LTE-R= use of LTE (Rel. 12) in Railway;*= Emerging technology introduced in Section 2.3;**= Emerging technology introduced in Section 2.4 using 3GPP Rel. 14 and beyond.

ranges of up to 450 m. In addition, it is very common to deploy these on board the train to provide wireless broadcast communications, internet access to users, and services directed to the operator (open and close the train doors or in video surveillance systems) among others [103]. Being this a broadband technology with a data rate in the order of megahertz.

Because of the rapid technology improvement, new WiFi variants are available on the market and may be deployed in railway networks in the near future, such is the case of 802.11ah called Wi-Fi HaLow. It works in the 900 MHz band with a data rate of up to 347 MHz and introduces new coding schemes, making it more robust against the Doppler effect. Another emerging variant is 802.11ad (WiGig) which operates in the 60 GHz millimeter band and provides a data rate of up to 7 GHz. However, its transmission range is small about 10 m; to compensate this limitation, manufacturers such as IgniteNed have used high transmission powers and high gain antennas, achieving a transmission range of up to 1.5 km.

Another emerging protocol is 802.11p that operates in the 5.9 GHz band adapted to support communications V2V, which was analyzed in detail in Section 2.2. In [104] the author concludes that 802.11p is more suitable for CBTC than 802.11a, using *end-to-end* latency and effective bit rate (throughput) as performance metrics. Nowadays, IEEE has been working in next evolution of 802.11p, called 802.11bd [39]. This oncoming protocol was introduced in Section 2.3 where a detailed description of its advanced physical layer was given. 802.11bd has been designed to support railway use cases. However, a prior evaluation process must be necessary before it is deployed in railway. The reader can find a performance evaluation of 802.11p/bd in Chapter 5 of this thesis for some T2T and T2I scenarios.

Another technology used to provide Internet access and service to users is WIMAX, which is a packet-switched network built on OFDM and has data rates of up to 78 Mbps. One of WIMAX attractive features for railways is that it offers QoS for the prioritization of different data flows in the network, which is important if the resources within the network are shared between critical and non-critical applications. In [105] the authors evaluate QoS performance in a T2I network to provide Internet access to users. However, QoS has not achieved great commercial success limiting its use in the railway environment because it does not guarantee long-term market continuity.

The emerging LTE-R technology is also being evaluated to replace GSM-R, which use the LTE mobile standard in railway environment. Compared to GSM-R, LTE offers greater capacity and significantly improves data transmission capabilities, so LTE is expected to be able of supporting a wide range of innovative applications. Besides, LTE-R infrastructure is likely to support both critical and non-critical services in a shared network. Thus, all railway companies mobile communication needs may possibly be supported by a single technology. For instant. the authors in [106] and [107] show the performance results of LTE in railway based on simulations and field measurements. The results show the validity of the transmission scheme to provide railway services in a practical LTE deployment. In addition, the new C-V2X emerging technologies are being designed to support railway use cases, which are based on LTE and presented in Section 2.4. Then, they are suitable technologies to be deployed in railway and covering communication needs. Hovewer, a prior evaluation process will be necessary before these are deployed, which is in an initial stage.

In [94] a model is offered to provide internet access to users on board the train based on whether using mobile repeaters or not, through mobile and satellite networks. To meet users' connection needs, railway operators frequently hire mobile operators services and share their network with 3G and 4G mobile technologies, such as LTE, UMTS and General Packet Radio Service (GPRS), among others. The aforementioned can cause interference problems between these systems and GSM-R, since they work in adjacent frequency bands.

Another technology used is Leaky Coaxial Cable (LCX), which is a coaxial cable with periodic openings on its surface allowing it to act as an antenna; this technique is also known as radiant cable. Its transmission range is generally small around ten meters between the radiant cable and the receiver on board the train, providing regular coverage while being less susceptible to interference. This is generally used in open locations where interference is significantly higher, or in critical locations where radio communications are extremely complicated (tunnels). LCX has successfully provided voice radio services in metro systems. It is also extensively used in Japan to provide Internet access to passengers through IPv4 [108]. However, this technology lacks acceptance among CBTC systems manufacturers, mainly due to high maintenance and installation costs [93]. For example, the manufacturer Bombardier, in its first design of CBTC used LCX as a communication platform, whose cost was 100 times higher than a solution built on 802.11.

There are also proprietary systems widely attractive in the railway market. For example, the TrainCom radio module systems, which provide interference-free, secure and high-performance data and information transmission to the user [101]. These devices use current technologies and techniques, entirely IP, providing bit rates of up to 32 Mbps and an availability of more than 99.999 %. The TrainCom data transmission can be used for a wide range of applications in the railway industry including CCTV, voice over radio, PIS, wireless internet access, passenger broadcast system, automatic passenger counting, and real-time news and television, as well as online train diagnosis and transport management system.

Another proprietary technology for mobile data broadcast communication is FLASH-OFDM, built on both OFDM and Frequency Hop Spread Spectral (FHSS) [102]. A mature technology that has mobility support of up to 250 km/h, transmission rates up to 3.2 Mbps and has greater efficiency than UMTS. Other wireless technologies are iBURST, Redline Communications, Faiveley and Martec, which are proprietary as well, deployed for railway access networks.

3.3.2 Global System for Mobile Communication–Railway (GSM-R)

GSM-R is a circuit-switched network, where each network connection, either a call or a data one, requires a dedicated *end-to-end* virtual circuit. This means that the network resources are reserved exclusively for a particular connection both in the radio access link and in the backbone network, which is suboptimal under the transmission of information data bursts. The first part of this section deals with GSM-R main features regarding its MAC and physical layer, while the next two sections are devoted to explain briefly its architecture and the main reasons why this standard is becoming obsolete.

3.3.2.1 Main features

Regarding frequency channeling, GSM uses a bandwidth of 4 MHz, operating in frequency bands of 876–880 MHz for the uplink and 921–925 MHz for the downlink [1]. These frequency bands are exclusive for the railway sector throughout EU, ensuring interoperability. Each frequency bands in both downlink and uplink is divided into 19 frequency channels of 200 KHz width plus a 100 KHz guard band at each end. These channels are used to separate neighboring cells transmissions, avoiding use of the same frequency, as the channels must be allocated among the cells safely. Each cell can use one or more channels depending on the expected capacity demand. A frequency channel used in one cell can be reused in another, but only if the distance between them guarantees that cells do not interfere. Generally, seven frequency channels are required to provide coverage over a wide area. On an open railway line, where only linear coverage is required, four frequency channels per cell may be enough [96].

For accessing the medium and sharing network resources in GSM-R, Time Division Multiple Access (TDMA) is used on each frequency channel, where a frame of length 4,615 ms is divided into 8 time slots, one of them is dedicated only to network signaling and the rest to voice calls and data connections. Given this, a typical cell offering up to three frequency channels has a capacity of 23 connections. The modulation technique used in GSM-R is Gaussian Minimum-Shift Keying (GMSK), which was selected due to its simplicity of implementation and low interference emission. However, regarding to modern modulation techniques, it transmits only one bit per symbol.

Since handover procedures, for example, are very frequent due to the high speeds reached by trains, it is necessary to design the network to ensure an excellent coverage of more than 99 % of the time to guarantee communications reliability and quality. The redundancy at a physical level is a common implementation of GSM-R; to achieve it, two design strategies are adopted. In the first one, two independent overlapping networks are used, having a coverage in two layers, fully redundant and independent from each other, allowing that if one or more base stations of a layer fail, an automatic roaming occurs to the other layer ensuring communication. The adjacent cells overlap each other around 600 meters, equivalent to 7 seconds at 300 km/h approximately. Currently, in many configurations, the traffic of a layer is assigned depending on the train movement direction. The other strategy uses a single network with twice the amount of base stations used in the first strategy, allowing a strong overlap in radio coverage, so that if one cell fails its neighboring cell automatically compensates its coverage. In both cases, a high coverage is achieved guaranteeing the operation of the system.

GSM-R architecture

The basis of GSM-R is the same as GSM, so it provides all the features of GSM and adds new ones to meet the demands and requirements of the railway environment. Among them we have railway emergency call, group voice call services, location-dependent addressing, among others. As shown in Fig. 3.7 below, the basic architecture of GSM-R falls into four subsystems, as follows:

- Mobile Station (MS): It is the user terminal wirelessly connected to the GSM-R network, which can be from a portable voice terminal to an OBU.
- Base Station Subsystem (BSS): It is composed of a Base Station Controller (BSC) and a certain number of Base Transceiver Stations (BTS), managed by the BSC of the area to which it belongs. The BTS is a base radio station responsible for wireless communication with the MS.
- Network and Switching Subsystem (NSS): Represents the network core, built on Mobile Switching Center (MSC), which performs all the signaling and switching functions (call establishment, call routing, and mobility management, among others) for the MS located in a geographic area assigned to it. In addition, this subsystem includes a set of databases for call control and network management such as Home Location Register (HLR), Visited Location Register (VLR), Authentication Center (AUC) and Equipment Identity Register (EIR).
- GSM-R subsystem: Includes servers responsible for offering railway services, such as the Operations and Maintenance Center (OMC) for the operation and maintenance tests and RBC for managing and supervising the movement of the train.

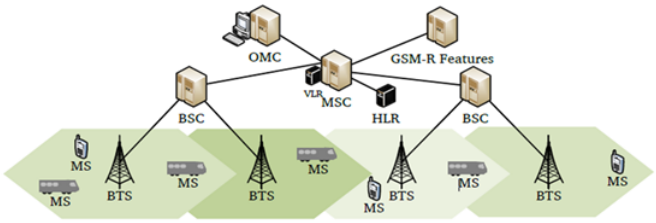

Figure 3.7: GSM-R Network Architecture [96].

3.3.2.2 GSM-R shortcomings and drawbacks

Nowadays, GSM-R is a successful and popular technology, but its lifetime is starting to run out due to its inability to adapt to the new requirements of railway services. In this section, some disadvantages and drawbacks of GSM-R are presented which could carry to its replacement by one of the current technologies in the near future [92].

GSM-R was designed for voice communication, a design choice in disagreement with modern railway systems needs. Future railway-communication networks should provide a good support for data transmission, which GSM-R lacks as it has a circuit-based transmission mode making data transmission inefficient while consuming more resources than needed. This means that network resources cannot be allocated based on actual demand since data are transmitted over virtual circuits, just like voice frames. However,

as opposed to voice, data communication tends to be at bursts, where the transmitter sends a variable amount of data at irregular intervals. Such burst transmission does not fit well into the fixed circuit concept provided by GSM-R. As a result, circuits are often under-utilized and network resources are wasted.

As stated above, GSM-R coexists with other mobile technologies in the same infrastructure to support both the critical and non-critical services. Therefore, there is an increasing interference between GSM-R and public networks, since both network operators want good coverage along the railway and operate on frequency channels close to each other. Furthermore, instead of cooperating in network planning, they strive for the best possible coverage. Interference can result in several deficiencies in voice and data communication links, as well as network coverage loss over several hundred meters on the railway track. In the future, interference may increase due to the growth of deployed GSM-R networks and the potential development of public networks.

Furthermore, GSM-R supports frequency channels of 200 KHz, which are enough for voice communications, since they are limited in time and do not occupy radio resources continuously. Such an allocation is inefficient in the case of the new generation railway systems, where each train needs to establish a continuous data connection with the wayside equipment, so a time slot is constantly needed. The maximum transmission rate is 9.6 kbps, sufficient only for low demand applications. Furthermore the messages delay is about 400 ms, which is very high to support any real-time application and emergency communications. The capacity of radio link can be improved by using more radio resources.

Another drawback is that TDMA allocates a time slot to a frame for each connection. This fits well with voice coders that encode voice into a periodic frame. Data connections are by bursts, as in ETCS, which could benefit from the use of more time slots per frame. However, a single connection cannot have more than one time slot, even if extra time slots are available. Thus, radio resources may remain unallocated even if there is data traffic waiting for transmission. Finally, another disadvantage is that the bit rates are insufficient for many modern applications, mainly for those based on multimedia transmission requiring more than 1 Mbps. Another modulation scheme can be used to transmit at higher bit rates, such as OFDM, since Gaussian Minimun-Shift Keying (GMSK). is a binary modulation that allows only one bit per symbol.

3.3.3 Terrestrial Trunked Radio (TETRA)

TETRA is a standard formulated by ETSI in [109], aimed to unify several alternatives of digital radio interfaces for public safety communication, that is, for use by the police, civil protection, fire departments, etc. This section deals with TETRA main features regarding its MAC and physical layer.

3.3.3.1 Main features

TETRA allows communications in two modes: Trunking Mode Operation (TMO) and Direct Mode Operation (DMO) which is an attractive feature for railways. The latter allows direct communication of mobile terminals or users without the use of the network infrastructure, increasing network coverage especially in those places with insufficient, overloaded or faulty network infrastructure. Furthermore, Short Data Send

(SDS) transmission is possible for both modes of operation, but is rather limited as it is a narrowband technology supporting a data rate of 7.2 Kbps per channel.

TETRA channeling differs from GSM-R, since it uses 8 frequency channels with 25 KHz bandwidth carriers, using TDMA frames with 4 time slots. However, it is insufficient for services that require a high bit rate, so it has almost the same limitations as GSM-R, as previously explained. It is a technology operating in the 380–470 MHz band, which implies a significant base stations saving compared to GSM-R (which does so in the 900 MHz band in Europe), due to their greater range by having better deployment conditions. However, TETRA can be used to a lesser extent in the 870–921 MHz band, finding interference from mobile systems operating in this band.

The robustness of TETRA, as well as its railway applicability is very significant especially for voice and, to a lesser extent, data transmission. In addition, the operation in DMO in the railway environment enables direct T2T communication, opening a wide range of research in which new railway applications aim to improve the reliability, safety and efficiency of this means of transport. These new applications can be related to critical train services that require high reliability and low latency, such as trains virtual coupling, collision avoidance systems, and decentralized CBTC systems, among others. For example, TrainCAS is a collision avoidance system, which is supported under TETRA and developed by DLR, which allows train drivers to have an updated knowledge of the traffic situation in their vicinity, and act accordingly.

The main task of this TrainCAS system is calculating its own position and motion vector and transmitting this information, as well as additional train data to the rest of the trains in the area [110]. The driver's cabin can be equipped with a display showing the position of the other trains in the region, in which a computational analysis is performed to determine the position and movement vector and display them on an electronic tracking map. The aforementioned allows detecting possible collisions, showing warning signs and instructing the driver of the most convenient strategies to avoid dangerous situations. The system enables a transmission range that is often 12 times greater than the braking distance of the train, hence its great availability.

3.4 Summary and conclusions

The telecommunication system associated with railway infrastructure is a strategic element not only for train safety, but also for the efficiency and capacity of the entire transport system. In this chapter, we have addressed the last statement where the main features of the wireless communication technologies deployed in railway have been described as well as their application field. Nowadays, GSM-R and 802.11 solutions are the technological options preferred by manufacturers. These technologies are used to support critical and non-critical application such as signaling systems like CBTC and ERTMS, avoidance collision systems, monitoring and maintenance systems or internet access, among others. For instance, while ERTMS implements GSM-R in its architecture (Section 3.3.2), most of CBTC implementations use Wireless Local Area Network (WLAN) solutions, mainly its 802.11a version.

However, GSM-R is an obsolete technology with more than 20 years of exploitation that does not support services based on packet switching nor ones that demand a high bit rate (in the order of megabits per second). Furthermore, the fast development of wireless standard based in cellular and WLAN solutions have taken attention by manufactures of

railway technologies. Thus, 802.11p/bd and C-V2X are wideband technologies with a great potential to be deployed in railway in next years. In this thesis we address this topic with a focus on 802.11p/bd.

In addition, four railway use cases have been identified, where the railway communication has an important role in train integrity: Onboard Train, Train-to-Infrastructure, and Vehicle-to-Train. The T2T use case allows the implementation of virtual coupling, which would increase the line capacity by decreasing the T2T distance beyond the train braking distance.

4

Train to Train Channel Models

T2T communication is proposed as another auxiliary safety-guaranteed measure for railway communications. Nowadays, wireless communication technologies are being designed, tested, and standardized that support this kind of communication. Hence, it is essential to have a T2T channel model that can accurately simulate the railway propagation environment. In this chapter, we first examine some topics about railway channel modeling. Then, six TDL models are proposed for T2T communications in Hilly Terrain and Railway Station scenarios. The measurement based proposed channel models consider different T2T distances and relative speeds of up to 50 km/h with trains moving in an approaching maneuver. Also, a study about the Doppler-delay behavior in the considered scenarios is made using the scattering function, from which two modes to associate the Doppler spectrum to the TDL model are examined. Using the measured impulse responses and a 802.11bd framework, the proposed channel models are validated.

4.1 Introduction

T2T communications have won attention in the scientific community in the last decade, where several research projects have been carried out to modernize the railway communication infrastructure. It allows a reliable radio link that is capable of transferring data directly between trains. Then, this T2T link can handle critical time events with low end-to-end latency compared to a centralized system. This way trains can exchange information about their composition, position, relative speed and train length among others. T2T communications are foreseen as the enablers of new time-critical applications, which will allow to improve train safety, availability and operation. Critical applications such as collision avoidance systems, decentralized CBTC, and train composition coupling are under investigation [41].

Commercial technologies such as C-V2X, TETRA, 802.11, and WiMAX have capabilities to support T2T links. For instance, the analysis of ITS-G5 based on 802.11p was presented in a T2T link under high speed railway (HSR) conditions [6]. In addition, new communication protocols are being standardized which enable use cases in railway scenarios since a part of the 5.9 GHz band has been assigned to these. One of such protocols is 802.11bd, which will be the successor of 802.11p and adds new advanced processing techniques to its physical layer [7]. Another one is NR-V2X, which is expected to be standardized in the next release (17) by 3GPP.

The performance evaluation of the previous mentioned wireless technologies requires accurate channel models and measurement campaigns carried out in railway scenarios. In [11], the author provides a rich literature analysis of existing railway channel models based on measurement only for train-to-infrastructure (T2I) communications. Several channel models, measurement campaigns and propagation studies have been carried out for T2I communications [13],[14]. In comparison, only a few studies have been reported for T2T communications and a research gap is observed. In addition, in some works found in the literature, the authors have used frequency bands that are not standardized for railway T2T applications.

In this Chapter, based on the measurement campaign reported in [6], we derive six tapped delay line channel models available for train-to-train communications, which cover different T2T distances and two railway scenarios (Hilly Terrain and Railway Station). Also, a study of the stochastic channel parameters and the Doppler-delay behaviour are presented for the considered propagation scenarios. In addition, the performance of the channel models is assessed through simulations based on the 802.11bd protocol.

The research presented in this chapter was carried out together with the Vehicular Application Group from the Institute of Communications and Navigation, German Aerospace Center (DLR). As a result of this collaboration, a joint article was submitted for publishing in IEEE Transactions in Vehicular Technology on July 2021. The following articles have been derived from the results present in this chapter:

- S. Zelenbaba, L. Mayer, E. Mozo, F. Wirth, R. Hladik, A. Alonso-Gómez, L. Bernadó, M. Schiefer, and T. Zemen, "Characterization of Time-Variant Wireless Channels in Railway Communication Scenarios," in IEEE 2nd 5G World Forum (5GWF), 2019, p. 6.
- E. Mozo, P. Unterhuber, A. Alonso-Gómez, S. Sand, and M. Mendicute, "Measurement based Tapped Delay Line Model for Train-to-Train Communications," submitted to IEEE Transactions on Vehicular Technology (28-07-2021), p. 13. (resubmitted 25-01-2022, under review)

The chapter is organized as follows: In Section 4.2, the theory underlying railway channel modelling is briefly described. Next in Section 4.3, the methodology used to calculated the parameters of a TDL model is presented in detail. In Section 4.4, we introduce the DLR measurement campaign where the channel impulse responses for some T2T scenarios were measured and stored. Next, using the stored data, six TDL models are developed and results are shown in section 4.5. Finally in the last two Sections 4.6 and 4.7, the proposed channel models are validated and the conclusions are presented, respectively.

4.2 Railway channel modelling

Modelling the wireless channel is one of the most difficult tasks of radio system design, and is usually done in a statistical way, based on measurements made specifically for an intended communication system and spectrum allocation. The channel models are generally based on a mathematical representation of the impulse response of a multipath channel $h(t, \tau)$, where t and τ represent time and delay, respectively. $h(t, \tau)$ contains all

information required to simulate or analyze any type of radio transmission through the channel.

A baseband representation for $h(t,\tau)$ was given by [111] as:

$$h(t,\tau) = \sum_{i=0}^{M-1} a_i(t,\tau) e^{j\theta_i(t,\tau)} \delta(\tau - \tau_i(t)), \tag{1}$$

being $\theta_i(t,\tau) = 2\pi\eta_i(t,\tau)\tau_i + \phi_i(t,\tau)$ the total phase term. The terms $a_i(t,\tau)$, $\phi_i(t,\tau)$, and $\tau_i(t)$ represent the real amplitude, phase, and delay of the i^{th} multipath component encountered in the channel at time t, respectively. The M phase components $\phi_i(t,\tau)$ are mutually independent random variables uniformly distributed over [-π; π], where M is the number of multipath components in the channel, including the first arriving component or LoS component. Moreover, δ(t) is the Dirac-delta function. Each multipath component experiences a Doppler frequency $\eta_i(t,\tau)$ due to dual mobility of the transmitter and receiver [112, page 42].

Fig 4.1a shows a snapshot of squared magnitude of $h(t,\tau)$ obtained during a T2T measurement campaign whose results were presented in [6]. The multipath components as well as LoS component can be identified very clear in Fig 4.1b which is the top view of Fig 4.1a. Here, the LoS component is defined how the multipath component with higher power.

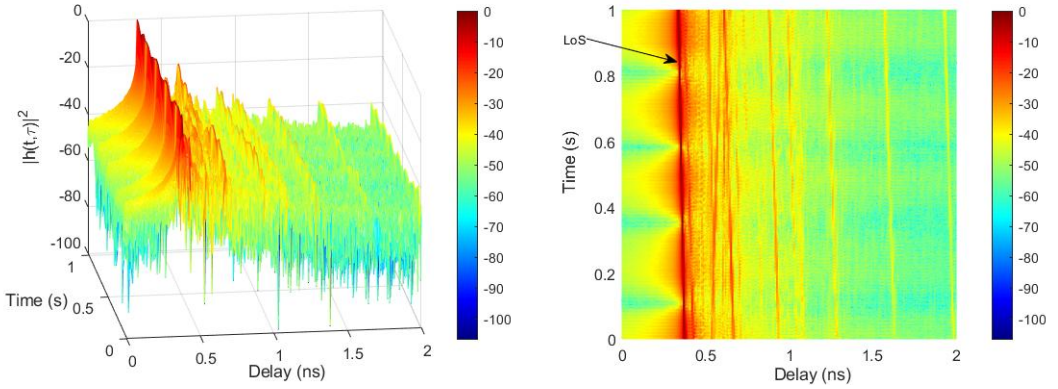

(a) Normalized $|h(t,\tau)|^2$ (b) Top view of $|h(t,\tau)|^2$

Figure 4.1: Squared magnitude of the channel impulse response, $|h(t,\tau)|^2$, measured during approaching maneuver [6] in Hilly Terrain: T2T distance of 100 meters, snapshot of 1 s, and carrier frequency of 5.2 GHz.

In addition, each multipath component has associated an angle of arrival $\alpha_i(t,\tau)$, whose statistical distribution determines the power spectral density or Doppler spectrum of $\eta_i(t,\tau)$. For instance, when $\alpha_i(t,\tau)$ exhibits a uniform distribution [11], the Doppler spectrum is represented by the *Jakes*' spectrum. The knowledge of the Doppler spectrum is very important in order to model a wireless channel since it determines how fast $h(t,\tau)$ varies in time. Then, the Doppler frequency of LoS component is expressed as:

$$\eta_{\text{los}}(t,\tau) = \frac{\Delta v f_c}{c} \cos\left(\alpha_{\text{los}}(t,\tau)\right), \tag{2}$$

where Δv represents the relative speed, f_c represents the carrier frequency of the transmitted signal, and c is the speed of light. The term $\alpha_{\text{los}}(t,\tau)$ represents angle of arrival of LoS component which includes the arrival direction and the movement direction.

Please note that as $h(t, \tau)$ is a function of two variables, we can perform the continuous Fourier transform (FT) with respect to both variables. As a consequence of that, four different, but equivalent, representations are obtained which are shown in Fig. 4.2. In this figure, $H(t, f)$ represents the transfer function or frequency response, $p(\tau, \nu)$ represents the Delay-Doppler spread function or the scattering function, and $D(f, \nu)$ represents the Doppler spread function. These functions which were firtly presented by Bello in [113] and used too in [114], characterize stochastic channel and are used to calculated the power density and auto-correlation functions of the channel.

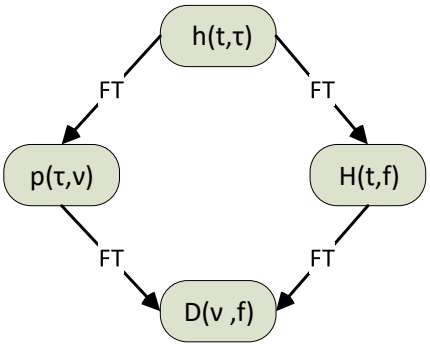

Figure 4.2: Interrelation among functions that characterize wireless channel [113].

Channel autocorrelation function

The wireless channel is modelled like a stochastic process, which can be characterized using the Auto-Correlation Function (ACF). This function describes the similarity between a function with a delayed copy of itself over time intervals Δt. The autocorrelation function of $h(t, \tau)$ was given by [114] as

$$R(t, t'; \tau, t') = E(h(t, \tau), h^*(t', \tau')), \tag{3}$$

where t' and τ' represent time and delay variables, E represents the expectation of the ensemble process, and $()^*$ indicates the complex conjugate. Note that ACF of the channel depends on four variables since the underlying stochastic process is two-dimensional. As a result, it is rather complicated to characterize the stochastic channel and more assumption must be taken in account.

In order to beat this drawback, Wide-Sense Stationary and Uncorrelated Scatterers (WSSUS) assumption is frequently used in the literature [115], which simplifies the autocorrelation function. This condition means that over a short period, the wireless channel is assumed to be stationary, which indicates that the statistical properties of the channel do not change with time. Furthermore, the contribution of two multipath components in the channel gain with different delay $\tau \neq \tau^{'}$ are uncorrelated, since both are caused by different scatteres. Then, (3) is simplified as

$$R(\Delta t, \tau) = E(h(t, \tau), h^*(t', \tau')) \cdot \delta(\tau - \tau'), \tag{4}$$

which is a two-dimensional function being $\Delta t = t - t'$.

4.2.1 Wideband channel sounder

A channel sounder is a system that measures the electromagnetic wave transmitted via a particular communication channel to determine either its time-vary impulse response or its time-vary frequency response. Also, it allows to estimate channel statistical parameters such as fading statistics, path loss, frequency and time correlation functions, phase information and Doppler spectrum among other. Thus, the channel sounding allows to understand the behavior of the wireless channel to develop more accurate channel models, which could be used to validate algorithms and communication techniques. In this subsection, we briefly introduce the main features of a channel sounder and how it can be used to estimate $h(t, \tau)$. A deep description about the operating principle of the channel sounder can be found in [116], [117].

The channel sounding can be classified depending on measurement bandwidth into two categories: narrowband and wideband sounding. Using the narrowband sounding, the transmitter sents a series of unmodulated continuous wave carriers with different frequencies [118]. Then, the carriers are measured by the receiver and collected using a Vector Network Analyzer (VNA). . Processing the stored data, the time-varying channel impulse response can be estimated. However, the narrowband sounding technique is inefficient to capture some wideband parameters such as the frequency and time coherence behavior, maximum delay spread or Doppler spectrum among others. Theses parameters are very important in order to determine the small-scale effect, which can be obtained by sounding signal with wide bandwidth.

On the other hand, using the wideband sounding, the measurement bandwidth of channel sounder W is much greater than the channel bandwidth and pulse compression methods based on pseudo noise (PN) sequences are normally used. A PN sequence is a finite-length binary sequence that shares some properties of noise. For instance, the PN choice sequence must have a flat spectrum over W [117]. Using the correlation of the received signal with the original transmitted sequence, the impulse response can be directly estimated. This kind of wideband channel sounders are named correlative channel sounders in the literature. A detailed classification of wideband channel sounders can be seen in [118].

The correlative channel sounders have had a great interest in the industry and academic, and have been used in several measurement campaign ,[19]. Some channel sounder systems are available in the marker such as SIMOCS 2000 produced by Siemens, the RUSK sounders family manufactured by MEDAV GmbH, and the 5G channel sounder manufactured by Keysight [119], among others. Next, we would like to review briefly the theory behind correlative channel sounding, which was presented in detail in [117].

4.2.1.1 Correlative channel sounder

Fig. 4.3 shows the diagram of a correlative channel sounder where the transmitted signal consists of a finite pulse sequence denoted by

$$S_{\mathrm{p}}(t) = \sum_{i=0}^{L_{\mathrm{n}}-1} c_i p(t - iT_{\mathrm{n}}) \qquad T_{\mathrm{o}} \leq t \leq T_{\mathrm{o}} + T_{\mathrm{L}}, \tag{5}$$

where $p(t)$ represents the pulse form used, L_{n} represents the PN sequence length, T_{n} represents the PN sequence chip period, and c_i represents the i^{th} pulse amplitude. The

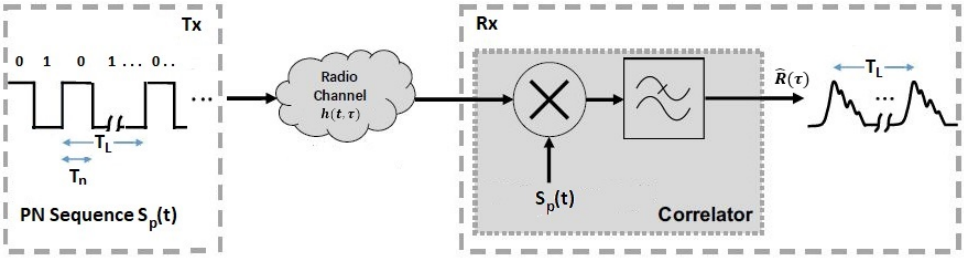

Figure 4.3: Basic diagram of a correlative channel sounder [118].

pulse amplitude $c_i = \{1, -1\}$ is mapped directly from the binary PN sequence. In addition, $S_{\mathrm{p}}(t)$ is a periodic signal with a period $T_{\mathrm{L}} = L_{\mathrm{n}}T_{\mathrm{n}}$, being $S_{\mathrm{p}}(t) = S_{\mathrm{p}}(t - T_{\mathrm{L}})$. Then, the start point of a PN sequence T_{o} is multiple of T_{L}. Assuming a linear channel, the output of the channel $y(t)$ is the convolution of the transmitted signal $S_{\mathrm{p}}(t)$ and $h(t, \tau)$ such as

$$y(t) = \int_{-\infty}^{\infty} S_{\mathrm{p}}(t - \tau)h(t, \tau)d\tau, \tag{6}$$

where $h(t, \tau)$ was defined in 4.2. Then, substituting (14) in (6), we obtain that

$$y(t) = \sum_{i=0}^{M-1} S_{\mathrm{p}}(t - \tau_i(t))h_i(t, \tau_i(t)), \tag{7}$$

being $h_i(t, \tau) = a_i(t, \tau)e^{j2\pi f_{\mathrm{c}}\tau + j\phi_i(t,\tau)}$ the complex channel gain of the i^{th} multipath component. Then, the channel output $y(t)$ is correlated with the transmitted periodic sequence to estimate the autocorrelation function as

$$\hat{R}(\Delta t, \tau) = \frac{1}{\Delta t}\int_{t=T_{\mathrm{o}}}^{T_{\mathrm{o}}+\Delta t} y(t)S_{\mathrm{p}}(t - \tau)dt, \tag{8}$$

being Δt the correlation interval. The last equation is implemented in the receiver side by applying a low-pass filter to the obtained result from multiplying the received signal $y(t)$ with the PN known sequence as seen in Fig. 4.3.

Combining (5) and (7) in (8), and choosing $\Delta t = T_{\mathrm{L}}$, the autocorrelation function is expressed as

$$\hat{R}(T_{\mathrm{L}}, \tau) = \sum_{i=0}^{M-1}\sum_{k=0}^{L_{\mathrm{n}}-1}\sum_{j=0}^{L_{\mathrm{n}}-1} c_j c_k \frac{1}{L_{\mathrm{T}}}\int_{t=T_{\mathrm{o}}}^{T_{\mathrm{o}}+T_{\mathrm{L}}} h_i(t, \tau_i(t))p(t - \tau_j - iL_{\mathrm{n}})\cdot$$
$$p(t - \tau - kL_{\mathrm{n}})dt. \tag{9}$$

Please note that the integral in the last equation is calculated in an interval $\Delta t = T_{\mathrm{L}}$, where the channel impulse response must vary slowly in time, and it can be assumed to be stationary. This statement means that $h_i(t, \tau_i(t)) = h_i(\tau_i)$ in that interval. To analyze (9), it is expressed as

$$\hat{R}(\tau) = \sum_{i=0}^{M-1} h_i(\tau_i)R_i(\tau), \tag{10}$$

being

$$R_i(\tau) = \frac{1}{L_{\mathrm{T}}} \sum_{j=0}^{Ln-1} \sum_{k=0}^{L_{\mathrm{n}}-1} c_j c_k \int_{t=T_{\mathrm{o}}}^{T_{\mathrm{o}}+T_{\mathrm{L}}} p(t-\tau_j - iL_{\mathrm{n}}) p(t-\tau-kL_{\mathrm{n}}) dt \tag{11}$$

a continous function that depends on the pulse form $p(t)$ used, which is known in advance. Then, $\hat{R}(\tau)$ represents an estimate of the auto-correlation function of the PN sequence in the analysed interval $[T_{\mathrm{o}}, T_{\mathrm{o}} + T_{\mathrm{L}}]$, where it contains information about the channel gain $h(\tau)$. Thus, the choice of the PN sequence is vital in order to achieve a unbiased estimate of $h(\tau)$. For instance, the chosen PN sequence must be balanced, which means the number of 1s in the sequence exeeds in one to the number of 0s. In [117], the author show how the PN sequence can be generated using shift registers and what characteristic should it have.

In orden to obtain $h(\tau)$ in the analysed interval, we need to calculate the auto-correlation function of the PN sequence $R(\tau)$ by

$$\begin{aligned} R(\tau) &= \frac{1}{L_{\mathrm{T}}} \int_{t=T_{\mathrm{o}}}^{T_{\mathrm{o}}+T_{\mathrm{L}}} p(t) p(t-\tau) dt \\ &= \left\{ \begin{array}{ll} 1 & \tau = T_{\mathrm{o}} \\ 1/L_{\mathrm{T}} & T_{\mathrm{o}} < \tau < T_{\mathrm{o}} + T_{\mathrm{L}} \end{array} \right\}. \end{aligned} \tag{12}$$

Please note that only one segment of $R(\tau)$ has been used in (12) since it is a periodic function with a period T_{L}. Finally, $h(\tau) = \sum_{i=0}^{M-1} h_i(\tau_i)\delta(\tau - \tau_i)$ can be estimated by combining (10) and (12). Using this approach, we can obtain a channel realization every interval $[T_{\mathrm{o}}, T_{\mathrm{o}} + T_{\mathrm{L}}]$. In a channel sounder, T_{L} is generally named as snapshot time, and it is the time that channel sounder need to estimate a realization of the channel impulse response. Moreover, the delay resolution is determined by chip time T_{n}.

4.2.2 **Measuring impulse response**

Using a channel sounder, it is possible to obtain a band-limited discrete representation for $h(t, \tau)$, denoted by $h[n, m]$, being n and m the time and delay indexes, respectively. The last result is normally taken sampling the impulse response $h(t, \tau)$ at equidistant time intervals Δt and at samples spaced $\Delta\tau$ in the delay domain. The delay resolution $\Delta\tau = 1/W$ takes into account the sampling theorem, where W represents the measurement bandwidth used in the channel sounder. Then, the discrete representation of the band-limited baseband wireless channel in a geographic area S is given by

$$h[n, m] = \sum_{i=0}^{N_{\mathrm{b}}-1} a_i[n, m] e^{j\theta_i[n,m]} h_{\mathrm{BL}}(m\Delta\tau - \tau_i[n]), \tag{13}$$

where N_{b} represents the total number of bins of the channel sounder, $\theta_i[n, m]$ represents the total discrete phase term, and $a_i[n, m]$ represents the discrete amplitude term. Also, $h_{\mathrm{BL}}(\tau)$ is the convolution of the band-limiting filters used at the transmitter and receiver side in the channel sounder.

In vehicular communications, the received signal fades owing to the mobility and the multipath propagation conditions. The fading can be described by a non-stationary

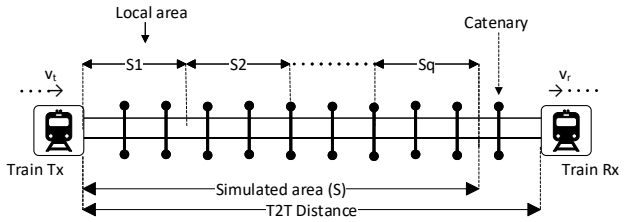

Figure 4.4: Simulation model for a railway approaching maneuver based on stationary region.

process, in which the channel statistics including $h[n, m]$ can change within a rather short period of time [120]. As a result, the implementation of (13) can not be performed assuming WSSUS for longer periods of time. To manage this drawback, the fading process can be considered locally stationary for an local area or stationary region S_q with finite extent in time, where $q = 1, \cdots, Q$ represents the local area index [121], and Q the total number of local areas in S. For instance, Fig. 4.4 shows how a geographic area S is divided into Q equally spaced areas S_q. Please note, S is the disjoint union of all S_q, such that $S = S_1 \cup S_2 \cdots \cup S_Q$.

The last approach is possible because the channel parameters change with a finite rate which usually represents a stationary distance d_s in the range of 20 to 40 λ, where $\lambda = c/f_\mathrm{c}$ represents the wavelength of the received signal [122]. The stationary time $t_\mathrm{s} = d_\mathrm{s}/\Delta v$ used in this thesis is chosen based on [20], where a stationarity analysis was carried out using the same data set and scenarios as in this thesis.

The measured impulse response in q^{th} local area is given by

$$h[n', m; q] = h[(q-1)N_\mathrm{s} + n', m], \tag{14}$$

where $n' = 0, \cdots, N_\mathrm{s} - 1$ is the time index in a local area, and $N_\mathrm{s} = t_\mathrm{s}/\Delta t$ is the number of measured impulse responses in a local area, being $\lceil x \rceil$ the ceiling function. Then, $h[n', m; q]$ represents a subset of $h[n, m]$ located in the q^{th} local area and limited by the time interval $[(q-1)N_\mathrm{s}; qN_\mathrm{s} - 1]$. This approach has been used in [121] to describe the non-stationary behavior of the channel using the local scattering function $P[n, m; q]$. In our case, we use $P[n, m; q]$ to estimate the scattering function $P[n, m]$ as the expectation of all $P[n, m; q]$ calculated in S.

4.2.3 Scattering function

In this subsection, we are particularly interested in characterizing the dispersion of the received signal through the wireless channel in the Doppler-delay domain. The estimation of the Doppler-delay spectrum, called scattering function in [123], is essential for this target. The scattering function $P[m, d]$ is a two-dimensional function of the propagation delay index m and the Doppler index d.

The procedure for calculating $P[m, d; q]$ from the measurement data consists of two steps as described in [19], where the WSSUS assumption is assumed for the local area. First, the local Doppler-variant impulse response is calculated using the discrete Fourier

transform by

$$s[m,d;q] = \frac{1}{N_{\mathrm{s}}} \sum_{n'=0}^{N_{\mathrm{s}}-1} h[n',m;q] e^{-j2\pi dn'/N_{\mathrm{s}}}, \tag{15}$$

and the local scattering function is then obtained by

$$P[m,d;q] = |s[m,d;q]|^2, \tag{16}$$

where $|x|$ is the magnitud of x and the Doppler domain has a resolution $\Delta\eta = 1/(\Delta t N_{\mathrm{s}})$. Please note, for each q^{th} local area, we estimated a value of the scattering function.

In addition, (16) is used in [121] to analyze the behavior of the local power delay profile $P_\tau[m;q]$, as well as the local Doppler spectral density $P_\eta[d;q]$. Both are defined by

$$P_\tau[m;q] = \frac{1}{N_{\mathrm{s}}} \sum_{i=-N_{\mathrm{s}}/2}^{N_{\mathrm{s}}/2-1} P[m,i;q], \tag{17}$$

and,

$$P_\eta[d;q] = \frac{1}{N_{\mathrm{b}}} \sum_{i=0}^{N_{\mathrm{b}}-1} P[i,d;q]. \tag{18}$$

The Doppler frequency in $P_\eta[d;q]$ varies from a positive value to a negative one, depending on the direction of the vehicle movement and the location of scatterers. Finally, an estimation of the scattering function in the wireless channel is carried out taking the expectation E[·] of $P[m,d;q]$, averaging the Q independent estimates of the scattering function as

$$P[m,d] = E[P[m,d;q]] = \frac{1}{Q} \sum_{q=1}^{Q} P[m,d;q]. \tag{19}$$

This approach allows balancing the noise variance. Furthermore, $P[m,d]$ can significantly change within a single scenario due to the change of relative speed and the emergence of moving scatterers.

4.2.3.1 **Processing the scattering function**

The WSSUS channel statistics, which are essential for the design of a communication system, are derived from the scattering function [123]. In this part of the chapter, we describe briefly how they are determined from $P[m,d]$ using the Fourier transform and integration techniques.

Relationships between the correlation functions, power spectral densities, and characteristic quantities of a WSSUS model were firstly shown by Bello in [113]. Fig. 4.5 shows a simplified diagram of these relationships, where, $C_\tau[d']$ is the frequency correlation function, $C_\eta[m']$ is the time correlation function, $P_\tau[m]$ is the average power delay profile, and $P_\eta[d]$ is the average Doppler spectral density.

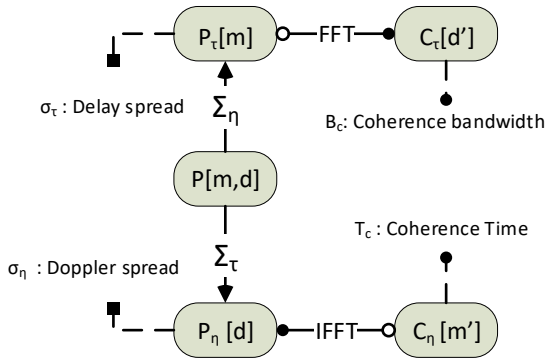

Figure 4.5: Processing the Doppler-delay spectrum in a WSSUS channel model.

The first and second central moments represent the mean and the variance of a function. These are used to estimate the delay spread σ_τ and Doppler spread σ_η from power spectral densities, using the following expressions:

$$\sigma_\tau = \sqrt{\frac{\sum_{i=0}^{N_\mathrm{b}-1} (i\Delta\tau - \bar{\tau})^2 P_\tau[i]}{\sum_{i=0}^{N_\mathrm{b}-1} P_\tau[i]}}. \tag{20}$$

and,

$$\sigma_\eta = \sqrt{\frac{\sum_{i=-N_\mathrm{s}/2}^{N_\mathrm{s}/2-1} (i\Delta\eta - \bar{\eta})^2 P_\eta[i]}{\sum_{i=-N_\mathrm{s}/2}^{N_\mathrm{s}/2-1} P_\eta[i]}}, \tag{21}$$

where $\bar{\tau}$ and $\bar{\eta}$ represent the mean delay and mean Doppler, which are calculated as

$$\bar{\tau} = \frac{\sum_{n=0}^{N_\mathrm{b}-1} i\Delta\tau P_\tau[i]}{\sum_{i=0}^{N_\mathrm{b}-1} P_\tau[i]}. \tag{22}$$

and,

$$\bar{\eta} = \frac{\sum_{n=-N_\mathrm{s}/2}^{N_\mathrm{s}/2-1} i\Delta\eta P_\eta[i]}{\sum_{i=-N_\mathrm{s}/2}^{N_\mathrm{s}/2-1} P_\eta[i]}. \tag{23}$$

Other important statistic parameters are the coherence time T_c and coherence bandwidth B_c, which can be estimated from the correlation functions based on a correlation

threshold β_c as

$$|C_\tau[B_c]| = \beta_c/C_\tau[0]$$
$$|C_\eta[T_c]| = \beta_c/C_\eta[0].$$

For instance, when β_c is defined above 0.5, it is estimated as the positive frequency in which the frequency correlation function drops 3 dB from its maximum value [123]. β_c and σ_τ are quantities which describe the dispersive nature of the channel. Instead, T_c and σ_η describe the time variation of the channel. Please note that all these quantities are statistical measures estimated from the scattering function, which characterizes the channel in a geographic area. The frequency and time selectivity of the channel can be derived from these quantities.

4.2.4 Signal fading

Using the statistic analysis of the channel impulse response presented in the previous sections, it is possible to obtain different parameters that characterize the channel fading. This phenomenon is considered as a stochastic process which causes that the transmitted signal undergoes a variation on the attenuation induced by the wireless channel. The fading can be classified as large-scale fading and small-scale fading depending on different propagation phenomena. Fig. 4.6 shows the kind of fading suffered by a signal which will be briefly introduced in the next subsection and are explained in detail in [111].

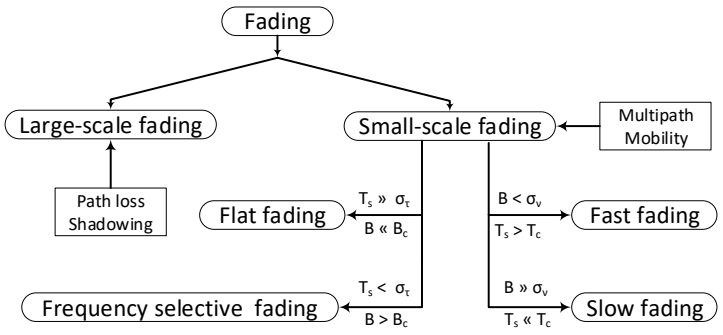

Figure 4.6: Types of fading in wireless signal.

4.2.4.1 Small-scale fading

Small-scale fading refers to the rapid changes of the amplitude and phase of a radio signal over short distance in relation to wavelength. For instance, the instantaneous received signal power may vary as much as 30 to 40 dB when the receiver is moved by only a fraction of a wavelength. Other effects of the small-scale fading over the signal are time and frequency dispersion. Whereas that time dispersion is caused by multipath propagation, the frequency dispersion is caused by random frequency modulation due to variations of Doppler spread on different multipath signals.

Fig. 4.6 shows how the type of fading that the transmitted signal undergoes when it is propagated through a channel depends on the relation of signal and channel parameters.

Given that, different transmitted signals can experience different types of fading on the same channel. The relevant parameters of the transmitted signal are bandwidth B and the symbol time T_s, while the channel parameters are the coherence time T_c, Doppler spread σ_ν, coherence bandwidth B_c and delay spread σ_τ. These parameters were introduced in the previous section. Please note, B_c and σ_τ as well as T_c and σ_ν, are inversely proportional.

Using delay spread as metric, if the wireless channel has a constant gain and linear phase response over a bandwidth which is smaller than the bandwidth of transmitted signal, the fading is classified as frequency selective fading. When this happens, the received signal includes multiples copies of the transmitted signal which are attenuated and delayed in time. In this case, the impulse response at any instant time $h(t = t_0, \tau)$, has multiples multipath components in the delay domain. On the other hand, the received signal will undergo a flat fading, where the channel impulse response can be approximated as a simple time-varying delta function $h(t)$, i.e, it has only one component in $\tau = 0$. Hence, no copies of the transmitted signal are observed in the receptor. The channel with flat fading causes deep fades, and thus a communication system may require more power to obtain a target bit error rate during the fade periods.

Using the Doppler spread as metric, if the coherence time of the channel is smaller than the symbol time of the transmitted signal, the fading is classified as fast fading. When this happens, the channel impulse response changes within the symbol duration, which causes frequency dispersion. The coherence time determines how fast $h(t, \tau)$ varies in time. Using a popular rule in digital communications, it can be calculated by $T_c = 0.423/\nu_m$, being ν_m the maximum Doppler spread which is calculated using (2). On the other hand, the received signal will undergo slow fading. The channel with slow fading can be considered to be static over one or several symbol intervals where $h(t, \tau)$ do not vary.

The aforementioned classification criteria, based on Doppler spread and delay spread, are independent. Then, a transmitted signal can experiment a frequency selective fading and slow fading at the same time. For instance, a wireless channel with slow and frequency selective fading is frequently observed in vehicular communication, where the amplitude and phase of the multipath components in $h(t, \tau)$ may assumed to be constant over M OFDM symbols.

4.2.4.2 **Large-scale fading**

Large-scale fading represents the average signal-power attenuation due to motion over large areas in relation to wavelength. It can affect the performance of a communication system when the received power is close to the receiver sensitivity. Large-scale fading is characterized by two known phenomena: path loss and shadowing. The path loss reflects the attenuation of the signal strength due to its propagation. A log-distance path loss model allows to calculate the path loss PL and assumes that average received signal power decreases logarithmically with the distance. Using this model, the path loss at a distance d is determined by

$$PL(d) = PL(d_0) + 10n \log(\frac{d}{d_0}), \tag{24}$$

where n is the path loss exponent which depends on the propagation space, and d_0 is a reference distance. When the propagation is carried out in free space, $n = 2$ and PL is calculated using Friis's equation [20].

Furthermore, the shadowing reflects a variation in the path loss calculated using (24) when the transmitted signal is obstructed by large objects. This effect is observed in a large number of measurement locations which have the same distance d, but have different levels of obstacles on the propagation path. As a result, the measured path loss $PL(d)$ is different although d has been kept constant. The measurement based results of $PL(d)$ indicate that it has a random behavior [111]. In orden to have in account the shadowing, a zero-mean Gaussian distribution random variable X_σ is added to (24), where X_σ and its standard deviation σ are expressed in dB.

The knowledge of propagation characteristic of a signal is essential to design a communication system. For instance, the choice of channel estimation method is different if the channel posses a fast or slow fading. For instance, the LS channel estimation method used in 802.11p works well in slow fading channels, but it decreases considerably its performance in fast fading channels. Also, the coverage area of the system can be optimized using accurate path loss models where parameters such as transmission power and receiver sensitivity are properly determined.

4.2.5 Channel modelling

The modeling techniques of a wireless channel may be split into three categories: deterministic modeling, stochastic modeling, and geometry-based stochastic modelling. Deterministic models characterize propagation by solving Maxwell's equations, usually applying techniques such as the finite difference method in the time domain or ray tracing in environments whose geometric and electromagnetic properties are fully defined. The ray tracing method is named in this way due to it attempts to trace every single ray from transmitter to the receiver [124]. The deterministic modeling technique is very exact, since for a specific propagation environment all the propagation mechanisms are considered at the cost of a higher computational complexity.

Geometry based stochastic channel modelling allows to incorporate the geometry of the propagation environment, thus introducing the non-stationarity of the channel. Using this model, the spatial distribution of scatterers are chosen stochastically [125]. Then, over this geometry, the laws of propagation of the electromagnetic waves are applied to determine the contribution of the scatterers to CIR.

Finally, stochastic channel models provide a suitable description of the channel without taking in account the geometry [113]. The stochastic channel models are extracted from measurement campaigns carried out in a target scenario. Then, a statistical analysis of CIR is carried out, extracting subsequently the channel statistics and parameters such as delay spread, Doppler spread, and coherent time among others. This type of channel model is of interest for this thesis. In the following, a methodology to derive a stochastic channel model based on measurements using a TDL technique will be introduced.

4.2.5.1 Tapped Delay Line (TDL) model

If WSSUS is assumed, a TDL model is an efficient way to model (14) using both (17) and (19). The TDL model has been widely used to model the wideband impulse response as the sum of delayed multipath components [126]. It is based on statistical parameters, where each tap is associated with an amplitude coefficient a_i, a delay τ_i, and a Doppler spectrum P_{η_i} that determines how fast a_i changes over time.

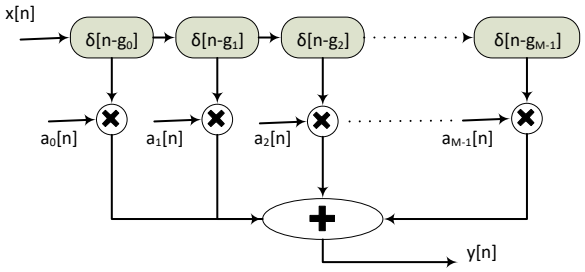

Figure 4.7: Representation of a TDL model as a time-varying FIR filter.

Fig. 4.7 shows a simplified representation of the TDL model as a time-varying finite impulse response (FIR) filter, where $g_i = \lceil (\tau_i - \tau_{i-1})/\Delta\tau \rceil$ represents the relative discrete delay and $a_i[n]$ represents the complex channel gain which depends on the amplitude coefficient of the tap and its Doppler spectrum. In addition, the Doppler spectrum for each tap P_{η_i} in a TDL model can be obtained from $P[m, d]$. Then, the implementation of a TDL model requires the knowledge of the following parameters:

- Number of taps M
- Delay associated with each tap τ_i
- Magnitude associated with each tap a_i
- Doppler spectrum associated with each tap P_{η_i}
- Distribution of tap amplitudes
- Speed range, distance, and bandwidth considered

The procedure for estimating all listed parameters from $h[n, m]$ will be explained in detail in the next sections.

The TDL model only simulates the small-scale channel behavior which is due to multipath effect and mobility. The maximum Doppler frequency simulated in a TDL model depends on f_c which can cause frequency distortions in the received signal. Please note that the Doppler frequency and the channel coherence time are inversely proportional [111]. Hence, measured channels with different f_c have different channel statistics. Thus, f_c must be chosen according to the intended communication system. In the literature, we have found two T2T channel models valid for frequencies below 1 GHz [15],[17], so they are not valid to evaluate the behavior of any vehicular communication system which operates in the 5.9 GHz band or millimeter band.

4.3 Computation of TDL model parameters

In this subsection, the methodology to derive the channel parameters is presented in detail, which allows to simulate a measured T2T wireless channel using a tapped delay line model.

4.3.1 Delay and power values in a TDL model

As it has been said, the TDL channel model is implemented as a transversal filter structure. It consists of M taps with a resolution in delay equal to $R_\tau = 1/W_\mathrm{p}$, where W_p is the bandwidth of the communication system whose performance will be evaluated through simulations employing the TDL channel model. The taps are characterized by a delay τ_i and a magnitude a_i $(i = 1, ..., M)$. Their estimates are based on the local power delay profile $P_\tau[m; q]$ which can be related to $h[n', m; q]$ substituting (15) and (16) in (17) as

$$P_\tau[m; q] = \frac{1}{N_\mathrm{s}} \sum_{n'=0}^{N_\mathrm{s}-1} |h[n', m; q]|^2, \tag{25}$$

where the square magnitudes of N_s impulse responses in the q^{th} local area were averaged. By taking the average power, we result in the slow fading characteristics of the local area. The definition of a local area has been introduced in Section 4.2.2.

In the following, the dynamic range in the interval $[i_q, i_q + bM]$ is established for each $P_\tau[m; q]$ based on a threshold β_t, where the part of the power density below the threshold is set to zero. Also, M is chosen based on both β_t and R_τ similar to [127], where β_t is used to eliminate noise which could be mistaken as a multipath component. The dynamic range is divided into M groups with $b = R_\tau/\Delta\tau$ samples. After that, the first sample of each group is indexed by m_i, where $i = 1, ..., M$ and m_1 is the index of the first nonzero sample after applying the threshold [128]. Next, the average delay for the i^{th} tap and q^{th} local area is calculated using the first moment of $P_\tau[m; q]$ as

$$\tau_{i;q} = \frac{\sum_{m'=m_i}^{m_i+b-1} m' \Delta\tau P_\tau[m'; q]}{\sum_{m'=m_i}^{m_i+b-1} P_\tau[m'; q]}. \tag{26}$$

From (26), Q independent samples of τ are obtained for each tap (one sample for each local area). An estimate of the average delay for each tap is achieved taking the expectation over $\tau_{i;q}$ as

$$\tau_i = E[\tau_{i;q}] = \frac{1}{Q} \sum_{q=1}^{Q} \tau_{i;q}. \tag{27}$$

Please note that the aforementioned τ_i values are generally not equidistant in delay. Also, the average power in each tap at S_q is calculated as

$$a_{i;q} = \frac{1}{b} \sum_{m'=m_i}^{m_i+b-1} P_\tau[m'; q], \tag{28}$$

and finally $a_i = E[a_{i;q}]$. The authors in[128] and [129] used (26) and (28) to develop a TDL model based on mobile radio propagation measurements. However, these models were not tested with a communication system to validate its performance.

Also, applying the dynamic range in $h[n', m; q]$, N_s complex amplitude samples for each tap are obtained by averaging the amplitudes in the delay domain as

$$r_{n',i;q} = \frac{1}{b} \sum_{m'=m_i}^{m_i+b-1} h[n', m'; q], \tag{29}$$

which are grouped into a three-dimensional complex matrix with $N_s \times M \times Q$ elements. This matrix will be used to estimate the Rice factor for each tap k_i in the next subsection.

4.3.2 Envelope amplitude distribution: k-factor

The amplitude distribution of the complex channel tap gain $r_{n',i;q}$ is analyzed in orden to take the statistical properties of the channel in a S_q. This gain can be modelled as a Gaussian random variable, and consists of a fixed component plus a zero-mean fluctuating component [130]. When there is a dominant component or LoS situation, a Ricean distribution is expected for the envelope of the complex channel tap gain R. The normalized Ricean probability density function (PDF) in [131] is given by

$$f_y(y) = 2y(1+k)e^{-k-(1+k)y^2} I_0[2y\sqrt{k(1+k)}], \tag{30}$$

where $y = R/E(R^2)$ represents the normalized envelope regarding the total mean power, $I_n[x]$ is the n^{th} order modified Bessel function, and k is the Rice factor. Also, y is calculated as the second moment of Rician distribution.

The Rician distribution is characterized by the k-factor, which indicates the severity of the fading in the channel. It can take values from $k = 0$, which represents a channel with deep fading, up to $k = \infty$, which corresponds to a channel without fading. If $k = 0$, the envelope of the complex gain is modelled as a Rayleigh distribution. In the literature, several methods have been shown to estimate the k-factor based on the envelope of received complex signal [130],[131],[132]. The two most common techniques are the method of moments (MoMs) and the method of maximun likelihood estimation (MLE).

MoMs is based on calculating the first and second moments of the time series data (envelope), where the theoretical PDF is matched with the moments of data for estimating the parameters of the distribution. Using this technique, the k-factor was estimated in [122] for a twelve-tap channel model. Furthermore, while the amplitude variation of the first tap was modelled following a Rician distribution, the rest of it followed a Rayleigh distribution.

On the other hand, MLE is based on maximizing the log-likelihood function of the joint PDF of N independent envelope outcomes. MLE is more reliable than MoMs and posses desirable features such as consistency and minimum squared error while having higher computational complexity.

4.3.2.1 Maximum Likelihood Estimation (MLE) method

The MLE method was derived by Talukdar in [131], where an explicit maximum-likelihood solution for (30) involves finding the k variable for which the joint density (J) of N_s independent outcomes will be maximum. Given that, we need to maximize

$$J = 2^{N_s}(1+k)^{N_s} y_1 \cdots y_{N_s} e^{-kN_s-(k'(y_1^2 \cdots y_{N_s}^2)} I_0[2y_1\sqrt{kk'}] \cdots I_0[2y_{N_s}\sqrt{kk'}], \tag{31}$$

being $k' = k + 1$. The maximum of the last expression can be obtained taking the logarithm of J and maximizing it with respect to k as

$$\ln J = N_{\mathrm{s}} \ln 2(1+k) - N_{\mathrm{s}} k - (1+k) \sum_{i=1}^{N_{\mathrm{s}}} y_i^2 + \sum_{i=1}^{N_{\mathrm{s}}} \ln I_0[2y_i \sqrt{k(1+k)}], \tag{32}$$

$$\frac{d}{dk} \ln J = 0, \tag{33}$$

where J is a function of one dimension which depend only on k. Working on the last equation, we can obtain a solution by finding the root of the equation

$$\frac{1}{1+k} + \frac{1+2k}{N_{\mathrm{s}}\sqrt{k(1+k)}} \cdot \sum_{n=1}^{N_{\mathrm{s}}} \frac{y'_j I_1(y'_n)}{I_0(y'_n)} = 1 + \frac{1}{N_{\mathrm{s}}} \cdot \sum_{n=1}^{N_{\mathrm{s}}} y_n^2, \tag{34}$$

where $y'_n = 2y_n\sqrt{k(k+1)}$. Equation (34) is non-linear and depends only on k so that it is difficult to find a closed-form solution. In order to solve this equation, a numerical method based on an exhaustive search of roots at a regular intervals was implemented in this thesis.

4.3.2.2 Using MLE to estimate the k-factor

The procedure for estimating the $k_{i;q}$ (k-factor of i^{th} tap at a local area S_q) is summarized as follows

- For each tap in a S_q, N_{s} independent samples of $r_{n',i;q}$ are taken ($r_{0,i;q}, r_{1,i;q}, \cdots, r_{N_{\mathrm{s}}-1,i;q}$), and its envelope $R_{n'}$ is calculated.
- The envelope is normalized with respect to the total mean power, i.e. normalized envelope $y_{n'} = R_{n'}/E[R_{n'}^2]$.
- Finally, the roots of (34) are calculated to estimate $k_{i;q}$.

Having estimated $k_{i;q}$, the k-factor for each tap i is obtained by the expectation $k_i = E[k_{i;q}]$. It will be used to characterize the amplitude distribution of the envelope.

4.3.3 Doppler spectrum per tap

The variation of $h[n,m]$ determines the Doppler spectrum of each resolvable tap. For implementing these Doppler spectra into the TDL channel model only the shape and the distribution are required to generate a channel representation with similar statistics and Doppler behaviour like the measured channel [128]. An estimation of the Doppler spectrum for the i^{th} tap can be obtained using the scattering function by

$$P_{\eta_i}[d] = \frac{1}{b} \sum_{n=0}^{b-1} P[m_n, d], \tag{35}$$

where $m_n = m_{\mathrm{los}} + ib + n$, and m_{los} is the average delay of the LoS component which can be estimated from $P_\tau[m]$. (35) allows to obtain a Doppler spectrum for each tap, which might have different statistical distributions [133].

Another approach is to use the same Doppler spectral shape for each tap. Given that, the Doppler spectrum for each tap is considered as a constant, and defined by

$$P_{\eta_i}[d] = P_{\eta}[d], \tag{36}$$

where $P_{\eta}[d]$ was defined in Section 4.2.3. This choice simplifies the model and reduces the implementation complexity. Then, the implementation of $P_{\eta_i}[d]$ into the TDL model is carried out using two operation modes which are named: DSP0 and DSP1. The DSP0 mode uses a Doppler spectrum approach by applying (36), while the DSP1 mode uses the Doppler spectrum approach based on $P[m, d]$ as defined in (35). Hence, we will validate in Section 4.6 how well these modes performs compared to measured channel impulse responses.

4.3.3.1 Shape of Doppler spectra

According to the shape of the Doppler spectrum, it can be classified as "Jakes", "Narrow", "Gaussian", "Flat" or "Bell" among others [134]. For instance, $P_{\nu_i}[d]$ was characterized for mobile communication at 5.3 GHz based on measurements and simulation results in [135]. In this article, it is asserted that the "Narrow" spectrum or "Rice" spectrum might be caused by a wave directly coming from the transmitter, which dominates the scattered waves. Instead, the "Flat" spectrum might be a consequence of the fact that both the scattering and the antenna are isotropic. The "Jakes" spectrum is mainly used for fixed-to-mobile communications, where one can assume that the contribution from the scattering comes equally from all directions. A detailed description of the derivation of the "Jakes" spectrum can be found in [125]. The "Gaussian" spectrum is mainly used in aeronautical channel models where the Doppler frequency possesses a strong directivity and decays exponentially .

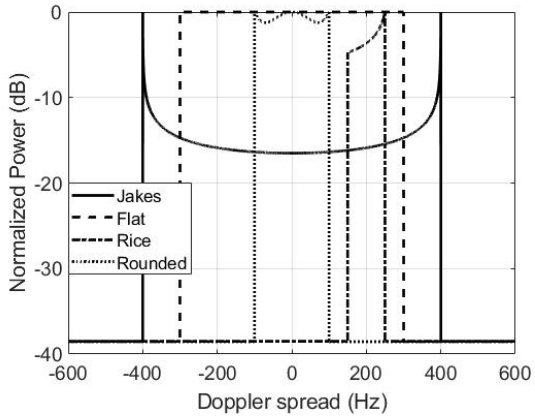

Figure 4.8: Shape of some Doppler spectra used in vehicular environments.

As was mentioned before, the knowledge of the shape of Doppler spectra is sufficient to define the time variation of the tapped delay line model. Then, Fig. 4.8 shows the shapes of some Doppler spectra which are widely used in vehicular channel models. These spectra are defined using the following analytical equations:

- "Jakes" spectrum:

$$P_\eta[d] = \frac{1}{\pi d_1 \Delta\eta \sqrt{1-(d/d_1)^2}}, |d| \leq d_1 \tag{37}$$

- "Flat" spectrum

$$P_\eta[d] = \frac{1}{2 d_1 \Delta\eta}, |d| \leq d_1 \tag{38}$$

- "Rice" spectrum

$$P_\eta[d] = \frac{A_a}{\pi d_1 \Delta\eta \sqrt{1-(d/d_m)^2}}, d_1 \leq d \leq d_2, \tag{39}$$

being

$$A_a = \frac{\pi}{2[\arcsin(d_2/d_m) - \arcsin(d_1/d_m)]}$$

- "Rounded" spectrum:

$$P_\eta[d] = C_r[a_o + a_2(\frac{d}{d_1})^2 + a_4(\frac{d}{d_1})^4], |d| \leq d_1, \tag{40}$$

being

$$C_r = \frac{1}{2\Delta\eta d_1[a_o + \frac{a_2}{3} + \frac{a_4}{5}]} \tag{41}$$

These equations are used in Matlab to simulate the Doppler frequency in a TDL model, where $\eta_{d_i} = d_i \Delta\eta$, being $d_i \in [-N_s/2; N_s/2 - 1]$, $i = 1, 2$ and $d_m = N_s/2 - 1$. Also, these free variables (η_{d_1} and η_{d_2}) are calculated applying a threshold to $P_{\eta_i}[d]$ between 20 and 30 dB with respect to its peak value. Also, the constants a_o, a_2, and a_4 determine the envelope of the "Rounded" spectrum, which are fixed to 1,-1, and 1 in Fig. 4.8, respectively. Furthermore, the analytical equations are used to determine the spectral shape that fits best with the measured Doppler spectrum such that the mean squared error is minimized.

4.4 Railway channel measurement campaigns

The wireless channels are generally modelled in a stochastic way, that means, the behavior of the channel is determined in a probabilistic way which can assume or not the underlying geometry of the scenario. This model can be extracted from measurement campaigns, where a statistic analysis of impulse response is carried out and some channel parameters (metrics) are extracted such as: delay spread, doppler spread among others.

Table 4.1: Research works on measurement based railway channel models.

	Train-to-infrastructure channel model					Train-to-train channel models			
No	**Scenario**	**Metric**	**Freq. (GHz)**	**TDL**	**No**	**Scenario**	**Metric**	**Freq. (GHz)**	**TDL**
[12]	Open field	-	< 6	yes	[15],[3]	RS, yard, shunting	PL,η, σ_τ	0.4	yes
[136],[137]	Hilly terrain, Rural	-	0.9	yes	[2],[19]	RS, Open field	PL,σ_η, σ_τ	5.8	-
[83],[138]	Viaduct	PL,k,ρ, AoA, η	0.93,2.35	-	[6]	RS, Open field, HT	PL,σ_η, σ_τ, k	5.2	-
[139]	Viaduct, tunnel, cutting	σ_τ, σ_η, η, τ, PL	0.95,2.15	yes	[18]	mixed	PL, τ, PER	0.45	-
[140]	Rural, cutting,HT,RS	k, η	2.6	yes	[18]	mixed	PL, τ, PER	0.45	-
[107],[141]	Rural	k,PL,σ_τ,η, τ	2.6, 1.89	-	[17]	Viaduct	PL, k, σ_τ	0.9	*
[142],[19]	RS	LC,AF,PL,k	0.93,5.2	-					

* A geometry based stochastic model (GBSCM) is presented;ρ =autocovariance ;PL=propagation loss;LC=level crossing rate;AF=average fade duration;RS=Railway Station;HT=Hilly terrain

4.4.1 State of the Art on Railway channel models

In this subsection, a summary of the most relevant measurement based railway channel models is carried out. Table 4.1 shows a summary of published channel models, although a review more detailed can be found in [11], [13]. These works are used to characterize the railway propagation environment. In some cases, they provide a TDL model which can be implemented in a channel emulator and used to evaluated the performance of any candidate railway technology.

In [11], the author provides a rich literature analysis of existing railway channel models based on measurements only for T2I communications. The work has permitted to identify a set of suitable TDL-based channel models for the following railway-related scenarios: hilly, rural, cutting and viaduct. Then, they were implemented in the Propsim F32 channel emulator and used to evaluate the performance of the Emulradio4Rail platform [11]. One of the conclusions of this work was that there is an urgent need for further work on channel characterization and modelling in railway environments, and especially for some specific measurement campaigns in the railway frequency bands.

Furthermore, the WINNER II channel model (link D2a), that was standardized by 3GPP, provides a TDL channel model for frequencies up to 6 GHz which is used for railways [12]. It was used in [143] to evaluated the performance of LTR-R in a HSR environment, where all OFDM configuration parameters are determined from the statistic of the channel, whose maximum delay is of 210 ns. Several channel models, measurement campaigns and propagation studies have been carried out for T2I communications [13],[14].

On the other hand, only a few studies have been reported for T2T communications and a research gap is observed. The first T2T studies based on measurements were carried out in [15],[3], where a TDL model was presented. These articles cover different radio phenomena in the 400 MHz band which include path loss, Doppler, fading, and delay spread. In [17] a geometry based stochastic model (GBSCM) is presented for a viaduct T2T environment in the 900 MHz band. The wireless channel is characterized with the propagation loss, the root mean square of the delay spread (RMS-DS), the k-factor and the covariance of the envelope.

In addition, some measurement campaigns have been carried out to characterize the propagation phenomena in T2T scenario and the results have been reported in [6],[2],[18]. In [20], the author presents a exhaustive study of stochastic T2T channel parameters for different scenarios, and how these can vary with the T2T distance and the selected scenario. Also, the stationarity behavior of the T2T propagation channel in time and frequency is investigated when the WSSUS condition is assumed. The results show that the quasi-stationary behavior is obtained for a time window of 65.5 ms. Also in [19], a wideband channel sounding campaign was carried out in the 5.9 GHz band, after which

time-variant statistical parameters of the T2T channel were derived for some use cases and driving maneuvers.

4.4.2 Measurement scenarios

In this chapter, we will develop a TDL model for some T2T scenarios based on a measurement campaign developed by DLR within the scope of the Roll2Rail project. Setting of the T2T measurement campaign are listed in Table 4.2 and are explained in detail in [6]. The DLR RUSK channel sounder was used in SISO mode to measure the time-varying channel impulse response $h[n, m]$ for some scenarios and maneuvers. For all measurements, the operating center frequency was 5.2 GHz with a bandwidth W = 120 MHz and a snapshot rate of 488 Hz.

Table 4.2: Settings of DLR RUSK channel sounder[6].

Parameters	Value
Central Frequency f_c	5.2 GHz
Bandwidth W	120 MHz
Snapshot rate Δt	1.024 ms
EIRP	33 dB
Number of bins N_b	1537
Antenna type	omnidirectional
Antenna Gain	6 dBi

EIRP = Effective Isotropic Radiated Power

The measurements were conducted on a 205 km long high speed railway (HSR) track between Naples and Rome, where Trenitalia Frecciarossa ETR 500 trains were used (Fig. 4.9). The trains were driving on parallel tracks for safety reasons. In the measurement, two HUBER+SUHNER (SWA-0859/360/4/0/DFRX302) rail antennas of 6 dBi gain were used, which were mounted in the roof of each train. These antennas were designed to meet the special requirements of railway applications including high current and high voltage protection [144]. They fit best in case of RF characteristics at 5.2 GHz as well as for 5.9 GHz. Also, each train was equipped with two GNSS receivers and inertial measurement units, which allow to record the train position, velocity and raw measurements. These raw measurements include pseudo range, carrier phase and Doppler [6].

Figure 4.9: Trenitalia Frecciarossa ETR 500 HST [6].

From the DLR measurement campaign, we analyze the following scenarios:

- Hilly Terrain: It is characterized by dense scatterers throughout the environment with objects distributed irregularly and non uniformly (Fig. 4.10a). Thus, the received signal will be subject to multipath fading. The LoS component can be observable for large distances up to 800 m as the railway track runs straight and no larger obstacles occur (please see Fig. 4.11). Also, long lasting multipath components can be received, which can provoke the dispersion in both delay and Doppler domains. In this scenario, both trains travel in the same direction in an approaching maneuver with a constant relative speed of 40 km/h.
- Railway Station: It is characterized by a dense network of railway infrastructure like platforms, buildings, other trains, overhead systems, and signaling systems as depicted in Fig. 4.10b. As a result, this scenario is rich of reflecting and scattering objects. Hence, low values of k-factor can be expected, although the LoS component is constantly observable. In this scenario, an approaching maneuver was carried out, where one train was standing on the platform and the other one decelerated from 50 km/h to 0 km/h.

(a) Hilly Terrain scenario

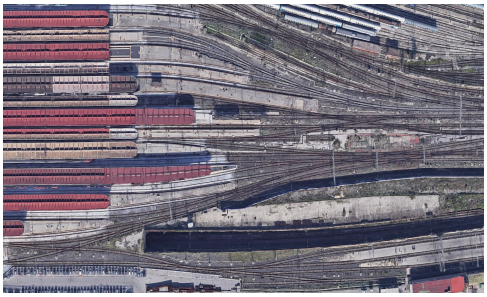

(b) Napoli Centrale Railway Station

Figure 4.10: Considered scenarios in the DLR measurement campaign [86].

In both scenarios, the overhead line system with the catenary and the supporting masts are kept in all environments and have a significant influence on the wireless propagation [86]. The distance between the adjustable catenaries can be up to 60 meters and it represents a propagation delay of about 200 ns.

4.4.3 Considered T2T distances

The channel statistics for each considered scenario are analyzed in three segments as

- Short distance: 5-100 m
- Medium distance: 400-500 m
- Large distance: 800-900 m

The subdivision in segments is motivated by the number of resolvable multipath components N_{rm}, which is correlated with the T2T distance. This effect can be seen in Fig. 4.11, where N_{rm} changes for the analyzed local areas. As a result, different dynamic ranges for the power are obtained for the local areas based on a threshold β_{t}. Thus, a multipath component is resolvable when its normalized power is higher than β_{t}.

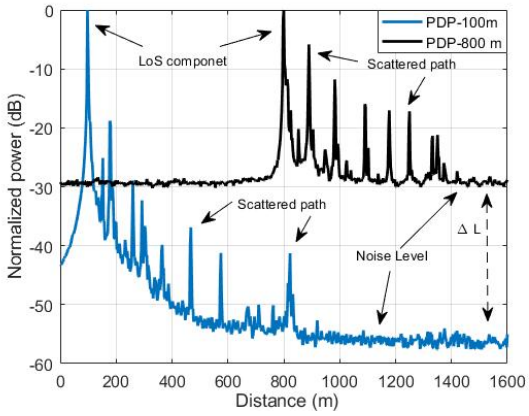

Figure 4.11: Measured normalized power delay profile (PDP) for two local areas located at train-to-train distances of 100 and 800 meters, values on the distance axis are obtained multiplying the delay with the speed of light.

In addition, different noise levels are observed as a consequence of the normalization operation in Fig. 4.11. The power interval between them (ΔL) can be interpreted as the path loss that the transmitted signal suffers in $[r_1; r_2]$ interval. Then, $\Delta L \approx 10\gamma \log(r_1/r_2)$ can be obtained considering that the shadow fading is assumed to be a Gaussian distributed random variable with zero mean and variance σ^2. γ describes the path loss exponent, and r_1 and r_2 the average distances in two local areas (S_q and $S_{q'}$) in S. Using the path loss model shown in [86] for this scenario, where $\gamma = 3.1$, it gives as a result $\Delta L \approx 28$ dB. This result matches well with what is observed in Fig. 4.11.

For future T2T applications, it is important to know the statistics of the wireless channel at certain T2T distances. For instance, in the use case of smart train composition coupling, the T2T distance must be kept within a certain distance range when both trains become virtually coupled [2].

4.5 Results and analysis of the proposed T2T models

In this section, the procedure shown in the previous sections is applied to six different propagation scenarios and the obtained results are shown and analyzed. The considered wireless channels are named from MD1 to MD6, which differ in the propagation scenarios (Hilly Terrain and Railway Station) and the considered T2T distances (short, medium and large). Also, the doppler, delay and time magnitudes are related and analyzed using the spectral density functions.

4.5.1 Spectral analysis

In the following, we use the power density functions defined in Section 4.2.3 to show how the power is distributed in time, delay and Doppler domains. This analysis will help us understand how the driving maneuver, scatterers density, and relative speed of the train influence the channel variability and gain.

4.5.1.1 Doppler-delay spectrum

The Hilly Terrain scenario and short distances are considered in the MD1 channel model. Fig. 4.12a shows the normalized Doppler-delay spectrum for this scenario, where the delay and the Doppler frequency can be related to the power of any received multipath component. Given that the relative speed Δv is constant, we can clearly identify the Doppler frequency η_{los} of the LoS component and the maximum Doppler frequency η_{max} of the reflecting and scattering obstacles located along the track. Using (2) with $\alpha = 0$, these Doppler frequencies can be calculated by

$$\eta_{\text{los,max}} = \frac{(v_{\text{t}} \mp v_{\text{r}}) f_{\text{c}}}{c},$$

where $v_{\text{t}} = 50.00$ km/h and $v_{\text{r}} = 10.00$ km/h, as shown in Fig. 4.4, represent the speed of the rear and front trains, respectively. Then, the LoS component is located at $\eta_{\text{los}} = 193$ Hz and it describes a red vertical line in the spectrum. Positive η_{los} indicates that the trains are approaching. In contrast, the scattering components, with less power, exhibit a maximum Doppler of $\eta_{\text{max}} = 289$ Hz.

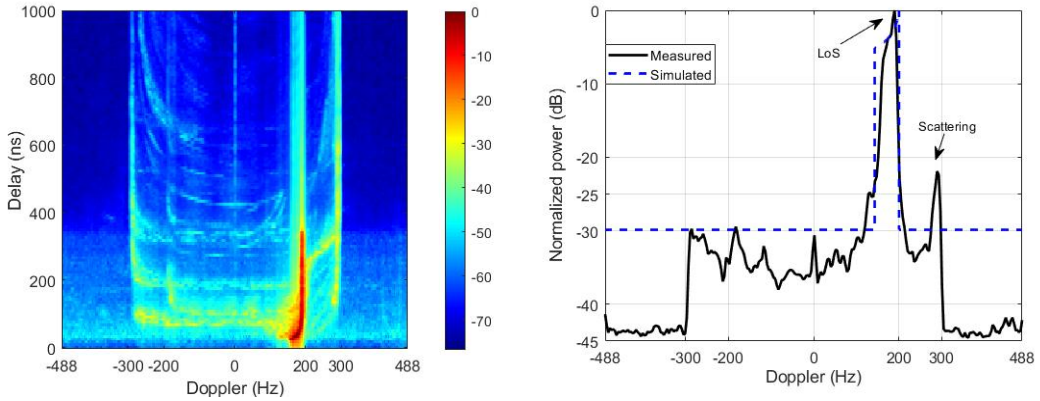

(a) Normalized Doppler delay spectrum $P[m, d]$ (b) Average Doppler spectrum $P_{\eta}[d]$

Figure 4.12: MD1 channel model is modelled in a Hilly Terrain scenario with short distance.

Please note, that when the angle of arrival α of the scattered path varies from 0 to π radians, the scattering Doppler frequency can become negative and takes a minimum value of $-\eta_{\text{max}}$. Moreover, the delay of the LoS component varies from 341 to 25 ns, which corresponds with the analyzed interval (100-5 m). In addition, when the T2T distance gets close to 15 m, both trains are about to cross and η_{los} starts to decrease since its angle of arrival begins to vary from 0 to $\pi/2$ radians. Moreover, the number of multipath components increases due to reflection from the metal structure of the train and multipath components with similar power to LoS component can be observed. These effects can be seen in Fig. 6a for delay below of 50 ns.

The average Doppler spectrum is computed for this scenario and shown in Fig. 4.12b, where the Doppler frequencies $\eta_{\text{los,max}}$ can be easily determined since they reach the peak power. The power of the LoS component exceeds the maximum multipath component by more than 20 dB. As it can be observed, the shape of the Doppler spectrum matches a “Rice” type. The “Rice” spectrum is expected to occur in scenarios where the LoS component is dominant [135]. In addition, the simulated Doppler spectrum is shown in

this figure as dashed blue line. The analytical expressions of all simulated Doppler spectra were presented in Section 4.3.3.1.

Different propagation conditions can be obtained if we select the MD4 channel model, where the Railway Station scenario and medium distance are considered. In this scenario, $v_r = 0$ and v_t varies from 40.82 to 36.08 km/h. Since the relative speed is not constant, $\eta_{los,max}$ can overlap and scattering components can be observed close to $\pm\eta_{los}$. Fig. 4.13a shows the normalized Doppler-delay spectrum for this scenario. The maximum Doppler component is determined by the LoS component, which slightly varies from 196.54 to 173.71 Hz (semi-curved red line). In addition, some scattering Doppler frequencies are densely located close to η_{los}. This finding indicates that this scenario is very rich in reflecting obstacles and a high rate of scatterers is expected.

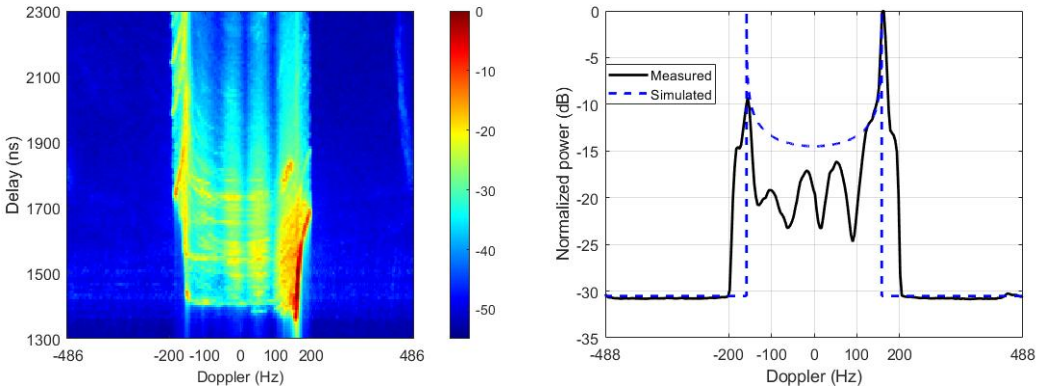

(a) Normalized Doppler-delay spectrum $P[m, d]$ (b) Average Doppler spectrum $P_\eta[d]$

Figure 4.13: MD5 channel model is modelled in a Railway Station scenario with medium distance, where the part of $P[m, d]$ below 1300 ns is not shown as it corresponds to noise.

The delay of the LoS component varies from 1692 to 1350 ns, which corresponds with the analyzed interval (500-400 m). Also, if the delay is constant, for instance 1550 ns, there are scatterers with significant power around -20 dB, whose Doppler vary in the $[-\eta_{los}, \eta_{los}]$ interval. In the spectrum, they can describe a horizontal line and it might be identified as reflections stemming from the catenaries. Then, some horizontal lines are seen in $P[m, d]$ in both scenarios, since the catenaries are periodically located long the track.

Fig. 4.13b shows the average Doppler spectrum for this scenario, where scatterers with both positive and negative Doppler frequencies can be observed. Also, two peak powers are located with a Doppler frequency at ± 158 Hz of different powers. The difference in power may be attributed to both the non-uniform distribution of the scatterers in the scenario and the LoS component that appears with positive Doppler, which can be verified in Fig. 4.13a. In this scenario, the shape of the Doppler spectrum is identified as "Jakes" type.

4.5.1.2 **Delay-time spectrum**

Using the time-varying power delay profile $P_\tau[m; q]$, we can analyze the amount of energy that arrives at the receiver with certain delay. Fig. 4.14 shows the behavior of $P_\tau[m; q]$ for the scenarios aforementioned using a time interval of 60 s. The results

indicate that the multipath components (MPCs) have a regular pattern, which can be seen in the delay-time spectrum with parallel lines that are oblique to the LoS component. Hence, we have a very strong indication that regularly appearing strong MPCs are caused by the overhead line support [86], which is located regularly along the track.

Also, by analysing the LoS component in Fig. 4.14, it is easy to note that the delay of the LoS component describes the trajectory carried out during the driving maneuver. For instance, in the first 30 s in Fig. 4.14a, both trains are approaching, the T2T distance decreases from 500 to 5 meters and the delay of the LoS component decreases proportionally to this.

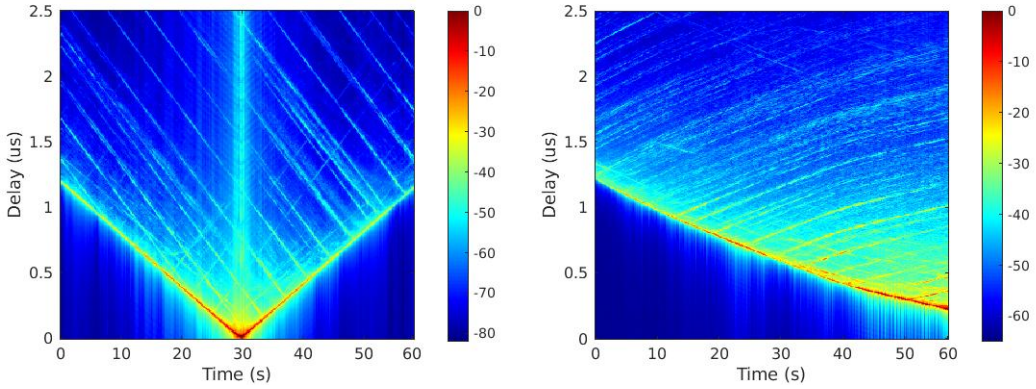

(a) Overtaking maneuver in Hilly Terrain (b) Approach maneuver Railway Station

Figure 4.14: Time-varying power delay profile $P_\tau[m;q]$ using a time interval of 60 s.

Fig. 4.14a shows the PDP for an overtaking maneuver, where both trains cross around of 30 s (crossing point). In this point, the amplitude of LoS component reaches its maximum value. Also, as expected it is inversely proportional to the delay since propagation losses decreases with the T2T distance. For instance, if the delay of LoS component vary from 1107.8 ns to 18.7 ns, its normalized power varies from -28 dB to 0 dB, respectively. It is important to note that the longer $P_\tau[m;q]$ around the crossing point are caused by the energy spreading effect of Inverse Discrete Fourier Transform (IDFT). This effect is not so noticeable for other point since their power is much lower.

On the other hand, Fig. 4.14b shows the PDP for an approach maneuver. In this case, the relative speed is not constant, it vary from to 40 km/h to 10 km/h. As a result, the delay of the LoS component describes a semi-curve line, whose minimum values is of 600 ns and the T2T distance decreases from 500 to 88 meters. Also it can see that this scenario presents a higher rate of multipath components that the scenario shown in Fig. 4.14a, which is expected due to the high density of reflective objects in a Railway Station scenario.

Using the segment division done in the previous section, the delay of the energy that arrives at the receiver in short and medium distances can be identified in Fig. 4.14a using time intervals of 36-45 s and 0-9 s, respectively. On the other hand in Fig. 4.14b, a time gap of 0-11 s for medium distance can be described.

4.5.1.3 Doppler-time spectrum

Using the time-varying Doppler spectrum density $P_\eta[d;q]$, we can analyze how much energy arrives at the receiver with certain Doppler. Fig. 4.15 shows the behavior of $P_\eta[d;q]$ for the previously analyzed scenarios in a time interval of 60 s. Although, the Doppler of the LoS component is concentrated around $\pm\eta_{\text{los}}$ in Fig. 4.15a, it varies from 204 to 100 Hz in 4.15b since the relative speed is not constant in this case.

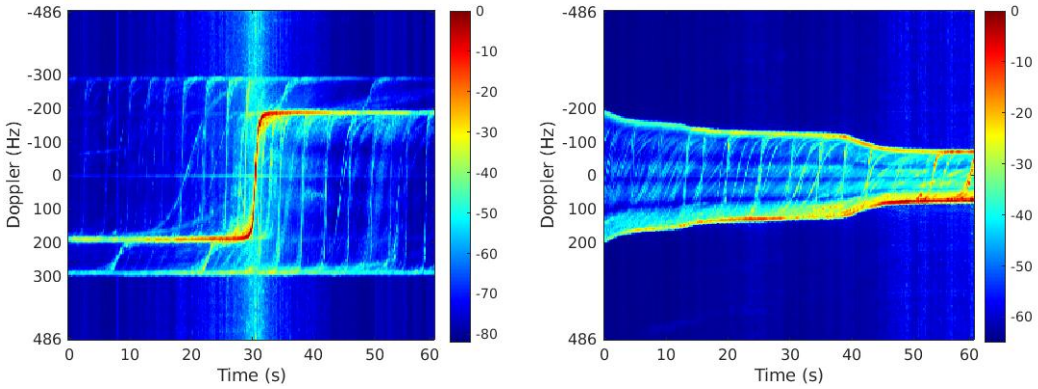

(a) Overtaking maneuver in Hilly Terrain (b) Approach maneuver Railway Station

Figure 4.15: Time-varying power spectrum density $P_\eta[d;q]$ using a time interval of 60 s.

The Doppler power spectral density is related to the angle of arrivals of the multipath components and the direction of movement of the receiver, as shown in (2). The sign of the instantaneous Doppler frequency depends on the direction of the velocity vector of the train with respect to the transmitter. This causes the effect shown in Fig. 4.15a, where the Doppler frequency of LoS component concentrates around $\pm\eta_1$ and it changes abruptly when the trains cross in the crossing point. In this case, the transmitter is located in the rear train and the receiver in the front train. A abrupt change is observed around 30 s where η_{los} change from 188 Hz to -188 Hz.

In addition, the Doppler of MCPs are fully resolved in both scenario. They are concentrated in the $[-\eta_{\max}, \eta_{\max}]$ interval, being $\eta_{\max}$ equal to 288 Hz and 204 Hz in the analyzed scenarios, Hilly Terrain and Railway Station, respectively. Remember that, $\eta_{\max}$ represents the maximum Doppler of the scatterings component, and it was introduced in Section 4.5.1.1. Also, the MCPs would be identified as replicas of the LoS component in Hilly Terrain scenario (Fig. 4.15a)

Using the segment division done in the previous section, the Doppler of the energy that arrives in short and medium distances at the receiver, can be identified in Fig. 4.15a using a time intervals of 36-45 s and 0-9 s, respectively. On the other hand, in the Fig. 4.15b, it can be identified using a time interval of 0-11 s for medium distance.

4.5.2 T2T Channel parameters

In this section, the results of channel parameters for all considered scenarios are shown. Then, they can be used to model the T2T wireless channel using a TDL model.

4.5.2.1 Doppler spectrum per tap

The distribution of Doppler spectra in all considered scenarios are listed in Table 4.3, where the η_{d_1} and η_{d_2} frequencies, which are expressed in Hertz (Hz), specify the spectrum (see Section 4.3.3.1). Using this table, the modelled Doppler spectra can be implemented in the TDL model using the DSP0 and DSP1 modes, as explained in Section 4.3.3. In addition, it is observed that in all analyzed scenarios, the first tap follows a "Rice" type Doppler spectrum, which indicates that the LoS component is always dominant even though large distances are considered. Another finding is that the taps can exhibit different spectrum types for the same scenario.

Table 4.3: Proposed Doppler spectrum for each tap.

		MD1			MD2			MD3			MD4			MD5			MD6		
Mode	**Taps**	η_{d_1}	η_{d_2}	**shape**	η_{d_1}	η_{d_2}	**shape**	η_{d_1}	η_{d_2}	**shape**	η_{d_1}	η_{d_2}	**shape**	η_{d_1}	η_{d_2}	**shape**	η_{d_1}	η_{d_2}	**shape**
DSP0	$1 \rightarrow M$	143	200	Rice	178	216	Rice	280	312	Rice	75	-	Flat	158	-	Jakes	266	-	Jakes
DSP1	1	116	201	Rice	174	271	Rice	166	220	Rice	6	36	Rice	120	170	Rice	185	277	Rice
	2	147	208	Rice	174	216	Rice	181	224	Rice	31	-	Jakes	109	174	Rice	32	281	Rice
	3	170	224	Rice	174	212	Rice	174	312	Rice	73	-	Jakes	166	-	Jakes	-78	277	Rice
	4	155	204	Rice	170	212	Rice	185	250	Rice	79	-	Flat	190	-	Jakes	262	-	Jakes
	5	304	-	Jakes	170	304	Rice	166	315	Rice	78	-	Flat	174	-	Jakes	266	-	Jakes
	6	304	-	Jakes	292	-	Jakes	189	312	Rice	76	-	flat	151	-	Jakes	269	-	Jakes
	7	304	-	Jakes	250	304	Rice	185	315	Rice	76	-	Flat	157	-	Jakes	262	-	Jakes
	8				289	-	Jakes	269	315	Rice	76	-	Flat	162	-	Jakes	262	-	Jakes
	9				289	-	Jakes	266	315	Rice	74	-	Flat	158	-	Jakes	266	-	Jakes
	10				289	-	Jakes	277	315	Rice	74	-	Flat	158	-	Jakes	269	-	Jakes
	11				292	-	Jakes	266	315	Rice	74	-	Flat	166	-	Jakes	262	-	Jakes
	12				266	-	Jakes	281	315	Rice				158	-	Jakes	266	-	Jakes
	13							273	315	Rice				158	-	Jakes	262	-	Jakes
	14							289	315	Rice				158	-	Jakes	266	-	Jakes
	15							285	315	Rice				158	-	Jakes	266	-	Jakes
	16							281	315	Rice				158	-	Jakes	266	-	Jakes

η_{d_1} and η_{d_2} are expressed in Hertz (Hz) which define the modelled Doppler spectra (see Appendix A)

4.5.2.2 Amplitude, delay and k factor per tap

Following the procedure explained in Section 4.3, the parameters of the TDL model were calculated for all considered scenarios. The tap resolution is equal to 100 ns since $W_{\mathrm{p}} = 10$ MHz (bandwidth considered for 802.11bd). The accuracy of estimated parameters were chosen using an confidence interval of 95 %, where a accuracy of one digit after the decimal point for a_i, 2 ns for τ_i and 0.5 dB for k_i were used. Please see Appendix 1 where the confidence interval for the proposed TDL models are shown.

Table 4.4 shows the power, delay, and k-factor for each resolvable tap in each considered model.As expected, the results always show that the first tap exhibits higher k-factor

Table 4.4: Parameters of the proposed channel models: Power, delay and k-factor.

	MD1			MD2			MD3			MD4			MD5			MD6		
Taps	a_i (dB)	τ_i (ns)	k_i (dB)	a_i (dB)	τ_i (ns)	k_i (dB)	a_i (dB)	τ_i (ns)	k_i (dB)	a_i (dB)	τ_i (ns)	k_i (dB)	a_i (dB)	τ_i (ns)	k_i (dB)	a_i (dB)	τ_i (ns)	k_i (dB)
1	0	0	12.5	0	0	9.0	0	0	6.0	0	0	6.0	0	0	4.0	0	0	4.0
2	-17.3	58	-6.0	-16.3	110	-4.0	-11	104	-4.0	-16.0	94	-5.0	-8.1	106	-8.5	-7.4	100	-9.0
3	-21.5	178	0.5	-20.3	204	-0.5	-14.4	200	-8.0	-18.5	194	1.0	-11.6	200	-7.5	-10.2	196	-7.0
4	-24.8	260	0.0	-18.0	320	0.0	-13.1	320	-2.0	-21.6	298	0.5	-14.2	308	-7.0	-12.1	304	-7.0
5	-30.2	380	-4.5	-18.8	410	-3.5	-13.2	406	-2.0	-21.7	400	0.5	-15.7	408	-7.0	-12.5	402	-5.0
6	-28.4	460	-4.0	-23.0	522	-5.5	-17.4	510	-9.5	-22.9	496	-2.0	-15.7	514	-3.5	-13.6	504	-4.5
7	-29.9	538	-3.0	-18.8	610	1.0	-14.7	620	-4.0	-25.3	598	-2.0	-16.4	608	-1.5	-15.0	604	-2.5
8				-24.1	722	-7.0	-11.3	708	2.5	-25.2	688	0.0	-18.2	706	-3.0	-16.0	704	-9.0
9				-20.9	836	-4.5	-17.3	806	-8.0	-27.1	798	-3.5	-19.2	808	-3.0	-16.3	804	-5.5
10				-23.9	914	-2.5	-19.3	912	-16.0	-27.0	902	-2.5	-20.2	908	-2.5	-16.5	904	-2.0
11				-23.9	1024	-10.0	-15.1	1014	-5.0	-21.1	1008	-0.5	-20.7	1006	-5.0	-17.2	1002	-4.5
12				-19.7	1106	-2.5	-16.2	1104	-1.5				-21.5	1110	-4.5	-18.1	1098	-4.5
13							-19.0	1212	-12.5				-22.8	1214	-3.0	-18.4	1200	-5.0
14							-15.4	1312	-5.5				-21.9	1310	-4.5	-18.5	1302	-8.5
15							-17.3	1404	-6.0				-20.3	1414	-3.5	-18.2	1404	-3.0
16							-17.5	1512	-12.0				-22.5	1502	-3.0	-19.4	1500	-7.5

than the rest. As a consequence, the amplitude of the first tap is simulated following a Rician distribution, while the other ones follow a Rayleigh distribution. The maximum delay $\tau_{\max} = \tau_{\mathrm{M}} - \tau_1$ is higher than 1 μs except in the MD1 model, where $\tau_{\max}$ is equal to 537 ns. The maximum number of resolvable taps is equal to 16 in the MD3, MD5 and MD6 models. Thus, the proposed channel models can be emulated using a channel emulator which allows to carry out a system-level simulation [145].

Furthermore, we consider that the differences among the three proposed channel models (MD4, MD5 and MD6) in Railway Station are caused by two variables: T2T distance and relative speed. While the T2T distance is correlated with the number of multipath components (see Section 4.4.3) which affects the obtained value M and the relative power of each tap, Δv determines the free degrees (η_{d1} and η_{d2}) of the shape of P_{η_i}. On the other hand, these differences in Hilly Terrain would only be caused by the T2T distance since Δv is constant for the three considered propagation scenarios.

4.5.2.3 Statistics of the proposed channel model

Channel statistics change considerably from one environment to another, over time and along T2T distance [19]. We are interested in investigating their averaged values and its dependence on the T2T distance. They are obtained based on $P[m, n]$ by using the diagram shown in Fig. 4.5. The obtained statistics of the analyzed channels are shown in Table 4.5. It is observed that both delay spread σ_τ and Doppler spread σ_η are correlated with the T2T distance. For instance, when we move from short distance (MD1) to medium distance (MD2), the σ_τ increases from 83.13 to 192.91 ns, while σ_η increases from 37.44 to 106.85 Hz.

Table 4.5: Channel statistics of the analyzed wireless channels.

Model	Scenario	Distance (m)	σ_τ(ns)	$\bar{\tau}$(ns)	σ_η(Hz)	$\bar{\eta}$ (Hz)	T_c (ms)	B_c (MHz)	k_1 (dB)	M	β_t (dB)	t_s (ms)	N_h	Δv (km/h)
MD1	HT	5-100	84	96	37	178	74.8	4.87	12.5	7	30	207.7	8777	40.00
MD2	HT	400-500	192	1522	107	177	59.7	1.94	9.0	12	20	207.7	8777	40.00
MD3	HT	800-900	820	2974	218	137	46.2	1.58	6.0	16	20	207.7	8777	40.00
MD4	RS	5-100	86	106	18	27	77.2	5.57	6.0	11	25	756.5	39000	5.49
MD5	RS	400-500	290	1600	126	96	63.0	1.81	4.0	16	20	216.1	10250	38.45
MD6	RS	800-900	572	2940	233	92	26.2	1.34	4.0	16	20	167.5	6408	49.61

HT = Hilly Terrain; RS = Railway Station; N_h = total number of used impulse responses; $\bar{\tau}$ = mean delay; $\bar{\eta}$ = mean Doppler

These results indicate that the channel dispersion in time-frequency domains increases with the distance, which is reasonable to expect since the number of resolvable multipath components increases with distance (see Fig. 4.11). Please note that the T2T distance determines the geometric relation between the trains and the environment, thereby this relation would be reflected in the channel statistics. The distance-dependent effect is also seen in k_1, which relates the power of the LoS component and the scattered paths. Thus, k_1 varies from 12.5 to 6.0 dB when short (MD1) and large (MD3) distances are considered in Hilly Terrain.

These finding match with the results shown in [20] where the behaviour of the k_1, σ_τ, and σ_η parameters with respect to T2T distance are shown. In addition, the coherence time T_c and the coherence bandwidth B_c are also shown in Table 4.5, being both dependent on the distance too. The knowledge of the wireless channel statistics is very important in order to optimize the design of any communication system. For instance, σ_τ determines the length of cyclic prefix in orthogonal frequency division multiplexing (OFDM) systems[146], while σ_η determines the separation of midambles in 802.11bd.

4.6 Analysis and validation of the Proposed Channel Models

In this section, the novel 802.11bd protocol and measured channel impulse response (CIR) are used to validate the proposed TDL channel models. A validation framework is proposed and the obtained results are shown and analyzed. 802.11bd introduced in Section 2.3 has been chosen for the validation, since the T2T communication is one of its use cases [41].

4.6.1 Performance-based validation

In order to evaluate the performance and the accuracy of the TDL models proposed in the previous section, a validation framework is implemented where the wireless channel is modelled in two different paths: using the measured channel impulse response $h[n, m]$ or the TDL channel model. Then, the performance results for both validation paths are compared and analyzed using packet error rate (PER) versus E_b/N_0, where E_b denotes the energy per bit and N_0 the noise power spectral density which is defined as in [51].

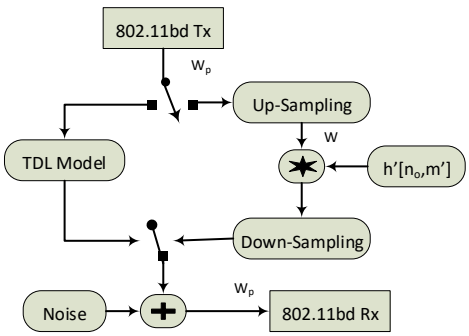

Figure 4.16: Diagram of the validation framework of the proposed channel models.

The baseband validation framework is shown in Fig. 4.16. Using the reference validation path, the switch will move to the right. Firstly, the 802.11bd signal has to be up-sampled as its bandwidth W_p is usually lower than the measurement bandwidth W. Secondly, the convolution process is carried out to emulate the impairments of the wireless channel. On the convolution, the normalized impulse response $h'[n_o, m']$ with discrete time index n_o is obtained by taking the samples within the dynamic range and normalizing them as

$$h'[n_o, m'] = \frac{h[n_o, i_p + m']}{\sum_{i=0}^{Mb-1} |h[n_o, i_p + i]|^2} \tag{42}$$

being $p = \lceil n_o/Q \rceil$ and $m' \in [0, Mb-1]$. Please note that $h[n_o, m']$ is a sample of the CIR from stored measurement data.

The dynamic range $[i_p; i_p + bM]$ is the same as the one applied in Section 4.3.1 and contains the significant energy of $h[n, m]$, smoothing in this way the noise. The normalization process in (42) removes the large-scale fading effect and its dependence with distance. Finally, the convolved output is downsampled. After adding the noise, it is processed at the receiver.

For the left path, the proposed TDL channel models are used to implement a Rician channel whose parameters are chosen from Table 4.3 and 4.4, according to chosen TDL model. Please note, the Doppler spectrum $P_{\eta_i}[d]$ can be simulated in the Rician model in two different modes: DSP0 or DSP1, as was explained in Section 4.3.3. Then, noise is added and the signal is processed at the receiver.

4.6.2 Simulations results

Using the diagram in Fig. 4.16, the performance results of 802.11bd are shown for each proposed path. Next, the PER performance of 802.11bd and 802.11p are compared using the MD1 channel model at different MCS. The simulation parameters are shown in Table 4.6, in which the packet size is set up to 400 bytes.

Table 4.6: Simulation parameters.

Parameters	**802.11bd**	**802.11p**
Bandwidth (MHz)	10	10
Data carriers	52	48
Modulation order	2,4,16,64,256	2,4,16,64
Coding rate R_c	1/2,2/3,3/4	1/2, 2/3
Type coder	LDPC	BCC
Channel estimation	Midamble	Least square
Midamble rate	4	-
Payload (bytes)	400	400
Simulated packets	40000	40000

BCC = Binary Convolutional Code

Fig. 4.17a shows how the performance of 802.11bd is degraded when the T2T distance is increased in Hilly Terrain by changing the channel model. For instance, there are 5 dB of penalty when switching the channel model from MD1 to MD2 and PER $= 10^{-2}$. The QPSK modulation and 1/2 coding rate (QPSK-1/2) are used in this test. For any considered channel model, significant differences are hardly observed between the two options of simulated Doppler spectra (DSP0 and DSP1 modes). In both cases, the obtained performances match well. Finally, the proposed channel models (MD1, MD2 and MD3) degrade performance of 802.11bd in a similar way as in the case of using the measured channel impulse response (CIR). For instance, choosing $E_b/N_0 = 25$ dB, a PER $= 2.0 \cdot 10^{-3}$ ($2.5 \cdot 10^{-3}$) is reached through MD2 in the DSP1 (DSP0) mode while a PER $= 1.8 \cdot 10^{-3}$ is reached if CIR is used.

Similar findings are obtained when the MD4, MD5 and MD6 channel models are tested, whose results are shown in Fig. 4.17b. Also, we can verify that Railway Station scenario is more demanding than Hilly Terrain scenario. For instance, to reach a PER $= 10^{-2}$ at short distances, an E_b/N_0 of 11 dB is necessary for the MD1 model, while an E_b/N_0 of 19 dB is necessary for the MD4 model.

Moreover, an error floor close to 10 % of packect loss is observed for the MD3 and MD6 channel models. This effect can be caused by orthogonality loss of subcarriers in OFDM modulation due to both timing and channel estimation errors. As a result, inter-symbol interference degrades system performance. Although, the transmission of error-free packets is possible for the MD1 model, a low error floor is still seen for the MD2 and MD4 channel models.

In addition, it is verified in Fig. 4.18 that using another performance indicator (BER), the modelled impulse response using any of the proposed channel models is correlated

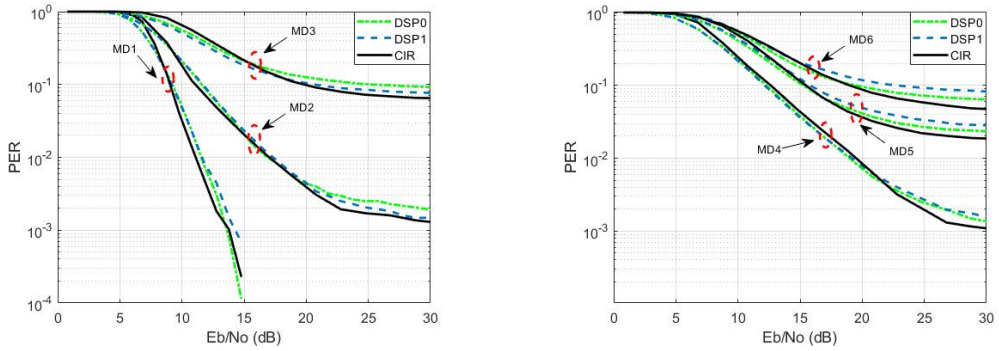

(a) Hilly Terrain scenario. (b) Railway Station scenario

Figure 4.17: Validation results of the proposed channel models based on PER performance of 80211.bd using QPSK-1/2 at different T2T distances.

with the measured impulse response since the 802.11bd performance using these are close. In both scenarios with high E_b/N_0, little performance differences are observed for both operation modes (DSP0 and DSP1). In general, the DSP1 mode matches better than the DSP0 mode to simulate the Doppler spectra in Hilly terrain scenario (Figs. 4.17a and 4.18a). On the contrary, a reverse situation is observed in the Railway Station scenario. For instance, using MD5 and $E_b/N_0 = 26$ dB, a PER $= 3.1 \cdot 10^{-2}$ is obtained to DSP1, while a PER $= 2.5 \cdot 10^{-2}$ is obtained to DSP0, being PER $= 2.0 \cdot 10^{-2}$ when CIR is used.

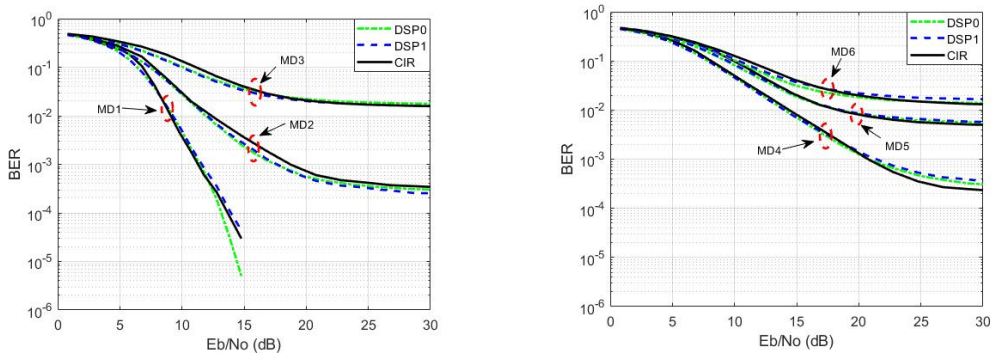

(a) Hilly Terrain scenario. (b) Railway Station scenario

Figure 4.18: Validation results of the proposed channel models based on BER performance of 80211.bd using QPSK-1/2 at different T2T distances.

The performance results of 802.11p and 802.11bd for different MCS are shown in Fig. 4.19. The results reveal that using 16QAM-1/2 scheme and a target PER $=10^{-3}$, a performance gain of 2 dB in E_b/N_0 is obtained when 802.11bd is used instead of 802.11p. Also, 802.11bd achieves a gain of 0.5 dB and 5 dB for BPSK-1/2 and 64QAM-2/3 schemes, respectively. These results match with the ones shown in [147], where a gain of 1-3 dB was obtained by 802.11bd using other channel models. Finally, the behavior of 802.11bd using a higher order modulation (256QAM) is shown in this figure too, where a PER $<10^{-2}$ is obtained for $E_b/N_0 > 36$ dB. This modulation is only available for 802.11bd which is used with $R_c = 3/4$.

The findings in this subsection indicate that the statistics of the proposed channel

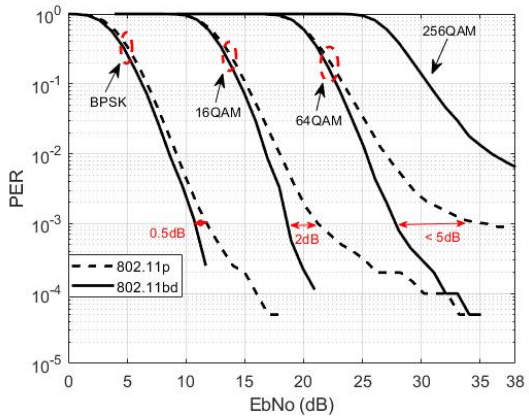

Figure 4.19: Comparison between 802.11p and 802.11bd using the MD1 model (DSP0) for different modulation schemes. The BPSK, 16QAM, 64QAM, and 256QAM modulations are combined with a coding rate of 1/2, 1/2, 2/3, and 3/4 respectively.

models follow the statistics of the measured wireless channel in both scenarios.

4.7 Summary and conclusions

Modelling the wireless channel is one of the most difficult and relevant tasks of radio system design. In this chapter, we have proposed six channel models for train-to-train communications. The Hilly Terrain and Railway Station scenarios are covered for large, medium, and short distances. The results indicate that the simulated channel using any of the proposed tapped delay line models is correlated with the measurements carried out with the DLR channel sounder, since both channels degrade the 802.11bd performance in a similar way. The proposed models can be modelled using a maximum tap number of 16, and hence can be implemented in any modern channel emulator. Also, the maximum delay is higher than 1 μs except for the MD1 model, whose maximum delay is 537 ns.

It is observed that the stochastic channel parameters are related with the considered train-to-train distance. For instance, delay spread σ_τ varies from 83 ns to 819 ns when short or large distances are considered in Hilly Terrain. Also, the analysis of Doppler-delay spectrum reveals that the Railway Station scenario is densely covered with reflector obstacles, which deteriorates the propagation conditions. The DSP0 and DSP1 modes, which describe how the Doppler spectrum is simulated, cause only small differences in the 802.11bd performance although the DSP0 mode is much simpler to implement. Finally, 802.11bd achieves a performance gain over 802.11p from 0.5 dB to 5 dB depending on the used modulation and coding scheme.

5

Channel estimation methods for 802.11-based technologies

In this chapter, several channel estimation methods are examined for channel tracking in 802.11p/bd. Although the MCE method is the candidate for 802.11bd, a CPCE method is proposed for 802.11bd, which increases the number of pilot subcarriers in comparison to MCE, and uses them to track the channel for each OFDM symbol. The method is also benchmarked against MCE, and combined with DCM. The performance analysis report includes different channel tracking algorithms, packet lengths, data rates and railway channel models. The simulations in Matlab show that the proposed CPCE method achieves better results than MCE for tracking the impairments of channels, with Doppler spreads of up 1000 Hz. It has a performance gain of about an order of magnitude over MCE in terms of PER, as well as a E_{b}/N_0 gain of greater than 3 dB for a target PER equal to 10^{-3}.

5.1 Introduction

The 802.11p protocol has been the one used in vehicular networks in the last decade, which was introduced in Section 2.2. Its performance, based on field measurements and numerical simulations, has been widely reported in the literature [8, 47, 64]. It was originally designed to support a basic set of vehicular applications which issue driver alerts to indicate potentially dangerous situations. These applications require an end-to-end latency of around 100 ms and transmission of periodic messages. However, they do not achieve the quality of service demanded by advanced applications, and fail to provide consistent high data rate transmissions [52],[30]. Advanced applications require latencies of less than 10 ms and a reliability of 99.999 % in some use cases [40]. They are thus much more stringent than those of basic safety applications.

Furthermore, when the traffic density increases, 802.11p experiences a degradation of its performance, resulting in an increase of PER. This is due to collisions between packets transmitted simultaneously by different vehicles. Additionally, the insufficient number of pilot carriers and the channel estimation method implemented in 802.11p penalize its performance in NLoS and high mobility situations [8]. Given that 802.11p was developed more than a decade ago [148], advanced processing techniques introduced in 802.11n/ac/ax can be leveraged to enhance 802.11p, increasing its throughput, extending

its transmission range, and improving its reliability and efficiency. IEEE created the TGbd working group in May 2018, which is preparing the upcoming 802.11bd amendment [39]. This draft includes new advanced technologies with the purpose of improving its reliability. The set of technologies that could be part of the new protocol, are currently under study [7]. For instance, the MCE method has been proposed for channel tracking. This updates the channel response estimation by periodically inserting training symbols into the sequence of OFDM data symbols [149]. This was successfully implemented in the 802.11ac amendment to perform channel estimation. Nevertheless, further investigation should be conducted to evaluate the performance of the 802.11bd candidate techniques, since very little research has been published on this topic [30],[147],[150].

In the literature, several methods of channel estimation for 802.11p have been reported to improve the performance [9]. Some of these methods increase the number of pilot carriers expanding the sampling points in the frequency domain, and thus improving channel response estimation [151][10]. This approach could be successful in a fast fading channel and could be considered as a candidate technique for 802.11bd.

In this chapter, an exhaustive study about channel estimation in 802.11p is carried out. Also, a CPCE method for channel tracking in 802.11bd is proposed, where the channel estimate is performed for each OFDM symbol using pilot subcarriers. The analyzed channel estimation methods are evaluated using the measurement-based railway channel models proposed, and the metric-based performance results are shown.

The research presented in this chapter was carried out within the SCOTT project and the InSectt project, which studied the performance of communication standards for railway domain amongst other use cases. Within the framework of these two European projects, an enhancement of the 802.11p communication standard and a performance analysis of next evolution 802.11bd was carried out. The following articles have been derived from the results present in this chapter:

- E. Mozo, A. Alonso-Gómez, and M. Mendicute, “Performance Analysis of Pilot Patterns for Channel Estimation for OFDM Systems in High-Speed Trains Scenarios,” in IEEE 30th Annual International Symposium on Personal, Indoor and Mobile Radio Communications (PIMRC), 2019, p. 7.
- E. Mozo, A. Alonso-Gómez, and M. Mendicute, “Channel estimation methods for IEEE 802.11 bd in vehicular channels with high Doppler,” Sensors, 2022. (Pending of submission)

The chapter is organized as follows: In Section 5.2, the state of the art of channel estimation methods in 802.11p is presented, where the relevant estimation methods are explained in detail. Next in Section 5.3, the estimation methods for 802.11bd are introduced where a CPCE method is proposed for 802.11bd. Furthermore, Section 5.4 shows relevant aspects to take into account in the time-frequency grid design in a OFDM multi-carrier system. Then, the performance results using railway channel models are shown in Section 5.5 and the conclusions are summarized in Section 5.6 .

5.2 Channel estimation in 802.11p

Channel estimation is one of the key tasks that affects system performance, as it needs to be able to cope with rapidly changing channel conditions. 802.11p estimates the

channel using training symbols at the beginning of each frame (preamble) by means of the well-known Least Square (LS) estimator. This estimation is used to equalize the rest of the symbols within the frame. This approach comes from 802.11a, which was initially designed for the estimation of indoor channels with low mobility. As a consequence, 802.11p cannot track rapidly changing channel variations because of an insufficient number of pilots or training symbols for channel estimation. For this reason, the preamble and the rest of symbols are affected differently in double dispersive channels. To overcome this limitation, various channel estimation techniques have been studied in the literature, some of which are shown in Table 5.1.

Table 5.1: Research works on 802.11p channel estimation

Ref.	Scheme	Main feature
[9]	LS	Effective when the channel is stationary (802.11p choice)
[8]	STA	Decreases the noise level by exploring the correlation function
[152][153]	DFT	Better performance than LS and STA on low Doppler
[9][154]	CDP	Improves performance on high Doppler
[155]	SFD	Better performance than CDP with less computational complexity
[149]	MCE	Increases the bit error rate but decreases the throughput
[10]	CPCE	Changes the location and number of pilot carriers
[146]	GDPS	Low iteration level is required for better performance
[156]	Winner	Sub-optimal implementation
[157]	TDLSE	Inserts a PN sequence in the prefix
[158]	Self Organizing	Good performance for low and medium SNR
[159]	Cross Layer	Same approach as MCE but does not modify the frame
[160]	Semi Blind	Based on time domain truncation, better performance than STA
[161][162]	Adaptive	Smart combination of some previous schemes
[163]	MMSE	Improve the performance of the LS in term of mean square error

Some of these schemes modify the structure of the 802.11p frame to adapt it to the variable conditions of the vehicular channel. This improves performance but it is incompatible with the standard and in some cases, a greater computational complexity is necessary. For example, in [157], a scheme called Time Domain Least Square Estimation (TDLSE) was proposed. This method inserts a pseudo noise sequence into the prefix in each OFDM symbol to further facilitate channel estimation. Then, the estimate is averaged with the adjacent symbols to reduce the effects of noise.

Other methods explore novel pilot numbers and distribution schemes for 802.11p. In [151], the authors redistribute pilot subcarriers on adjacent symbols. Then a time-frequency interpolation is used to obtain the channel impulse response. On the other hand, the number of pilot subcarriers is increased in [10], and a CPCE method is adapted to the 802.11p frame structure. In [149], the channel response is continually updated by means of a MCE method. This approach was used in 802.11ac, being MCE the candidate estimation method for 802.11bd. These two estimation methods will be analyzed in detail in Section 5.3.

On the other hand, other methods are compatible with the standard and only require a software update on the receiver side. An Spectral-Temporal Averaging (STA) based scheme is presented to estimate the dynamic nature of the communication channel in [8]. STA is based on the correlation between each carrier and its neighboring carriers in the frequency domain, as well as the time correlation between successive OFDM symbols. An extension to this, called Constructs Data Pilot (CDP) scheme, was proposed in [9]. It exploits the correlation between adjacent symbols to determine channel variability and decides whether to update or not the channel estimate following a STA method. The CDP estimator achieves a higher performance than STA in high SNR at the expense of

increased computational complexity.

In addition, a State Feedback Decision (SFD) algorithm was proposed by [155] which enables us to extract reliable data pilots within a few received symbols without the aid of conventional decoders. This algorithm allows to minimize error propagation effect and reduces the computational complexity in comparison with the CDP method. Given that, the SFD algorithm can process P data bits at the same time, the reliability level of the data and the receiver complexity can be adjusted depending on the situation.

Another method is the Wiener filter, which seeks for the optimal coefficients to minimize Mean Square Error (MSE) of the channel response at its input and output [156]. The optimal implementation of the filter depends on a prior statistical characterization of the channel (maximum excess delay and power delay profile), as well as the received SNR. These parameters are not known precisely beforehand, so its practical implementation is sub-optimal. Nevertheless, this approach can achieve a SNR gain of several decibels (dB) for different modulation and coding schemes.

The following subsection describes in detail some basic channel estimation methods available for 802.11p which are suitable for slow fading channel, namely LS and DFT methods. In addition, we examine different options of Data Aided Channel Estimation (DACE) method which improves the 802.11p performance in fast fading channels where the Doppler spread achieves medium and high values. Please note, CDP and DACE approaches are similar, since they use data subcarriers to improve channel estimation. The only difference between them is how they manage error propagation, which can cause a performance loss.

5.2.1 Least square channel estimation

In this subsection, we introduce the LS method which is a basic channel estimation technique. The LS estimator is usually implemented in OFDM systems using training sequences, which are transmitted in an OFDM symbol with N subcarriers. Assuming that X is a matrix of size $N \times N$ with the elements of the transmitted training sequence in its diagonal, Y is a $N \times 1$ vector with the received training sequence, H is a $N \times 1$ vector with the channel gain, and W is a $N \times 1$ vector of AWGN with mean zero and variance σ_{w}^2. The relation input-output of channel is given by

$$Y = HX + W. \tag{1}$$

The LS channel estimator of H, denoted by $\hat{H}_{\mathrm{LS}}$, minimizes the following objective function:

$$J_{\mathrm{LS}} = (Y - \hat{H}_{\mathrm{LS}}X)^H (Y - \hat{H}_{\mathrm{LS}}X), \tag{2}$$

where $(\cdot)^H$ denotes the conjugate transpose. Then, the final estimation of $\hat{H}_{\mathrm{LS}}$ is obtained taking $\partial J_{\mathrm{LS}}/\partial H = 0$, and expressed it as

$$\hat{H}_{\mathrm{LS}} = \frac{Y}{X} = H + \frac{W}{X}. \tag{3}$$

Please note, the noise on the second term in (3) directly determines the accuracy of the estimator.

The mean and variance of the LS estimator are estimated by

$$E(\hat{H}_{LS}) = E(H) \tag{4}$$

and

$$Var(\hat{H}_{LS}) = Var(H) + \frac{\sigma_w^2}{X}, \tag{5}$$

respectively. Where $E(\cdot)$ is expected value and $Var(\cdot)$ is variance. Please note, the LS estimator has a bias equal to σ_w^2/X, which depends only on the power of the noise σ_w^2 since the training sequence X is a constant which is known in the receiver. Although, LS estimator offers an implementation with a very low complexity, it has an important disadvantage: its performance is very sensitive to noise. Then, the accuracy of the estimator is reduced at low SNR.

5.2.1.1 Using LS estimation in 802.11p

The 802.11p packet structure was introduced in Section 2.2, being is composed of three fields: the Preamble field for time-frequency synchronization, the Signal field for control information and signaling, and the Data field for data bits. The part of preamble includes two LTS symbols which are used for the channel estimation. These symbols are known by the transmitter and receiver and can be used to obtain a LS channel estimation. The receiver firstly obtains the initial channel estimation $\hat{H}_{LS}^{(i)}$ from the two long training symbols using (3) as

$$\hat{H}_{\mathrm{LS}}^{(i)} = \frac{Y^{(i)}}{X^{(i)}}, \tag{6}$$

where $i \in \{1, 2\}$ represents the index of training symbol used, $Y^{(i)}$ is the i^{th} received training symbol, and $X^{(i)}$ is a matrix whose main diagonal contains the i^{th} transmitted training symbol, respectively. Subsequently, the final channel estimation is achieved averaging the obtained estimation in both training periods as

$$\hat{H}_{\mathrm{LS}} = \frac{\hat{H}_{\mathrm{LS}}^{(1)} + \hat{H}_{\mathrm{LS}}^{(2)}}{2}. \tag{7}$$

This approach minimizes the noise variance and has a low implementation complexity. Afterwards, $\hat{H}_{\mathrm{LS}}$ is used to equalize all the data symbols within the 802.11p packet. Note, that this approach is only suitable for slow fading channels where the coherence time of the channel is higher than packet time. Therefore, fast fading can cause a complete loss of estimated channel parameters. In order to overcome that, 802.11bd will use midamble symbols for channel tracking, which are transmitted every M OFDM data symbols. Lastly, the midambles are used to update the channel using an LS estimator.

5.2.2 DFT-based channel estimation

In order to improve the performance of the LS estimator in situations with low SNR, $\hat{H}_{\mathrm{LS}}$ can be smoothed based on the fact that channel impulse response $h[n]$ is short compared to the length of the considered cyclic prefix G in an OFDM system. In other words, the energy of channel coefficients in $h[n]$ decreases rapidly outside the first G taps of the channel, while the noise energy is assumed to be constant over the entire range.

Using this approach, the channel estimation is firstly obtained in frequency domain based on LS estimation. Then, using the IDFT, it is converted to the time domain as

$$\hat{h}_{\mathrm{LS}}[n] = \frac{1}{N} \sum_{k=0}^{N-1} \hat{H}_{\mathrm{LS}}[k] e^{j2\pi \frac{nk}{N}}, \tag{8}$$

being k and n the carrier and time indexes respectively, where $k, n \in \{0, ..., N-1\}$. In order to restrain the effects of noise, the considered coefficients with low energy are approximated to zero. Thus, the smoothed impulse response is obtained by

$$\hat{h}_{\mathrm{FT}}[n] = \left\{ \begin{array}{cc} \hat{h}_{\mathrm{LS}}[n] & 0 \leq n \leq G-1 \\ 0 & otherwise \end{array} \right\}. \tag{9}$$

Now, it is transformed to the frequency domain using Discrete Fourier Transform (DFT) as

$$\hat{H}_{\mathrm{FT}}[k] = \sum_{n=0}^{N-1} \hat{h}_{\mathrm{FT}}[n] e^{-j2\pi \frac{nk}{N}}. \tag{10}$$

This channel estimation approach is known as DFT method. It improves accuracy in the estimation, and the implementation complexity is not very high since the IDFT/DFT transforms can be implemented using the fast Fourier algorithms as shown in Fig. 5.1.

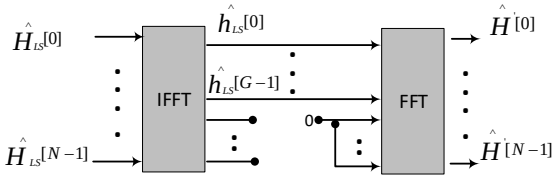

Figure 5.1: Smoothing the LS estimation $\hat{H}_{LS}$ using DFT.

5.2.3 Data Aided Channel Estimation (DACE)

In order to address the problem of the insufficient number of pilot subcarriers and to track the fast fading channel in 802.11p, the data subcarriers in an OFDM symbol can also be used to estimate the frequency response of channel. This approach is known as Data Aided Channel Estimation (DACE) method. The main idea behind DACE is the reconstruction of the transmitted OFDM symbol, so that the received data can be considered as a training sequence and used to perform channel estimation exploiting the new available information [164]. This approach improves the 802.11p performance in low and high SNR as well as in fast fading channel [9]. Nowadays, most of the 802.11p chipsets implement this channel estimation method which provides a performance gain over the conventional estimation method. In this section, we show and test different strategies underlying the DACE implementation.

5.2.3.1 DACE algorithm

The DACE algorithm can use different processing block to build the data symbols in the frequency domain [164], [9]. Fig. 5.2 shows a generic diagram of a DACE algorithm. In this section, $Y_i[k]$ denotes the i^{th} received data OFDM symbol at frequency domain before the equalization process is carried out, being k the subcarrier index.

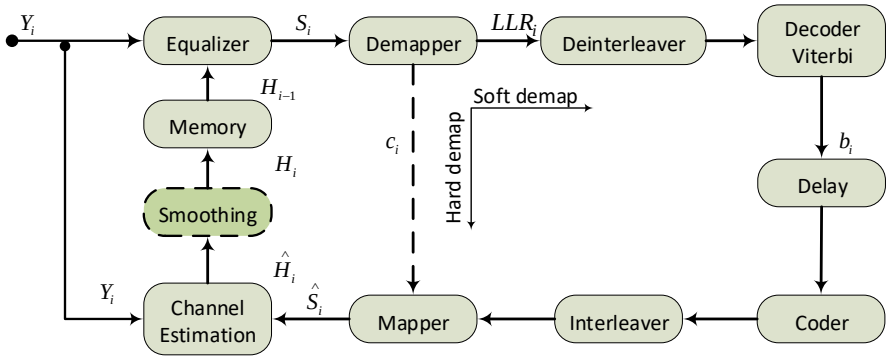

Figure 5.2: Generic diagram of a data aided channel estimation (DACE) method.

The following steps are carried out to implement a DACE algorithm:

- $Y_i[k]$ is equalized with most recent available channel estimate $H_{i-1}[k]$. The zero forcing equalizer is the most common approach given its simplicity. The initial channel estimate $H_o[k]$ is obtained using the training symbols.
- The equalized symbol $S_i[k]$ is introduced into demapper block which can provide a soft or hard output.
- Using the soft output of the demapper block, log likelihood rate coefficients $LLR_i[j']$ are calculated to obtained decoded bits $b_i[j]$ by a two block sequence composed of a deinterleaver and a Viterbi decoder. Indexes, $j = 1, ..., N_{\text{bps}}$ and $j' = 1, ..., N_{\text{bcps}}$ depend on MCS used, being N_{bps} and N_{bcps} the number of bits and number of coded bits per OFDM symbol, respectively.
- The decoded bits must be delayed to manage the delay introduced by the Viterbi decoder block due to its convergence time T_g.
- To rebuild the transmitted OFDM symbol $\tilde{S}_i[k]$, the delayed decoded bits are again encoded, interleaved and mapped. On the other hand, if the hard demapper output is used, the interleaved-coded bits $C_i[j']$ are only mapped again in the Mapper block.
- The updated channel estimate $\hat{H}_i[k]$ is computed substituting $Y_i[k]$ and $\tilde{S}_i[k]$ in (3).
- Optionally a smoothing block can be used to improve accuracy in the estimation in $\hat{H}_i[k]$, which allows to combat the impact of the noise and to smooth the propagation of errors in the loopback.
- The smoothed channel estimate $H_i[k]$ is stored in memory and used with the following received OFDM symbol.

The DACE implementation in Fig. 5.2 is carried out at OFDM symbol level, which means that every block works with a period corresponding to an OFDM symbol. For instance, the decoder block operates on blocks of N_{bcps} bits. The last restriction is a requirement of the interleaver/deinterlever blocks which has an OFDM symbol approach. As a result, the DACE technique is not compatible with processing algorithms that work with the frame approach. This approach requires that decoder block receives the coded bits of whole packet to provide an output result. Therefore, DACE has not been considered by TGbd as a channel estimation method in the oncoming 802.11bd standard, since its receiver is based on LDPC coding, which has an frame approach.

Furthermore, the Viterbi decoder convergence time introduces a delay of $b_{\mathrm{d}} = T_{\mathrm{g}}/T_{\mathrm{b}}$ bits in the sequence $b_i[j]$, being T_{b} the bit time. As a consequence, the data bits corresponding to the i^{th} OFDM symbol is decoded only after the $(i+1)^{th}$ OFDM symbol has been processed, which represents a latency of one OFDM symbol. Also, b_{d} has to be greater than or equal to N_{bps} in orden that Viterbi algorithm converges. The 802.11p/bd protocols have been designed with multiple MCS where the minimum value of N_{bps} is 24 (BPSK-1/2). Then, $b_{\mathrm{d}} = 24$ could be a good choice to set up the Viterbi decoder.

5.2.3.2 DACE implementing strategy

Depending on the number of Viterbi decoders and the demapper mode used, different strategies can be followed to implement the DACE algorithm. Three schemes are identified in DACE, which can be denoted by:

- Hard DACE (hDACE): It uses hard demapping of the equalized symbol $S_i[k]$ which associates the closest symbol $S[c]$ from the constellation to $S_i[k]$, being $c = \{1, .., M\}$, and M the order of the modulation used [164]. This association uses the reference of the Euclidean distance from the equalized symbol. Fig 5.3 shows how Hard DACE scheme is implemented which is similar to the STA method shown in [8]. Please note, the $C_i[j']$ output has to be deinterleaved, decoded, and descrambled in order to recover the transmitted bits. The hDACE scheme suffers from errors due to the impacts of noise, other interferences and synchronization errors. As a consequence to that, $S_i[k]$ can be easily demapped into an incorrect constellation point, and thus errors can spread to the next OFDM symbol which degrades the system performance. In order to solve this drawback, an alternative strategy should be considered with a smoothing block, as depicted in Fig. 5.2.

- Simple decoding DACE (sDACE): It uses soft demapping of $S_i[k]$ which implies the estimation of $LLR_i[j']$. These coefficients can be calculated as

$$LLR_i[j'] = \log\left(\frac{P(b'_i[j'] = 0 \mid Y_i[k], H_{i-1}[k])}{P(b'_i[j'] = 1 \mid Y_i[k], H_{i-1}[k])}\right), \tag{11}$$

  being $b'_i[j']$ the j'-th interleaved coded bit in the i-th OFDM symbol and $P(a|b)$ the conditional probability of a given b. Fig 5.4 shows how this sDACE scheme is implemented. Error mitigation can be achieved, since soft channel coding is used to estimate $\hat{S}_i[k]$. sDACE has a higher computational complexity than the hDACE scheme. Also, it is a sub-optimal implementation since $Y_i[k]$ is equalized with the channel estimation of the previous symbol $H_{i-1}[k]$. However, it achieves a good performance-complexity relation [164].

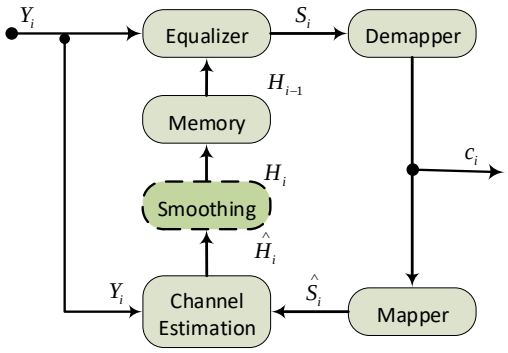

Figure 5.3: Implementation of the data aided channel estimation method using hard demapping.

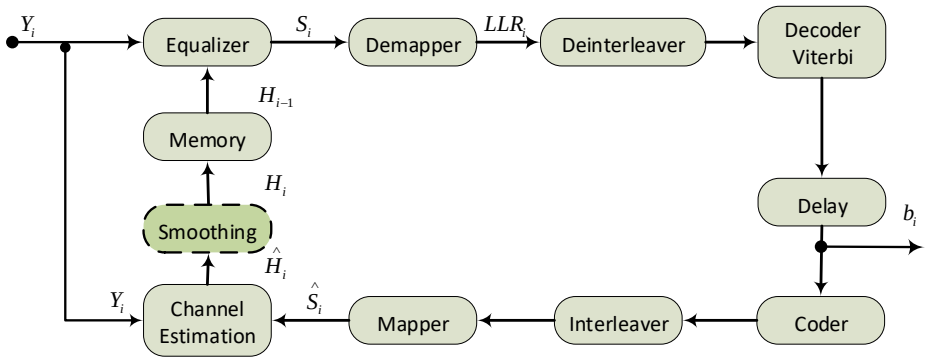

Figure 5.4: Implementation of the data aided channel estimation method using soft demapping.

- Double decoding DACE (dDACE): It uses the updated channel estimation $H_i[k]$ to equalize the received symbol $Y_i[k]$. Fig 5.5 shows how the dDACE scheme is implemented using soft demapping. The scheme requires that the block composed by equalizer-demapper-deinterleaver-decoding is done twice. As a result, the dDACE scheme has a higher latency and computational complexity than the previous analyzed schemes.

The main difference between sDACE and dDACE schemes is that $H_i[k]$ is used to equalize $Y_i[k]$ in dDACE. In contrast, $Y_i[k]$ is equalized with the channel estimate in the previous symbol $H_{i-1}[k]$ in sDACE. Then, the dDACE scheme would achieves a performance gain over sDACE in fast fading channels, whose gain would depend on the channel correlation of two adjacent OFDM symbols.

In addition, the error propagation is inherent to all DACE schemes due to the decoded bits are fed back to the input through loopback. Then, several strategies can be considered to mitigate the effects of the error propagation. For instance, averaging in both the frequency and time domains can help in improving accuracy in the estimation. The averaging in the frequency domain is given by

$$H_i[k] = \sum_{\lambda=-\beta}^{\beta} \varpi_\lambda \hat{H}_i[k+\lambda], \tag{12}$$

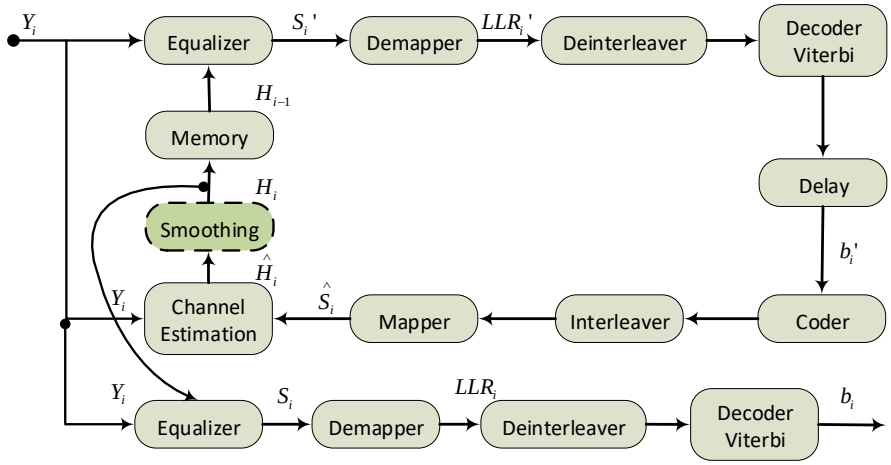

Figure 5.5: Implementation of the data aided channel estimation method using soft demapping with double decoding.

being $H_i(k)$ the smoothed channel estimation in the i^{th} OFDM symbol and k^{th} subcarrier. Also, ϖ_λ is a set of weighting coefficients with unit sum, β is a integer number, and $2\beta+1$ represents the number of subcarriers that are averaged [154],[165]. On the other hand, the averaging in the time domain is given by

$$H_i[k] = (1-\alpha)H_{i-1}[k] + \alpha\hat{H}_i[k], \tag{13}$$

where α is an updating parameter related to the Doppler shift.

The values α and β are dependent on the types of channel and scenario. Significant accuracy can be achieved by adjusting these values according to the knowledge of the vehicular channel environment [154]. However, such kind of information is hard to obtain in reality. Fixed values of these parameters would be a good balance of algorithm simplicity and an acceptable performance degradation. In addition, the averaging in time domain can be done too using DFT transforms, similar to (9).

Furthermore, the authors in [9] exploit the channel correlation characteristics between two adjacent data symbols in time domain ($H_{i-1}[k]$ and $H_i[k]$) as well as between adjacent subcarriers in frequency domain ($H_i[k-1]$ and $H_i[k]$). Then, the correlation coefficient is used to decide whether or not to update the channel estimate, which helps to minimize the error propagation. The results show that the BER performance of this approach outperforms currently relevant schemes, eg., STA scheme, especially in a high SNR regime. In addition, the SFD algorithm proposed in [155] minimizes error propagation effect and reduces the computational complexity in comparison with the DACE methods reported in the literature.

5.3 Channel estimation method proposed for 802.11bd

In this section, we examine two additional channel estimation methods considered for channel tracking in 802.11bd. First, the Midamble based Channel Estimation (MCE) scheme is analyzed, which updates the channel response estimation by periodically inserting training symbols into the sequence of data OFDM symbols. A Comb-type Pilot-based

Channel Estimation (CPCE) scheme is then proposed for 802.11bd. The latter increases the number of pilot subcarriers N_p in comparison to 802.11p and keeps the same nominal bandwidth as 802.11bd. Finally, a study of frequency-time grid in a OFDM system is presented, where the channel parameters are related with system design parameters.

5.3.1 Midamble-based Channel Estimation (MCE)

TGbd has defined a set of advanced technologies that could be part of the new protocol, which are currently under study [7]. For instance, the MCE method has been proposed for channel tracking. This was successfully implemented in 802.11ac to perform channel estimation. Nevertheless, further investigation should be conducted to evaluate the performance of the 802.11bd candidate techniques, since very little research has been published on this topic [30],[150],[147].

Using MCE, training symbols $X_m[k]$ are periodically transmitted with a rate equal to M, which means that for every M data symbol, one training symbol is transmitted [149]. The training symbols are normally called midambles since they are mixed with the data OFDM symbols. The total number of midambles N_M in an 802.11bd packet of N_{SIMB} OFDM symbols is given by

$$N_M = \left\lceil \frac{N_{\text{SIMB}} - 1}{M} \right\rceil, \tag{14}$$

being $\lceil x \rceil$ the whole part function. The midambles serve to update the channel response estimation (channel tracking) using a LS estimator as

$$\hat{H}_m[k] = \frac{Y_m[k]}{X_m[k]}, \tag{15}$$

where $Y_m[k]$ represents the m^{th} received midamble in a frame, being $m = 1, ..., N_M$. In order to improve the estimation of $\hat{H}_m[k]$, an averaging in frequency domain can be done as in (12). Then, the final estimation $H_m[k]$ is used to equalize the rest of the OFDM symbols within a frame until a new midamble is received, as shown in Fig. 5.6. In this figure, the initial estimation $H_o[k]$ is obtained using the NGV_LTF training symbol, which has been introduced in Section 2.3.2. Please note that using MCE, the averaging in time domain with (13) is not possible since $H_m[k]$ is estimated every $M + 1$ OFDM symbols.

MCE obtains performance improvement at the expense of spectrum efficiency, i.e, increasing the midamble rate improves the performance, but makes the overhead grow. Thus, it is very important to choose the optimal M according to channel parameters, packet lengths and Doppler shift. The computational requirement of MCE is lower than all the DACE schemes shown in Section 5.2.3. The efficiency penalty caused by inserting midamble symbols can be defined by:

$$\varepsilon_{\text{MCE}} = \frac{M}{M+1}. \tag{16}$$

5.3.2 Proposed channel estimation method

The CPCE method computes the channel estimate using the pilot subcarriers on each OFDM symbol within the same frame [10]. Firstly, the channel response for each pilot

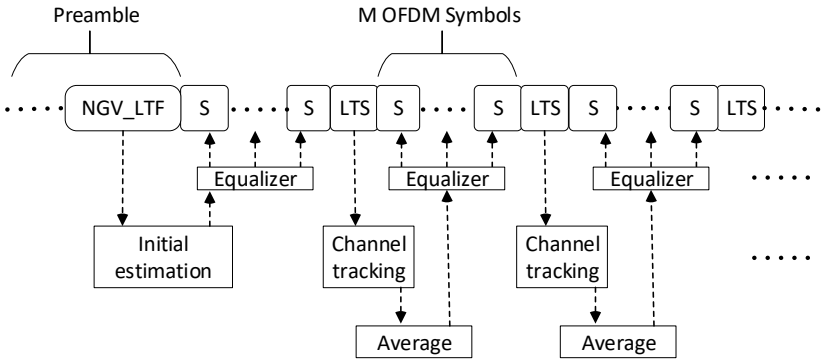

Figure 5.6: Midamble based channel estimation (MCE).

subcarrier is estimated. Then, this estimation is used to determine the channel response for the rest of the data subcarriers by means of a linear interpolation technique. Finally, the last estimation is averaged in time to reduce the effect of noise. This process is described in Fig. 5.7.

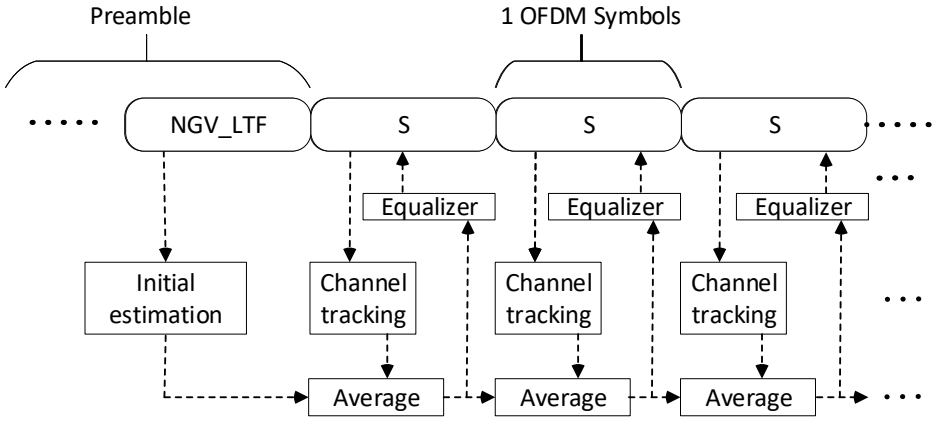

Figure 5.7: Comb-type pilot-based channel estimation (CPCE).

The 802.11bd draft locates the pilot carriers in the positions $\{9, 25, 41, 55\}$, while the pilot pattern would be {1,1,1,-1} as described in [7]. In our proposal, the number of pilot subcarriers N_{p} is increased and these pilots are distributed almost uniformly over the entire bandwidth. In addition, two of the pilot subcarriers are located at the edge of the band (position 5 and 61 considering 64 subcarriers). This pilot distribution is due to the requirement of interpolation method, in order to minimize the mean squared error in the estimation of the channel response and decrease the computational requirement [10]. The chosen pilot pattern is a periodic extension of the pattern used in 802.11bd.

With the previous modification, the channel response $H_i[k_p]$ is first estimated for every pilot subcarrier and OFDM symbol using an LS estimator as:

$$\hat{H}_i[k_p] = \frac{Y_i[k_p]}{X_i[k_p]}, \tag{17}$$

where $Y_i[k_p]$ and $X_i[k_p]$ represent the transmitted and received symbols at the k_p-th subcarrier and i-th OFDM symbol, respectively, being $p = 1, 2.., N_p$ the pilot subcarrier index. Then, an interpolation technique is used to estimate the channel response $\hat{H}_i[k_d]$ of any other data subcarrier d in the frequency domain. The number of nominal subcarrier N_{ac} (data and pilot subcarriers) in 802.11bd is 56 or 114 for bandwidth of 10 or 20 MHz, respectively. Then, the linear interpolation can be expressed by

$$\hat{H}_i[k_d] = (\hat{H}_i[k_{p+1}] - \hat{H}_1[k_p])\frac{l}{L} + \hat{H}_i[p], \tag{18}$$

given that,

$$pL < k_d < (p+1)L, \tag{19}$$

where $k_d = pL + l$, and L represents the number of data subcarriers between two consecutive pilot subcarriers [166]. Finally, once the estimate of $\hat{H}_i[k]$ is computed, it is combined in time with the estimate from the previous symbol using (13) to obtain the final estimation $H_i[k]$.

The efficiency penalty caused by increasing the number of pilot subcarriers in CPCE can be defined by

$$\varepsilon_{\text{CPCE}} = \frac{N_{\text{ac}} - N_{\text{p}}}{N_{\text{da}}}, \tag{20}$$

where N_{da} represents the number of nominal data subcarriers, which is equal to 52 or 108 depending on the bandwidth used.

5.4 Time-Frequency grid design

Adding pilot carriers or midamble symbols improves the system performance. However, it decreases the system throughput, so N_{p} and M must be properly chosen to achieve a balance between system performance and throughput. In this case, the design of the time-frequency grid plays a significant role in how it can efficiently track the channel impairments. The grid utilizes N carriers over a bandwidth B and P OFDM symbols. Also, each symbol uses a cyclic prefix with length G. For instance, Fig. 5.8 shows how the grid is set up when a packet of 350 bytes of length is transmitted using the MCS7 mode (64QAM-2/3). In the grid in Fig. 5.8, the guard subcarriers are not shown, and a bandwidth of 10 MHz is used.

The pilot placement in the time-frequency grid needs to fulfill the sampling theorem. In addition, two basic parameters of the wireless channel must be taken into account for the design: maximum excess delay $\tau_{\max}$ and the Doppler spread σ_ν. The maximum excess delay determines how dense pilot subcarriers must be in frequency domain [146], while, the Doppler spread determines how dense pilot symbols must be in time. As discussed in [167], the maximum pilot spacing Δf (number of data subcarriers) will satisfy

$$\Delta f \leq \frac{N}{\tau_{\max} B}. \tag{21}$$

From this, a lower bound of the number of pilot subcarriers is obtained as

$$N_p \geq \tau_{\max} B. \tag{22}$$

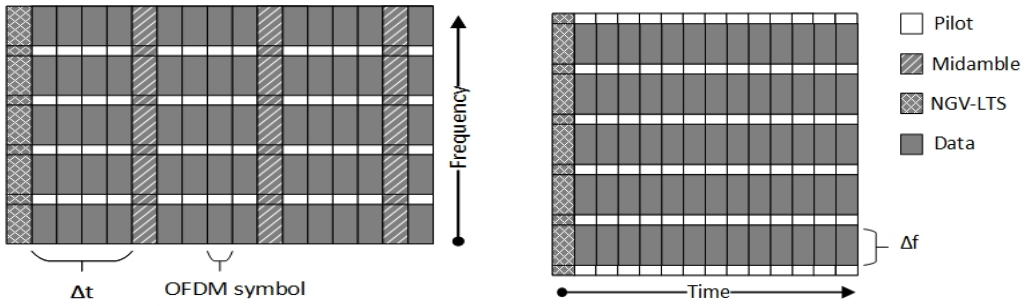

(a) MCE with M=4 and Δf = 500 KHz. (b) CPCE with N_{p}=6 and $\Delta f = 600$ KHz.

Figure 5.8: Distribution of subcarriers in a time-frequency grid for the analyzed channel estimation methods.

This equation indicates that, the minimum number of pilot carriers in 802.11bd must be equal to 16, since the protocol was designed to support a maximum delay of 1.6 us (length of cyclic prefix). In addition, the maximum pilot symbols spacing Δt (number of OFDM symbols) will satisfy

$$\Delta t \leq \frac{B}{2\sigma_{\nu}(N+G)}. \tag{23}$$

From this, an upper bound of midamble rate is obtained as

$$M \leq \Delta t - 1. \tag{24}$$

These equations establish the bounds that must be fulfilled to avoid aliasing. 802.11p has only four pilot subcarriers and does not use midamble symbols (similar to choosing M greater than P). In time-variant channels with high σ_{ν} (higher than 800 Hz) and high $\tau_{\max}$ (higher than 400 ns), the conditions above are not met if the number of 802.11p OFDM symbols is higher than 80. This situation will cause a degradation of the channel estimates due to aliasing. In vehicular environments, this last condition is very common, due to high vehicle speeds and the high density of scatterers. For this reason, the channel coefficients could change between OFDM symbols within a frame.

802.11bd uses midamble symbols to relax the restriction in Equation (23), but it keeps the same number of pilot carriers as 802.11p. This configuration indicates that 802.11bd faces the same problem as 802.11p (in scenarios with high τ_{max}) and its performance could thus be degraded. On the other hand, the approach of increasing the number of pilot subcarriers for each OFDM symbol relaxes such limitations, and would be more robust with regard to the impairment of wireless channel.

Equations (22) and (24) only give a bound about N_{p} and M. Both variables depend on the statistics of the wireless channel ($\tau_{\max}$, σ_{ν}) which can be estimated from a measurement campaign [19]. Please note, that both statistics may change considerably for different environments and over time, it would be hard to choose an optimum value for them (N_{p}, M). Given that 802.11bd has to support different scenarios and use cases, TGbd chose different rates of M, to allow the protocol to adapt its settings to the propagation environment and traffic statistics. These rates were 4, 8 or 12 symbols, and their selection was based on a previous study of the protocol performance in several vehicular environments [7]. Based on this last approach, we propose that N_{p} be equal to 14, 10, or 6 pilot subcarriers in a 10 MHz bandwidth.

For a fair comparison between both methods (MCE and CPCE), the efficiency penalty using them must be as equal as possible. Hence, if we select $M = 4$ (choice of TGbd), then N_{p} must be fixed to 14, and a penalty of 0.8 is obtained for both methods. This condition ensures that the obtained results reflect the behavior of each method in more detail.

5.5 Simulation results

In order to evaluate the performance of the channel estimation methods previously described, a 802.11p/bd simulation framework is implemented assuming a link between the transmitter and the receiver for different configurations. In this section, first, simulation settings are briefly described. Next, the performance result obtained by 802.11p/bd are shown, compared, and contrasted.

5.5.1 Simulation Setup

In this section, the configuration parameters and details of the simulations are presented. Monte Carlo simulations are performed in Matlab to compare the performance of MCE and CPCE, and to evaluate how they would match with other 802.11bd candidate technologies such as LDPC and DCM. Also, different channel estimation methods are evaluated for 802.11p and the results are taken as reference. Three configurations are chosen and denoted as

- 11*bd* (802.11*bd* using the MCE candidate method)
- 11bd^{+} (802.11*bd* using the proposed CPCE method)
- 11*p* (802.11*p* using the LS, DFT, sDACE, dDACE, and hDACE methods)

The only difference between 11*bd* and 11bd^{+} is the used channel estimation method, because they have different placement of pilot subcarriers in the time-frequency grid. The simulation configuration parameters are shown in Table 5.2, in which different channel estimation methods, coding and modulation schemes, channel models and payload sizes are used. The comparison considers railway channel models available for T2I and T2T communications. While the T2I link is modelled using the Winner II channel model described by [12], the T2T link is modelled using the T2T channel models (T2T-MD) proposed in Chapter 4.

The baseband processing of 802.11p/bd complex signal was shown in Section 2.3.3, where both the transmitter and receiver structure were described in detail. After generating the complex signal at the transmitter side, it passes first through a railway wireless channel (frequency-time selective). Next, AWGN is added to the received signal and finally the result is processed at the receiver side. Finally, performance indicators are calculated in order to evaluate the behaviour of the chosen configuration.

5.5.2 Performance results for 802.11p

The channel estimation methods available for 802.11p were described in Section 5.2. The performance results in the literature show that the DACE channel estimation method

Table 5.2: Simulation parameters.

Parameter	Value
Bandwidth (MHz)	10
FFT Length	64
Modulation	BPSK, QPSK, 16QAM, 64QAM, 256QAM
Channel estimation	MCE, CPCE, DACE, LS, DFT
Channel coding	LDPC, BCC
Simulated packets	40000
Payload (bytes)	100-1500
Channel types	Winner II, T2T-MD, AWGN

obtains the best performance with respect to others estimation methods such as LS, STA, DFT. These results only consider vehicular propagation environments, such as Marrun in [127] and ETSI in [112]. Then, this result has not yet been evaluated in the literature for railway scenarios, where channel variability may be greater than in vehicular scenarios. In this section, the performance results of 802.11p for different railway propagation scenarios are shown and the following questions are answered:

- Which is the channel estimation method used in 802.11p that will provide the best performance on railway channels?
- Which is the effective bit rate that 802.11p can provide on the railway communication link?
- Which is the behavior of 802.11p in terms of PER performance when the Doppler frequency varies?

Comparison of channel estimation algorithms

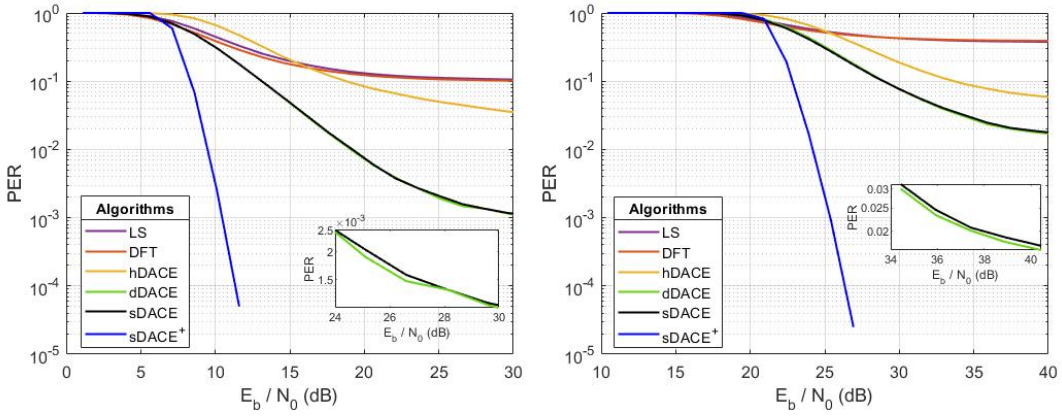

(a) QPSK-1/2 (b) 64QAM-2/3

Figure 5.9: Behavior of 802.11p for different channel estimation algorithms using Winner II channel model with maximum Doppler frequency of 1000 Hz.

Fig. 5.9 shows the performance results of 802.11p for different channel estimation methods using a Winner II channel model with a maximum Doppler frequency of 1000

Hz. In the simulations, the QPSK-1/2 and 64QAM-2/3 schemes and a packet length of 400 bytes are considered. The results indicate that using both MCS modes, the performance of LS and DFT is close and heavily degraded since their PER performance is always higher than 10^{-1} at any E_b/N_0 considered. This result is expected since both methods estimate the channel only at the beginning of the packet, which is inefficient in channels with fast fading as in this case (high Doppler). Moreover, the hDACE method improves the 802.11p performance with respect to the LS and DFT methods for $E_b/N_0 > 15$ dB. However, its PER performance continues being high, equal to $3 \cdot 10^{-2}$ at $Eb/N_0 = 30$ dB in Fig. 5.9a.

In addition, Fig. 5.9a and Fig. 5.9b show also the performance of sDACE when only AWGN is considered. In that situation, denoted by sDACE$^+$, the multipath effect is not simulated. Finally, the sDACE and dDACE methods have the best performance, obtaining a PER performance below 10^{-2} when $E_b/N_0 > 20$ dB in Fig. 5.9a. Please note that using sDACE and dDACE, significant differences are hardly observed in the 802.11p performance for the two MCS schemes used. In order to visualize these differences, a snapshot of the performance of both methods is included in Fig. 5.9a and Fig. 5.9b. These results would be caused since the channel frequency responses estimated in two consecutive OFDM symbols are correlated (please see Section 5.2.3.2).

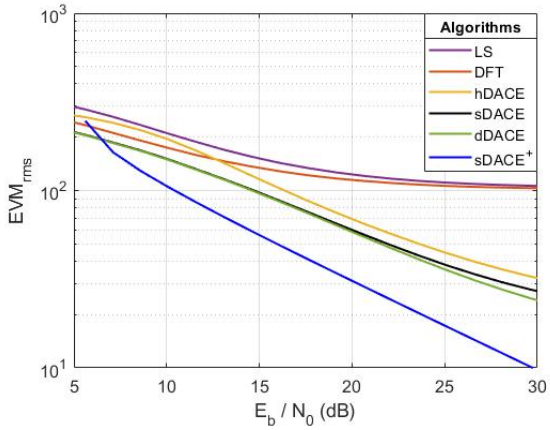

Figure 5.10: Error vector magnitude EVM$_{rms}$ for different channel estimation algorithms using Winner II channel model, QPSK-1/2, and maximum Doppler frequency of 1000 Hz.

Another metric to evaluate the performance of the analysed channel estimation methods, is the error vector magnitude EVM$_{\text{rms}}$. Fig. 5.10 shows EVM$_{\text{rms}}$ for different channel estimation algorithms using Winner II channel model, a Doppler frequency of 1000 Hz, and a payload of 400 bytes. The results show again that the sDACE and dDACE methods obtain the best performance in terms of EVM$_{\text{rms}}$ in comparison to the others, while LS obtains the worst one. Also, a slight improvement in EVM$_{\text{rms}}$ is obtained by dDACE over sDACE for $Eb/N_0 > 25$ dB, but it does not achieve an improvement in the PER performance (see Fig. 5.9a).

Furthermore, given that the performance of 802.11p would change drastically from a T2I to a T2T scenario, we also investigate the performance of the analyzed channel estimation algorithms for a T2T link. Fig. 5.11 shows the 802.11p performance results for different channel estimation methods using the MD1 channel model, which considers T2T distances between 5-100 meters and a maximum Doppler frequency of 200 Hz. Also, two MCS schemes and a packet length of 400 bytes are considered in this test. The results

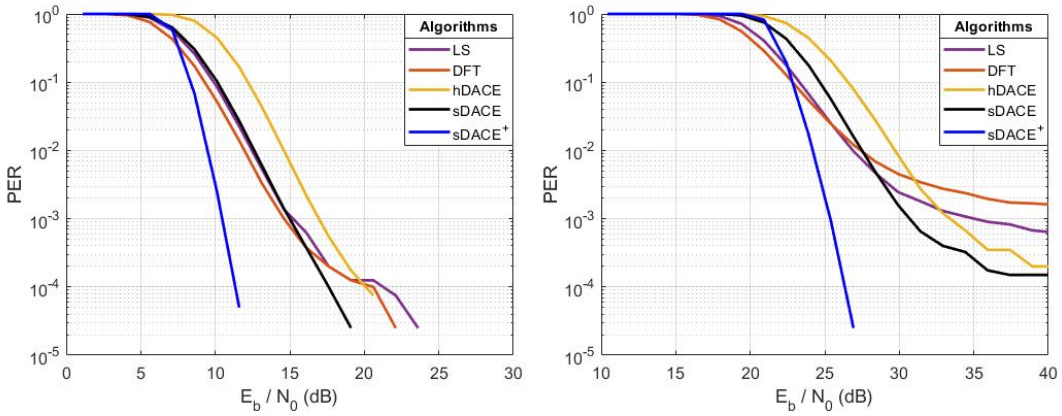

(a) QPSK-1/2 (b) 64QAM-2/3

Figure 5.11: Behavior of 802.11p for different channel estimation algorithms using the MD1 proposed channel model, maximum Doppler frequency of 200 Hz, and payload of 400 bytes.

show that error-free transmission, considered when PER $< 10^{-5}$, is possible for all the channel estimation algorithms analyzed. However, the hDACE method has the worst performance, which has a loss in E_b/N_0 about of 2 dB at a PER of 10^{-3} with respect to the other algorithms analyzed, as shown in Fig. 5.11a. This behavior would be caused by error propagation in the algorithm feedback loop, because it does not use the Viterbi decoder.

Moreover, the performance curves of the DFT, LS, and sDACE methods are close with a slight improvement of PER performance for the DFT method when $E_b/N_0 < 15$ dB (see Fig. 5.11a). Please note that the maximum Doppler frequency in the MD1 model is about 200 Hz, thus performance of DFT and LS is not affected, unlike in Fig. 5.9a. However, when a higher modulation is used (Fig. 5.11b), the performance of DFT and LS is degraded for $E_b/N_0 > 27$ dB and a noise floor is obtained. In addition, sDACE achieves again the best performance for $E_b/N_0 > 30$ dB as well as a gain about 2 dB over hDACE for any target PER. The performance of dDACE is not shown in Fig 5.11 as it has a similar performance to sDACE but a higher computational requirement.

Throughput of communication link

The effective data rate or throughput of a communication link is a relevant metric that indicates how many data bits can be transmitted per unit of time. Fig. 5.12 shows the throughput of 802.11p for two different situations. First, obtained throughput for each channel estimation method analyzed previously are shown in Fig. 5.12a. In this situation, the T2I link is modelled using the Winner II model. The results show again that sDACE obtains the best performance in terms of throughput, performing closer to the reference one (blue line). As a result, the sDACE method in next simulations will be used.

Furthermore, Fig. 5.12b shows the throughput of 802.11p when sDACE is used, together with three of the proposed channel models in this thesis. These models simulate a T2T link in Hilly Terrain propagation scenario. When the T2T distance increases, the throughput should decrease since propagation conditions worsen, increasing the packet loss. For instance, the throughput varies from 20 to 15 Mbps when the channel changes from MD1 to MD2, respectively. Please note that while MD1 considers T2T distances

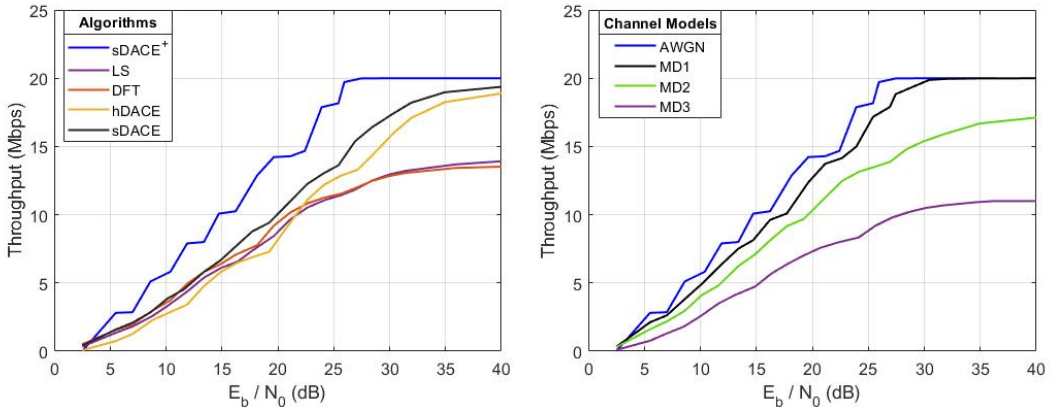

(a) Using Winner model, Doppler 1000 Hz (b) Using T2T-MD models, sDACE algorithm

Figure 5.12: Behavior of throughput versus E_b/N_0 with 400 bytes of payload.

of 5-100 meters, MD2 considers T2T distances of 400-500 meters. These results are consistent with what was expected.

802.11p defines eight modulation and coding schemes and has a maximum data rate of 27 Mbps (see Section 2.2.1). These schemes are identified in Fig. 5.12a and Fig. 5.12b as the eight steps over the blue reference line, where only AWGN is simulated and a maximum throughput of 20 Mbps is achieved. Channel impairments cause that in the proposed channel models, the 802.11p maximum throughput is 20 Mbps, which is only obtained in the MD1 channel at $E_b/N_0 = 30$ dB (please see Fig 5.12b).

Impact of varying Doppler frequency

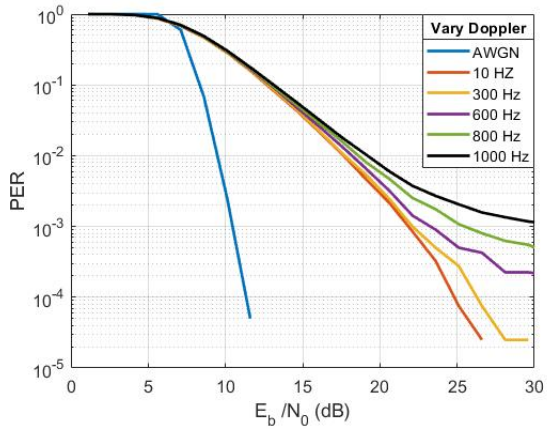

Figure 5.13: Behavior of 802.11p using the sDACE channel estimation method, the Winner II model with different Doppler, QPSk-1/2 and 400 bytes of payload.

Fig. 5.13 shows the behavior of 802.11p when the maximum Doppler frequency $\eta_{\max}$ varies from 10 to 1000 Hz. The results indicate that the performance of 802.11p is progressively degraded. For instance at $E_b/N_0 = 25$ dB, the PER performance is degraded by more than an order of magnitude when $\eta_{\max}$ varies from 10 to 1000 Hz. Based on this result, the oncoming protocol 802.11bd should include more advanced

techniques and algorithms for channel tracking, and their performance must be verified with realistic channel models. Thus, the use of midamble symbols is one of the alternatives included in 802.11bd for better channel tracking.

5.5.3 Performance results for 802.11bd

The channel estimation methods available for 802.11bd were presented in Section 5.3, where DACE and CPCE were described in detail. In this section, the obtained results for 11*bd* and 11bd^+ are shown and analyzed for different configurations and railway channel scenarios. The results also include the ones for 11*p*, as they are taken as a reference. Please note that for these simulations, 11*p* implements the sDACE method which obtained the best performance for 802.11p in the previous section. Then, the performance results of 11*bd* and 11bd^+ are compared and the following questions are answered:

- Which is the optimal value of M and N_p in the simulated scenarios?
- What is the performance gain provided by DCM?
- How is the system performance affected when the payload size is incremented?
- Which is the effective bit rate that 802.11bd can provide on a railway communication link?
- Which is the behavior of 802.11bd in terms of PER performance when the Doppler frequency varies?

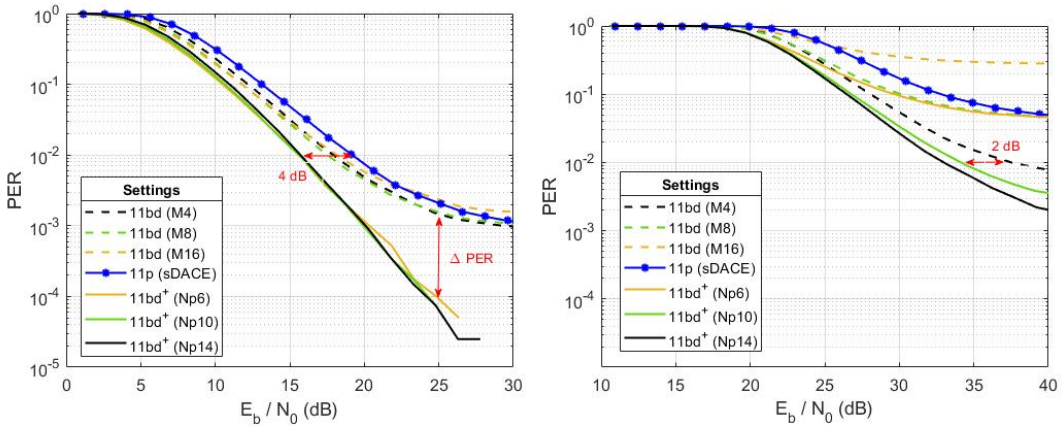

(a) QPSK-1/2 scheme (b) 64QAM-3/4 scheme

Figure 5.14: Comparison of PER performance of 11*bd* (M = 4,8,16) and 11bd^+ (Np = 14,10,6) using a Winner II channel model, maximum Doppler frequency of 1000 Hz, and payload of 400 bytes.

Analysis of M and N_p

Fig. 5.14 show the performance of 11*bd* and 11bd^+ configurations for two MCS schemes QPSK-1/2 and 64QAM-3/4, different choices of (M,N_p), Winner II channel model, and payload of 400 bytes. For both schemes, the performance of 11bd^+ (solid

lines) is higher than $11bd$ (dashed lines) for any combination of midamble rate M and pilot subcarriers N_p used. As results, a E_b/N_0 gain greater than 5 dB can be obtained for a target PER equal to 10^{-3}. In addition, for $E_b/N_0 = 25$ dB, there is a performance improvement ΔPER of about an order of magnitude if $11bd^+$ is used instead of $11bd$ (see Fig. 5.14a). Please note that using QPSK-1/2, small performance differences are hard to observe among the N_p values used in $11bd^+$, as well as among the M values used in $11bd$. However, when a higher MCS is considered in Fig. 5.14b, these differences are clearly observed, where $11bd$ ($M = 16$) and $11bd^+$ ($N_p = 6$) get the worst result. In consequence. these options are not used in the next simulations. In addition, $11bd^+$ ($N_p = 10, 14$) obtains the best performance and a E_b/N_0 gain of 2 dB at PER $= 10^{-2}$ is obtained over $11bd$ ($M = 4$) .

Furthermore, Fig. 5.14 also shows that the $11p$ performance is poorer than the $11bd^+$ and $11bd$ performance. For instance, $11bd^+$ and $11bd$ achieve a E_b/N_0 gain at PER $= 10^{-2}$ of 3 and 1 dB over $11p$ in Fig. 5.14a, respectively. These gains are obtained since the LDPC coding technique used in $11bd^+$ and $11bd$ has a gain over the convolutional coding used in $11p$, as stated in [147].

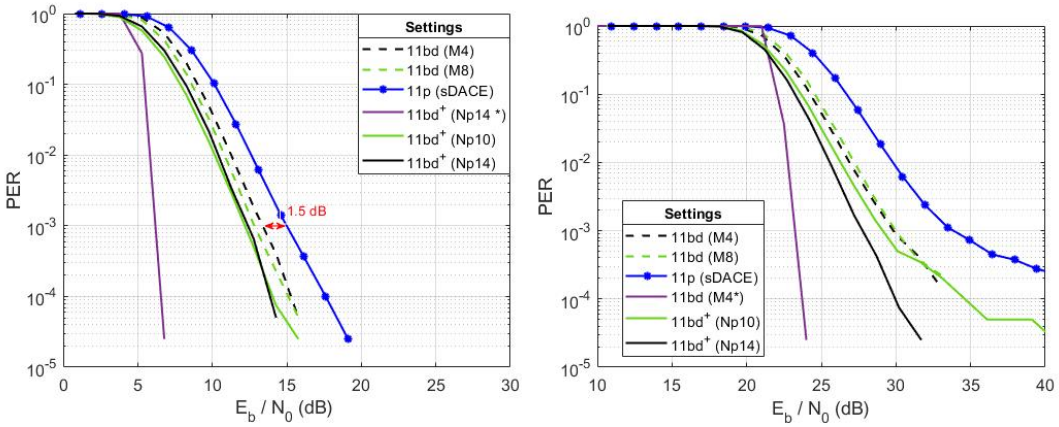

(a) QPSK-1/2 scheme (b) 64QAM-3/4 scheme

Figure 5.15: Comparison of PER performance of $11bd$ (M = 4,8) and $11bd^+$ (Np = 14,10) using MD1 channel model, maximum Doppler frequency of 200 Hz, and payload of 400 bytes.

On the other hand, Fig. 5.15 shows the performance of $11bd$ and $11bd^+$ for the previously mentioned configuration, but in this case the MD1 channel model is used. The obtained results show that although the error-free transmission (PER $< 10^{-5}$) is possible for $E_b/N_0 > 20$ dB in Fig.5.15a, $11bd^+$ again achieves better PER performance than $11bd$, since a performance improvement is always observed for any E_b/N_0, MCS, and used combination of M and N_p. Moreover, a slight performance improvement is observed when $11bd^+$ is set up with $N_p = 10$ instead of $N_p = 14$, as well as when $11bd$ is set up with $M = 8$ instead of $M = 4$ (see Fig. 5.15a). It is important to remark that in the last situation, the packet length for $N_p = 10$ and $M = 8$ is smaller than $N_p = 14$ and $M = 4$. On account of this, the throughput would be increased since fewer overhead symbols are transmitted. A recommendation in this scenario is to implement adaptive algorithms to select the most suitable M and N_p at time.

Also, $11bd^+$ and $11bd$ achieve a E_b/N_0 gain at PER $= 10^{-3}$ with respect to $11p$ between 1.5 and 5 dB, respectively (see Fig. 5.15), depending on the MCS, and the choice of M and N_p. For instance, using $N_p = 10$ and $M = 8$ with 64QAM-3/4, the E_b/N_0 gain

is about of 4 and 3.5 dB respectively. In addition, Fig. 5.15 shows also the performance behavior of $11bd^{+}$ ($N_p = 14$) and $11bd^{+}$ ($M = 4$), when only AWGN is considered. In that situation, denoted by $11bd^{+}$ ($N_p = 14^{*}$) and $11bd$ ($M = 4^{*}$), the multipath effect is not simulated.

Performance gain of DCM modulation

The behavior of the DCM modulation using a Winner II channel model(with a Doppler of 1000 Hz) is shown in Fig. 5.16a. For both MCS modes, MCS0 and MCS10, the system performance is clearly improved when $11bd^{+}$ is used instead of $11bd$ for any combination of considered MCS and SNR > 8 dB. Please note, while MCS0 mode uses the BPSK-1/2 scheme, MCS10 mode combines the MCS0 mode with DCM modulation (see Section 2.3.3.1). Given a target PER, the SNR interval between the performance curves for both MCS0 and MCS10 modes is defined by the DCM gain and denoted as ΔDCM in Fig. 5.16. Using $11bd^{+}$, a $\Delta\text{DCM} = 2.1$ dB at $\text{PER} = 10^{-3}$ is achieved which is held for any target PER considered. However using $11bd$, this gain is about 1.8 dB at $\text{PER} = 10^{-1}$ but this begins to decrease progressively and becomes $\Delta\text{DCM} = 0$ dB.

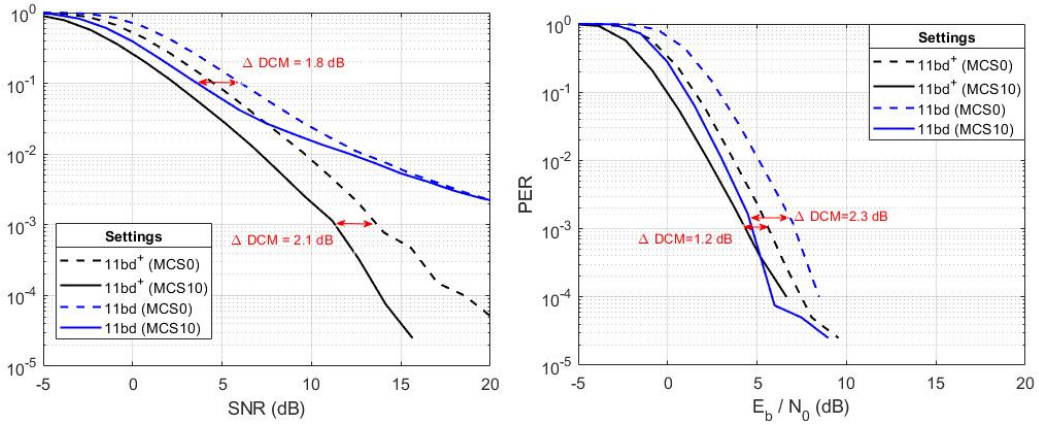

(a) T2I link using the Winner II channel model (b) T2T link using the MD1 channel model

Figure 5.16: Behavior of DCM modulation for $11bd$ ($M = 4$) and $11bd^{+}$ ($N_p = 14$) using a payload of 400 bytes.

On the other hand, the behavior of the DCM modulation in a T2T link (MD1 channel model) is shown in Fig. 5.16b. Again, $11bd^{+}$ achieve better performance than $11bd$ for both MCS options (MCS0 and MCS10). In addition, ΔDCM for $11bd^{+}$ is about of 1.2 dB at 10^{-3}, which is lower in comparison to the previous scenario (T2I link). This result is obtained because the channel variability in simulated T2I link (Doppler 1000 Hz) is higher than in the simulated T2T link (Doppler 200 Hz). However, a different result is obtained for $11bd$ where $\Delta\text{DCM} = 2.3$ dB at $\text{PER} = 10^{-3}$ and it is held for any target PER. Moreover, the error-free transmission is possible for all the used configurations in this scenario (MD1 channel model), which considers T2T distances of 5-100 meters.

These results indicate that the CPCE method used in $11bd^{+}$ matches better with DCM modulation than the MCE method used in $11bd$ in the analyzed scenarios.

Impact of Payload size

As discussed in Section 2.3.1, 802.11bd will need to support a wide variety of use cases, which demand different system requirements. For example, advanced sensors require payload sizes greater than 1000 bytes [25], while T2T requires packet lengths below 400 bytes [41]. As a consequence to this, the new protocol should have a stable performance with respect to payload variations. The PER performance results of $11bd$, $11bd^{+}$ and $11p$ for a varying the packet size are shown in Fig. 5.17 for two channel models and a $E_b/N_0 = 15$ dB. Please note, the MD2 proposed channel model is used to simulate the T2T communication link which considers T2T distances of 400–500 meters. Again, $11bd^{+}$ reaches better performance (lower PER) than $11bd$ and $11p$ for any chosen payload size and channel model.

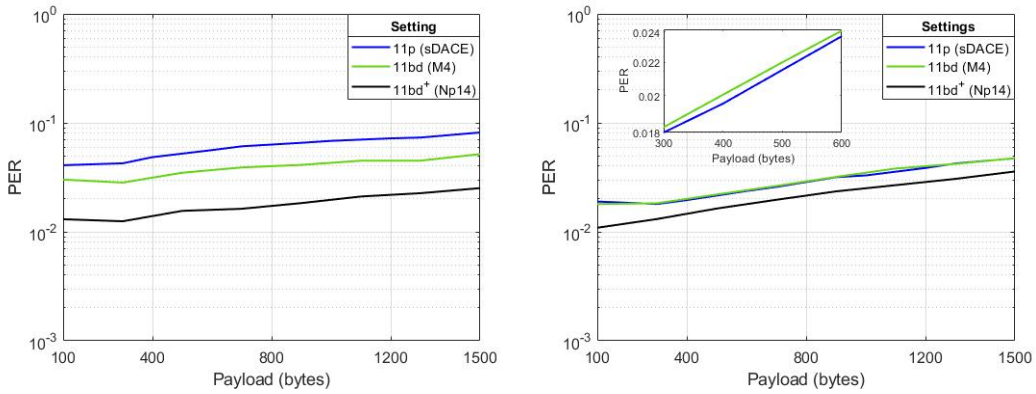

(a) T2I link using the Winner II channel model (b) T2T link using the MD2 channel model

Figure 5.17: Behavior of PER versus Payload for $11bd$ ($M = 4$), $11bd^{+}$ ($N_p = 14$), and $11bd^{+}$ (sDACE) with QPSK-1/2 scheme and $E_b/N_0 = 15$ dB.

PER performance curves tend to vary linearly with positive slope in both Fig. 5.17a and Fig. 5.17b. The envelopes look alike to those shown in [8], where the LS and STA methods are tested in 802.11p. In addition, using the MD2 model in Fig. 5.17b, significant differences are hardly observed between the performance curves of $11bd$ and $11p$, unlike what was observed in 5.17a. In order to visualize these differences, a snapshot of the performance of both configuration is included in Fig. 5.17b.

These results indicate that $11bd^{+}$ would have a better behaviour than $11bd$ when the communication link is carried out in mixed scenarios with or without infrastructure, where the requirements of packet size are different.

Throughput of the communication link

Fig. 5.18 shows the throughput of $11bd^{+}$ and $11bd$ for two different situations. First, the obtained throughput results for $11bd^{+}$ ($N_p = 14, 10$), $11bd$ ($M = 4, 8$), and $11p$ (reference curve) in a T2I link are shown in Fig. 5.18a. The results indicate that while $11bd^{+}$ ($N_p = 10$) achieves the best performance for $E_b/N_0 < 20$ dB between all the used configurations, $11p$ surpasses this for higher E_b/N_0. In addition, considering only $11bd$, the $M = 8$ option obtains the highest throughput for $E_b/N_0 < 32$ dB. The figure shows also a snapshot where the previously mentioned differences can be seen in detail.

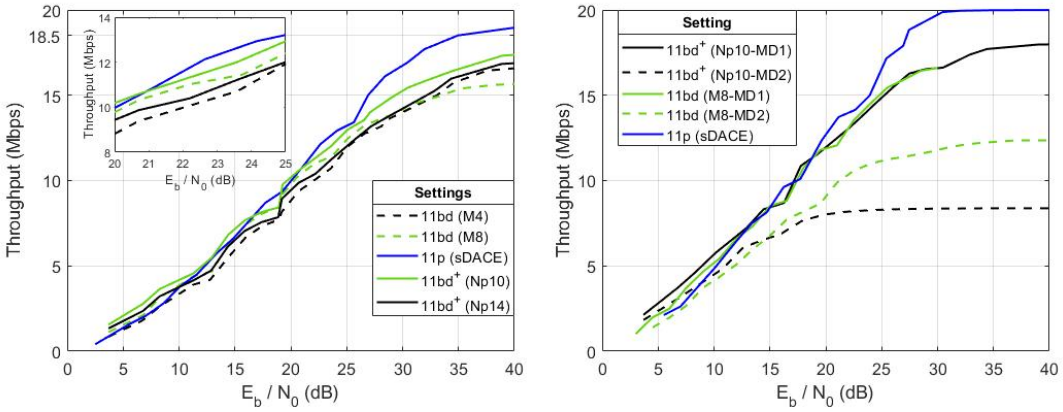

(a) T2I link using the Winner II model (b) T2T link using the MD1 and MD2 models

Figure 5.18: Behaviour of throughput for 11*b* (M=4,8), 11bd^+ (Np=14,10), and 11*p* (sDACE).

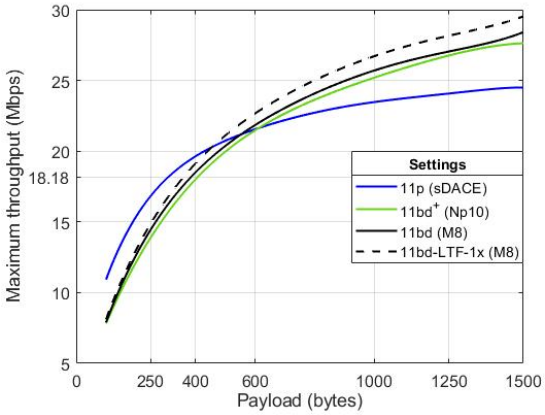

Figure 5.19: Maximum throughput considering PER $= 0$ and higher MCS mode.

In orden to explain why 11*p* achieves the best throughput in Fig. 5.18a for $E_\mathrm{b}/N_0 > 20$, we would like to show Fig. 5.19, where the behaviour of maximum throughput versus payload is shown. The maximum throughput Th_max is reached when PER $= 0$ and the higher MCS mode is used in Equation 24. The results indicate that 11*p* obtains higher Th_max than 11*bd* ($M = 8$) and 11bd^+ ($N_p = 10$) when payload is lower than 600 bytes. In addition, 11*bd* ($M = 8$) and 11bd^+ ($N_p = 10$) would obtain a Th_max about of 18.18 Mbps at a payload of 400 bytes, that is the case analyzed in Fig. 5.18a. Please note, both 11*bd* and 11bd^+ introduce overhead symbols in the frame with respect to 11*p* for backwards-compatibility and channel estimation purposes, which has a penalty in the throughput. In order to smoothing this situation, 11*bd* can use shorter midamble symbols by using TLF-1x mode (please see Section 2.3.2). Thus so, 11*bd* using the TLF-1x mode improves its throughput with respect to 11*p* for payload higher than 460 bytes as shown in 5.19. In addition, both 11*bd* and 11bd^+ can be set up in channels with 20 MHz bandwidth and so their throughput can be duplicated.

Moreover, similar results can be obtained when we use the MD1 and MD2 channel models in Fig. 5.18b. Please note that as these models depend on the T2T distance, the obtained throughput does it too. Thus, the throughput decreases when we change the model from MD1 to MD2. For instance, using 11*bd* ($M = 8$), the throughput at

$E_b/N_0 = 30$ dB varies from 16.59 to 11.70 Mbps when the channel model is changed from MD1 to MD2. The MD2 model considers T2T distances of 400-500 meters, has a delay spread higher than 1 ms, has a low variability with a Doppler frequency of 204 Hz. At this distances, the performance of higher modulations for $11bd$ and $11bd^+$ is hardly degraded caused by both synchronization and channel estimation errors.

Impact of varying Doppler frequency

Fig. 5.20 shows the behavior of $11bd$ and $11bd^+$ when the maximum Doppler frequency $\eta_{\max}$ varies from 10 to 1000 Hz. The results indicate that performance of both configurations is progressively degraded when $\eta_{\max}$ increases. For instant at $E_b/N_0 = 25$ dB, the PER performance of $11bd$ is degraded by more than an order of magnitude (10^{-1}) when $\eta_{\max}$ varies from 10 to 1000 Hz. While the error-free transmission is possible for $11bd^+$ when $\eta_{\max}$ varies, the $11bd^+$ performance curves would reach a noise floor for $\eta_{\max} > 600$ Hz and $E_b/N_0 > 28$ dB. In addition, the CPCE method used in $11bd^+$ is more robust to variations of $\eta_{\max}$ than the MCE method used in $11bd$, thus it always reaches a lower PER than 10^{-3} for $E_b/N_0 < 21$ dB and any simulated $\eta_{\max}$, see Fig. 5.20b. This result is obtained by $11bd$ when $\eta_{\max} < 300$ Hz in Fig. 5.20a. Please note that CPCE and MCE methods are used in 802.11bd for channel tracking.

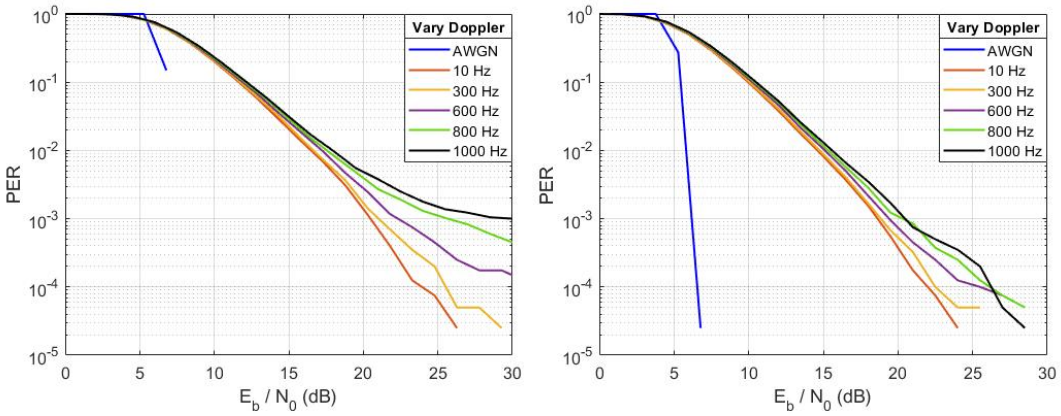

(a) $11bd$ using $M = 4$ (b) $11bd^+$ using $N_p = 4$

Figure 5.20: Behavior of packect error rate (PER) versus simulated maximum Doppler frequency using the Winner II model, QPSk-1/2 and 400 bytes de payload.

5.6 Summary and conclusions

802.11bd is a competitive candidate to be one of the most used protocols in vehicular communications in the near future. In this chapter, channel estimation for 802.11p/bd systems has been introduced and different channel estimation methods have been analyzed and compared for multiple railway propagation environments. In addition, a CPCE method has been proposed as an alternative to the MCE method (proposal at ETSI to be standardized in 802.11bd). Moreover, the LS, DFT, hDACE, sDACE, and dDACE channel estimation methods have been considered for 802.11p, which performance is taken as reference. Simulated channels consider two railway communication scenarios:

a T2I link using the Winner II channel model [12] and a T2T link using the proposed TDL channel models in Chapter 4.

Provided simulation results prove that $11bd^{+}$ (using the proposed CPCE method) is superior to both $11bd$ (using the MCE method) and $11p$ (using the sDACE method) in terms of PER in the analyzed scenarios. It can achieve a gain higher than 3 dB over $11bd$ for a target PER equal to 10^{-2}. In addition, a performance gain (ΔPER) of up to an order of magnitude can be obtained at high E_b/N_0 values. The performance gain of DCM has been analyzed and assesed with the considered channel estimation algorithms, showing that it improves the system performance and combines better with $11bd^{+}$ than $11bd$. Moreover, it is shown that the use of DCM with $11bd$ (MCS10 mode) is not recommended in some situations, for instance for $E_{\mathrm{b}}/N_0 = 15$ dB in T2I links (Winner II model). Also, it is verified that when low packet sizes are considered, i.e below of 600 bytes, the performance of $11p$ in term of maximum throughput is greater than $11bd$ and $11bd^{+}$.

6 Conclusions and future work

6.1 Conclusion

VANETs provide the opportunity to improve traffic safety and transportation management through the use of cooperative systems based on V2X communications. In this thesis we evaluated the use of the subset of V2X technologies considered to be the enablers for traffic safety services, i.e. the 802.11 amendments, in railway environments. Moreover, we introduced the current proposal for amendment 802.11bd, which is beyond the state of the art, and additionally evaluated its performance as railway wireless technology. The choice of the 802.11-based standards was made upon the completion of an state of the art analysis of the existing technologies, which can support T2T and T2I communications. The conclusion of this analysis showed that the ITS-G5 standard had desiable characteristics to support both communications links, in addition to high reliability and low latency.

Referring to the objectives and hypotheses stated in Sections 1.2 and 1.3 respectively, and based on the results shown and discussed in this thesis report, the conclusions are addressed into two research fields: channel modelling and communication protocol evaluation. In the first field, we derived the small-scale propagation characteristic of a T2T wireless channel based on measurement campaign results field and proposed six TDL models for Hilly Terrain and Railway Station scenarios. In the second topic, we incorporated the proposed TDL models and the Winner II channel model into a 802.11p/bd framework, in order to evaluate the performance of these protocols in both T2T and T2I communication links. Moreover, different channel estimation methods were considered, where a CPCE method was proposed as an alternative to the MCE method (included in the standardization of 802.11bd). CPCE increases the number of pilot subcarriers in comparison to MCE, and uses them to track the channel for each OFDM symbol.

Related to channel modeling, in line with the second objective in Section 1.2, the proposed TDL models consider different T2T distances and relative speeds of up to 50 km/h with trains moving in an approaching maneuver. The channel implementations of the proposed TDL models were closely following the results based on the measured channel impulse response, indicating a good accuracy of the theoretical derivation and the simulation method. Hence, the TDL channel models provide valid simulation results. Moreover, a study about the Doppler-delay behavior in the considered scenarios reveals that Railway Station scenario is very rich in reflecting obstacles, which deteriorates the

propagation conditions. As a consequence of that, more robust modulation and coding schemes should be used in this scenario.

Furthermore, it was observed that the stochastic channel parameters are time variant and T2T distance dependent. While delay spread σ_τ varies from 84 ns to 820 ns, Doppler spread σ_τ varies from 37 to 237 Hz, when short or large distances are considered in Hilly Terrain. Thus, the stochastic channel parameters obtained can be used as a reference in the design of future communication protocols. We also showed that the DSP0 and DSP1 modes, which describe how the Doppler spectrum is simulated in a TDL model, cause only small differences in the 802.11bd performance although the DSP0 mode is much simpler to implement.

In relation to communication protocol evaluation, in line with the first objective in Section 1.2, we developed an 802.11-based framework which incorporated the full physical layer of the 802.11p and 802.11bd standards using different channel estimation methods. Three configurations were chosen: 802.11p using the sDACE method denoted as $11p$, 802.11bd using the MCE candidate method denoted as $11bd$, and 802.11bd using the CPCE proposed method denoted as $11bd^+$. The proposed framework allows to evaluate the reliability of the chosen configurations in terms of packet error rate (PER) and throughput.

Provided simulation results prove that in scenarios with high Doppler frequency, the approach of increasing the number of pilot subcarrier is effective since $11bd^+$ archives a better performance in terms of PER than both $11bd$ and $11p$. For instance, on T2I scenario, $11bd^+$ ($N_p = 14, 10$) can obtain a E_b/N_0 gain greater than 2 dB over $11bd$ ($M = 4$) and $11p$ depending on the used MCS, chosen PER target and payload of 400 bytes. In this case, the worst performance is always obtained by $11p$. On T2T scenario where the simulated Doppler frequency is lower than in T2I, the performance gap of $11p$ with respect to $11bd$ and $11bd^+$ is reduced. Moreover, the use of overhead symbols (preambles, midambles and additional pilot subcarriers) in $11bd$ and $11bd^+$ due to compatibility issues, penalizes their throughput with respect to $11p$.

Related to communication protocol evaluation, in line with the third objective in Section 1.2, we proved that DCM modulation, candidate technique in 802.11bd, matches better with $11bd^+$ (using CPCE) than $11bd$ (using MCE) since the DCM gain obtained is held for any chosen values of SNR. In addition, the use of DCM with $11bd$ is not recommended in scenarios with high Doppler since DCM gain tends to zero as SNR increases. Moreover, we showed that an increment in the packet size provokes a degradation in the performance of the evaluated configurations which has a linear trend. In the considered scenarios, the configurations $11bd^+$ ($N_p = 10$) and $11bd$ ($M = 8$) provide the best performance in terms of both PER and throughput with respect to the configurations $11bd^+$ ($N_p = 6, 14$) and $11bd$ ($M = 4, 16$), respectively.

Considering all the aforementioned conclusions, we conclude that 802.11bd supports reliable V2X communications in railway environments. Thus, railway transport should progressively incorporate it and exploit its potential and proven advantages to benefit from cooperative connected services in railway. In addition, the use of a CPCE based alternative channel estimation method improves the performance of 802.11bd in scenarios with high Doppler.

6.2 Contributions

In this section we list the main contributions of this doctoral thesis and we show the publications derived from them.

- We have derived six tapped delay line channel models available for T2T communications in the 5.9 GHz band, which cover different T2T distances and two railway scenarios (Hilly Terrain and Railway Station). The results obtained in this thesis complement the works carried out on T2I channel modelling shown in the literature [11]. Thus, the proposed T2T channel models can be used to evaluate the performance of any communication protocol based on numerical simulations or laboratory measurements. For the best of our knowledge, there are no such results in the scientific bibliography.
- We have obtained and analyzed the stochastic T2T channel parameters at short, medium, and large distances in the considered scenarios. These parameters are necessary for the design of any communication protocol. For instance in 802.11bd, they determine the length of the cyclic prefix in the OFDM modulation and the midamble rate M. In addition, based on spectral analysis, we have shown how the energy of the transmitted signal is distributed in time, delay and Doppler domains. This contribution together with those shown in [19] and [20] help to fill in the research gap that is observed in the literature with respect to T2T channel characterization.
- We have evaluated the 802.11p/bd performance using T2I and T2T channel models for several configurations that include different modulation and coding schemes, midambles rate, payload sizes and channel estimation methods. This contribution complements the performance results shown by ETSI in [39] where vehicular channel models in the 5.9 GHz band [112] are considered.
- We have proposed and evaluated an alternative channel estimation method for the 802.11bd frame structure that improves its performance in railway channels with high Doppler frequency, named CPCE method. The proposed method is also benchmarked against the candidate channel estimation method (MCE) for 802.11bd using different performance indicators such as PER, BER and E_{b}/N_0.

These are the works related to channel modelling and estimation on which the author of this thesis appears as author.

- E. Mozo, A. Alonso-Gómez, and M. Mendicute, "Performance Analysis of Pilot Patterns for Channel Estimation for OFDM Systems in High-Speed Trains Scenarios," in IEEE 30th Annual International Symposium on Personal, Indoor and Mobile Radio Communications (PIMRC), 2019, p. 7.
- E. Mozo, A. Alonso-Gómez, and M. Mendicute, "Channel estimation methods for IEEE 802.11 bd in vehicular channels with high Doppler," Sensors, 2022. (Pending of submission)
- E. Mozo, P. Unterhuber, A. Alonso-Gómez, S. Sand, and M. Mendicute, "Measurement based Tapped Delay Line Model for Train-to-Train Communications," submitted to IEEE Transactions on Vehicular Technology (28-07-2021), p. 13. (resubmitted 25-01-2022, under review)

These are the works related to railway measurement campaigns on which the author of this thesis appears as co-author.

- A. Alonso-Gómez, E. Mozo, L. Bernadó, S. Zelenbaba, T. Zemen, F. Parrilla, and A. Alberdi, "Performance analysis of ITS-G5 for smart train composition coupling," in Proceedings of 2018 16th International Conference on Intelligent Transport System Telecommunications, 2018, p. 7.
- S. Zelenbaba, L. Mayer, E. Mozo, F. Wirth, R. Hladik, A. Alonso-Gómez, L. Bernadó, M. Schiefer, and T. Zemen, "Characterization of Time-Variant Wireless Channels in Railway Communication Scenarios," in IEEE 2nd 5G World Forum (5GWF), 2019, p. 6.

6.3 Future work

Considering the current state of our research and the work carried out during this doctoral thesis, some opportunities for future investigation have been identified which are presented in this section. These research opportunities are geared towards railway channel modeling and 802.11bd performance evaluation under more realistic conditions.

802.11bd should be evaluated both numerically and experimentally, verifying its potential for different use cases. TGbd defined in [7] the techniques and algorithms that could be part of the new amendment. In this thesis, processing techniques such as LDPC, DCM, 256QAM modulation, and MCE has been considered for 802.11bd and their performance evaluated. Then, other processing techniques and configurations that could be evaluated in 802.11bd including 20 MHz channels, MIMO capabilities, packet retransmission techniques. The performance results obtained could be used by hardware designers to optimize their physical layer.

In addition, an experimental evaluation of the protocol under real conditions could be performed using Software Defined Radio (SDR) platforms. They are programmable radios that provide access to data down to the physical layer, allowing to implement the full signal processing in software while the only RF part (antennas, frequency converters, power amplifiers ect) is made through hardware. This aspect makes them particularly well suited to build prototype transceivers and to experiment with novel signal processing algorithms. These platforms have been successfully used to experimentally evaluate other communication protocols in [47] and [168] such as LTE, WIMAX and 802.11p.

There are some parameters in the 802.11bd receiver design that must be optimized to obtain the best system performance. For example, the choice of β and α (see Section 5.3), as well as the detection threshold (see Section 2.3.3.2) can have a significant impact on system performance. In addition, increasing the number of pilot subcarriers N_p or the number of midamble symbols (decrease M), can improve performance, but decreases the throughput. In this sense, these variables must be appropriately chosen in relation to the conditions of the channel using adaptive algorithms.

Six TDL channel models have been proposed and validated for two T2T railway scenarios with trains moving with relative speeds up to 50 km/h. These speeds were chosen due to limitations on the measurement site and the channel sounder. In reality, although the trains could drive faster than 300 km/h, their relative speed $\Delta v'$ could be in the considered relative speed Δv range in this thesis. Given that, what would happen

with the parameters of the proposed TDL models if other Δv and driving maneuvers are considered? This last question is another research gap in T2T communications, where new studies must be carried out.

In addition, a measurement campaign was carried out in [107] for different relative speeds in a T2I scenario. The results show that the measured PDP for $\Delta v = 100$ km/h behave similar to the measured PDP for $\Delta v = 200$ km/h in the same scenario. Also, the T2T communication based on TETRA was analyzed in [18], where no evidence was found of a possible influence of Δv on the message error rate. Based on the shown results in these articles and the ones obtained in this thesis, the following ideas arise for future work in railway channel modelling:

- The average power delay profile $P_\tau[m]$ does not change when Δv changes since it only depends on the geometry of the scenario. As a result, the stochastic channel parameters shown in Table 4.4 should remain valid.
- The average Doppler spectral density $P_\eta[d]$ is spread or compressed when Δv changes since Doppler frequency depends on Δv as was shown in (2). As a consequence, the channel parameters (η_{d_1} and η_{d_2}) shown in Table 4.3 should be scaled by a constant $C_\mathrm{d} = \Delta v'/\Delta v$.
- The channel statistics shown in Table 4.5 should not change except $\bar{\eta}$, σ_η and T_c when Δv changes.

Therefore, measurements with different measurement settings e.g. higher velocities, higher bandwidth or MIMO setups would be of high interest. Additional parameters could be provided by a Train-to-Train Geometry based Stochastic Channel Model (T2T-GSCM) where different velocities and various maneuvers could be considered in different environments. Then, a T2T-GSCM for different railway environments should be derived.

I

Confidence interval for estimated parameters

The confidence interval I_{x} for the mean of a population $X = \{x_1, x_2, ..., x_{N_{\mathrm{c}}}\}$ with N_c elements and a confidence level of $100 \cdot (1 - 2 \cdot \alpha)\%$ is given by [169] as

$$I_{\mathrm{x}} = [I_1; I_2] = \left[\hat{m}_{\mathrm{x}} - t_{N_{\mathrm{c}}-1,\alpha} \cdot \frac{\hat{S}_{\mathrm{x}}}{\sqrt{N_{\mathrm{c}}}}; \hat{m}_{\mathrm{x}} + t_{N_{\mathrm{c}}-1,\alpha} \cdot \frac{\hat{S}_{\mathrm{x}}}{\sqrt{N_{\mathrm{c}}}}\right]. \tag{1}$$

Being $\hat{m}_{\mathrm{x}}$ and $\hat{S}_{\mathrm{x}}$ the mean and the standard deviation of X which are estimated by

$$\hat{m}_{\mathrm{x}} = \frac{1}{N_{\mathrm{c}}} \cdot \sum_{i=1}^{N_{\mathrm{c}}} x_i \tag{2}$$

and

$$\hat{S}_{\mathrm{x}} = \sqrt{\frac{1}{N_{\mathrm{c}} - 1} \cdot \sum_{i=1}^{N_{\mathrm{c}}} (\hat{m}_{\mathrm{x}} - x_i)^2}, \tag{3}$$

respectively. In addition, $t_{a,b}$ represents the t-student distribution with degree of freedom a and probabilistic sample b. The maximum error in the estimate for the confidence level used is given by

$$\varepsilon_{\mathrm{x}} = \frac{I_2 - I_1}{2}. \tag{4}$$

The confidence interval with 95% of confidence ($\alpha = 0.025$) for estimated variables in the proposed channel models is shown in the following tables:

Table I.1: Confidence interval for the MD1 proposed TDL model with 95 % confidence.

Taps	N_{c}	a_i (dB)			N_{c}	τ_i (ns)			N_{c}	k_i (dB)		
		I_{a}	$\hat{m}_{\mathrm{a}}$	ε_{a}		I_τ	$\hat{m}_\tau$	ε_τ		I_{k}	$\hat{m}_{\mathrm{k}}$	ε_{k}
1	43	[-0.1650;0.1650]	0	0.165	43	[-3.8646;3.8646]	0	3.86	43	[-10.3977;14.647]	12.522	2.125
2	43	[-18.3539;-16.1860]	-17.2700	1.084	43	[55.5683;60.0652]	57.8167	2.25	43	[-9.189;-3.105]	-6.147	3.042
3	37	[-22.3408;-20.6614]	-21.5011	0.840	37	[173.2276;180.8831]	177.0554	3.83	43	[-1.017;2.095]	0.539	1.556
4	25	[-26.8364;-22.8494]	-24.8429	1.994	25	[252.3580;266.4419]	259.4000	7.04	43	[-2.828;2.616]	-0.106	2.722
5	13	[-31.3455;-29.0695]	-30.2075	1.138	13	[369.0368;391.4267]	380.2318	11.19	43	[-7.982;-0.864]	-4.423	3.559
6	10	[-30.4651;-26.3048]	-28.3850	2.080	10	[445.3111;473.7311]	459.4211	14.21	43	[-8.411;0.102]	-4.256	4.155
7	2	[-32.1817;-27.7063]	-29.9440	2.238	2	[500.2073;574.2233]	537.2153	37.01	43	[-5.302;-0.237]	-2.770	2.533

Table I.2: Confidence interval for the MD2 proposed TDL model with 95 % confidence.

Taps	N_c	a_i (dB)			N_c	τ_i (ns)			N_c	k_i (dB)		
		I_{a}	$\hat{m}_{\mathrm{a}}$	ε_{a}		I_τ	$\hat{m}_\tau$	ε_τ		I_{k}	$\hat{m}_{\mathrm{k}}$	ε_{k}
1	43	[-0.0568;-0.0568]	0	-0.0568	43	[-1.6698;1.6698]	0	3.0136	43	[6.7403;10.8527]	8.7965	2.0562
2	29	[-17.2015;-15.4866]	-16.3441	0.8574	29	[104.1392;114.8074]	109.4733	2.5415	43	[-6.9904;-0.9194]	-3.9549	3.0355
3	23	[-21.0632;-19.5913]	-20.3272	0.7360	23	[198.8358;207.7427]	203.2892	2.0717	43	[-2.9622;2.1507]	-0.4057	2.5564
4	21	[-20.0240;-16.0143]	-18.7812	2.0048	21	[312.2032;327.1994]	319.7013	1.9641	43	[-2.7522;2.4847]	-0.1338	2.6185
5	8	[-20.3017;-17.2606]	-18.7812	1.5206	8	[396.4184;421.9023]	409.1604	2.1015	43	[-6.9693;0.2617]	-3.3538	3.6155
6	3	[-23.5383;-22.3285]	-22.9334	0.6049	3	[519.7089;525.5513]	522.6301	2.6416	43	[-8.2653;-3.1390]	-5.7021	2.5632
7	3	[-22.2291;-15.3285]	-18.7788	3.4503	3	[597.4188;623.1711]	610.2950	3.0277	43	[-2.2336;4.0040]	0.8852	3.1188
8	2	[-25.8634;-22.2746]	-24.0690	1.7944	2	[706.3306;737.1678]	721.7492	2.1037	43	[-10.6712;-4.1615]	-7.4164	3.2549
9	2	[-24.4899;-17.2724]	-20.8812	3.6087	2	[817.8784;852.9955]	835.4369	2.5447	43	[-8.4281;-0.0931]	-4.2606	4.1675
10	2	[-29.6141;-18.0803]	-23.8472	5.7669	2	[871.8395;955.8115]	913.8255	3.1775	43	[-5.5680;0.7883]	-2.3899	3.1782
11	2	[-25.3218;-22.4374]	-23.8796	1.4422	2	[1008.916;1037.680]	1023.298	3.6949	43	[-13.9987;-6.3753]	-10.1870	3.8117
12	2	[-36.8952;-2.3906]	-19.6429	17.2523	2	[1075.939;1137.743]	1106.841	5.2207	43	[-6.0020;0.8981]	-2.5519	3.4501

Table I.3: Confidence interval for the MD3 proposed TDL model with 95 % confidence.

Taps	N_c	a_i(dB)			N_c	τ_i(ns)			N_c	k_i(dB)		
		I_a	$\hat{m}_a$	ε_a		I_τ	$\hat{m}_\tau$	ε_τ		I_k	$\hat{m}_k$	ε_k
1	43	[-0.4275;0.4275]	0	0.4275	43	[-4.2315;4.2315]	0	4.2315	43	[3.2834;7.5760]	5.4297	2.1463
2	43	[-11.6889;10.3042]	-10.9965	0.6923	43	[100.4369;109.1484]	104.7927	4.3557	43	[-8.4711;0-0.9747]	-4.7229	3.7482
3	43	[-15.3246;-13.4984]	-14.4115	0.9131	43	[198.2943;203.0596]	200.6770	2.3827	43	[-12.1585;-4.3501]	-8.2543	3.9042
4	43	[-14.8060;-11.4762]	-13.1411	1.6649	43	[315.3955;323.4525]	319.4240	4.0285	43	[-6.6752;1.2798]	-2.6977	3.9775
5	43	[-14.4390;-11.9502]	-13.1946	1.2444	43	[402.2536;411.6558]	406.9547	4.7011	43	[-6.8539;2.0755]	-2.3892	4.4647
6	43	[-18.1994;-16.5551]	-17.3773	0.8222	43	[506.6294;513.0517]	509.8406	3.2111	43	[-13.7415;-6.7097]	-10.2256	3.5159
7	43	[-16.2082;-13.1317]	-14.6700	1.5383	43	[616.6899;624.8086]	620.7492	4.0593	43	[-9.2120;0.2454]	-4.4833	4.7287
8	43	[-12.9577;-9.7346]	-11.3461	1.6116	43	[703.0422,714;5107]	708.7764	5.7342	43	[-2.4813;6.4971]	2.0079	4.4892
9	43	[-18.5165;-16.1496]	-17.3330	1.1835	43	[803.8939;809.2474]	806.5707	2.6768	43	[-12.0210;-5.0180]	-8.5195	3.5015
10	43	[-19.8251;-188297]	-19.3274	0.4977	43	[911.1957;912.8247]	912.0102	0.8145	43	[-20.0537;-13.2795]	-16.6666	3.3871
11	43	[-16.4282;-13.8390]	-15.1336	1.2946	43	[1009.871;1019.337	1014.604	4.7329	43	[-11.3587;0.0397]	-5.6595	5.6992
12	43	[-17.3846;-150715]	-16.2281	1.1565	43	[1100.092;1109.159]	1104.625	4.5336	43	[-5.6275;2.0847]	-1.7714	3.8561
13	41	[-19.6502;-18.2610]	-18.9556	0.6946	41	[1210.095;1215.411]	1212.753	2.6580	43	[-16.7602;-9.2215]	-12.9908	3.7694
14	41	[-16.3165;-14.3225]	-15.3195	0.9970	41	[1305.390;1318.185]	1311.787	6.3976	43	[-12.1929;-0.0256]	-6.1092	6.0837
15	32	[-18.2180;16.2889]	-17.2535	0.9646	32	[1398.339;1409.469]	1403.904	5.5653	43	[-10.8694;-2.3142]	-6.5918	4.2776
16	20	[-18.3450;-16.7521]	-17.5485	0.7964	20	[1505.579;1518.014]	1511.797	6.2171	43	[-17.0561;-7.8724]	-12.4643	4.5918

Table I.4: Confidence interval for the MD4 proposed TDL model with 95 % confidence.

Taps	N_c	a_i (dB)			N_c	τ_i (ns)			N_c	k_i (dB)		
		I_{a}	$\hat{m}_{\mathrm{a}}$	ε_{a}		I_τ	$\hat{m}_\tau$	ε_τ		I_{k}	$\hat{m}_{\mathrm{k}}$	ε_{k}
1	52	[-0.0792;0.0792]	0	0.079	52	[-3.4769;3.4769]	0	3.477	52	[5.066;7.241]	6.154	1.0878
2	51	[-17.0436;-15.1387]	-16.0912	0.952	51	[90.8064;98.7409]	94.7736	3.97	52	[-7.865;-2.140]	-5.002	2.8623
3	50	[-19.6528;-17.3191]	-18.4859	1.167	50	[190.2298;196.6489]	193.4394	3.21	52	[-0.430;2.869]	1.220	1.6495
4	47	[-22.6338;-20.5978]	-21.6158	1.018	47	[292.6850;303.9480]	298.3165	5.63	52	[-2.079;2.973]	0.447	2.5258
5	31	[-22.9799;-20.4195]	-21.6997	1.280	31	[392.3706;406.7096]	399.5401	7.17	52	[-2.162;3.2751]	0.557	2.7186
6	21	[-24.2650;-21.4906]	-22.8778	1.387	21	[485.6432;504.7183]	495.1807	9.54	52	[-4.807;1.241]	-1.783	3.0239
7	10	[-27.8291;-22.8212]	-25.3251	2.504	10	[581.7966;615.7309]	598.7638	16.97	52	[-4.836;1.171]	-1.832	3.0032
8	5	[-27.2250;-23.2654]	-25.2452	1.980	5	[669.2486;705.8158]	687.5322	18.28	52	[-1.982;2.438]	0.228	2.2103
9	3	[-31.2433;-22.9578]	-27.1006	4.143	3	[777.4753;818.3429]	797.9091	20.43	52	[-7.277;-0.155]	-3.716	3.5610
10	3	[-29.4242;-24.5126]	-26.9684	2.456	3	[868.2518;934.0543]	901.1531	32.90	52	[-5.557;0.209]	-2.674	2.8830
11	2	[-21.3543;20.9516]	-21.1530	0.201	2	[828.2216;1189.2]	1008.7217	180.50	52	[-2.555;1.800]	-0.378	2.1774

Table I.5: Confidence interval for the MD5 proposed TDL model with 95 % confidence.

Taps	N_c	a_i(dB)			N_c	τ_i(ns)			N_c	k_i(dB)		
		I_a	$\hat{m}_{\mathrm{a}}$	ε_{a}		I_τ	$\hat{m}_\tau$	ε_τ		I_k	$\hat{m}_{\mathrm{k}}$	ε_{a}
1	48	[-0.2695;0.2695]	0	0.2695	48	[-2.9859;2.9859]	0	2.9859	48	[2.1502;6.0735]	4.1118	1.9617
2	48	[-9.0071;-7.2772]	-8.1421	0.8649	48	[102.2189;108.1777]	105.1983	2.9794	48	[-11.7917;-5.5573]	-8.6745	3.1172
3	45	[-12.3877;-10.8252]	-11.6064	0.7812	45	[198.1488;203.6128]	200.8808	2.7320	48	[-10.0488;-4.5615]	-7.3052	2.7437
4	38	[-14.6678;-13.7886]	-14.2282	0.4396	38	[304.2172;310.3590]	307.2881	3.0709	48	[-10.1757;-4.2940]	-7.2348	2.9409
5	34	[-16.4229;-15.0632]	-15.7430	0.6798	34	[403.9313;410.5913]	407.2613	3.3300	48	[-9.5906;-4.0012]	-6.7959	2.7947
6	31	[-16.4450;-15.0229]	-15.7340	0.7110	31	[511.1193;516.5210]	513.8201	2.7009	48	[-6.4777;-0.9987]	-3.7382	2.7395
7	31	[-17.2798;-15.5004]	-16.3901	0.8897	31	[601.2822;612.9442]	607.1132	5.8310	48	[-3.4021;0.7124]	-1.3449	2.0573
8	24	[-18.8478;-17.5293]	-18.1885	0.6592	24	[698.6012;711.5031]	705.0522	6.4509	48	[-4.8519;-0.8314]	-2.8416	2.0103
9	21	[-20.0692;-18.3436]	-19.2064	0.8628	21	[800.5458;814.5232]	807.5345	6.9887	48	[-5.7046;-0.0873]	-2.8960	2.8087
10	16	[-20.6695;-19.7468]	-20.2082	0.4614	16	[903.0180;914.0677]	908.5428	5.5249	48	[-5.3920;0.0033]	-2.6944	2.6976
11	13	[-21.6083;-19.7121]	-20.6602	0.9481	13	[997.7476;1012.554]	1005.151	7.4036	48	[-8.1113;-1.7308]	-4.9210	3.1902
12	12	[-22.1217;-20.7790]	-21.4504	0.6714	12	[1103.950;1116.944]	1110.447	6.4972	48	[-6.7700;-1.7861]	-4.2780	2.4919
13	12	[-24.1249;-21.5232]	-22.8240	1.3009	12	[1207.156;1220.078]	1213.617	6.4608	48	[-5.7012;-0.4998]	-3.1005	2.6007
14	12	[-23.5248;-20.3411]	-21.9329	1.5919	12	[1301.793;1317.541]	1309.667	7.8740	48	[-7.1939;-1.8259]	-4.5099	2.6840
15	10	[-21.6724;-18.9977]	-20.3351	1.3374	10	[1402.979;1424.969]	1413.974	10.9951	48	[-6.5280;-0.6983]	-3.6131	2.9149
16	6	[-23.3618;-21.6616]	-22.5117	0.8501	6	[1484.987;1517.588]	1501.287	16.3006	48	[-5.8684;0.0112]	-2.9398	2.9286

In order to obtain these tables, (1) has been applied to amplitude $a_{i,q}$, delay $\tau_{i,q}$ and k-factor $k_{i,q}$ for each i^{th} resolvable tap, being q the local area index. Please note, the mean of $a_{i,q}$ and $\tau_{i,q}$ denoted by $\hat{m}_{\mathrm{a}}$ and $\hat{m}_\tau$ on these tables, are normalized with respect to the

Table I.6: Confidence interval for the MD6 proposed TDL model with 95 % confidence.

Taps	N_c	a_i(dB)			N_c	τ_i(ns)			N_c	k_i(dB)		
		I_a	$\hat{m}_a$	ε_a		I_τ	$\hat{m}_\tau$	ε_τ		I_k	$\hat{m}_k$	ε_a
1	39	[-0.2404]	0	0.2404	39	[-3.0136;3.0136]	0	3.0136	39	[1.2220;6.6402]	3.9311	2.7091
2	39	[-7.9133;-6.8952]	-7.4042	0.5091	39	[96.5893;101.6723]	99.1308	2.5415	39	[-12.1364;-5.7849]	-8.9607	3.1758
3	39	[-10.5540;-9.8270]	-10.1905	0.3635	39	[194.8462;198.9896]	196.9179	2.0717	39	[-9.8629;-4.0434]	-6.9532	2.9098
4	39	[-12.5893;-11.6883]	-12.1388	0.4505	39	[301.3985;305.3267]	303.3626	1.9641	39	[-10.5570;-3.6410]	-7.0990	3.4580
5	39	[-12.9397;-12.1039]	-12.5243	0.4154	39	[399.4674;403.6704]	401.5689	2.1015	39	[-8.3984;-1.7859]	-5.0922	3.3062
6	39	[-14.1174;-13.1795]	-13.6485	0.4690	39	[501.1678;506.4510]	503.8094	2.6416	39	[-7.0601;-1.4418]	-4.2510	2.8092
7	38	[-15.3999;-14.5412]	-14.9706	0.4293	38	[600.0074;606.0627]	603.0351	3.0277	39	[-4.0195;-0.6594]	-2.3394	1.6800
8	37	[-16.6237;-15.4529]	-16.0383	0.5854	37	[701.3747;705.5820]	703.4784	2.1037	39	[-12.8699;-5.2190]	-9.0445	3.8254
9	37	[-16.8365;-15.7362]	-16.28.63	0.5502	37	[802.2812;807.3706]	804.8259	2.5447	39	[-9.0313;-2.0944]	-5.5629	3.4684
10	35	[-17.1994;-15.8612]	-16.5303	0.6691	35	[900.7959;907.1509]	903.9734	3.1775	39	[-4.4193;-0.2040]	-2.1076	2.3116
11	34	[-17.7932;-16.5352]	-17.1642	0.6290	34	[988.7460;1006.135]	1002.440	3.6949	39	[-7.7476;-1.6061]	-4.6769	3.0708
12	32	[-18.6966;-17.4466]	-18.0716	0.6250	32	[1091.815;1102.256]	1097.036	5.2207	39	[-7.6405;-1.0701]	-4.3553	3.2852
13	24	[-19.2917;-17.5560]	-18.4239	0.8678	24	[1194.367;1206.993]	1200.680	6.3131	39	[-8.6993;-1.4652]	-5.0822	3.6171
14	19	[-19.2379;-17.7088]	-18.4734	0.7646	19	[1297.251;1306.129]	1301.690	4.4389	39	[-12.0319;-4.8061]	-8.4190	3.6129
15	18	[-18.8874;-17.4537]	-18.1705	0.7169	18	[1398.536;1408.935]	1403.736	5.1995	39	[-5.9247;-0.3419]	-3.1333	2.7914
16	13	[-20.3425;-18.4635]	-19.4030	0.9395	13	[1491.550;1509.294]	1500.422	8.8721	39	[-11.2285;-3.8925]	-7.5605	3.6680

first tap. Also, ε_τ for each tap in these models is smaller than the tap resolution $R_\tau = 100$ ns, so the error can be assumed. Based on ε_x of each estimated variable, the accuracy of a_i, τ_i and k_i were chosen. Then, an accuracy of one digit after the decimal point for a_i, 2 ns for τ_i and 0.5 dB for k_i is assumed in Section 4.5.2.2.

Glossary

Symbols

3GPP 3rd Generation Partnership Project. 2, 3, 5, 34–37, 39, 42, 50, 56, 58, 65

A

AWGN Additive White Gaussian Noise. 26, 27, 30, 31, 102, 113, 115, 117, 120

B

BER Bit Error Rate. 4, 18, 32, 108, 127

BSM Basic Safety Message. 14, 36, 37

C

C-ITS Cooperative-Intelligent Transportation Systems. 9, 10

C-V2X Cellular Vehicular-to-Everything. 2, 9, 14, 15, 34, 35, 38, 57–59, 64, 143

CAM Cooperative Awareness Message. 14, 34, 36, 37

CBTC Communication Based Train Control. 2, 50–52, 58, 59, 63, 65

CCH Control Channels. 14, 15

CCTV Closed Circuit Television. 49, 59

CDP Constructs Data Pilot. 101, 102

CFO Coarse Frequency Offset. 26, 31

CIR Channel Impulse Response. 3, 5, 26, 48, 77, 96

CP Cyclic Prefix. 22, 24, 26, 39

CPCE Comb-type Pilot-based Channel Estimation. 3, 6, 99–101, 109, 111, 113, 118, 120, 123–127

D

D2D Device-to-Device. 1, 35

DACE Data Aided Channel Estimation. 102, 104–109, 113, 118

DCM Dual Constellation Modulation. 3, 24, 99, 113, 120, 126, 128

dDACE Double decoding DACE. 107, 113, 115, 116, 123

DFT Discrete Fourier Transform. 104, 108, 114–116, 123

DLR German Aerospace Center. 2, 5, 6, 63, 85

DMRS Demodulation Reference Signals. 37, 39, 40

DSRC Dedicated Short-Range Communications. 13, 15, 36

E

eNodeB Evolved Node B. 34, 35

ERTMS European Rail Traffic Management System. 45, 48, 50, 52, 53, 57, 63

ETCS European Train Control Systems. 53, 54, 62

ETSI European Telecommunications Standards Institute. 3, 6, 13–15, 23, 42, 62, 127

EU European Union. 44, 54, 57, 60

F

FFO Fine Frequency Offset. 26, 31

G

GoA Grades of Automation. 50, 51

GPS Global Positioning System. 11, 51

GSM Global Systems for Mobile Communication. 45, 53, 60, 61

GSM-R Global Systems for Mobile Communication-Railway. 1, 45, 49, 53, 57, 59–63

H

hDACE Hard DACE. 106, 113, 115, 116, 123

I

ICI Inter-Carrier Interference. 15, 30, 31

IDFT Inverse Discrete Fourier Transform. 90, 104

IEEE Institute of Electrical and Electronics Engineers. 13, 14, 17, 42, 50, 56, 58

ITS Intelligent Transportation Systems. 9–11, 14, 36, 40

L

LDPC Low Density Parity Check. 3, 22, 23, 41, 106, 113, 119, 128

LMA Limit of Movement Authority. 51, 52

LoS Line of Sight. 5, 46–48, 67, 90

LS Least Square. 101–104, 110, 114–116, 121, 123

LTE 4G Long Term Evolution. 33–35, 38, 39, 55, 59

LTE-R 4G Long Term Evolution for Railway. 57, 59

LTE-V2X LTE based Vehicular-to-Everything. 33–42

LTS Large Training Symbol. 16, 17, 25, 28, 29, 31, 103

M

MAC Medium Access Control. 13, 15–18, 41, 62

MCE Midamble-based Channel Estimation. 6, 99–101, 108, 109, 113, 120, 123–128

MCS Modulation and Coding Scheme. 5, 6, 17, 24, 33, 37, 105, 106, 115, 119, 120, 122, 126

MIMO Multiple-Input Multiple-Output. 24, 40, 128, 129

MSE Mean Square Error. 102

N

NGV Next Generation Vehicle-to-Everything. 17–19

NGV-Data NGV Data Field. 19

NGV-LTF NGV Large Training Field. 19–21, 23

NGV-SIG NGV Signal Field. 19–21

NLoS Non Line of Sight. 47, 48, 99

NR-V2X New Radio Vehicular-to-Everything. 2, 33–35, 37–42, 139

O

OBU On-Board Unit. 10, 12, 53, 54, 61

OC-BSS Outside the Context of a Basic Service Set. 13

OFDM Orthogonal Frequency Division Multiplexing. 2, 3, 15–20, 22–26, 31–33, 36–39, 41, 42, 58, 59, 62, 99–107, 109–112, 115, 125, 127

P

PER Packet Error Rate. 4, 17, 19, 32, 41, 42, 99, 114–117, 119, 121, 124, 126, 127

PIS Passenger Information System. 49, 59

PLCP Physical Layer Convergence Protocol. 15, 17

PMD Physical Medium Dependent. 15, 16

Q

QoS Quality of Service. 17, 58

R

R-SIG Repeated SIG. 19

RBC Radio Block Centre. 53, 54

RBs Resource Blocks. 36, 37

RNGV-SIG Repeated NGV-SIG. 19

RSU Road-Side Unit. 10–12, 39, 53

S

SCH Service Channels. 14, 15

sDACE Simple decoding DACE. 106, 107, 113, 115, 116, 118, 123, 124, 126

SFD State Feedback Decision. 102, 108

SIG Signal Field. 19, 20

SISO Single-Input Single-Output. 24, 40, 85

SL Sidelink. 34–37

SNR Signal to Noise Ratio. 5, 33, 101–104, 126

STA Spectral-Temporal Averaging. 101, 106, 114, 121

STCC Smart Trains Composition Coupling. 5, 55, 56

STF Short Training Field. 19, 26

STS Short Training Symbol. 16, 17, 25, 30

T

T2G Train-to-Ground. 48, 51

T2I Train-to-Infrastructure. 1–6, 19, 45, 52, 53, 57, 58, 84, 113, 116, 121, 124–126

T2T Train-to-Train. 1–6, 19, 26, 45, 48, 52, 55, 57, 58, 63, 65–67, 84, 85, 90, 113, 115–117, 120, 122, 124–127

TCMS Train Control and Monitoring System. 48, 49

TDL Tapped Delay Line. 3, 5, 6, 48, 65, 66, 79, 124–126

TDLSE Time Domain Least Square Estimation. 101

TDMA Time Division Multiple Access. 60, 62, 63

TETRA Terrestrial Trunked Radio. 2, 54–57, 62, 63

TGbd Task Group 802.11bd. 17, 18, 109, 112

U

UE User Equipment. 34–36, 39

UMTS Universal Mobile Telecommunications System. 49, 59

US United State. 13, 14, 42

V

V2I Vehicle-to-Infrastructure. 34, 41

V2V Vehicle-to-Vehicle. 11, 14, 34, 58

V2X Vehicular-to-Everything. 10–14, 19, 33, 34, 38–40, 42, 50, 125, 126

VANET Vehicular Ad-hoc Networks. 9, 10, 12, 13, 42, 125

W

WAVE Wireless Access in Vehicular Environment. 13, 14

WIMAX Worldwide Interoperability for Microwave. 49, 55, 58

WSSUS Wide-Sense Stationary and Uncorrelated Scatterers. 68, 72

List of Figures

Index of tables

Bibliography

[1] A. Sniady and J. Soler, "An overview of GSM-R technology and its shortcomings," *2012 12th International Conference on ITS Telecommunications, ITST 2012*, pp. 626–629, 2012.

[2] A. Alonso, E. Mozo, L. Bernado, S. Zelenbaba, T. Zemen, F. Parrilla, and A. Alberdi, "Performance analysis of ITS-G5 for smart train composition coupling," *Proceedings of 2018 16th International Conference on Intelligent Transport System Telecommunications, ITST 2018*, 2018.

[3] T. Strang, A. Festag, A. Vinel, R. Mehmood, C. R. Garcia, and M. Röckl, "Measurement and Analysis of the Direct Train to train Propagation Channel in hthe 70 cm UHF-Band," in *International Workshop on Communication Technologies for Vehicles*, vol. 6596 LNCS, no. March, 2011.

[4] Y. Liu, L. Yuan, and P. Wang, "A Study on the Application of Train to Train Communication in Train Control Systems," *International Journal of Simulation Systems, Science and Technology*, pp. 1–6.

[5] ALSTOM, "Lille metro RS and Urbalis Fluence." [Online]. Available: https://www.alstom.com/transport

[6] P. Unterhuber, S. Sand, M. Soliman, B. Siebler, A. Lehner, T. Strang, and D. Gera, "Wide band propagation in train-to-train scenarios - Measurement campaign and first results," in *2017 11th European Conference on Antennas and Propagation, EUCAP 2017*, 2017, p. 5.

[7] B. Sadeghi, "802.11bd Specification Framework Document," in *IEEE Meeting NGV*, 2019, p. 9. [Online]. Available: https://mentor.ieee.org/802.11/documents

[8] J. Fernandez, K. Borries, L. Cheng, V. Kumar, D. Stancil, and F. Bai, "Performance of the 802 . 11p Physical Layer in Vehicle-to-Vehicle Environments," *IEEE Transaction on Vehicle Technology*, vol. 61, no. 1, pp. 3–14, 2012.

[9] Z. Zhao, X. Cheng, M. Wen, B. Jiao, and C. Wang, "Channel Estimation Schemes for IEEE 802.11p Standard," *IEEE Intelligent Transportation Systems Magazine*, vol. 5, no. 4, p. 12, 2013.

[10] E. Mozo, A. Alonso, F. Parrila, and M. Mendicute, "Performance Analysis of Pilot Patterns for Channel Estimation for OFDM Systems in High-Speed Trains Scenarios," in *IEEE 30th Annual International Symposium on Personal, Indoor and Mobile Radio Communications (PIMRC)*. IEEE, 2019, p. 7.

[11] M. Berbineau, R. Behaegel, J. M. Garcia-Loygorri, R. Torrego, R. D'errico, A. Sabra, Y. Yan, and J. Soler, "Channel models for performance evaluation of wireless systems in railway environments," *IEEE Access*, vol. 4, pp. 1–14, 2021.

[12] P. Kyösti, J. Meinilä, L. Hentilä, X. Zhao, T. Jämsä, C. Schneider, M. Narandzić, M. Milojević, A. Hong, J. Ylitalo, V.-M. Holappa, M. Alatossava, R. Bultitude, Y. de Jong, and T. Rautiainen, "Ist-4-027756 Winner II Channel Model," pp. 1–206, 2007. [Online]. Available: http://projects.celtic-initiative.org/WINNER+/WINNER2-Deliverables/D4.6.1.pdf

[13] C. X. Wang, A. Ghazal, B. Ai, Y. Liu, and P. Fan, "Channel Measurements and Models for High-Speed Train Communication Systems: A Survey," *IEEE Communications Surveys and Tutorials*, vol. 18, no. 2, pp. 974–987, 2016.

[14] B. Ai, X. Cheng, T. Kürner, Z.-d. Zhong, K. Guan, R.-s. He, L. Xiong, D. W. Matolak, D. G. Michelson, and C. Briso-rodriguez, "Challenges toward wireless communications for high-speed railway," *IEEE Transactions on intelligent*, pp. 1–16, 2014.

[15] C. R. García, A. Lehner, T. Strang, and K. Frank, "Channel model for train to train communication using the 400 MHz band," *IEEE Vehicular Technology Conference*, pp. 3082–3086, 2008.

[16] P. Unterhuber, S. Pfletschinger, S. Sand, M. Soliman, T. Jost, A. Arriola, I. Val, C. Cruces, J. Moreno, J. P. García-Nieto, C. Rodríguez, M. Berbineau, E. Echeverría, and I. Baz, "A Survey of Channel Measurements and Models for Current and Future Railway Communication Systems," *Mobile Information Systems*, vol. 2016, 2016.

[17] J. J. H. Park, S. C. Chen, J. M. Gil, and N. Y. Yen, "Urban Viaduct Channel Characterization of train to train communication at 900 MHz," *Lecture Notes in Electrical Engineering*, vol. 308, pp. 353–360, 2014.

[18] A. Lehner, T. Strang, and P. Unterhuber, "Direct train-to-train communications at low UHF frequencies," *IET Microwaves, Antennas and Propagation*, vol. 12, no. 4, pp. 486–491, 2018.

[19] S. Zelenbaba, L. W. Mayer, E. Mozo, F. Wirth, R. Hladik, A. A. G, L. Bernad, M. Schiefer, and T. Zemen, "Characterization of Time-Variant Wireless Channels in Railway Communication Scenarios," in *IEEE 2nd 5G World Forum (5GWF)*, 2019, p. 6.

[20] P. Unterhuber, M. Walter, U. Fiebig, and K. Thomas, "Stochastic Channel Parameters for Train-to-Train Communications," *IEEE Open Journal of Antennas and Propagation*, vol. 2, pp. 778–792, 2021.

[21] DLR, "Institute of Communications and Navigation." [Online]. Available: https://www.dlr.de/kn/en

[22] M. Lee and T. Atkison, "VANET applications : Past , present , and future." *Vehicular Communications*, vol. 1, p. 100310, 2020. [Online]. Available: https://doi.org/10.1016/j.vehcom.2020.100310

[23] M. Alam, J. Ferreira, and J. Fonseca, *Intelligent transportation systems: Dependable Vehicular Communications for Improved Road Safety*, 2017.

[24] C. Campolo and A. Molinaro, *Vehicular ad hoc Networks*, 2015.

[25] 3rd Generation Partnership Project, "3GPP TS 22.185 V14.3.0 : Technical Specification Group Services and System Aspects; Service requirements for V2X services;(Release 14)," Tech. Rep., 2017.

[26] Vincent Tabora, "Improving Self-Driving Car Safety And Reliability With V2X Protocols," 2018. [Online]. Available: https://medium.com/self-driving-cars/improving-self-driving-car-safety-and-reliability-with-v2x-protocols-1408082bae54

[27] G. Llano, D. Ph, and R. Michoud, "Redes vehiculares Ad-hoc : aplicaciones basadas en simulación," *Ingenium*, vol. 6, pp. 11–22, 2012.

[28] B. Fernandes, J. Rufino, M. Alam, and J. Ferreira, "Implementation and Analysis of IEEE and ETSI Security Standards for Vehicular Communications," *Mobile Networks and Applications*, vol. 23, no. 3, pp. 469–478, 2018.

[29] C2C, "Urban Rail integration into ITS-G5," Tech. Rep., 2019. [Online]. Available: https://www.car-2-car.org/fileadmin/documents/General_Documents/C2CCC_TR2053_Urban_Rail.pdf

[30] W. Anwar, N. Franchi, and G. Fettweis, "Physical Layer Evaluation of V2X Communications Technologies: 5G NR-V2X, LTE-V2X, IEEE 802.11bd, and IEEE 802.11p," in *2019 IEEE 90th Vehicular Technology Conference (VTC2019-Fall)*. IEEE, 2019, p. 7.

[31] Auto-Talks, "One global V2X solution: DSRC and C-V2X." [Online]. Available: https://www.auto-talks.com/technology/global_v2x_dsrc-and-c-v2x/

[32] IEEE, "IEEE 802.11p-2010 - IEEE Standard for Information technology– Local and metropolitan area networks– Specific requirements– Part 11: Wireless LAN Medium Access Control (MAC) and Physical Layer (PHY) Specifications Amendment 6: Wireless Access in Vehicul," Tech. Rep., 2010. [Online]. Available: https://standards.ieee.org/standard/802_11p-2010.html

[33] Y. Zhang and L. C. Yang, "Design and simulation of physical layer of IEEE 802.11p vehicular ad-hoc networks," in *International Conference on Information System and Artificial Intelligence*, no. 5, 2017, p. 4.

[34] A. M. Abdelgader and W. Lenan, "The physical layer of the IEEE 802. 11p WAVE communication standard: The specifications and challenges," in *World Congress on Engineering and Computer Science*, vol. 2, 2014, pp. 691–698.

[35] S. Shah and N. Mustari, "Modeling and performance analysis of the IEEE 802.11P Enhanced Distributed Channel Access function for vehicular network," in *FTC 2016 - Proceedings of Future Technologies Conference*, no. December, 2017, pp. 173–178.

[36] C. Han, M. Dianati, R. Tafazolli, R. Kernchen, and X. Shen, "Analytical study of the IEEE 802.11p MAC sublayer in vehicular networks," *IEEE Transactions on Intelligent Transportation Systems*, vol. 13, no. 2, pp. 873–886, 2012.

[37] B. Erdem, "IEEE 802.11bd - A Seamless Evolutionary Access Layer For ITS-G5/DSRC," in *Car 2 Car Forum 2019*, no. 23, 2019, pp. 21–27. [Online]. Available: https://www.car-2-car.org/fileadmin/downloads/PDFs/car-2-car-journal/Journal_23_C2C-CC_Oct_2019_web.pdf

[38] S. Bo and H. Zhang, "802.11 NGV Proposed PAR," in *IEEE NGV Meeting*, 2018, p. 31. [Online]. Available: http://www.ieee802.org/11/Reports/tgbd_update.htm

[39] IEEE, "802.11 documents." [Online]. Available: https://mentor.ieee.org/802.11/documents?is_dcn=DCN%2CTitle%2CAuthororAffiliation&is_group=00bd

[40] G. T. . V15.2.0, "3rd Generation Partnership Project; Technical Specification Group Services and System Aspects; Enhancement of 3GPP support for V2X scenarios," Tech. Rep., 2017.

[41] S. Stephan, P. Unterhuber, M. Soliman, A. Lehner, F. Berens, and J. M. García-Loygorri, "Railway Use Cases for NGV," in *IEEE NGV Meeting*, 2018, p. 12. [Online]. Available: https://mentor.ieee.org/802.11/documents?is%5C_group=00bd

[42] I. S. 802.11™-2016, "Part 11 : Wireless LAN Medium Access Control (MAC) and Physical Layer (PHY) Specifications IEEE Computer Society Specific requirements Part 11 : Wireless LAN Medium Access Control (MAC) and Physical Layer (PHY) Specifications," p. 3534, 2016.

[43] S. BO, "NGV SG Use Cases (Next Generation V2X Study Group)," in *IEEE NGV Meeting*, 2018, p. 17. [Online]. Available: https://mentor.ieee.org/802.11/documents?is%5C_group=00bd,(accessed30July2020).

[44] IEEE, "Part 11 : Wireless LAN Medium Access Control (MAC) and Physical Layer (PHY) S pecifications," Tech. Rep. March, 2012.

[45] J. Liu, T. Pare, C. Wang, J. Wang, T. Wu, R. Huang, J. Yee, A. Jauh, and C. Hu, "Reliable Dual Sub-Carrier Modulations (DCM) for HE-SIG-B and Data," in *IEEE Meeting HE-SIG-B and Data*, 2015, p. 25. [Online]. Available: https://mentor.ieee.org/802.11/documents

[46] S. Tang, K. Gong, C. Pan, J. Wang, and Z. Yang, "Self-Cancellation of Intercarrier Interference in OFDM Systems with Phase Noise," in *2006 IEEE 17th International Symposium on Personal, Indoor and Mobile Radio Communications*, 2006, p. 5.

[47] B. Bloessl, M. Segata, C. Sommer, and F. Dressler, "Performance Assessment of IEEE 802.11p with an Open Source SDR based Prototype," *IEEE Transaction on Mobile Computing*, vol. 17, no. 5, p. 14, 2018.

[48] C. H. Liu, "On the Design of OFDM Signal Detection Algorithms for Hardware Implementation," in *IEEE Global Telecommunications Conference*, vol. 2, no. 2, 2003, pp. 596–599.

[49] E. Sourour, H. El-ghoroury, and D. Mcneill, "Frequency Offset Estimation and Correction in the IEEE 802.11a WLAN," in *IEEE 60th Vehicular Technology Conference*, 2004, pp. 4923–4927.

[50] M. Speth, S. Fechtel, G. Fock, and H. Meyr, "Optimum receiver design for wireless broad-band systems using OFDM-part I," *IEEE Transactions on Communications*, vol. 47, no. 11, pp. 1668–1677, 1999.

[51] S. Sand, P. Unterhuber, M. Soliman, M. Schmidhammer, and F. Ponte-Muller, "Performance Analysis of Outer RS Coding Scheme," in *IEEE NGV Meeting*, 2019. [Online]. Available: https://mentor.ieee.org/802.11/dcn/19/11-19-0364-00-00bd-performance-analysis-of-outer-rs-coding-scheme.pptx

[52] G. Naik, B. Choudhury, and J. M. Park, "IEEE 802.11bd 5G NR V2X: Evolution of Radio Access Technologies for V2X Communications," *IEEE Access*, vol. 7, pp. 70 169–70 184, 2019.

[53] M. Garcia, A. Molina, M. Boban, J. Gozalvez, B. Perales, T. Şahin, and A. Kousaridas, "A Tutorial on 5G NR V2X Communications," *IEEE Communications Surveys Tutorials journal*, p. 55, 2020.

[54] A. Rodríguez Saiz, "Tecnologías C-V2X Y Dsrc Para El Vehículo Conectado En Redes De Nueva Generación," Ph.D. dissertation, Universitat Oberta de Catalunya, 2020. [Online]. Available: http://openaccess.uoc.edu/webapps/o2/bitstream/10609/117806/6/arosa92TFM0620memoria.pdf

[55] Á. Knapp, A. Wippelhauser, D. Magyar, and G. Gódor, "An Overview of Current and Future Vehicular Communication Technologies," *Periodica Polytechnica Transportation Engineering*, vol. 48, no. 4, pp. 341–348, 2020.

[56] 3GPP, "TS 36.213 Evolved Universal Terrestrial Radio Access (E-UTRA); Physical layer procedures (v14.8.0, Release 14) (v15.7.0, Release 15)," 2018.

[57] Giovanni Nardini, A. Virdis, C. Campolo, and A. Molinaro, "Cellular-V2X Communications for Platooning : Design and Evaluation," *Sensor*, vol. 18, pp. 1–22, 2018.

[58] Wikiwand, "OFDMA." [Online]. Available: https://www.wikiwand.com/ca/OFDMA

[59] ETSI, "TS 136 211 - V14.9.0 - LTE; Evolved Universal Terrestrial Radio Access (E-UTRA); Physical channels and modulation (3GPP TS 36.211 version 14.9.0 Release 14)," Tech. Rep., 2017. [Online]. Available: https://portal.etsi.org/TB/ETSIDeliverableStatus.aspx

[60] 3GPP, "ETSI TS 138 211 - V16.3.0 - 5G; NR; Physical channels and modulation (3GPP TS 38.211 version 16.3.0 Release 16)," Tech. Rep., 2020. [Online]. Available: https://portal.etsi.org/TB/ETSIDeliverableStatus.aspx

[61] A. Zaidi, F. Athley, J. Medbo, U. Gustavsson, G. Durisi, and X. Chen, *5G Physical Layer: Principles, Models and Technology Components*, 2018.

[62] G. T. . V14.3.0, "3rd Generation Partnership Project; Technical Specification Group Services and System Aspects; Service requirements for V2X services; Stage 1 (Release 14)," 2017.

[63] A. Turley, K. Moerman, A. Filippi, and V. Martinez, "C-ITS: Three observations on LTE-V2X and ETSI ITS-G5-A comparison," Tech. Rep., 2018. [Online]. Available: www.simtd.de

[64] W. Anwar, K. Kulkarni, T. R. Augustin, N. Franchi, and G. Fettweis, "PHY Abstraction Techniques for IEEE 802.11p and LTE-V2V: Applications and Analysis," in *IEEE Globecom Workshops*, 2018, pp. 1–7.

[65] A. Bazzi, B. M. Masini, A. Zanella, S. Member, and I. Thibault, "On the performance of IEEE 802 . 11p and LTE-V2V for the Cooperative Awareness of Connected Vehicles," *IEEE Transaction on Vehicle Technology*, vol. 66, no. 11, p. 14, 2017.

[66] NXP, "Next Generation Vehicular Networks: IEEE802.11bd," in *Secure Connections a Smarter World*, 2019, p. 7. [Online]. Available: https://mentor.ieee.org/802.11/documents

[67] R. Molina-Masegosa, J. Gozalvez, and M. Sepulcre, "Comparison of IEEE 802.11p and LTE-V2X: An Evaluation with Periodic and Aperiodic Messages of Constant and Variable Size," *IEEE Access*, vol. 8, pp. 121 526–121 548, 2020.

[68] M. Saad, M. Raza, S. Ahmed, and D. Kim, "Advancements in Vehicular Communication Technologies: C-V2X and NR-V2X Comparison," *IEEE Communications Magazine*, vol. 59, no. 8, p. 8, 2021.

[69] J. Ferrándiz, "EL FERROCARRIL EN EL SISTEMA DE TRANSPORTES : ASPECTOS ECONÓMICOS Y," Tech. Rep.

[70] UE, "El transporte ferroviario," Tech. Rep., 2021. [Online]. Available: http://revistas.bancomext.gob.mx/rce/magazines/157/2/el_transporte.pdf

[71] J. Rodríguez-piñeiro, "Broadband Wireless Communication Systems for High Mobility Scenarios," Ph.D. dissertation, 2016.

[72] E. Masson and M. Berbineau, *Broadband wireless communications for railway applications*, 2017. [Online]. Available: https://books.google.com.co/books?id=O6VDDQAAQBAJ

[73] U. I. d. C. de Fer, "Prescriptions Techniques pour les Systèmes Analogues Radio Sol-Train en Service International (UIC 751-3)," Tech. Rep., 1984.

[74] U. Bock and J. Varchmin, "Enhancement of the Occupancy of Railroads Using Virtually Coupled Train Formations," in *World Congress on Railway Research*, 1999.

[75] NBW, "The Depths of Tring Railway Cutting." [Online]. Available: https://www.northbuckswanderer.com/2018/09/the-depths-of-tring-railway-cutting.html#gsc.tab=0

[76] M.J.Rees, "MERSEY RAIL TUNNEL." [Online]. Available: http://www.mjrees.co.uk/portfolio/mersey-rail-tunnel/

[77] XINHUANET, "China's high-speed railway length to top 30,000 km in 2019." [Online]. Available: http://www.xinhuanet.com/english/2019-01/03/c_137715444.htm

[78] BaneNor, "A modern Vestfold Line." [Online]. Available: https://www.banenor.no/en/startpage1/news/a-modern-vestfold-line/

[79] L. Tian, J. Zhang, and C. Pan, "Small scale fading characteristics of wideband radio channel in the U-shape cutting of high-speed railway," in *IEEE Vehicular Technology Conference*, 2013, p. 6.

[80] R. He, S. Member, B. Ai, S. Member, Z. Zhong, S. Member, M. Yang, S. Member, C. Huang, S. Member, and R. Chen, "Radio Communication Scenarios in 5G - Railways," in *CS - Networking and Internet Architecture*, no. 1, 2021, pp. 1–7.

[81] J. Li, Y. Zhao, J. Zhang, R. Jiang, C. Tao, and Z. Tan, "Radio channel measurements and analysis at 2.4/5GHz in subway tunnels," *China Communications*, vol. 12, no. 1, pp. 36–45, 2015.

[82] P. Unterhuber, S. Sand, U. C. Fiebig, and B. Siebler, "Path loss models for train-to-train communications in typical high speed railway environments," *IET Microwaves, Antennas and Propagation*, vol. 12, no. 4, pp. 492–500, 2018.

[83] R. He, Z. Zhong, B. Ai, G. Wang, J. Ding, and A. F. Molisch, "Measurements and analysis of propagation channels in high-speed railway viaducts," *IEEE Transactions on Wireless Communications*, vol. 12, no. 2, pp. 794–805, 2013.

[84] D. Wang, L. Song, X. Kong, and Z. Zhang, "Near-ground path loss measurements and modeling for wireless sensor networks at 2.4 GHz," *International Journal of Distributed Sensor Networks*, vol. 2012, 2012.

[85] Y. Zhang, Z. He, W. Zhang, L. Xiao, and S. Zhou, "Measurement-based delay and doppler characterizations for high-speed railway hilly scenario," *International Journal of Antennas and Propagation*, vol. 2014, 2014.

[86] P. Unterhuber, M. Walter, U.-c. Fiebig, and K. Thomas, "Stochastic Channel Parameters for Train-to-Train Communications," *IEEE Open Journal of Antennas and Propagation*, vol. 2, pp. 778 – 792, 2021.

[87] P. Fraga-Lamas, T. Fernández-Caramés, and L. Castedo, "Towards the internet of smart trains: A review on industrial IoT-connected railways," *Sensors (Switzerland)*, vol. 17, no. 6, pp. 0–44, 2017.

[88] J. Garcia-Loygorri, J. Goikoetxea, E. Echeverria, A. Arriola, I. Val, S. Sand, P. Unterhuber, and F. Del Rio, "The wireless train communication network: Roll2rail vision," *IEEE Vehicular Technology Magazine*, vol. 13, no. 3, pp. 135–143, 2018.

[89] 3GPP, "TS 122 289 - V16.1.0 - LTE; 5G; Mobile communication system for railways (3GPP TS 22.289 version 16.1.0 Release 16)," Tech. Rep., 2020.

[90] IEEE, "IEEE 1474.1-2004 Standard for Communications-Based Train Control (CBTC) Performance and Functional Requirements," Tech. Rep., 2005. [Online]. Available: https://www.techstreet.com/ieee/standards/ieee-1474-1-2004?product_id=1214446#jumps

[91] EUROPEAN-COMMISSION, "EN Delivering an effective and interoperable European Rail Traffic Management System (ERTMS) – the way ahead," p. 22, 2017.

[92] C. Briso-Rodríguez, J. M. García-Loygorri, and L. Zhang, "Transmission-Based Signaling Systems," *Modern Railway Engineering*, 2018.

[93] J. Farooq and J. Soler, "Radio Communication for Communications-Based Train Control (CBTC): A Tutorial and Survey," *IEEE Communications Surveys and Tutorials*, vol. 19, no. 3, pp. 1377–1402, 2017.

[94] J. Moreno, J. M. Riera, L. D. Haro, and C. Rodriguez, "A survey on future railway radio communications services: Challenges and opportunities," *IEEE Communications Magazine*, vol. 53, no. 10, pp. 62–68, 2015.

[95] Y. Shao, H. Jiang, and H. Zhao, "Stackelberg Game-Based Radio Resource Management Algorithm in an Urban Rail Transit Communication System," *Urban Rail Transit*, vol. 7, no. 2, pp. 128–138, 2021. [Online]. Available: https://doi.org/10.1007/s40864-021-00147-6

[96] A. Sniady, "Communication TechnologiesSupport to Railway Infrastructureand Operations," Ph.D. dissertation, 2020. [Online]. Available: www.aqua.dtu.dk/publikationer

[97] Peter Winter, *Compendium on ERTMS : European rail traffic management system*. Eurail Press, 2009.

[98] Rieles, "CAF Signalling suministrá 118 equipos ETCS embarcados en los nuevos Civity de Holanda," 2016. [Online]. Available: https://www.rieles.com/front/caf-signalling-suministra-118-equipos-etcs-embarcados-en-los-nuevos-civity-de-holanda/

[99] U. Bock and J. Varchmin, "Enhancement of the Occupancy of Railroads Using Virtually Coupled Train Formations," in *World Congress on Railway Research*, Tokio, 1999.

[100] MOVINGRAIL, "Deliverable D3.1 Virtual Coupling Communication Solutions Analysis," Tech. Rep., 2020. [Online]. Available: https://projects.shift2rail.org/

[101] TELEFUNKEN, "TELEFUNKEN Radio Communication Systems," 2017. [Online]. Available: http://www.railway-technology.com/contractors/signal/telefunken

[102] Flarion, "FLASH-OFDM." [Online]. Available: http://www.telecomabc.com/f/flash.html

[103] J. Moreno, "ESTUDIO SOBRE UN SISTEMA DE RADIOCOMUNICACIONES FERROVIARIAS DE ACUERDO AL PARADIGMA 4G," Ph.D. dissertation, Universidad Politécnica de Madrid, 2015.

[104] B. Nandha and A. Basha, "QoS enhancements using IEEE 802.11p WLANs for communication based train control systems," *International Journal of Advanced Research in Computer and Communication Engineering*, vol. 2, no. 5, pp. 1987–1990, 2013.

[105] M. Aguado, E. Jacob, M. Higuero, M. Berbineau, and P. Saiz, "Broadband Communication in the High Mobility Scenario: the WiMAX Opportunity," *Intech*, 2009.

[106] K. Guan, Z. Zhong, and B. Ai, "Assessment of LTE-R using high speed railway channel model," *Proceedings - 2011 3rd International Conference on Communications and Mobile Computing, CMC 2011*, vol. 2, pp. 461–464, 2011.

[107] T. Domínguez-bolaño, J. Rodríguez-piñeiro, J. A. García-naya, and L. Castedo, "Experimental Characterization of LTE Wireless Links in High-Speed Trains," *Wireless Communications and Mobile Computing*, vol. 2017, p. 21, 2017.

[108] S. Banerjee, M. Hempel, and H. Sharif, "A Survey of Wireless Communication Technologies Their Performance for High Speed Railways," *Journal of Transportation Technologies*, vol. 06, no. 01, pp. 15–29, 2016.

[109] ETSI, "ETSI EN 300 396-3: Terrestrial Trunked Radio (TETRA); Technical requirements for Direct Mode Operation (DMO); Part 3: Mobile station to mobile station (MS-MS) Air Interface (AI)protocol." European Standard (Telecommunications series), Tech. Rep., 2006.

[110] T. Strang, A. Festag, A. Vinel, R. Mehmood, C. R. Garcia, and M. Röckl, "Measurement and Analysis of the Direct Train to Train Propagation Channel in the 70 cm UHF-Band,," in *Nets4Cars/Nets4Trains 2011*, no. March, 2014, p. 12.

[111] T. Rappaport, *Wireless Communications: Principles and Practices*. Prentice Hall, 1999.

[112] ETSI, "TR 103 257-1 V1.1.1 Intelligent Transport Systems (ITS). Access Layer. Part 1: Channel Models for the 5,9 GHz frequency band." Tech. Rep., 2019.

[113] P. Bello, "Characterization of Randomly Time-Variant Linear Channels," *IEEE Transactions on Communications Systems*, pp. 360–393, 1963.

[114] A. Molisch, *WIRELESS COMMUNICATIONS*, John Wiley, Ed., 2011.

[115] J. Moreno, "Characterization of the railway environment : channel models general characteristics," pp. 1–57, 2021.

[116] S. Salous, "Radio Channel Sounders," in *Radio Propagation Measurement and Channel Modelling*, 2013, no. 1864.

[117] N. Costa and S. Haykin, *Multiple-input, multiple-output channel models*, 2010.

[118] L. Zhang, "Channel Measurement and Modeling in Complex Environments para la Sociedad de la Informaci ´ on," Ph.D. dissertation, Technical University of Madrid, 2016.

[119] K. Technologies, "5G Channel Sounding , Reference Solution," Tech. Rep. [Online]. Available: www.keysight.com

[120] A. F. Molisch, F. Tufvesson, S. Member, J. Karedal, S. Member, C. Mecklenbrauker, and S. Member, "Propagation aspects of vehicle-to-vehicle communications - an overview," pp. 1–4, 2009.

[121] L. Bernado, T. Zemen, F. Tufvesson, A. F. Molisch, and C. F. Mecklenbrauker, "Delay and doppler spreads of nonstationary vehicular channels for safety-relevant scenarios," *IEEE Transactions on Vehicular Technology*, vol. 63, no. 1, pp. 82–93, 2014.

[122] G. Acosta and M. A. Ingram, "Model development for the wideband expressway vehicle-to-vehicle 2.4 GHz channel," in *IEEE Wireless Communications and Networking Conference, WCNC*, vol. 3, no. c, 2006, pp. 1283–1288.

[123] M. Pätzold, *Mobile Radio Channels: Second Edition*, 2011.

[124] J. McKown and L. Hamilton, "Ray Tracing as a Design Tool for Radio Networks," *IEEE Network Magazine*, vol. 5, no. 6, pp. 27–30, 1991.

[125] M. Walter, "Scattering in Non-Stationary Mobile-to-Mobile Communications Channels," Ph.D. dissertation, Universit at Ulm, 2015.

[126] J. Sykora, "Tapped delay line model of linear randomly time-variant WSSUS channel," *Electronics Letters*, vol. 36, no. 19, 2000.

[127] G. Acosta-marum, "Measurement , Modeling , and OFDM Synchronization for the Wideband Mobile-to-Mobile Channel Measurement , Modeling , and OFDM Synchronization for the Wideband Mobile-to-Mobile Channel," *Test*, 2007.

[128] W. Mohr, "Wideband Mobile Radio Channels Based on Propagation Measurements," pp. 397–401, 1995.

[129] X. Zhao, J. Kivinen, and P. Vainikainen, "Tapped delay line channel models at 5.3 GHz in indoor environments," *IEEE Vehicular Technology Conference*, vol. 1, no. 52 ND, pp. 1–5, 2000.

[130] L. Greenstein, D. Michelson, and V. Erceg, "Moment-Method Estimation of the Ricean," *Communications Letters*, vol. 3, no. 6, pp. 175–176, 1999.

[131] K. Talukdar and W. Lawing, "Estimation of the parameters of the Rice distribution," *J. Acoust. Soc. Amer.*, vol. 89, no. May, pp. 1193–1197, 1990.

[132] B. Chen, Z. Zhong, B. Ai, K. Guan, R. He, and D. G. Michelson, "Channel characteristics in high-speed railway: A survey of channel propagation properties," *IEEE Vehicular Technology Magazine*, vol. 10, no. 2, pp. 67–78, 2015.

[133] M. Walter, D. Shutin, and U. C. Fiebig, "Delay-dependent doppler probability density functions for vehicle-to-vehicle scatter channels," *IEEE Transactions on Antennas and Propagation*, vol. 62, no. 4, pp. 2238–2249, 2014.

[134] J. Kivinen, X. Zhao, and P. Vainikainen, "Empirical characterization of wideband indoor radio channel at 5.3 GHz," *IEEE Transactions on Antennas and Propagation*, vol. 49, no. 8, pp. 1192–1203, 2001.

[135] X. Zhao, K. Jarmo, V. Pertti, and S. Kari, "Characterization of Doppler Spectra for Mobile Communications at 5.3 GHz," *IEEE Trans. Veh. Technol*, vol. 52, no. 1, pp. 14–23, 2003.

[136] W. Qian, X. Chunxiu, W. Muqing, Z. Min, and Y. Deshui, "Propagation characteristics of high speed railway radio channel based on broadband measurements at 2.6 GHz," *IEEE Wireless Communications and Networking Conference, WCNC*, vol. 1, pp. 166–170, 2014.

[137] ETSI TS 1, "Digital cellular telecomm mmunications system (Phase 2+) GSM/EDGE Radio transmission and reception (3GPP TS 45.005 version 13.3.0 Release 13))," vol. 0, 2017.

[138] R. Sun, C. Tao, L. Liu, Z. Tan, L. Zhang, and T. Zhou, "Nonisotropic scattering characteristic in an alternant tree-blocked viaduct scenario on high-speed railway at 2.35 GHz," *International Journal of Antennas and Propagation*, vol. 2014, 2014.

[139] J. Ding, L. Zhang, J. Yang, B. Sun, and J. Huang, "Broadband wireless channel in composite high-speed railway scenario: Measurements, simulation, and analysis," *Wireless Communications and Mobile Computing*, vol. 2017, 2017.

[140] L. Liu, C. Tao, T. Zhou, Y. Zhao, X. Yin, and H. Chen, "A highly efficient channel sounding method based on cellular communications for high-speed railway scenarios," *EURASIP Journal on Wireless Communications and Networking*, vol. 2012, no. 1, pp. 1–16, 2012.

[141] T. Zhou, C. Tao, S. Salous, L. Liu, and Z. Tan, "Implementation of an LTE-based channel measurement method for high-speed railway scenarios," *IEEE Transactions on Instrumentation and Measurement*, vol. 65, no. 1, pp. 25–36, 2016.

[142] K. Guan, Z. Zhong, B. Ai, and T. Kürner, "Propagation measurements and modeling of crossing bridges on high-speed railway at 930 MHz," *IEEE Transactions on Vehicular Technology*, vol. 63, no. 2, pp. 502–517, 2014.

[143] K. Guan, Z. Zhong, and B. Ai, "Assessment of LTE-R using high speed railway channel model," *Proceedings - 2011 3rd International Conference on Communications and Mobile Computing, CMC 2011*, vol. 2, pp. 461–464, 2011.

[144] Huber+Suhner, "Sencity Rail." [Online]. Available: https://www.hubersuhner.com/en/products/radio-frequency/antennas/railway/sencity-rail-en

[145] A. Dakic, M. Hofer, B. Rainer, S. Zelenbaba, L. Bernado, and T. Zemen, "Real-Time Vehicular Wireless System-Level Simulation," *IEEE Access*, vol. 9, pp. 23 202–23 217, 2021.

[146] T. Zemen, L. Bernadó, and N. Czink, "Iterative Time-Variant Channel Estimation for 802 . 11p Using Generalized Discrete Prolate Spheroidal Sequences," *IEEE Transaction on Vehicular Technology*, vol. 61, no. 3, pp. 1–12, 2012.

[147] S. Ioannis, "Considerations on NGV PHY design," in *IEEE Meeting NGV*, 2019, p. 25. [Online]. Available: https://mentor.ieee.org/802.11/documents?is%5C_group=00bd

[148] L. Miao, K. Djouani, B. Van, and Y. Hamam, "Evaluation and Enhancement of IEEE 802.11p Standard: A Survey," *Mobile Computing*, vol. 1, no. 1, 2012. [Online]. Available: https://www.researchgate.net/publication/258118237

[149] S. Kim, H. Oh, and H. Choi, "Mid-amble aided OFDM performance analysis in high mobility vehicular channel," in *IEEE Intelligent Vehicles Symposium*, 2008, pp. 751–754.

[150] W. Anwar, A. Traßl, N. Franchi, and G. Fettweis, "On the Reliability of NR-V2X and IEEE 802.11bd," in *2019 IEEE 30th Annual International Symposium on Personal, Indoor and Mobile Radio Communications (PIMRC)*, 201.

[151] M. Sybis, "Channel Estimation with Two-Dimensional Interpolation for the 802 . 11p Communication," in *International Conference on Connected Vehicles and Expo (ICCVE)*, 2014, pp. 693–694.

[152] Y. Kang, K. Kim, and H. Park, "Efficient DFT-based channel estimation for OFDM systems on multipath channels," *IET Commun*, vol. 1, no. 2, pp. 197–202, 2007.

[153] Y.-s. Lee, H.-c. Shin, and H.-n. Kim, "Channel Estimation Based on a Time-Domain Threshold for OFDM Systems," *IEEE Transaction on Broadcasting*, vol. 55, no. 3, pp. 656–662, 2009.

[154] T. Wang, A. Hussain, Y. Cao, and S. Gulomjon, "An Improved Channel Estimation Technique for IEEE 802.11p Standard in Vehicular Communications," *Sensors*, pp. 1–22, 2019.

[155] S. Baek, I. Lee, and C. Song, "A New Data Pilot-Aided Channel Estimation Scheme for Fast Time-Varying Channels in IEEE 802.11p Systems," *IEEE Transactions on Vehicular Technology*, vol. 68, no. 5, pp. 5169–5172, 2019.

[156] J. Nuckelt, M. Schack, and K. Thomas, "Performance Evaluation of Wiener Filter Designs for Channel Estimation in Vehicular Environments," in *2011 IEEE Vehicular Technology Conference (VTC Fall)*, no. 2. IEEE, 2011, p. 5.

[157] C.-s. Lin and J.-c. Lin, "Novel Channel Estimation Techniques in IEEE 802 . 11p Environments," in *IEEE 71st Vehicular Technology Conference*. IEEE, 2010, p. 5.

[158] R.-a. Stoica, S. Severi, and G. Thadeu, "A Self-Organizing Frequency Approach to 802 . 11p Channel Estimation," *IEEE Transactions on Intelligent Transportation Systems*, vol. 18, no. 7, p. 13, 2016.

[159] K. Nagalapur, F. Br, E. Str, F. Undi, and K. Mahler, "An 802 . 11p Cross-Layered Pilot Scheme for Time- and Frequency-Varying Channels and Its Hardware Implementation," *IEEE Transactions on Vehicular Technologytion*, vol. 65, no. 6, pp. 1–12, 2016.

[160] M. Awad, K. Seddik, S. Member, and A. Elezabi, "Low-Complexity Semi-Blind Channel Estimation Algorithms for Vehicular Communications Using the IEEE 802 . 11p Standard," *IEEE Transactions on Intellegent Transportation Systems*, vol. 20, no. 5, p. 10, 2018.

[161] J. Choi, H. Jo, C. Mun, and J. Yook, "Preamble-based adaptive channel estimation for IEEE 802.11p," *Sensors*, vol. 19, no. 13, pp. 1–20, 2019.

[162] C. Young, C. Mun, and J. Gwan, "Adaptive Channel Estimation Based on a Decision Method Using a Long Preamble for the IEEE 802 . 11p," in *2017 IEEE 85th Vehicular Technology Conference (VTC Spring)*, 2017, p. 5.

[163] M. Jie, Y. Hua, and L. Shouyin, "The MMSE channel estimation based on DFT for OFDM system," *Proceedings - 5th International Conference on Wireless Communications, Networking and Mobile Computing, WiCOM 2009*, pp. 0–3, 2009.

[164] A. Agnoletto, "Data Decoding Aided Channel Estimation Techniques for OFDM Systems in Vehicular Enviroment," Ph.D. dissertation, Universita Degli Studi di Padova, 2013.

[165] I. Sarris, "V2X baseband simulation model," 2018. [Online]. Available: https://github.com/u-blox/ubx-v2x/tree/ngv_ldpc_mce

[166] S. Coleri, M. Ergen, A. Puri, and A. Bahai, "A Study of Channel Estimation in OFDM Systems," in *Proceedings IEEE 56th Vehicular Technology Conference*, 2002, pp. 894–898.

[167] C. F. Mecklenbraüker, A. F. Molisch, J. Karedal, F. Tufvesson, A. Paier, L. Bernadó, T. Zemen, O. Klemp, and N. Czink, "Vehicular channel characterization and its implications for wireless system design and performance," *Proceedings of the IEEE*, vol. 99, no. 7, pp. 1189–1212, 2011.

[168] T. D. Bolaño, "Design and Evaluation of New Waveforms for High Mobility Communications," Ph.D. dissertation, Universidade da Coruña, 2018. [Online]. Available: https://ruc.udc.es/dspace/handle/2183/21081

[169] K. Chu, S. Dean, and B. Illowsky, *Elementary statistics*, 2006, vol. 207. [Online]. Available: http://cnx.org/content/col10966/1.4/

[170] T. Schmidl and D. Cox, "Robust frequency and timing synchronization for OFDM," *IEEE Transactions on Communications*, vol. 45, no. 12, pp. 1613–1621, 1997.

[171] S. S. Das, R. Rajakumar, M. Rahman, and A. Pal, "Low Complexity Residual Phase Tracking Algorithm for OFDM-based WLAN Systems," in *Communication Systems,Networks and Digital Signal Processing CSNDSP*, 2004, p. 4.

[172] Shift2Rail, "Shift2Rail Joint Undertaking (S2R JU) Amended Annual Work Plan and Budget for 2018," Tech. Rep., 2018. [Online]. Available: https://shift2rail.org/wp-content/uploads/2017/11/Decision-6-2017_-AWP2018_Annex.pdf

[173] J. M. Molina-Garcia-Pardo, J. V. Rodríguez, and L. Juan-Llácer, "Wide-band measurements and characterization at 2.1 GHz while entering in a small tunnel," *IEEE Transactions on Vehicular Technology*, vol. 53, no. 6, pp. 1794–1799, 2004.

[174] F. Luan, Y. Zhang, L. Xiao, C. Zhou, and S. Zhou, "Fading characteristics of wireless channel on high-speed railway in hilly terrain scenario," *International Journal of Antennas and Propagation*, vol. 2013, 2013.

[175] R. Sun, C. Tao, L. Liu, and Z. Tan, "Channel measurement and characterization for HSR u-shape groove scenarios at 2.35 GHz," in *IEEE Vehicular Technology Conference*, 2013, p. 5.

[176] A. Paier, J. Karedal, N. Czink, H. Hofstetter, C. Dumard, T. Zemen, F. Tufvesson, A. F. Molisch, and C. F. Mecklenbräuker, "Car-to-car radio channel measurements at 5 GHz: Pathloss, power-delay profile, and delay-Doppler spectrum," *Proceedings of 4th IEEE Internatilonal Symposium on Wireless Communication Systems 2007, ISWCS*, pp. 224–228, 2007.

[177] M. Pätzold, A. Szczepanski, and N. Youssef, "Methods for modeling of specified and measured multipath power-delay profiles," *IEEE Transactions on Vehicular Technology*, vol. 51, no. 5, pp. 978–988, 2002.

[178] G. Acosta-Marum and M. A. Ingram, "A BER-based partitioned model for a 2.4GHz vehicle-to-vehicle expressway channel," *Wireless Personal Communications*, vol. 37, no. 3-4, pp. 421–443, 2006.

[179] K. Guan, B. Ai, Z. Zhong, C. F. López, L. Zhang, C. Briso-Rodríguez, A. Hrovat, B. Zhang, R. He, and T. Tang, "Measurements and Analysis of Large-Scale Fading Characteristics in Curved Subway Tunnels at 920 MHz, 2400 MHz, and 5705 MHz," *IEEE Transactions on Intelligent Transportation Systems*, vol. 16, no. 5, pp. 2393–2405, 2015.

[180] J. J. van de Beek, O. Edfors, M. Sandell, S. K. Wilson, and P. O. Borjesson, "On channel estimation in OFDM systems," *IEEE Vehicular Technology Conference*, vol. 2, no. 1, pp. 815–819, 1995.

[181] O. Edfors, M. Sandell, J.-J. V. D. Beek, S. K. Wilson, P. O. Borjessonl, and W. Lafayette, "OFDM Channel Estimation By Singular Value Decomposition," *Computer Engineering*, pp. 0–4, 1996.

[182] E. Mozo, A. Gómez-Alonso, and M. Mendicute, "Pilot-based channel estimation technique for IEEE 802 . 11bd in vehicular channels with high Doppler," *Sensors*, 2022.